

Ghent University - Faculty of Sciences
Department of Analytical Chemistry
Krijgslaan 281, S12
9000 Ghent

Development, optimisation and application of Raman
spectroscopic and X-ray fluorescence spectroscopic
methodology in the field of cultural heritage.

Annelien Deneckere

Academic year 2011–2012

Dissertation submitted in fulfillment of the requirements for the degree of Doctor
(Ph.D.) in Sciences, Chemistry



Promotor: Prof. Dr. Luc Moens
Co-promotor: Prof. Dr. Peter Vandenabeele
Co-promotor: Dr. Bart Vekemans

Woord vooraf

Gedurende mijn licentiaatsthesis kreeg ik de Raman-microbe te pakken, al was het dan wel voor de analyse van geneesmiddelenvervalsingen. Tijdens mijn verblijf in de Ramangroep werd er een mogelijkheid om te doctoreren aangeboden, hetzij dan wel in de richting van kunst. Ik heb deze kans met beide handen gegrepen en de overstap gemaakt naar de analyse van kunstobjecten. Ik zal nooit vergeten hoe ontgoocheld ik was met de eerste noisy Raman spectra, die eigen zijn aan de kunstanalyse, die ik verkreeg; maar ik bleef volharden. In het tweede jaar van mijn doctoraat kreeg ik de mogelijkheid om naast Ramanspectroscopie ook X-straal fluorescentie spectroscopie te gebruiken. De combinatie van de beide technieken opende een hele nieuwe waaier aan mogelijkheden.

Door de aard van mijn onderzoek ben ik op plaatsen geweest, het nachtelijk verblijf in de Onze-Lieve-Vrouwekathedraal in Antwerpen; en in contact gekomen met waardevolle kunstobjecten, o.a. Middeleeuwse handschriften; waar anderen alleen maar kunnen van dromen. Het gevoel dat komt opborrelen wanneer je een waardevol kunstobject in je handen hebt is onbeschrijfelijk. Als ik dan toch een poging zou ondernemen om dit gevoel te beschrijven, zou ik de verwoording kiezen die Albert Einstein gebruikte:

The most beautiful experience we can have is the mysterious – the fundamental emotion which stands at the cradle of true art and true science.

Albert Einstein

Ik hoop dat jullie door het lezen van dit document ook kunnen meegenieten van dit onbeschrijfelijke gevoel.

Content

Abbreviations and acronyms

Chapter 1: Introduction and aim.....1

Chapter 2: Raman spectroscopy and X-ray fluorescence (XRF) spectroscopy:
theory and instrumentation.....9

2.1 Raman spectroscopy.....11

2.1.1 Raman spectroscopy: theory.....11

2.1.1.1 Introduction.....11

2.1.1.2 Raman effect: classical approach.....11

2.1.1.3 Raman effect: quantum chemical approach.....12

2.1.1.4 Raman spectrum: intensity as function of wavenumber.14

2.1.2 Raman spectroscopy: instrumentation.....17

2.1.2.1 The laser.....17

2.1.2.2 The neutral density filter.....18

2.1.2.3 The microscope.....19

2.1.2.4 The sample stage system.....20

2.1.2.5 The aperture.....20

2.1.2.6 The diffraction gratings.....21

2.1.2.7 The detector.....21

2.1.2.8 The wavelength stability of the Senterra Raman
spectrometer.....22

2.1.2.8.1 Short term wavelength stability.....22

2.1.2.8.2 Long term wavelength stability.....26

2.1.2.9 The Mobile Art Analyser (MArtA).....28

2.2 X-ray fluorescence (XRF) spectroscopy.....	30
2.2.1 XRF spectroscopy: theory.....	30
2.2.1.1 Introduction.....	30
2.2.1.2 Theory of X-ray fluorescence (XRF).....	30
2.2.1.3 XRF spectrum: intensity as function of energy.....	32
2.2.2 XRF spectroscopy: instrumentation.....	36
2.2.2.1 The X-ray tube.....	37
2.2.2.2 X-ray optics: the polycapillary.....	37
2.2.2.3 The detector.....	38
2.2.2.4 Analytical characteristics of the EDAX Eagle-III.....	41
2.2.2.4.1 Beam size characterisation.....	41
2.2.2.4.2 The relative minimum detection limits.....	43
2.2.2.5 Two mobile micro-XRF spectrometers: ArtTAX (Bruker, Germany) and the EDXRF system from the CEA (Liège, Belgium).....	45
Chapter 3: In-house developed software.....	51
3.1 Evaluation of XRF spectra by Iterative Least-squares (AXIL).....	53
3.1.1 Non-linear least-squares fitting.....	53
3.1.2 Background compensation method.....	54
3.2 Evaluation of Raman spectra by in-house developed software.....	56
3.2.1 File-format.....	56
3.2.2 Calculation of the parameters and estimation of the background.....	57
Chapter 4: Multivariate statistical techniques.....	63
4.1 Principal components analysis (PCA).....	65
4.2 K-means cluster analysis.....	69

Chapter 5: The use of mobile Raman spectroscopy to compare three full-page miniatures from the Breviary of Arnold of Egmond.....	73
5.1 Introduction.....	75
5.2 The Breviary Arnold of Egmond.....	76
5.3 Experimental.....	78
5.3.1 The analysed folios.....	78
5.3.2 Mobile Raman spectroscopy.....	80
5.4 Results and discussion.....	81
5.4.1 Visual examination based on style.....	81
5.4.2 Analysis with mobile Raman spectroscopy.....	82
5.4.2.1 White colour.....	82
5.4.2.2 Yellow colour.....	84
5.4.2.3 Blue colour.....	84
5.4.2.4 Green and grey colour.....	85
5.4.2.5 Brown colour.....	86
5.4.2.6 Red colour and incarnation.....	87
5.4.3 Interpretation of the results.....	88
5.5 Conclusions.....	90
Chapter 6: <i>In situ</i> investigations of vault paintings in the Antwerp cathedral.....	95
6.1 Introduction.....	97
6.2 The Site.....	99
6.2.1 Mediaeval vault painting.....	99
6.2.2 Renaissance vault painting.....	100
6.3 Experimental.....	101
6.3.1 XRF spectroscopy.....	101
6.3.2 Raman spectroscopy.....	102
6.4 Results and discussion.....	103

6.4.1 Conditions.....	103
6.4.2 Pigment identification of the mediaeval vault painting.....	104
6.4.2.1 Supporting layer.....	104
6.4.2.2 Red layers.....	105
6.4.2.3 Green layers.....	108
6.4.2.4 Blue layers.....	112
6.4.3 Pigment identification of the renaissance vault painting.....	114
6.4.3.1 Supporting layer.....	114
6.4.3.2 Red layers.....	115
6.4.3.3 Gold and tin layer.....	117
6.4.2.4 Blue layers.....	119
6.5 Conclusions.....	120

Chapter 7: The use of a multi-method approach to identify the pigments in the 12 th century manuscript <i>Liber Floridus</i>	127
7.1 Introduction.....	129
7.2 The manuscript ‘ <i>Liber Floridus</i> ’.....	130
7.3 Experimental.....	132
7.3.1 Samples and sample preparation.....	132
7.3.2 Instrumentation.....	134
7.3.2.1 <i>In situ</i> Raman spectroscopy.....	134
7.3.2.2 Confocal micro-Raman spectroscopy.....	134
7.3.2.3 Energy dispersive X-ray fluorescence spectroscopy (EDXRF).....	135
7.3.2.4 UV-fluorescence photography.....	136
7.3.2.5 Infrared reflectography (IRR).....	136
7.4 Results and discussion.....	137
7.4.1 Underdrawing.....	138

7.4.2 Blue.....	141
7.4.3 Green.....	145
7.4.4 Purple.....	145
7.4.5 Red.....	146
7.4.6 Yellow.....	151
7.4.7 White.....	152
7. 5 Conclusions.....	154

Chapter 8: Direct analysis of the central panel of the so-called Wyts triptych after Jan van Eyck.....163

8.1 Introduction.....	165
8.2 The Wyts Triptych.....	167
8.3 Experimental.....	170
8.3.1 Energy dispersive X-ray fluorescence spectroscopy.....	170
8.3.2 Raman spectroscopy.....	171
8.4 Results and discussion.....	173
8.4.1 Direct energy dispersive X-ray fluorescence analysis.....	173
8.4.1.1 Red, brown and flesh colour.....	173
8.4.1.2 Blue and green colour.....	174
8.4.1.3 White colour.....	175
8.4.1.4 Yellow colour.....	176
8.4.1.5 Restored areas and two-dimensional elemental mapping.....	176
8.4.2 Direct Raman spectroscopic analysis.....	178
8.4.2.1 Red, brown and flesh colour.....	179
8.4.2.2 Blue colour.....	181
8.4.2.3 White colour.....	183
8.4.2.4 Yellow colour.....	183

8.4.1.5 Discussion.....	183
8.4.3 Integration of the results.....	184
8.4.3.1 Red, brown and flesh colour.....	184
8.4.3.2 Blue and green colour.....	185
8.4.2.3 White and yellow colour.....	186
8.5 Conclusions.....	186

Chapter 9: Feasibility study of the application of micro-Raman imaging as

complement to micro-XRF imaging.....	195
9.1 Introduction.....	197
9.2 Techniques.....	199
9.2.1 Raman spectroscopy.....	199
9.2.2 X-ray fluorescence (XRF) spectroscopy.....	202
9.2.3 Combined techniques.....	205
9.3 Experimental.....	207
9.3.1 Confocal micro-Raman spectroscopy.....	207
9.3.2 Energy dispersive X-ray fluorescence (EDXRF) spectroscopy.....	208
9.4 Results and discussion.....	209
9.4.1 X-ray fluorescence (XRF) spectroscopy.....	209
9.4.1.1 Identification of the pigments.....	209
9.4.1.2 Chemometrical data processing	211
9.4.1.2.1 Principal components analysis (PCA).....	211
9.4.1.2.2 K-means cluster analysis.....	214
9.4.2 Raman spectroscopy.....	218
9.4.2.1 Identification of the pigments.....	219
9.4.2.2 The influence of spectral resolution and measurement time.....	221

9.5 Conclusions.....	225
Chapter 10: Identification of inorganic pigments used in porcelain cards based on fusing Raman and XRF data.....	243
10.1 Introduction.....	245
10.2 Experimental.....	249
10.2.1 Samples.....	249
10.2.2 Instrumentation.....	250
10.2.2.1 Micro-Raman spectroscopy.....	250
10.2.2.2 Energy dispersive X-ray fluorescence (EDXRF) spectroscopy.....	252
10.3 Results and discussion.....	252
10.3.1 Fusion of the data: proposed methodology.....	252
10.3.2 Identification procedure applied on the fused data.....	256
10.3.3 Porcelain cards.....	262
10.3.3.1 Raman classification.....	262
10.3.3.2 XRF classification.....	264
10.3.3.3 Raman and XRF data fusion.....	264
10.3.4 Reference pigments.....	268
10.3.4.1 Raman and XRF data fusion.....	268
10.3.4.2 Identification procedure.....	269
10.4 Conclusions.....	272
Chapter 11: Conclusions and future prospects.....	281
Summary/Samenvatting.....	287
Dankwoord.....	301

Appendix A: Idl routines read_jcamp_dx.pro and calc_jcamp_dx_parameters.pro....	303
A.1 read_jcamp_dx.pro.....	303
A.2 calc_jcamp_dx_parameters.pro.....	308
Appendix B: Publications and activities.....	317
B.1 List of (contributions to) publications.....	317
B.2 List of (contributions to) oral presentations.....	318
B.3 List of (contributions to) poster presentations.....	320

Abbreviations and acronyms

General

CCD	charged coupled device
CEA	Centre Européen d'Archéométrie
EDXRF	energy dispersive X-ray fluorescence
FCA	fuzzy cluster analysis
FWHM	full width at half maximum
HCA	hierarchical cluster analysis
IRR	infrared reflectography
KCA	K-means cluster analysis
MArtA	Mobile Art Analyser
MDL	minimum detection limit
ND	neutral density
NMR	nuclear magnetic resonance
PC	principal component
PCA	principal components analysis
PLS-DA	partial least-square discriminant analysis
PLSR	partial least-squares regression
PR	pigment red
UV	ultraviolet
rMDL	relative minimum detection limit
RGB	red-green-blue
ROI	region of interest
SDD	silicon drift detector
TXRF	total reflection X-ray fluorescence
XRF	X-ray fluorescence

Spectral descriptions

vw	very weak
w	weak
m	medium
s	strong
vs	very strong

Chapter 1: Introduction and aim

There are different reasons to investigate art objects such as; amongst others, art historical questions concerning the authenticity or dating of the artefact, the fundamental interest in materials and techniques used in the past, the possibility to identify new materials and manufacturing techniques, interests concerning the relationship between a particular work and similar works, and concerns related to the damage and the degradation of specific artefacts, most of the time in the context of conservation and remediation.

When analysing precious art objects, it is of great importance to gather as much as possible information with a minimum of (or preferably no) damage to the art object. Sometimes taking small amounts of material or moving the whole art object to the laboratory is allowed. For the analysis of these micro-samples or artworks, the use of laboratory instrumentation is recommended. This allows a careful optimisation of the experimental parameters when acquiring the data. However, in other cases moving or sampling the art object is not allowed. In order to accommodate to these situations, mobile or portable equipment was developed to perform direct or *in situ* analysis. When performing *in situ* analysis some experimental conditions might not be optimal: time might be a limiting factor, because the study needs to be done in only a few hours, or in the best case a few days; and environmental parameters have to be considered, such as the use of scaffoldings, the limited dimensions of the measurement room, not being able to darken the room,...

The connection between spectroscopic analysis of art objects and the art historical questions of the conservators or art historians is called archaeometry. According to M.S. Tite¹, Archaeometry is a meeting ground for a series of collaborations between disciplines: archaeology on the one hand and on the other hand the full range of natural sciences (physics, chemistry, biology, biochemistry, earth sciences, material science, mathematics, statistics, etc.). The main areas of archaeometry are: dating, artefact studies, man and his environment, mathematical methods, remote sensing

and conservation science¹. So, performing archaeometrical studies implies the necessity of a multidisciplinary approach.

In this work, two analytical techniques, Raman spectroscopy and X-ray fluorescence (XRF) spectroscopy, were used to analyse different art objects. These two techniques are complementary: Raman spectroscopy provides molecular information, while XRF spectroscopy supplies the researcher with elemental information.

Raman spectroscopy is a powerful technique for the analysis of artworks, due to the ability to perform non-destructive molecularly specific analysis. It is increasingly applied for the analysis of objects of art over the last 20 years. The technique was used for the analysis of, amongst others, manuscripts, panel paintings, polychrome objects, rock paintings, lithographs, etc.²

XRF spectroscopy is also a non-destructive technique, but gives elemental information on the analysed work. The many examples found in literature^{3,4}, indicate that also XRF spectroscopy was extensively used for the analysis of art objects during the last decades.

The main aim of this work is exploring the possibilities for the identification of pigments while combining both techniques. This study includes the use of different Raman and XRF spectrometers: mobile spectrometers, as well as laboratory spectrometers. For the Raman analysis the Mobile Art Analyser⁵ was used for *in situ* measurements (Chapters 5, 6, 7 & 8). Whereas for the Raman analysis in the laboratory the newly acquired Senterra Raman spectrometer (Bruker) was used (Chapter 7, 9 & 10). An attempt to characterise this new spectrometer is also discussed in this work (Chapter 2). For the *in situ* XRF analysis two transportable XRF spectrometers were used: the portable ArtTAX (Bruker) from the Royal Institute for Cultural Heritage (Chapter 6) and the EDXRF system⁶ from the University of Liège (Chapter 8). For the laboratory XRF analysis, the recently

acquired EDAX Eagle-III was used (Chapter 7, 9 & 10). The characteristics of this XRF spectrometer will also be discussed in this work (Chapter 2).

The first part of this thesis discusses some theoretical considerations on Raman spectroscopy and XRF spectroscopy (Chapter 2). Because one of the important goals of this research is the interpretation of combined Raman and XRF data, there was a need to develop dedicated software to evaluate Raman spectra. The details of this in-house developed software are presented in Chapter 3. Chapter 4 describes two multivariate statistical techniques: principal components analysis (PCA) and K-means cluster analysis.

The following chapters (5–9) present case studies where a combination of mobile and laboratory Raman or XRF are used. Chapter 5 describes the analysis of the pigments used for three miniatures from the Breviary of Arnold of Egmond by using mobile Raman spectroscopy. These analyses were performed in the museum Het Valkhof, Nijmegen (The Netherlands), as the three individual miniatures belong to three different collections and were brought together for an exposition.

In Chapter 6, a combination of mobile Raman spectroscopy and mobile XRF spectroscopy is used to analyse two vault paintings in the Our Lady's Cathedral in Antwerp (Belgium). The Raman analysis was performed during the night, because of the interference with stray light during the day.

For the analysis of the manuscript *Liber Floridus* a combination of mobile Raman spectroscopy, laboratory Raman spectroscopy, laboratory XRF spectroscopy, UV-fluorescence photography and infrared reflectography (IRR) was used. The results of this study are presented in Chapter 7. The direct Raman analysis, UV-fluorescence photography and IRR were performed in the central library of Ghent University. Because of the promising results of the direct Raman analysis, we

were allowed to take micro-samples. These samples were in the laboratory analysed with Raman spectroscopy and XRF spectroscopy.

Chapter 8 describes the analysis of the so-called ‘Wyts Triptych’ after Jan van Eyck with mobile Raman spectroscopy and mobile XRF spectroscopy. The analyses were performed under the authority of the Bruges Groeningemuseum. For the first time in this work, mapping of a small area of the panel with XRF spectroscopy was executed to gather information on the restoration of this area.

In the previous chapters, Raman and XRF point analyses were performed for the identification of the pigments used in art objects. In Chapter 9, a methodology was explored based on Raman and XRF mapping on the same sample areas in order to identify the pigments and to study the spatial distribution in porcelain cards. Porcelain cards can be considered as the “business cards” from the 19th century. After performing a mapping of the selected area and the interpretation of the results, point measurements are performed on the areas of interest.

In all presented cases, except for one (Chapter 5), Raman and XRF spectroscopy are used as complementary analytical techniques for the identification of pigments. In Chapter 10, a very first attempt was made to explore the pigment identification based on fusing data obtained from the two analytical techniques. For this, Raman and XRF analysis were performed on the same sample positions so that the fusion of the data is straightforward. Comparison was made between the results after performing PCA on the Raman data, the XRF data and the fused Raman–XRF data. In this research also an attempt for identification of pigments by a general identification procedure is introduced. Finally, in Chapter 11 general conclusions are formulated and suggestions for further research are made.

References

1. Tite, M.S. (1991) Archaeological Science – Past Achievements and Future–Prospects. *Archaeometry* 33: 139–151.
2. Vandenabeele, P., Edwards, H.G.M., Moens, L. (2007) A decade of Raman spectroscopy in art and archaeology. *Chemical Reviews* 107: 675–686.
3. Janssens, K., Adams, F., Rindbay, A. (2000) *Microscopic X-Ray Fluorescence Analysis*. Chapter 9 Applications in Art and Archaeology, John & Wiley and Sons Ltd., Chichester, 291–314.
4. Lindgren, E. (2000). Special Millenium Issue on Cultural Heritage. *X-ray spectrometry* 29.
5. Vandenabeele, P., Weis, T.L., Grant, E.R., Moens, L.J. (2004) A new instrument adapted to in situ Raman analysis of objects of art. *Analytical and Bioanalytical Chemistry* 379: 137–142.
6. Hocquet, F.P., Garnir, H.P., Marchal, A., Clar, M., Oger, C., Strivay, D. (2008) A remote controlled XRF system for field analysis of cultural heritage objects. *X-Ray Spectrometry* 37: 304–308.

Chapter 2: Raman spectroscopy and X-ray fluorescence (XRF) spectroscopy: theory and instrumentation

In this chapter some theoretical aspects of Raman spectroscopy and X-ray fluorescence (XRF) spectroscopy are presented. Not only the theory, but also the instrumental properties are discussed. Besides this, a comparison between different Raman spectrometers and different XRF spectrometers is made.

2.1 Raman spectroscopy

2.1.1 Raman spectroscopy: theory

2.1.1.1 Introduction

In 1923, Smekal theoretically predicted the inelastic scattering of light molecules analogous to the Compton effect¹, but the first experimental observation was made by Raman and Krishnan in 1928². During this experiment, Sir Raman used the sun as light source, a telescope as collector and his eyes as detector. In 1930 Raman received the Nobel Prize in Physics for this important phenomenon that since then is known as the Raman effect, Raman scattering or Raman spectroscopy.

Raman spectroscopy as analytical technique gained importance with the introduction of lasers as light sources (1960's) and other instrumental developments³ (1980's), such as charge coupled device (CCD) detectors, holographic gratings and fibre-optics.

2.1.1.2 Raman effect: classical approach

In a classical approach, the Raman effect⁴ is explained by considering molecules as a collection of atoms undergoing harmonic vibrations. An external electrical field can distort the electron cloud that forms a chemical bond away from its equilibrium position. To express how easily an electron can be moved, the polarizability is used.

Light, which can be considered as an oscillating electric and magnetic field, can therefore cause the position of the electron cloud in a chemical bond to oscillate. This re-emission of light from the light-induced oscillation in the electron cloud is called scattering (Fig. 2.1). The scattered light can have a frequency equal to the incident light (*Rayleigh scattering*), equal to the frequency of the inherent light minus the vibration frequency (*Stokes scattering*) or equal to the frequency of the inherent light plus the vibration frequency (*anti-Stokes scattering*). The intensity of the Stokes and anti-Stokes scattering is not equivalent in all directions, therefore Raman scattering is usually observed at 90° or 180° from the direction of the incident light. These scattering geometries are called respectively right-angle scattering and backscattering.

2.1.1.3 Raman effect: quantum chemical approach

When using a quantum chemical approach towards the Raman effect, it is considered as a light scattering effect and can be described by an energy distribution diagram⁵ (Fig. 2.1). When monochromatic light interacts with a molecule, it can be excited to a virtual state. This virtual state is not stable and the molecule can relax in three different ways. In the first way (Fig. 2.1) the molecule transfers from the vibrational ground state to the virtual state and relaxes by emitting a photon to the vibrational ground state. The energy of the incident light is equal to the energy of the emitted photon. This type of elastic scattering is called *Rayleigh scattering* and is the most intense scattering. In a very small number of cases the molecule relaxes in a second way: the molecule again transfers from the vibrational ground state to the virtual state, but relaxes, by emitting a photon, to the first vibrational excited state (Fig. 2.1). The energy of the incident light is now higher than the energy of the emitted photon. This type of inelastic scattering is called the *Stokes scattering*. In the third way, the molecule transfers from the first vibrational excited state to the

virtual state and relaxes, by emitting a photon, to the vibrational ground state (Fig. 2.1). The energy of the incident light is lower than the energy of the emitted photon. This type of inelastic scattering is called *anti-Stokes scattering*.

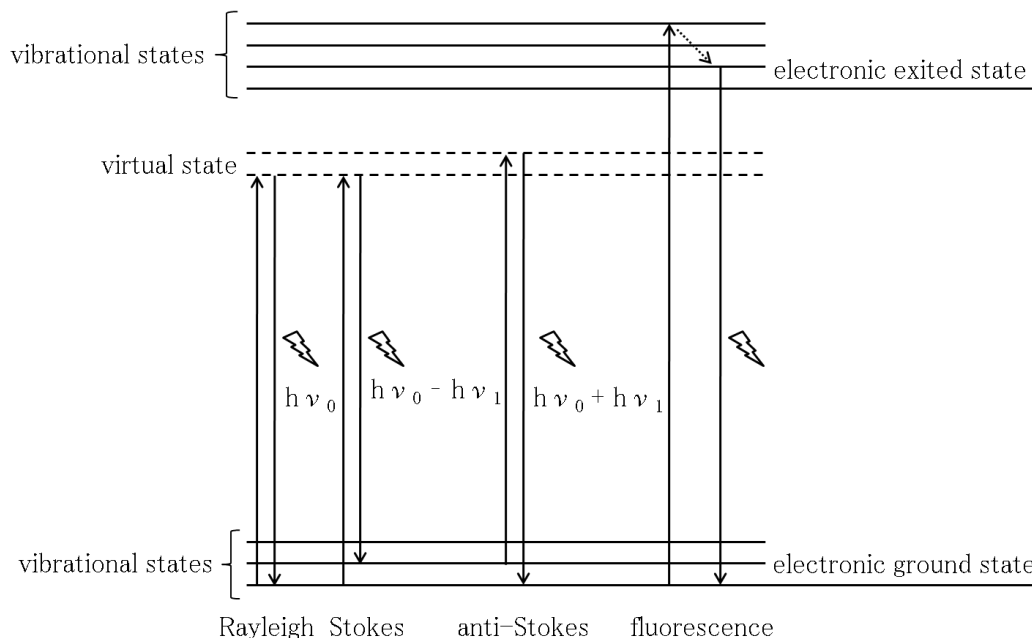


Figure 2.1 Energy diagram that illustrates the different types of scattering and fluorescence⁵. $h\nu_0$ indicates the energy of the laser light, while $h\nu_1$ indicates the energy difference between the vibrational ground state and the 1st vibrational excited state.

The shift in energy between the incident light and the Stokes or anti-Stokes scattering gives information on the vibrational states of the molecule. The intensity of the inelastic scattering processes is proportional to the population of molecules present in the different states. The relation between the population in higher and lower vibrational energy levels is given by the Boltzmann distribution⁴:

$$\frac{N_1}{N_0} \sim e^{\frac{-\Delta E}{kT}} \quad (2.1)$$

Where N_i = number of molecules in a higher vibrational energy level

N_0 = number of molecules in a lower vibrational energy level

ΔE = energy difference between the higher and lower vibrational energy levels

k = Boltzmann constant ($1.38 \cdot 10^{-23}$ J/K)

T = temperature, K

According to the Boltzmann distribution, the number of molecules at thermal equilibrium in a lower vibrational energy level is higher than in a higher vibrational energy level. This means that the Stokes intensity is usually higher than the anti-Stokes intensity and is therefore commonly used in Raman spectroscopy.

2.1.1.4 Raman spectrum: intensity as function of wavenumber

In a Raman spectrum the intensity, expressed in counts is plotted as a function of the Raman wavenumber, expressed in reciprocal centimetres (cm^{-1}).

The expression for the Raman scattering intensity⁴ is:

$$I = \frac{2^4 \pi^3}{45 \cdot 3^2 c^4} * \frac{\hbar I_L N (\nu_0 - \nu)^4}{\mu \nu (1 - e^{-\hbar \nu / kT})} [45 (\alpha'_a)^2 + 7 (\gamma'_a)^2] \quad (2.2)$$

Where c = speed of light ($2.99 \cdot 10^8$ m/s)

h = Planck constant ($6.63 \cdot 10^{-34}$ J·s)

I_L = excitation intensity

N = number of scattering molecules

ν = molecular vibrational frequency, s^{-1}

ν_0 = laser excitation frequency, s^{-1}

μ = reduced mass of the vibrating atoms

k = Boltzmann constant ($1.38 \cdot 10^{-23}$ J/K)

T = absolute temperature, K

α_a' = mean invariant of the polarizability tensor

γ_a' = anisotropy invariant of the polarizability tensor

Equation 2.2 shows that the Raman scattering intensity is dependent of different factors:

- The Raman scattering intensity is proportional to N , the number of molecules that are irradiated. Therefore, a higher concentration results in a higher intensity of the Raman signal.
- The Raman scattering intensity is proportional to the intensity of the incident light, I_L . Using attenuation filters to reduce the power of the laser light results in a weaker Raman scattering intensity. Some analyses are performed using a reduced power to avoid any possible sample damaging.
- The Raman scattering intensity is proportional to $(\nu_o - \nu)^4$. By choosing a laser with a higher frequency, ν_o , (shorter wavelength) the intensity of the Raman signal increases. However, by choosing a laser with a higher frequency the chance of interference due to fluorescence (Fig. 2.1) is much higher.

The Raman wavenumber⁴ or Raman shift is defined as the difference between the excitation wavelength and the Raman wavelength expressed in wavenumbers:

$$shift_{Raman} (cm^{-1}) = \left(\frac{1}{\lambda_{inc}(nm)} - \frac{1}{\lambda_{Stokes}(nm)} \right) 10^7 \quad (2.3)$$

Where λ_{inc} = wavelength of the incident light

λ_{Stokes} = wavelength of the Stokes scattering

The relation⁴ between energy, wavelength and frequency is given by equation 2.4

$$E = h\nu = \frac{hc}{\lambda} \quad (2.4)$$

Where h = Planck constant ($6.63 \cdot 10^{-34}$ J.s)

ν = frequency of the light

c = speed of light ($2.99 \cdot 10^8$ m/s)

λ = wavelength of the light

The position of the Raman band in the spectrum is determined by the energy difference between the vibrational ground state and the vibrational excited state (Fig. 2.1). Because the molecules undergo harmonic vibrations, the vibration frequency can be expressed as follows:

$$\nu = \frac{1}{2\pi} \sqrt{\frac{\kappa}{\mu}} \quad (2.5)$$

Where κ = force constant of the bond

$$\mu = \text{reduced mass of the atoms present in the bond} \left(\frac{1}{\mu} = \frac{1}{m_1} + \frac{1}{m_2} \right) \quad (2.6)$$

According to equation 2.5 the position of the Raman band is dependent of two factors: the force constant of the binding for the considered vibration type (κ) and the reduced mass (μ).

2.1.2 Raman spectroscopy: instrumentation

In this research, two different types of Raman spectrometers were used: the laboratory Senterra spectrometer (Bruker), recently acquired and installed at UGent, and the Mobile Art Analyser (MArtA)⁶. The different components of a dispersive Raman spectrometer are discussed using the laboratory Senterra spectrometer as example (Fig. 2.2). The difference between the laboratory spectrometer and the mobile spectrometer will be discussed in a separate paragraph.

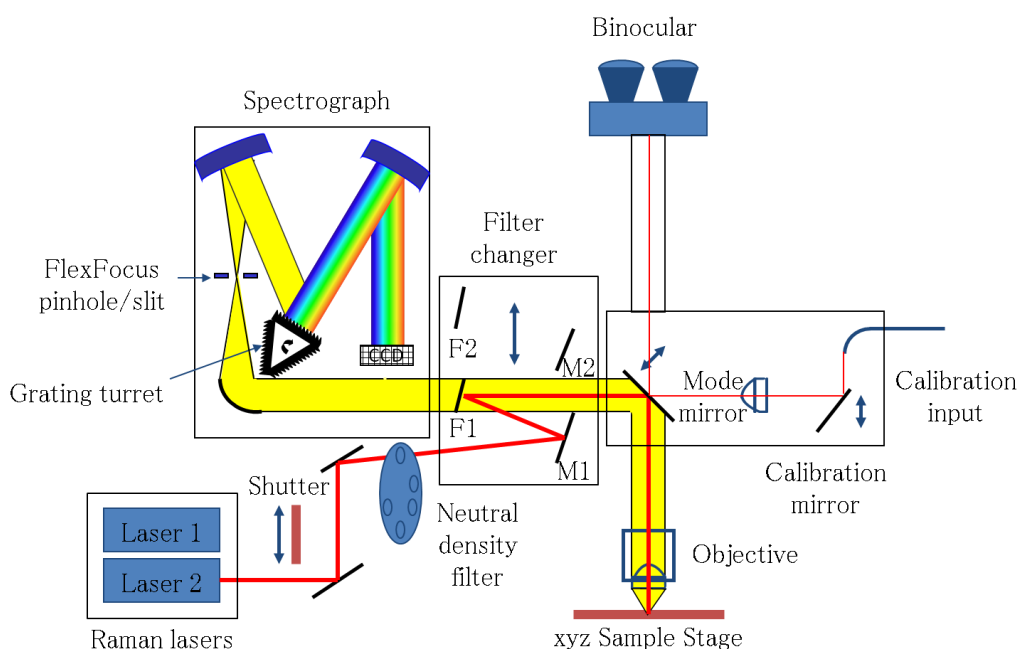


Figure 2.2 Schematic view of the light path of the Senterra Raman spectrometer⁷.

2.1.2.1 The laser

Lasers are ideal excitation sources for Raman spectroscopy due to the following characteristics⁸:

- Single lines from large continuous-wave lasers can easily provide a power of 1–2 W (intense).

- Laser beams are highly monochromatic.
- Most laser beams have small diameters (1–2 mm), which can be reduced to 0.1 mm by using simple lens systems (small divergence).

The Senterra Raman spectrometer contains two different lasers: a red diode laser with a wavelength of 785 nm and a green frequency doubled solid state Neodymium-YAG (Nd:YAG) laser with a wavelength of 532 nm.

Most of the experiments in this work were performed using the red diode laser (785 nm), because choosing a laser with a longer wavelength (smaller energy) decreases the contribution of fluorescence (Fig. 2.1) for many samples. By absorbing laser light with a short wavelength, the molecule is excited from the electronic ground state to an excited electronic state. After internal conversion, the molecule falls back to the electronic ground state by emitting fluorescence light, which results in broad fluorescence bands in the Raman spectrum. By using a laser with a longer wavelength, the energy of the light will probably be too small to bring the molecule in the electronic excited state.

2.1.2.2 The neutral density filter.

For some samples, it is necessary to reduce the laser intensity to avoid any possible sample damaging. Therefore, the Senterra spectrometer uses neutral density (ND) filters. These ND filters reduce only the intensity of the laser light passing through it, without altering the relative distribution of energy. The intensity can be reduced from 100% (no filter) down to 50%, 25%, 10% and 1% of the original laser intensity. For quantitative analysis it is very important to know the exact value of these filters. The exact values of the different ND filters were checked by measuring the intensity of the ring breathing band of cyclohexane, after excitation with the red (Fig. 2.3) and green laser.

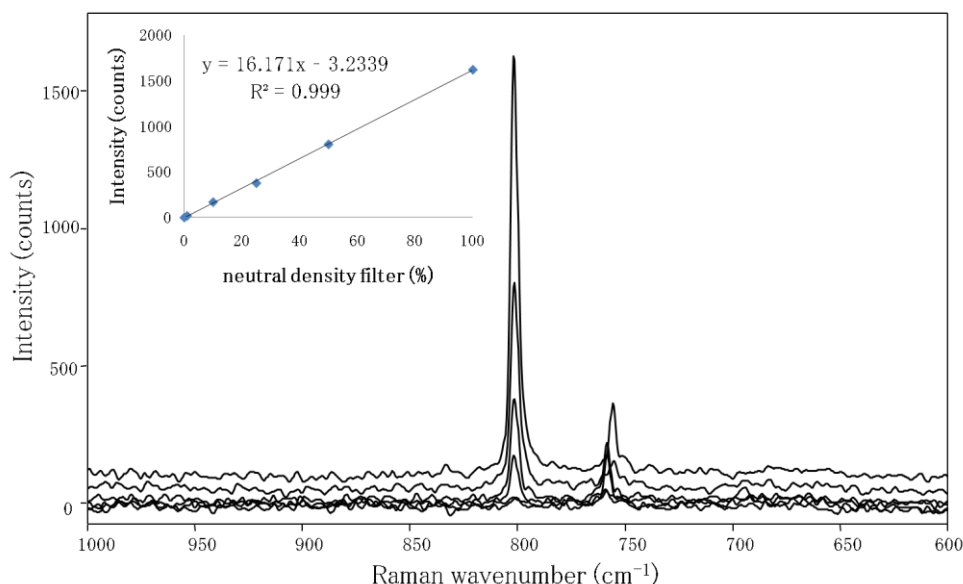


Figure 2.3 Raman spectra of the ring breathing of cyclohexane (802 cm^{-1}), measured with alternating density filters and a measurement time of 20 s. Graph: the intensity of the Raman band as function of the neutral density filter.

2.1.2.3 The microscope

In the Senterra spectrometer an Olympus microscope is used to visualise the sample and to focus the laser beam on it. A digital video camera is coupled to the microscope, delivering digital images of the samples. The laser light or the visible light is focussed on the sample using the objectives of the microscope. This microscope is equipped with 3 objectives (5 \times , 20 \times and 50 \times). The resulting minimal reflected spot sizes, measured using the objective micrometer (0–1mm/100), which was delivered with the spectrometer, are shown in table 2.1.

objective	numerical aperture	spot size (μm)
5 \times	0.1	50
20 \times	0.4	10
50 \times	0.75	4

Table 2.1 Overview of a few characteristics⁷ of the available objectives, together with the resulting maximal spot size of the laser beam on the sample.

2.1.2.4 The sample stage system

A motorised stage is used to select the region of interest of the sample. This motorised stage can be controlled by the OPUS software and by a joystick. The maximum adjustment range of this motorised stage⁷ is 100 mm × 80 mm and the positioning accuracy 0.1 µm. In contrast to a manually operating stage, a motorised stage provides some additional possibilities:

- automatic generation of a large overview image of the sample by joining the snapshots together (=composite image).
- computer-controlled/joystick-controlled stage movement in the x- and y-direction allowing navigating across the live video image of the sample.
- automatic measurement of a predefined linear or rectangular measurement raster.
- automatic point measurements of a list of predefined spots on the sample.

For this Senterra spectrometer, the motorised stage is equipped with a third motor, which allows movement in the z-direction. Because of this additional movement, depth profiling measurements can be performed.

2.1.2.5 The aperture

The scattered light is reflected by a mirror and then sent to the dielectric filter. This filter suppresses the very intense Rayleigh light in favor of the weak Raman scattering. Before the scattered light reaches the diffraction grating, the light has to pass through a narrow slit, the aperture. The Senterra spectrometer has two different types of apertures⁷: a slit-type aperture of 25×1000 µm and one of 50×1000 µm for high-throughput; and two pinhole-type apertures of 25 µm and 50 µm for confocal spectroscopy and depth profiling.

2.1.2.6 The diffraction gratings

The Senterra spectrometer contains two different diffraction gratings⁷: one with 400 lines/mm to measure in low resolution mode and one with 1200 lines/mm to measure in high resolution mode. When measuring in low resolution mode a spectrum is recorded with a spectral range of 90–3500 cm^{-1} for the red laser (70–4450 cm^{-1} for the green laser). Measuring in high resolution mode is executed in three different steps. First, a spectrum is recorded with a spectral range of 80–1525 cm^{-1} (46–1544 cm^{-1} for the green laser), next the grating is turned and a spectrum with a spectral range of 1520–2660 cm^{-1} (1530–2750 cm^{-1} for the green laser) is recorded, then the grating is turned again and a spectrum with a spectral range of 2650–3500 cm^{-1} (2700–3700 cm^{-1} for the green laser) is recorded and finally the spectra with different spectral ranges are composed together.

2.1.2.7 The detector

The Senterra spectrometer contains a thermoelectrically cooled charge-coupled device (CCD) detector. A CCD⁸ is a silicon-based semiconductor arranged as an array of positive elements, of which each generates photoelectrons and stores them as a small charge. The charges stored on each individual pixel are proportional to the number of photons striking that pixel. The diffraction grating separates the photons according to their wavenumber, so that photons with the same energy hit on the same row of the CCD, while the photons with a different frequency reach different rows. The row number of the CCD is thus proportional to the Raman wavenumber, while the accumulated charges are proportional to the intensity. The format of the CCD in the Senterra spectrometer is 1024×256 pixels. The advantages of a CCD compared to other multichannel detectors are: low readout noise and high quantum efficiency.

2.1.2.8 The wavelength stability of the Senterra Raman spectrometer.

Comparing Raman spectra with each other implies that each data point in all the spectra corresponds with the exact Raman wavenumber. This is not always the case due to shifts in optical pathway and/or shifts in laser wavelength. In this part, the wavelength stability of the Senterra spectrometer is evaluated over a short and long period.

2.1.2.8.1 Short term wavelength stability

To evaluate the short term stability of the Senterra spectrometer, repetitive point measurements of neon light were performed. The positions of the neon lines are exactly known and listed extensively in literature⁹. The emission lines are most often given in wavelength units (nm) in literature, which means that one has to do the conversion to the Raman wavenumbers depending on the wavelength of the laser (equation 2.3). Because of this, the stability of the laser wavelength can be evaluated by recording a spectrum of neon. To evaluate the short term wavelength stability the intensity of the emission line of neon showed in the spectrum at 1005 cm^{-1} , was selected. The wavelength of the emission line can be calculated using equation (2.3). Solving this equation for the red laser with a wavelength of 785 nm results in a wavelength of 852.5 nm for this neon emission line. If we compare the spectrum of the neon emission lines with the one presented in literature⁹, the wavelength of the selected emission line should be 849.5 nm. This means that the wavelength of the laser is 782.5 nm instead of 785 nm. Because of the fluctuation of the laser wavelength, it is important to calibrate the Raman spectrometer before performing analysis.

For these repetitive measurements a measuring time of 30 s was chosen, the 5× objective was used, a spectral range of $80\text{--}1525\text{ cm}^{-1}$ was chosen and the point

measurement was repeated 750 times, which results in a total measuring time of 20 hours. Figure 2.4 shows the Raman wavenumber (cm^{-1}) as function of the time (hours) for the emission line of neon with a wavelength of 849.5 nm.

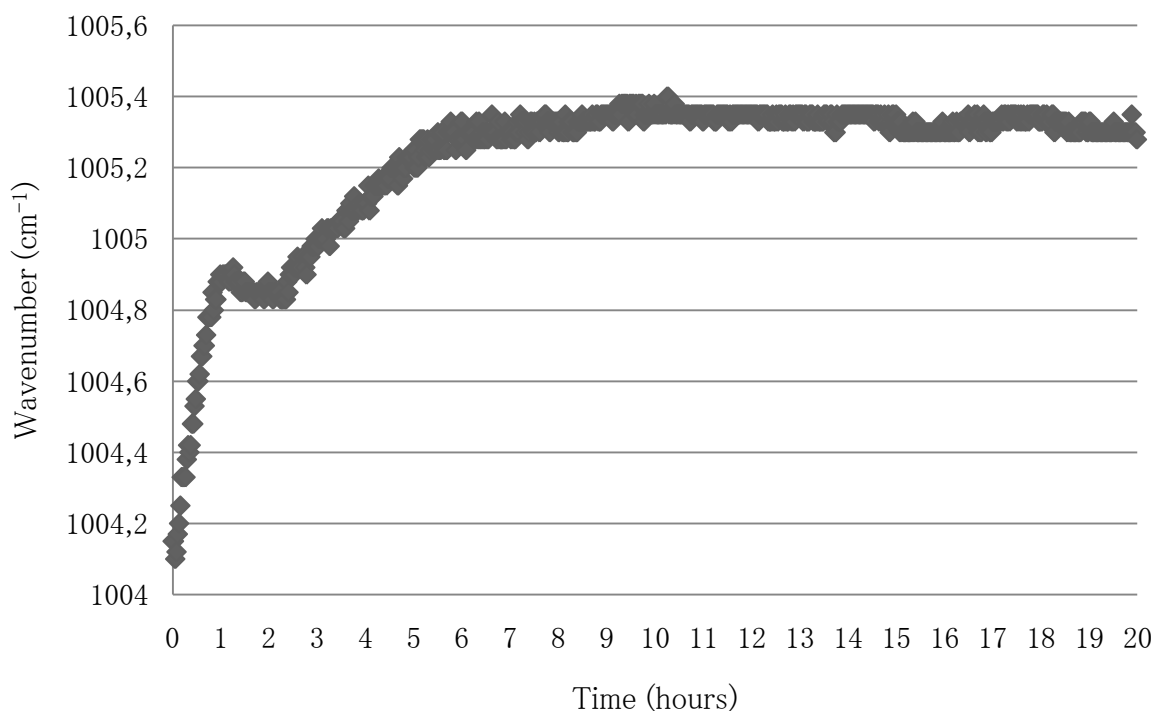


Figure 2.4 The Raman wavenumber (cm^{-1}) as a function of the time (hours) for the emission line of neon with a wavelength of 849.5 nm.

The graph shows that the laser is not stable during the 20 hours of measurement time. Especially the first 5 hours the Raman wavenumber at approximately 1005 cm^{-1} is shifting towards a lower wavenumber. After these 5 hours the stability of the laser increases.

To evaluate if the Senterra instrument corrects for the instability of the laser wavelength, a silicium standard (Kaiser Optical Systems) was placed on top of the neon lamp during the repetitive point measurements. This resulted in a combined Raman spectrum of the neon light and the silicium standard. Figure 2.5 shows the Raman wavenumber (cm^{-1}) as function of the time (hours) for the Raman signal of silicium at 520 cm^{-1} .

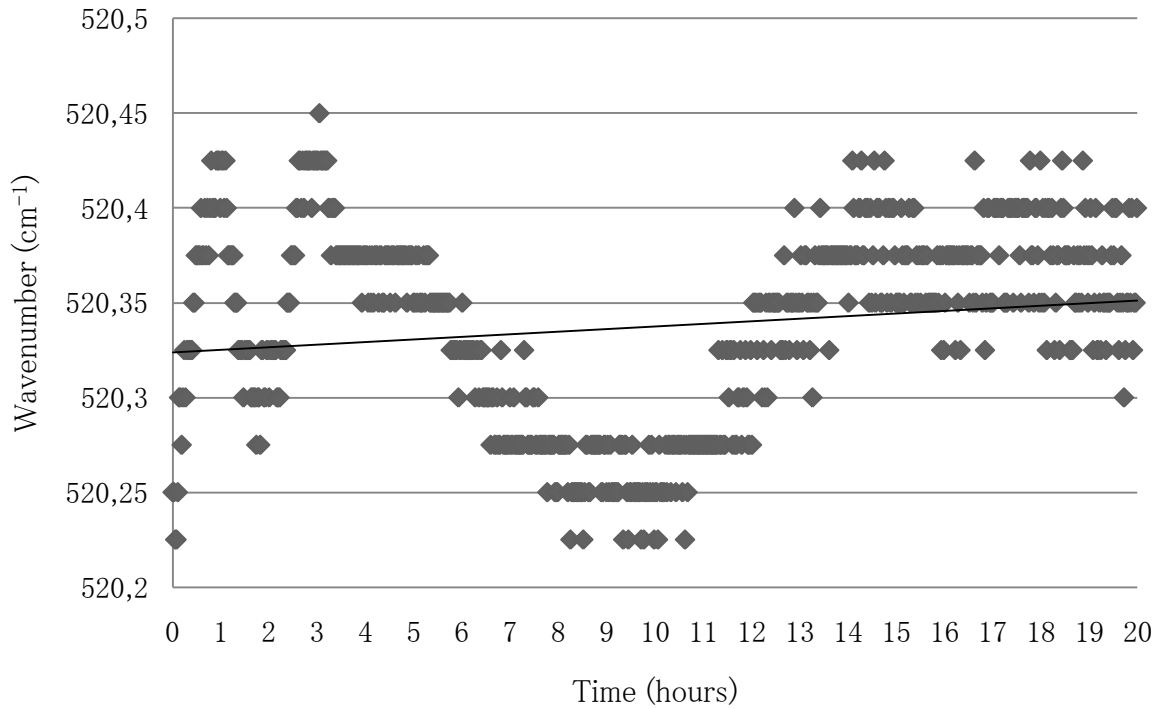


Figure 2.5 The Raman wavenumber (cm^{-1}) as function of the time (hours) for the Raman signal of silicium at 520 cm^{-1} .

The graph shows that the signal fluctuates over time. To evaluate this, linear regression analysis was used¹⁰. In order to be able to apply linear regression analysis on a dataset, the dataset has to fulfil three conditions: the variance of the residues has to be constant, this means independent from x and y ; the residues have to be mutual independent; and the residues have to be normally distributed. According to figure 2.5 the first two conditions are fulfilled. To evaluate whether the residues are normally distributed, the Q-Q plot¹⁰ can be used. A Q-Q plot is a probability plot, which is a graphical method for comparing two probability distributions by plotting the expected normal value and the observed value of the quantiles against each other. Figure 2.6 shows a Q-Q plot for the distribution of the Raman wavenumber of silicium at 520 cm^{-1} .

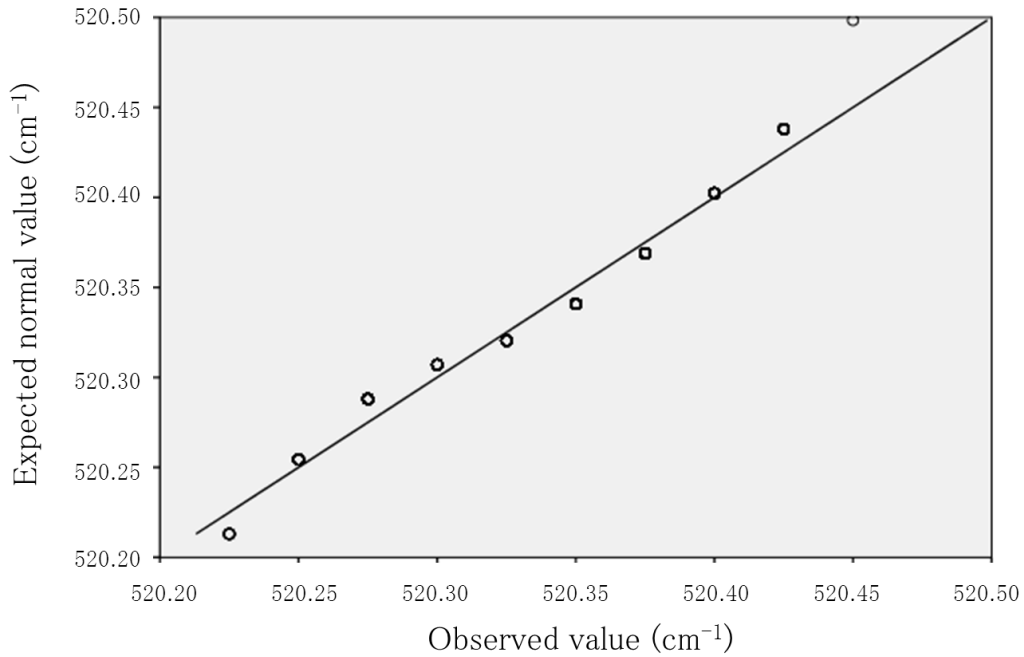


Figure 2.6 The Q-Q plot of the Raman band of silicium at approximately 520 cm⁻¹, calculated using SPSS.

The points in the graph are approximately situated along a straight line, which confirms the normal distribution of the dataset. Because all three conditions are fulfilled linear regression analysis can be applied on the dataset.

If the Senterra spectrometer corrects for the instability of the laser, the slope of the best fit regression line for the data (Fig. 2.5) should be equal to zero. Calculating the slope (b) and standard deviation (s) using excel gives $b=0.0014$ and $s= 0.0511$. To check whether the slope significantly differs from μ , which is zero, the Student t-test¹¹ was used. Taking the null hypothesis, that b is equal μ into account, the statistical t is calculated:

$$t = \frac{(b-\mu)\sqrt{n}}{s} \quad (2.7)$$

For this dataset $|t|= 0.7310$. This value does not exceed the critical value $|t|_{750}(0.95) = 1.96$, so the null hypothesis, that b is equal to μ is accepted for the

95% confidence level. From this result we can conclude that for a short term the Senterra spectrometer corrects for the instability of the laser.

2.1.2.8.2 Long term wavelength stability

To evaluate the long term wavelength stability of the spectrometer, every measuring day since the new spectrometer was installed, a Raman spectrum of cyclohexane was recorded with following measurement characteristics: 30 s measuring time, 5× objective, 100 % laser power and a spectral range of 80–1525 cm^{-1} . To evaluate the long wavelength stability the same procedure was followed, using linear regression analysis. Figure 2.7 shows the Raman wavenumber (cm^{-1}) as a function of the time (days) for the Raman signal of cyclohexane at 802 cm^{-1} .

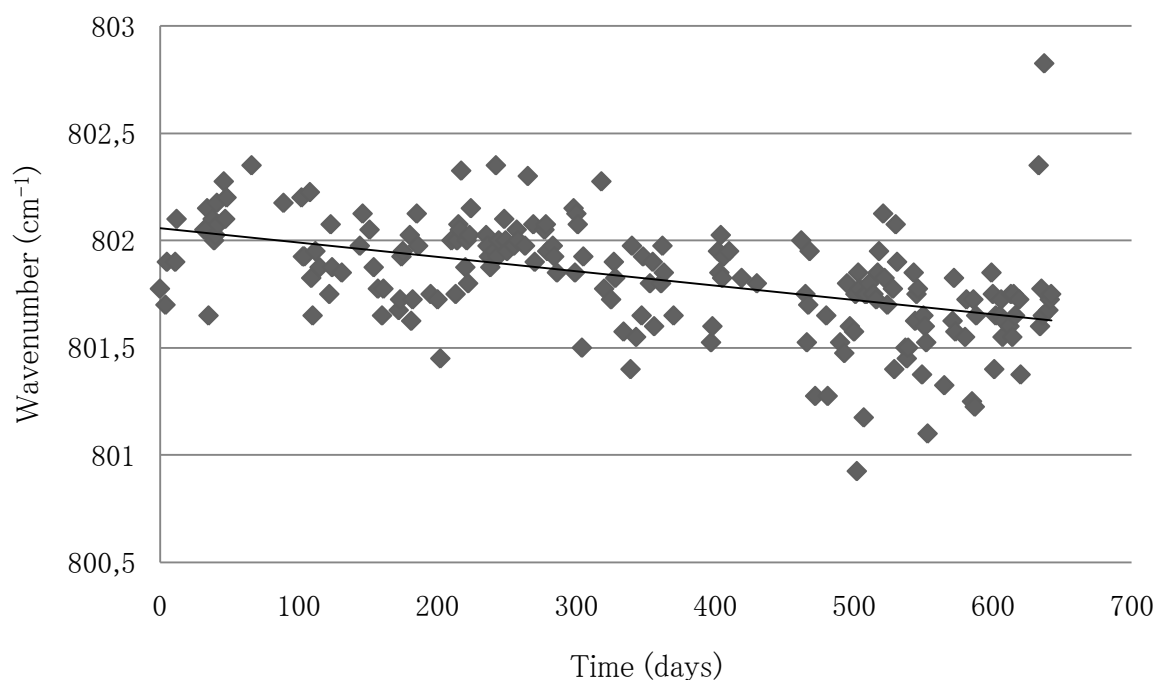


Figure 2.7 The Raman wavenumber (cm^{-1}) as a function of the time (days) for the Raman signal of cyclohexane at 802 cm^{-1} .

The graph in figure 2.7 shows that the first two conditions are fulfilled in order to be able to apply linear regression analysis on this dataset. To check the normality of the distribution of this dataset a Q-Q plot was made (Fig. 2.8).

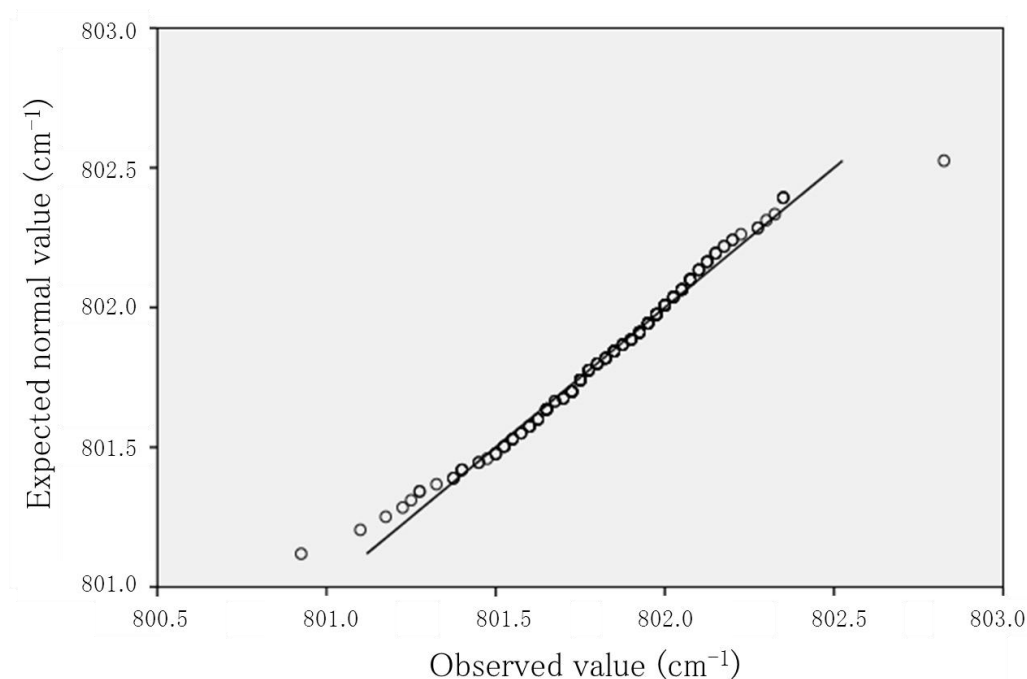


Figure 2.8 The Q-Q plot of the Raman band of cyclohexane at approximately 802 cm^{-1} , calculated using SPSS.

The points in the graph are approximately situated along a straight line, which confirms the normal distribution of the dataset. Because all three conditions are fulfilled, linear regression analysis can be applied on the dataset.

If the Senterra Raman spectrometer corrects for the instability of the laser for a long time, the slope of the best fit regression line for the data (Fig. 2.7) should be equal to zero. Calculating the slope (b) and standard deviation (s) using excel gives $b = -0.0007$ and $s = 0.2572$. Equation 2.7 gives for this dataset $|t| = 0.0365$. This value does not exceed the critical value $|t|_{196}(0.95) = 1.96$, so the null hypothesis, that b is equal to μ is accepted for the 95% confidence level. From this result we can conclude that for a long term the Senterra spectrometer corrects for the instability of the laser.

2.1.2.9 The Mobile Art Analyser (MArtA)

The Mobile Art Analyser (MArtA) was used for the analysis of the three full-page miniatures from the Breviary of Arnold of Egmond (Chapter 5), the analysis of the vault paintings in the Antwerp cathedral (Chapter 6), the analysis of the manuscript *Liber Floridus* (Chapter 7) and the analysis of the central panel of the so-called ‘Wyts Triptych’ (Chapter 8). Table 2.2 shows the characteristics of the MArtA spectrometer in comparison with the characteristics of the Senterra spectrometer.

The most important advantage of the MArtA spectrometer is the mobility of the spectrometer, which makes *in situ* analysis possible. Another advantage is that the probe head is coupled with optical fibres to focus the laser beam on the sample and to gather the Raman scattering. Using a probe head instead of a microscope allows performing direct analysis on bigger works of art, typically only art works with dimensions smaller than approximately $15 \times 15 \times 3 \text{ cm}^3$ can be measured with the Senterra spectrometer. Using fibre optics also allows to measure on difficult accessible places, such as ceilings.

Measurements with the MArtA spectrometer always have to be performed in a dark place where the windows are covered, or during the night because of the interference of stray light. This was done in several projects (Chapters 5,6,7 & 8).

In contrary, measuring with the Senterra spectrometer can be performed during the day, because the microscope contains a covering cylinder, which prevents the stray light to interfere. The Senterra spectrometer has also the advantages of measuring in confocal mode and the possibility to switch to the second laser with a different wavelength: if fluorescence bands interfere with the Raman spectrum, another laser can be selected.

characteristics	Senterra spectrometer	Mobile Art analyser (MArtA)
type	laboratory spectrometer (desktop)	mobile spectrometer
focussing device	OLYMPUS microscope	probe head
positioning equipment	motorised stage: range of movement: 100 mm \times 80 mm, step size: 0.1 μ m, positioning accuracy: 1.0 μ m.	manual & motorised: micro-and macro-positioning (vertical post, articulating arm, translation stage)
camera	Infinity 1 colour video camera	colour camera
gratings	1200 and 400 lines mm ⁻¹	1200 and 600 lines mm ⁻¹
detector	1024 \times 256 thermoelectrically cooled CCD	1024 \times 512 thermoelectrically cooled CCD
laser(s)	785nm diode laser, 300 mW 532 nm Nd:YAG frequency doubled solid state laser, 20 mW	785 nm diode laser, 300 mW
objective(s)	5 \times , 20 \times and 50 \times	6 \times
spot size	50, 10 and 4 μ m	25 μ m
type of analysis	only analysis on samples with dimensions smaller than approximately 15 \times 15 \times 3 cm ³	direct or <i>in situ</i> analysis possible, next to analysis of samples
developed by	Bruker	in-house developed

Table 2.2 Overview of some characteristics of the Senterra spectrometer and the Mobile Art Analyser (MArtA).

2.2 X-ray fluorescence (XRF) spectroscopy

2.2.1 XRF spectroscopy: theory

2.2.1.1 Introduction

In 1895 Wilhelm Conrad Röntgen discovered X-rays¹² at the University of Würzburg, Germany. Röntgen discovered the X-rays by accident, while he was studying the conduction of the electric current through gasses at low pressure using an experimental discharge tube called a Crookes' tube. He noticed that a barium platinocyanide screen placed at a short distance of the tube suddenly started to glow. For this work Röntgen received in 1901 the first Nobel Prize in Physics. In 1903, Moseley showed that the wavelengths of the emitted lines were characteristic for the elements in the periodic table and showed that they had the same sequence as the atomic numbers, thus enabling the atomic numbers determined unambiguously for the first time. XRF spectroscopy as analytical technique gained significantly in terms of accessibility and importance with the introduction of energy-dispersive detectors, such as a Si(Li) detector (1980's). The introduction of X-ray focussing devices starting from the 1990's, e.g. polycapillary optics, has resulted in the development of scanning-XRF with microscopic spatial resolution.

2.2.1.2 Theory of X-ray fluorescence (XRF)

The aim of XRF spectroscopy is the identification of the elemental composition by detection of the fluorescent X-rays that the sample emits, when it is irradiated with a primary X-ray beam. When this primary X-ray beam hits the sample, three different interaction processes are possible:

- The first type of interaction process is elastic scattering, called the *Rayleigh scattering*. The incident X-ray beam is elastically scattered by the electrons of the sample atom. The scattered X-ray photon has the same energy of the incident X-ray photon, but changes in direction.
- In a second type of interaction the incident X-ray beam is inelastic scattered by the electrons of the sample atom. The total energy of the incident X-ray photon is distributed over the electron and the scattered X-ray photon. The energy and direction of the scattered X-ray photon changes. This type of inelastic scattering is called *Compton scattering*. Compton scattering results in a continuous spectrum, because of the many possibilities of distributing the energy between the electron and the scattered X-ray photon.
- The third, most important interaction process is the *photoelectric effect*. This effect can be explained by Bohr's atom model (Fig. 2.9).

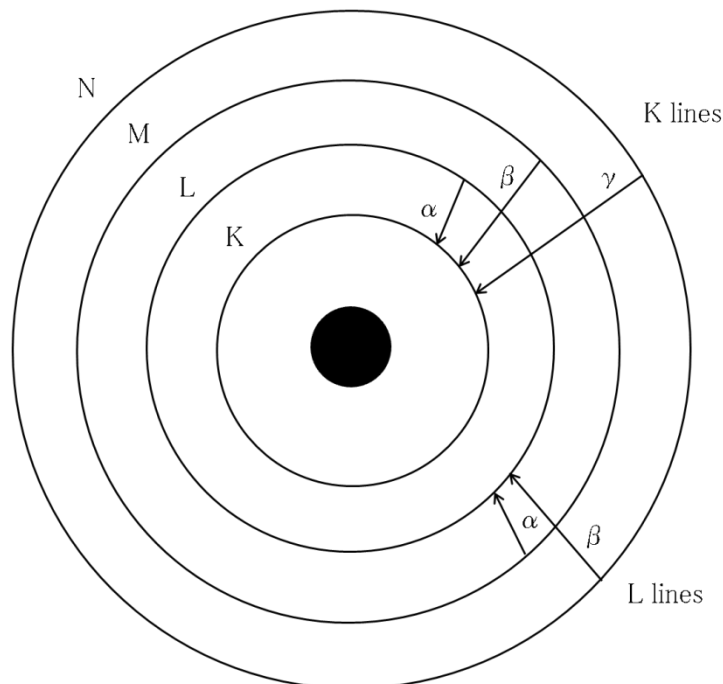


Figure 2.9 Simplified figure of the characteristic X-ray lines in Bohr's atom model.

The incident X-ray beam interacts with the atom by transferring all the energy to an electron on one of the inner shells. This energy is sufficient to remove the electron from the shell, creating a vacancy in this shell. Subsequently, the vacancy is filled by an electron transition from an outer orbital, which can either result in the emission of an X-ray photon (XRF emission) with an energy corresponding to the difference between the binding energies of two orbitals, or in the emission of an Auger electron.

2.2.1.3 XRF spectrum: intensity as function of energy

In an XRF spectrum the intensity, expressed in counts, is plotted as a function of the energy, expressed in keV.

The intensity of the incident X-ray beam decreases when passing through the sample due to absorption. The degree of absorption is calculated using the well-known law of Lambert–Beer¹²:

$$I = I_0 e^{-\mu_L x} \quad (2.8)$$

Where I_0 = incident intensity of the X-ray beam

I = intensity of the X-ray beam after passing through the sample

μ_L = linear absorption coefficient, cm^{-1}

x = layer thickness of the sample, cm

The linear absorption coefficient, μ_L , depends of the energy of the incident X-ray beam (cross section) and the number of atoms in the sample.

$$\mu_L = n\sigma = \frac{N_A \rho}{m_a} \sigma \quad (2.9)$$

Where n = number of atoms per volume unit

σ = total atomic cross-section

N_A = Avogadro's number ($6.022 \cdot 10^{23} \text{ mol}^{-1}$)

ρ = density (kg/m^3)

m_a = atomic mass ($1.66 \cdot 10^{-27} \text{ kg}$)

The total atomic cross section depends on the energy of the incident X-ray beam and the atomic number of the element; and is the sum of the individual cross sections:

$$\sigma_{total}(E, Z) = \sigma_{Rayleigh}(E, Z) + \sigma_{Compton}(E, Z) + \sigma_{photoelectric}(E, Z) \quad (2.10)$$

Fig 2.10 shows that for Cu the photoelectric cross section is the most important in the analytical X-ray region (1–100 keV).

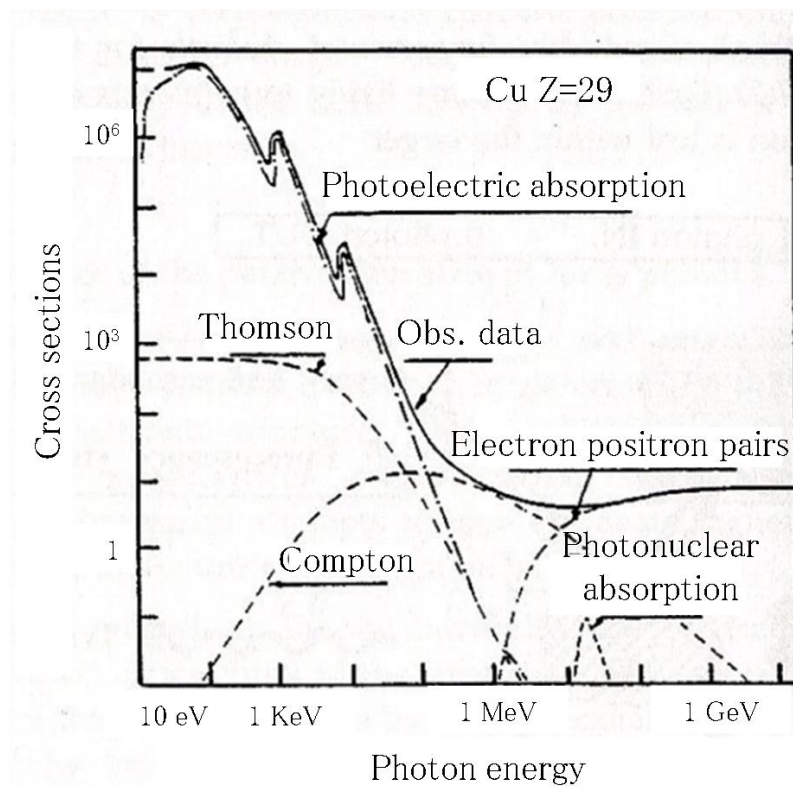


Figure 2.10 The contribution of each individual cross section to the total cross section of Cu as a function of the photon energy ¹³.

In practice however, the absorptive characteristics of an element are not indicated by the linear absorption coefficient, but by the mass attenuation coefficient, μ_ρ , expressed in cm^2/g .

$$\mu_\rho = \frac{\mu_L}{\rho} \quad (2.11)$$

The mass attenuation coefficient only depends on the atomic number of the absorbing element and the energy of the X-ray beam.

The calculation of the energy of the X-ray (electromagnetic radiation) is given by equation 2.12.

$$\Delta E = h\nu = \frac{hc}{\lambda} \quad (2.12)$$

Where h = Planck constant ($6.63 \cdot 10^{-34}$ J·s)

ν = frequency of the incident X-ray beam

c = speed of light ($2.99 \cdot 10^8$ m/s)

λ = wavelength of the incident X-ray beam

The energy of the emitted fluorescence X-rays can be approximated by the following formulation of Moseley's Law:

$$\Delta E = c_1(Z - c_2)^2 \quad (2.13)$$

Where c_1 and c_2 are constants for different line types and Z the atomic number. The closer the energy of the incident X-ray beam is to the necessary energy to eject the electron, the higher the probability that the photoelectric effect will happen.

Figure 2.11 shows the XRF spectrum of standard NIST SRM 621, with the characteristic lines of the elements, as indicated in the certificate of the standard.

The broad background in the X-ray spectrum is called bremsstrahlung. These continuous production of X-rays is produced when electrons, or other high-energy charged particles, such as protons or α -particles, lose energy when passing through the Coulomb field of the nucleus¹². On this continuous bremsstrahlung, the characteristic X-lines of the elements are plotted. Also the Compton and Rayleigh scattering are visible in the XRF spectrum. The artefacts, sometimes present in the XRF spectrum are discussed in part 2.2.2.3, which discusses the characteristics of the detector.

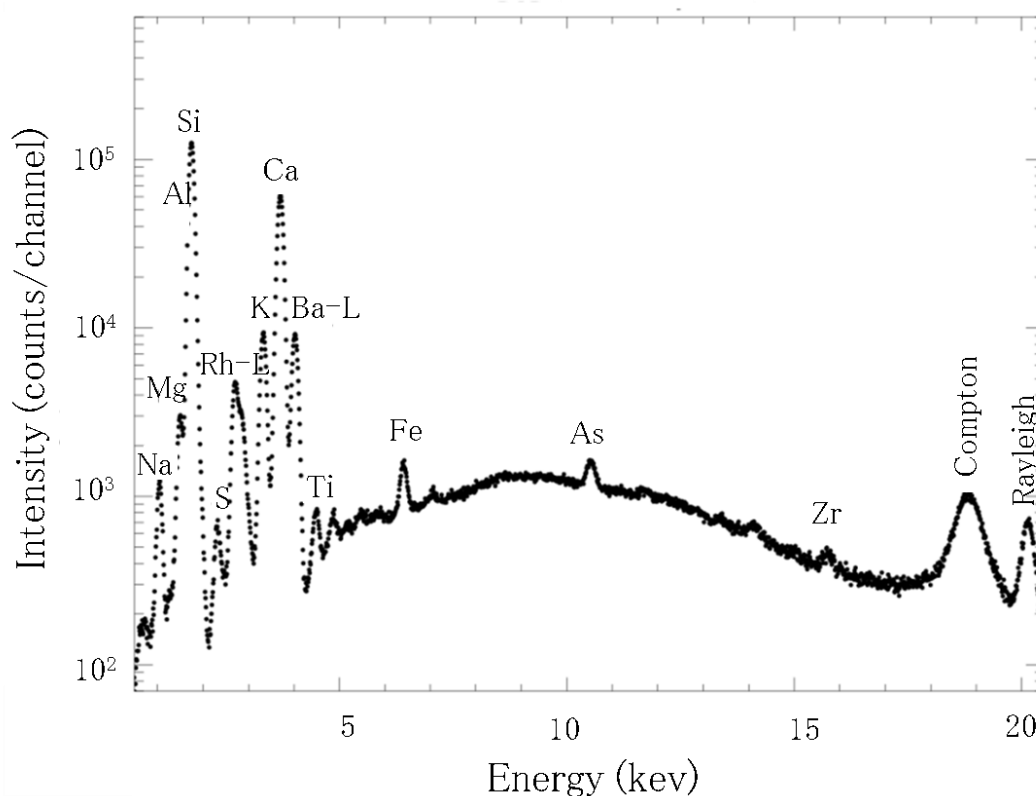


Figure 2.11 Example of an X-ray spectrum. Scan of the NIST SRM 621 measured with the EDAX Eagle-III (25 μm , 1000 s, 40 kV and 135 μA).

2.2.2 XRF spectroscopy: instrumentation

In this research, three different types of XRF spectrometers were used: the laboratory EDAX Eagle-III scanning micro-XRF spectrometer of the Ghent University X-ray Microspectroscopy and Imaging group (UGent XMI) (Chapters 7, 9 & 10), the mobile micro-XRF spectrometer ArtTAX of the Royal Institute for Cultural Heritage (Chapter 6), and the mobile EDXRF system from the University of Liège (Chapter 8). The different components of an XRF spectrometer are discussed using the laboratory EDAX Eagle-III spectrometer (Fig. 2.12). A comparison between this conventional spectrometer and the two mobile spectrometers will be made in a separate paragraph.



Figure 2.12 Picture of the UGent EDAX Eagle-III scanning micro-XRF spectrometer. The XYZ sample motor stage is attached to the door of the sample chamber. The characteristics of this micro-XRF spectrometer are summarised in table 2.5.

2.2.2.1 The X-ray tube

An applied high voltage between the negatively charged cathode, a tungsten filament, and the positively charged Rh-anode¹⁴ accelerates the electrons towards the anode surface, where the electron beam interactions generate X-rays¹⁵. The generated X-ray spectrum consists of the characteristic lines of the anode material, and a continuous component, called Bremsstrahlung, due to the braking radiation emitted by the decelerating electrons.

2.2.2.2 X-ray optics: the polycapillary

A polycapillary optic¹⁶ consists of an array of a large number of small glass tubes formed into a specific shape. This polycapillary collects X-rays from an X-ray source within a large solid angle and redirects them, by multiple total reflections, to form a focused beam (Fig. 2.13). The direction of the X-ray radiation can be changed when X-rays undergo multiple total reflections within a bent capillary, as long as the incident angle at each reflection is less than the critical angle (mrad) (Fig. 2.14). The critical angle of total reflection (mrad) for glass material can be approximated as follows:

$$\theta_c \approx \frac{30}{E} \quad (2.14)$$

Where E = energy of the incident X-ray radiation, in keV.

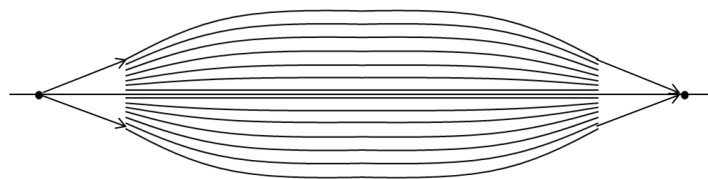


Figure 2.13 Polycapillary X-ray optics that produce a focused beam¹².

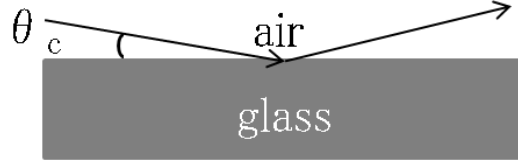


Figure 2.14 Schematic presentation of the principle of X-ray total reflection occurring at the air/glass interface within the hollow fibers of the polycapillary optics, with θ_c the critical angle for total reflection¹⁷.

Due to this total reflection condition the curvature of the capillary has to be gentle and the capillary diameter has to be small.

2.2.2.3 The detector

For the detection of the emitted X-rays the EDAX Eagle-III uses a liquid N₂ cooled Si(Li) semiconductor detector, with an active area of 80 mm². In this type of detector¹⁵, the total ionization produced by each X-ray photon striking the detector is converted to a voltage signal with amplitude proportional to the incident energy. The energy resolution of the semiconductor determines the ability of a given system to resolve characteristic X-rays from multi-element samples and is defined as the full width at half maximum (FWHM) of the pulse-height distribution measured for a monochromatic X-ray at a specific energy¹⁵. The instrumental energy resolution of a semiconductor detector is, when neglecting the natural line width of the X-rays, a function of two independent factors: one determined by the properties of the detector itself and the other dependent on the nature of the electronic pulse processing employed. According to this, the measured FWHM of the X-ray line (ΔE_{total}) can be described as follows:

$$\Delta E_{total} = \sqrt{\Delta E_{det}^2 + \Delta E_{elec}^2} \quad (2.15)$$

Where ΔE_{det}^2 = contribution due to the detector

ΔE_{elec}^2 = contribution associated with the electronic pulse processing

The contribution of the detector ΔE_{det} is determined by the statistics of the free-charge production process occurring in the depleted volume of the diode. The average number of electron-hole pairs produced by an incident photon can be calculated as the total photon energy (E) divided by the mean energy required to produce a single electron-hole pair (ϵ)¹⁵. If the fluctuation of this mean could be described by the Poisson statistics, the standard deviation could be described as follows:

$$\sigma = \sqrt{n} = \sqrt{\frac{E}{\epsilon}} \quad (2.16)$$

For semiconductor detectors the Fano factor (F) has to be taken into account, to correct for the fact that during the energy-loss process the individual events are not strictly independent. Taking into account the Fano factor, the FWHM can be described as follows:

$$\sigma = \sqrt{Fn} = \sqrt{\frac{FE}{\epsilon}} \quad (2.17)$$

Using

$$\frac{\sigma(E)}{E} = \sqrt{Fn} \quad (2.18)$$

Gives the following equation for the contribution of the detector ΔE_{det} to the measured FWHM of the X-ray line:

$$\Delta E_{det} = 2.35\sqrt{F\epsilon E} \quad (2.19)$$

The FWHM indicates the quality of an EDXRF system. However, other factors such as the presence of the background and artefacts in the XRF spectrum play also an important role for analytical applications.

Background

Effects associated with the partial collection of the photoelectrical signal by the detector have a small effect on its efficiency. The effect of incomplete charge collection results in tailing of the low energy-side of a peak. In addition, it produces a continuum of events appear as a shelf on the low-energy side of the major peaks in the spectrum¹⁵.

Artefacts

1. Escape peaks

For an incident X-ray with an energy higher than the Si-K absorption edge, the detection process will involve the generation, because of the X-ray fluorescence of the detector material, of Si-K X-rays. The majority of these will immediately be absorbed in the detector volume and contribute to the overall charge collected for the original incident X-ray photon. However, a finite probability will escape from the detector volume. The resulting energy detected will be reduced by 1.740 keV, which is the energy of the Si-K α X-ray that escaped.

2. Sum peaks

Sum peaks arise when two high intensity peaks arrive at the detector so close to each other that the detector cannot recognize them as two separate signals. The effect is that a signal will appear at an energy, which is equal to the sum of the energy of the two signals.

3. Diffraction peaks

Whenever a crystalline sample is measured in an EDXRF spectrometer, there is the possibility that the conditions of the Bragg diffraction will be fulfilled. The more monochromatic the excitation beam, the smaller the chance that the Bragg conditions will be satisfied.

2.2.2.4 Analytical characteristics of the EDAX Eagle-III

2.2.2.4.1 Beam size characterisation

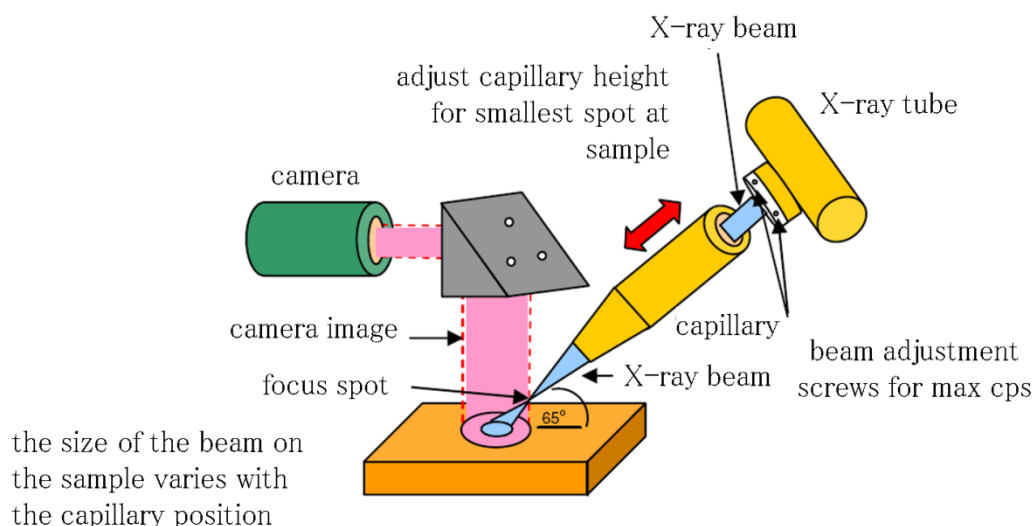


Figure 2.15 Working principle of the varispot option of the EDAX Eagle-III¹¹.

In the EDAX Eagle-III the module consisting of the X-ray tube and the polycapillary optic is motorised and can therefore move further away or closer to the sample (Fig. 2.15). Using this varispot system, a variable spot size of the incident X-ray micro-beam can be obtained. By increasing the polycapillary-sample distance, beam spots of approximately 25, 100, 225 and 300 μm can be obtained.

To calculate the size of the X-ray beam, a scan over a 10 μm thin copper wire using a measurement time of 50 s was performed with an adapted step size according to

the beam size, using the different varislot settings¹⁷. For the first two settings (being close to the ideal polycapillary focal distance producing the smallest beam sizes), a step size of 5 μm was chosen, for the larger beam sizes 10 and 25 μm respectively. Figure 2.16 shows the distance as a function of the intensity of the X-ray signal.

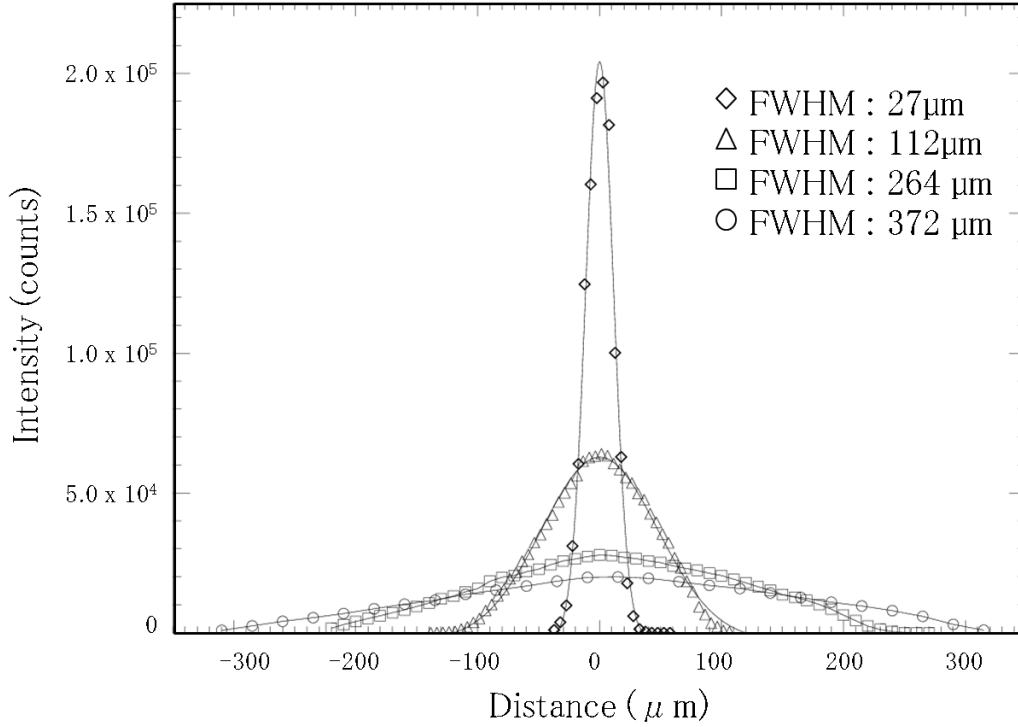


Figure 2.16 Line scan of a 10 μm copper wire with different varislot settings.

All the different modes show a clear Gaussian beam profile, which is used to calculate the full width at half maximum (FWHM)¹⁸:

$$FWHM = 2 * \sqrt{2\ln 2} * \sigma \quad (2.20)$$

Where σ = standard deviation

The relation between the $FWHM$ and the beam size, s , taking the thickness of the wire into account, is given by:

$$s = \sqrt{(FWHM)^2 - (T_w)^2} \quad (2.21)$$

Where $FWHM$ = full width at half maximum, μm

T_w = thickness of the copper wire, μm

Table 2.3 shows the different beam sizes using the different varispot modes.

position	beam size (μm)
position A	25
position B	112
position C	264
position D	372

Table 2.3 Overview of the different beam sizes using the different varispot modes.

2.2.2.4.2 The relative minimum detection limits.

To calculate the relative minimum detection limits the NIST SRM 621 was measured with a beam size of 25 μm for 1000 s at a voltage of 40 keV and a current of 135 μA . The certificate (Table 2.4) of this standard shows the exact concentration of different elements as oxides.

The mathematical definition of minimum detection limit (MDL) is based on the standard counting deviation. The MDL¹⁸ is defined as the amount of analyte which gives a net intensity equal to three times the standard counting error of the background intensity. The MDL can be calculated as follows:

$$MDL_i = 3 * c_{cert,i} * \sigma_{B,i} * I_{N,i} \quad (2.22)$$

Where $c_{cert,i}$ = certificated concentration of the element i

$\sigma_{B,i}$ = standard deviation of the background of element i

$I_{N,i}$ = netto intensity of the element i

constituent	% by weight	uncertainty
SiO ₂	71.13	0.03
Na ₂ O	12.74	0.05
CaO	10.71	0.05
Al ₂ O ₃	2.76	0.04
K ₂ O	2.01	0.03
MgO	0.27	0.03
SO ₃	0.13	0.02
BaO	0.12	0.05
Fe ₂ O ₃	0.040	0.003
As ₂ O ₃	0.030	0.001
TiO ₂	0.014	0.003
ZrO ₂	0.007	0.001

Table 2.4 Overview of the certificated values and the uncertainty of the different elements present in the NIST SRM 621 standard (trace elements in glass). The certified values are the present best estimates of the “true” values based on the results of a cooperative analytical program.

Figure 2.17 shows the relative minimum detection limit (rMDL), in ppm ($\mu\text{g/g}$), as a function of the atomic number, Z . The rMDL from the elements with $Z = 16$ until $Z = 40$, is approximately around 10 ppm, while from $Z = 15$ and lighter elements the rMDL increases exponentially. The rMDL for the lowest Z ($Z=11$, Na) that still can be seen by the instrument is approximately 2000 ppm (0.2%) when measuring this glass for 1000 s.

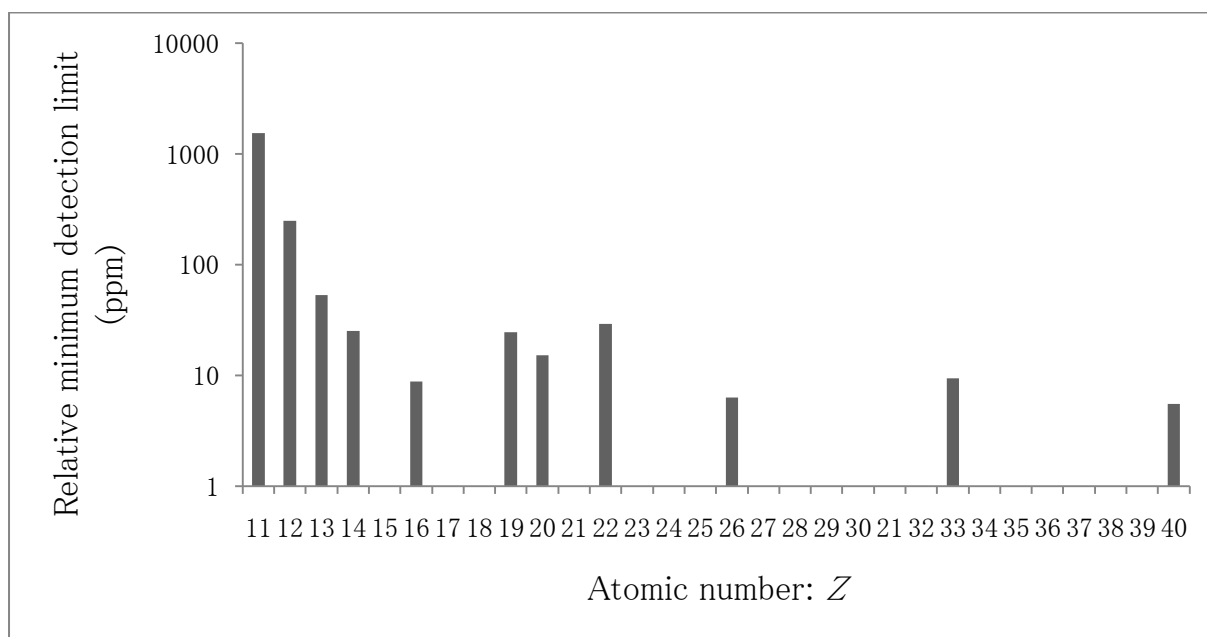


Figure 2.17 Relative minimum detection limits in ppm or $\mu\text{g/g}$ for NIST SRM 621 (beam size: 25 μm , time: 1000 s, voltage: 40 kV, a current: 135 μA , in vacuum and no filter).

2.2.2.5 Two mobile micro-XRF spectrometers: ArtTAX (Bruker, Germany) and the EDXRF system from the CEA (Liège, Belgium)

For a few of the analysis the mobile micro-XRF spectrometer ArtTAX of the Royal Institute for Cultural Heritage (Chapter 6), and the mobile EDXRF system from the University of Liège (Chapter 8) were used. Table 2.5 makes a comparison between the characteristics of the EDAX Eagle-III, the ArtTAX and the EDXRF.

The main advantage of the two mobile spectrometers is the possibility of *in situ* measurements. However the EDAX Eagle-III has the advantage that measuring in vacuum is possible, which results in a better sensitivity of the lower Z elements (down to Na). The EDXRF (CEA) has a very large spot size, 2 mm, while the portable ArtTAX system has a smaller spot size of 100 μm and smaller.

characteristics	EDAX Eagle-III	ArtTAX ¹⁹	EDXRF ²⁰
instrument type	laboratory	mobile	mobile
X-ray anode	Rh	W	Rh, W
max. voltage	50 kV	50 kV	50 kV
max. power	50 W	50 W	50 W
X-ray optic	XOS polycapillary incident angle 60°	polycapillary	collimator
spot size	25, 100, 225, 300 µm	< 100 µm	2 mm
detector type	liquid N ₂ cooled 80 mm ² Si(Li) detector	thermo-electrically cooled 10 mm ² silicon drift detector (X-flash)	Peltier-cooled 5 mm ² silicon drift detector
stage	axis: XYZ Step size: 5 µm max. sample size: 250×200×120 mm ³ max. load: 5kg	axis: XYZ Step size: 10 µm	Axis: X, Y, Z, θ Step size : 10 µm Two rails (1 m) placed perpendicular to each other
sample chamber	vacuum	open	open
camera	2 CCD colour cameras: high mag. (100×) low mag. (10×)	colour CCD camera, 500×582 pixels (20×)	2 micro-cameras
type of analysis	small samples (250×200×120 mm ³)	direct or <i>in situ</i> analysis possible, next to analysis of samples	direct or <i>in situ</i> analysis possible, next to analysis of samples
developed by	EDAX	Bruker	CEA (in house)

Table 2.5 Overview of some characteristics of the EDAX Eagle-III, the ArtTAX spectrometer and the EDXRF spectrometer.

In this chapter, theoretical considerations concerning Raman and XRF spectroscopy, and some instrumental properties of both techniques were discussed. The next chapter discusses the in-house developed software used to evaluate the Raman spectra and to calculate different parameters, which will enable us to fuse the data in Chapter 10. Also the evaluation of the XRF spectra, using the existing AXIL software package will shortly be discussed.

References

1. Smekal, A. (1923) Zur Quantentheorie de Dispersion. *Naturwiss* 11: 873–875.
2. Raman, C.V, Krishnan, K.S. (1928) A new type of secondary radiation. *Nature* 121: 501.
3. Ferraro, J.R., Nakamoto, K., Brown, C.W. (1994) *Introductory Raman spectroscopy*. Chapter 1 Basic Theory. Elsevier Science, USA, 1–94.
4. Peltier, M.J. (1999) *Analytical applications of Raman spectroscopy*. Chapter 1 Introduction to applied Raman spectroscopy. Blackwell Science Ltd, Oxford, 1–52.
5. McCreery, R.L. (2000) *Raman spectroscopy for chemical analysis (Chemical analysis series vol. 157)*. Chapter 1 Introduction and scope. John Wiley and Sons, New York, 1–14.
6. Vandenabeele, P., Weis, T.L., Grant, E.R., Moens, L.J. (2004) A new instrument adapted to in situ Raman analysis of objects of art. *Analytical and Bioanalytical Chemistry* 379: 137–142.
7. User manual Senterra (2008) Bruker optic.
8. Ferraro, J.R., Nakamoto, K., Brown, C.W. (1994) *Introductory Raman spectroscopy*. Chapter 2 Instrumentation and Experimental Techniques. Elsevier Science, USA, 95–146.
9. Hamaguchi, H.O. (1988) Calibrating Multichannel Raman Spectrometers. *Applied Spectroscopy Reviews* 24: 137–174.
10. Brereton, R.G (2007) *Applied Chemometrics for Scientists*. Chapter 3 Statistical concepts. John Wiley and Sons Ltd., Chichester, 63–110.

11. Miller, J.N., Miller, J.C. (2005) *Statistics and Chemometrics for Analytical Chemistry (5th edition)*. Chapter 3 Significance tests. Ellis Horwood imprint, England, 39–73.
12. Van Grieken, R.E., Markowicz, A.A. (2002) *Handbook of X-ray spectrometry (2nd editon)*. Chapter 1 X-ray Physiscs. Marcel Dekker, Inc., New Yok, 1–94.
13. <http://commons.wikimedia.org/>
14. User manual EDAX eagle-III (2003) EDAX.
15. Van Grieken, R.E., Markowicz, A.A. (2002) *Handbook of X-ray spectrometry (2nd editon)*. Chapter 3 Energy-dispersive X-ray Fluorescence Analysis using X-ray tube Excitation. Marcel Dekker, Inc., New Yok, 199–238.
16. Van Grieken, R.E., Markowicz, A.A. (2002) *Handbook of X-ray spectrometry (2nd editon)*. Chapter 2 Wavelength-dispersive X-ray Fluorescence. Marcel Dekker, Inc., New Yok, 95–198.
17. De Samber B. (2010) *Spatially resolved X-ray micro/nano-spectroscopy and imaging on the model organism Daphnia Magna using laboratory and synchrotron sources*. PhD thesis UGent.
18. Geo, N., Janssens, K. (2004) *X-ray spectrometry: Recent Technological advances*. Chapter 3 X-ray optics, John Wiley & Sons, Ltd., USA, 63–132.
19. Deneckere, A., Hocquet, F.P., Born, A., Klein, P., Rakkaa, S., Lycke, S., De Langhe, K., Martens, M.P.J., Strivay, D., Vandenabeele, P., Moens, L. (2010) Direct analysis of the central panel of the so-called Wyts triptych after Jan van Eyck. *Journal of Raman Spectroscopy* 41: 1210–1219.

20. Hocquet, F.P., Garnir, H.P., Marchal, A., Clar, M., Oger, C., Strivay, D. (2008) A remote controlled XRF system for field analysis of cultural heritage objects. *X-Ray Spectrometry* 37: 304–308.

Chapter 3: In-house developed software

Chapter 2 described the theory of Raman spectroscopy and XRF spectroscopy, and some properties of the instruments used in this work. In order to extract information from the collected Raman and XRF spectra, we should be able to evaluate both spectrum types with data processing software. Normally, the Raman spectra are processed using GRAMSTM or OPUSTM, but these programs have some drawbacks, especially for large datasets. Therefore, software to evaluate Raman spectra was developed. To evaluate the XRF spectra, the existing AXIL^{1,2} software package was used. In the first part of this chapter some details of AXIL will be described, while in the second part the in-house developed software to evaluate Raman spectra, is presented.

3.1 Evaluation of XRF spectra by Iterative Least-squares (AXIL)

XRF data evaluation is necessary because the XRF spectra contain different types of artefacts, such as: the background, peak overlap, sum peaks, escape peaks and diffraction peaks (see Chapter 2). The program AXIL (analysis of X-ray spectra by iterative least-squares) is based on the non-linear fitting of a mathematical function, which describes the photopeaks and the spectral background, to experimental data.

3.1.1 Non-linear least-squares fitting

A mathematical model is built by specifying the region of interest (ROI), selection of a suitable background, selection of the X-ray line groups to be included in the model and by establishing approximately correct values for the energy and the resolution of the spectrometer. These parameters are in a next step optimised by means of a non-linear least-squares strategy, which uses a modified Marquardt algorithm¹ to minimise the weighted sum of the differences χ^2 between the experimental data y_i and the mathematical model function $y_{model}(i)$:

$$\chi^2 = \frac{1}{n-m} \sum_i \frac{[y_i - y_{model}(i)]^2}{y_i} \quad (3.1)$$

Where n = total number of channels in the ROI

m = number of parameters optimised during the fitting process

The model parameters can be divided in 4 groups: peak group areas, calibration parameters (energy and resolution), background model parameters and peak shape parameters. For the spectrum evaluation the peak group area parameters are of primary interest. The model function $y_{model}(i)$ can therefore be described as a function of the spectral background and the photopeaks:

$$y_{model}(i) = y_{back}(i) + \sum_j A_j \sum_{k=1}^{N_j} R_{jk} y_j(i, E_{jk}) \quad (3.2)$$

Where E_{jk} represents the energy of the photopeaks and A_j represents the total area of all photopeaks (e.g. Fe-K α and Fe-K β) belonging to group j . The parameter A_j can be optimised during the least squares fitting process. The index k runs over all lines in group j , each line having a relative abundance R_{jk} and $\sum_k R_{jk} = 1$.

3.1.2 Background compensation method

For the XRF spectra, the LINEAR method¹ was used as background compensation method. This type of background compensation method attempt to adjust the parameters of a suitable mathematical method $y_{back}(i)$ to the background shape during the fitting process simultaneously with all the other parameters of $y_{model}(i)$. This background compensation model (ORTPOL method) uses a linear combination of mutually orthogonal polynomials:

$$y_{back}(i) = \sum_{l=0}^L a_l P_l(i) \quad (3.3)$$

Where L = degree of the polynomial

The orthogonal polynomials $P_l(i)$ are constructed by means of the following recurrent relationship:

$$\begin{aligned} P_0(i) &= 1 \\ P_1(i) &= i - \alpha_0 \\ P_l(i) &= (i - \alpha_{l-1})P_{l-1}(i) - \beta_{l-1}P_{l-2}(i) \text{ with } l = 2, \dots, L-1 \end{aligned} \quad (3.4)$$

Where

$$\begin{aligned} \alpha_0 &= \frac{\sum_{i=1}^n w(i)i}{\sum_{i=1}^n w(i)} \\ \alpha_l &= \frac{\sum_{i=1}^n w(i)i[P_l(i)]^2}{\sum_i w(i)[P_l(i)]^2} \\ \beta_0 &= 0 \\ \beta_l &= \frac{\sum_{i=1}^n w(i)i[P_l(i)P_{l-1}(i)]}{\sum_i w(i)[P_{l-1}(i)]^2} \end{aligned}$$

Where $w(i)$ = the weight of channel i (equal to $1/b(i)$ when channel i belongs to a background region of the spectrum; equal to 0 when channel i is part of a peak)

The values of the coefficients a_l can be calculated by the weighted sum of the polynomials:

$$a_l = \sum_i \frac{w(i)y_i P_l(i)}{w(i)[P_l(i)]^2} \quad (3.5)$$

Since prior to the calibration the background estimation is unknown, all channel weights are initially set to $1/y_i$. After calculating a first estimate of the coefficients

a_i , the channel weights are adjusted and the whole procedure is repeated. Channel i is identified as part of a peak when y_i is found to be significantly higher than the current estimate $b(i)$. This procedure is repeated until a stable set of weights $w(i)$ is obtained. During the fitting process the background coefficients a_i are adjusted together with the other parameters in the fitting model.

3.2 Evaluation of Raman spectra by in-house developed software

The Raman data evaluation proposed here is based on simple arithmetic routines such as, using derivatives in order to find the peak maxima. In order to be able to correct for the background, the SNIP background estimation method was found to be very effective.

3.2.1 File-format

In the field of spectroscopy, the publication and successful implementation of the JCAMP-DX (Joint Committee on Atomic and Molecular Physical Data-Data Exchange) protocols³ made it possible to exchange infrared, Raman, nuclear magnetic resonance and mass spectroscopic datasets. The JCAMP-DX protocols are based on delivering scientific data using ASCII encoding to ensure maximum compatibility and life span of the encoded data. Depending on the encoding software, it is possible to produce data exchange files with absolutely no loss of data.

Obviously, we chose this type of input file for the software. The Raman spectrometers owned by the research group are able to convert the data in a JCAMP-DX file format. The JCAMP-DX files are read by the software using the program *read_jcamp_dx.pro*. This program can also read JCAMP-DX files, which contain more than one spectrum. Details of this program can be found in the

appendix A. The development of the described software tools in this thesis was done in the high-level software environment of IDL (ITT Visual Information Solutions).

3.2.2 Calculation of the parameters and estimation of the background

In a second program, *calc_jcamp_dx_paramaters.pro* (see appendix A), the parameters of the Raman spectra are calculated. In a first step a least-squares polynomial of the second order is fitted through the Raman spectrum. Next, the first and second derivative of the function are calculated to determine respectively the maxima and minima of the spectrum, and the points of inflection (Fig. 3.1).

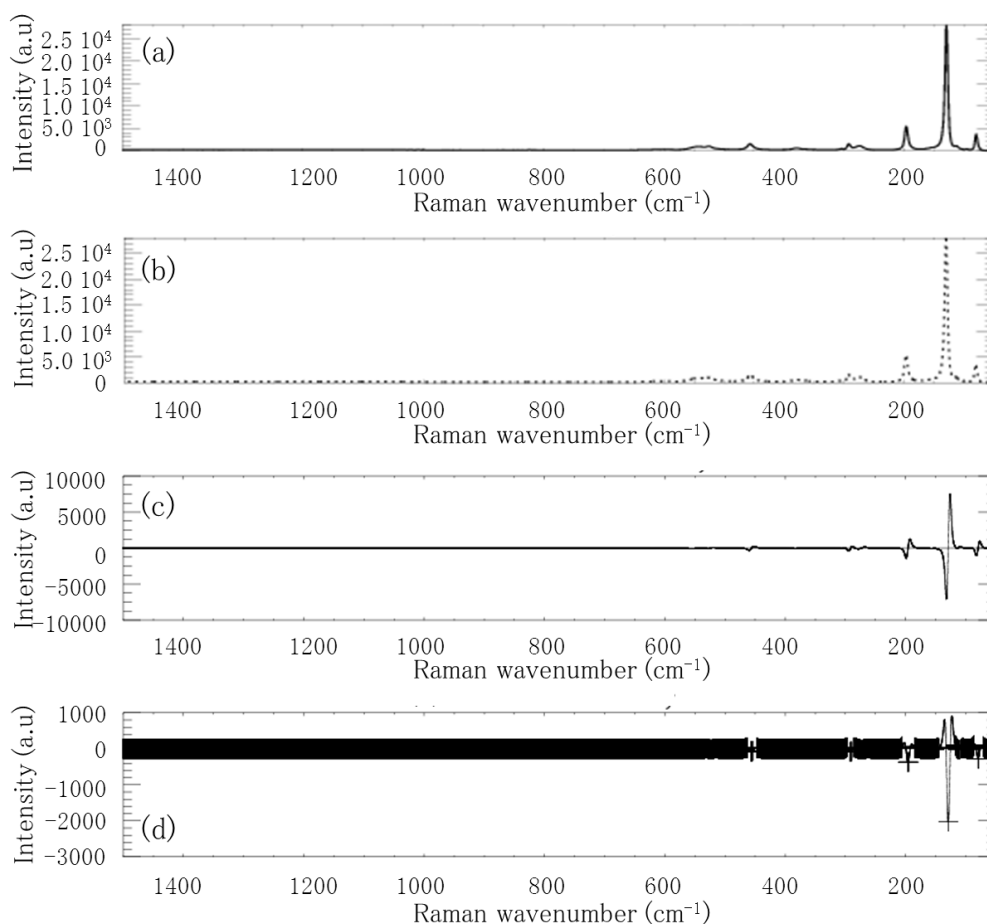


Figure 3.1 Spectra of (a) the raw y, (b) the smoothed y, (c) the first derivative of the smoothed y and (d) the second derivative of the smoothed y for the Raman spectrum of lead-tin yellow type I.

As background estimation procedure the SNIP method¹ was used. This type of background estimation method estimates the background shape $b(i)$ and subtracts the estimated background from the original spectrum y_i . The resulting spectrum $n_i = y_i - b(i)$ is then further evaluated. The Statistical Non-linear Iterative Peak clipping (SNIP) is based on the comparison of the content y_i of channel i with the mean m_i of the contents of the neighbouring channels a distance w away from the channel i . If m_i is smaller than y_i , the content of this channel is replaced by the mean m_i :

$$m_i = \frac{y_{i-w} + y_{i+w}}{2} \quad (3.6)$$

If after the replacement m_i is still smaller than y_i , then is m_i replaced by y_i .

The width w is initially set to twice the peak full width at half maximum. In this research, a fixed number, 50, was chosen as width w . This procedure is executed for all the channels of the ROI. Repeating this procedure, in our case 8 times, gradually causes peaks to be ‘stripped’ away from the original spectral data, so that only the estimate of the background shape $b(i)$ remains.

For the identification and extraction of the peaks the user can select the peaks by adapting the threshold values (d1_threshold and d2_threshold) for the first and second derivative. Figure 3.2(c) shows also the uncertainty expressed by the standard deviation (95.6% for 2σ). By means of the standard deviation, a selection has to be made between the noise and a ‘real’ signal. Equations 3.7 and 3.8 respectively calculate the maximum value of the estimated background and the most pessimistic value of the peak intensity taking the uncertainty into account:

$$b_{max}(i) = b(i) + 2\sqrt{2y_n(i) + b(i)} \quad (3.7)$$

$$y_{min}(i) = y_n(i) - 2\sqrt{y_n(i) + 2b(i)} \quad (3.8)$$

Where $b(i)$ = value for the estimated background

$y_n(i)$ = net intensity of the peak

Decisions can now be made using 5 different selection rules:

$$y_{min}(i) > 3\sqrt{b_{max}(i)} \quad (99 \%) \quad (1)$$

$$y_{min}(i) > 2\sqrt{b_{max}(i)} \quad (95 \%) \quad (2)$$

$$y_n(i) > 3\sqrt{b_{max}(i)} \quad (3)$$

$$y_n(i) > 2\sqrt{b_{max}(i)} \quad (4)$$

$$y_n(i) > 3\sqrt{b(i)} \quad (\text{most optimistic}) \quad (5)$$

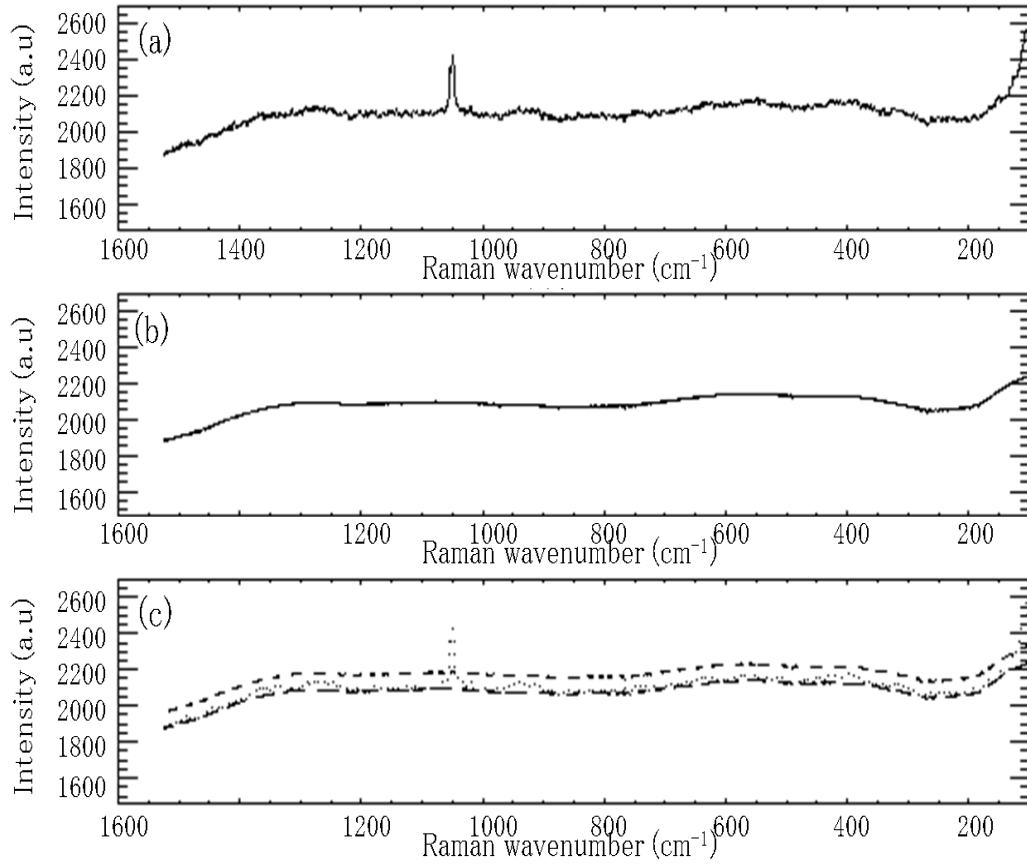


Figure 3.2 (a) Raman spectrum of lead white, (b) estimated background $b(i)$, (c) estimated background $b(i)$ together with the uncertainty spectrum $(2\sqrt{b(i)})$.

The user can decide which of the 5 selection rules will be used. In this research, we chose to use the 3rd selection rule. After the selection of the thresholds of the 1st and 2nd derivative, and the selection rule for the background estimation, the Raman spectra can be plotted and labelled (Fig. 3.3)

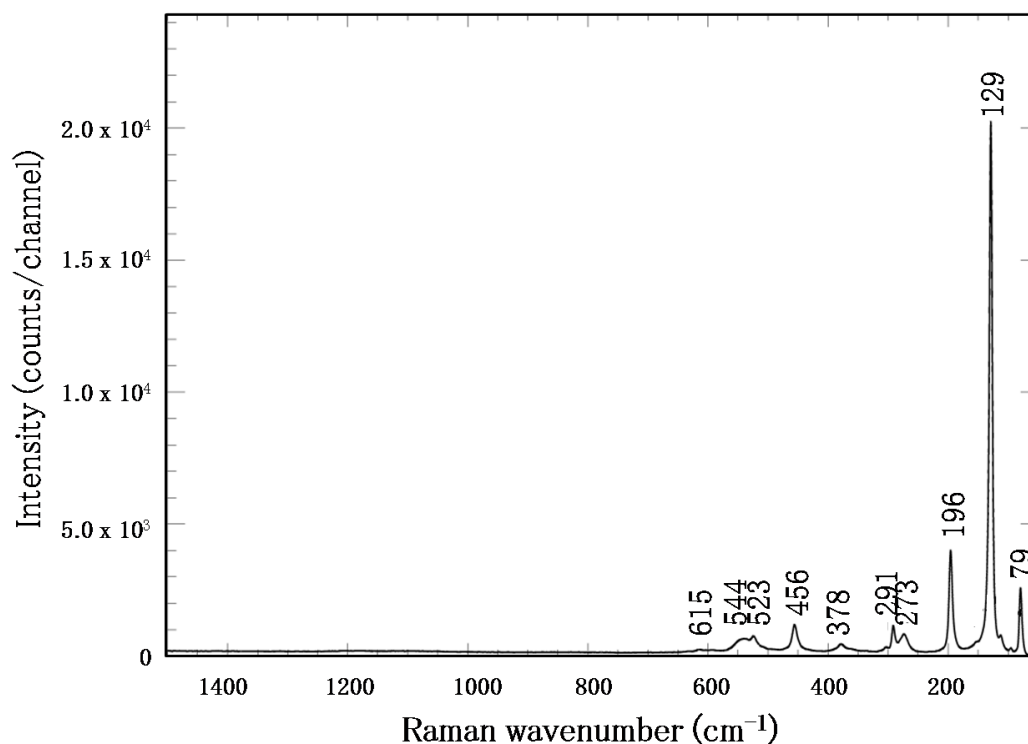


Figure 3.3 Raman spectrum of lead-tin yellow type I (background corrected).

In this chapter, the details of the existing AXIL software package to evaluate XRF spectra were discussed. Also the in-house developed software to evaluate Raman spectra was described in detail. The evaluation of the Raman and XRF spectra will be used in Chapter 9, to process the Raman and XRF mappings of a porcelain card separately, and as a first step for the fusion of Raman and XRF data (Chapter 10). The next chapter discusses two statistical multivariate methods, used in Chapter 9 and 10 for the characterisation and classification of unknown inorganic pigments and inorganic reference pigments.

References

1. Vekemans, B., Janssens, K., Vincze, L., Adams, F., Vanespen, P. (1994) Analysis of X-Ray-Spectra by Iterative Least-Squares (Axil) – New Developments. *X-Ray Spectrometry* 23: 278–285.
2. Vanespen, P., Janssens, K., Nobels, J. (1986) Axil-Pc, Software for the Analysis of Complex-X-Ray Spectra. *Chemometrics and Intelligent Laboratory Systems* 1: 109–114.
3. Lampen, P., Lambert, J., Lancashire, R.J., McDonald, R.S., McIntyre, P.S., Rutledge, D.N., Frohlich, T., Davies, A.N. (1999) An extension to the JCAMP-DX standard file format, JCAMP-DX V.5.01 (IUPAC Recommendations 1999). *Pure and Applied Chemistry* 71: 1549–1556.

Chapter 4: Multivariate statistical techniques

In chapter 3, the in-house developed software to evaluate Raman spectra and the existing AXIL software package to evaluate XRF spectra were presented. After the evaluation of the spectra, the results are used for characterisation of pigments, binding media, etc. For the identification and classification of the pigments used for the porcelain cards (Chapters 9 & 10), an appropriate statistical data processing method was necessary. In this chapter principal components analysis (PCA) and K-means cluster analysis are introduced as multivariate statistical techniques.

4.1 Principal components analysis (PCA)

Principal components analysis¹⁻³ (PCA) can be applied as a pattern recognition data reducing method which aims to determine the underlying information from multivariate raw data by interpreting the principal components (PCs) and observing patterns.

In this work, PCA is done mathematically as follows: a data matrix **X** (for example a set of Raman or XRF spectra) can be written as a combination of smaller matrices and some noise.

$$\begin{array}{ccccccc}
 \text{data matrix} & & \text{contribution of} & & \text{single} & & \text{noise} \\
 & & \text{each component} & & \text{component} & & \\
 N_{\text{var}} & & a & & N_{\text{var}} & & N_{\text{var}} \\
 N_{\text{obj}} \boxed{\mathbf{X}} & = & N_{\text{obj}} \boxed{\mathbf{C}} & \cdot & a \boxed{\mathbf{S}} & + & N_{\text{obj}} \boxed{\mathbf{E}} \quad (4.1)
 \end{array}$$

Where **X** = data matrix (rows = objects/spectra, columns = variables)

C = contribution of each component

S = spectra of each single component

E = noise

It is possible to predict \mathbf{C} and \mathbf{S} , but they can never be observed directly and perfectly. In order to observe the most important features and trends in the dataset PCA can be used to reduce the data matrix. PCA provides an approximation of a data matrix, \mathbf{X} , in terms of the product of two small matrices \mathbf{T} and \mathbf{P} . These matrices, \mathbf{T} and \mathbf{P} , capture the essential data patterns of \mathbf{X} (Fig. 4.1).

$$\begin{array}{ccccccc}
 & \text{data matrix} & & \text{scores} & & \text{loadings} & \text{noise} \\
 & N_{\text{var}} & & N_{\text{PCs}} & & N_{\text{var}} & \\
 N_{\text{obj}} \begin{array}{|c|} \hline \mathbf{X} \\ \hline \end{array} & = & N_{\text{obj}} \begin{array}{|c|} \hline \mathbf{T} \\ \hline \end{array} & \cdot & N_{\text{PCs}} \begin{array}{|c|} \hline \mathbf{P} \\ \hline \end{array} & + & \mathbf{E} \quad (4.2)
 \end{array}$$

Where \mathbf{T} = loadings

\mathbf{P} = scores

\mathbf{E} = noise

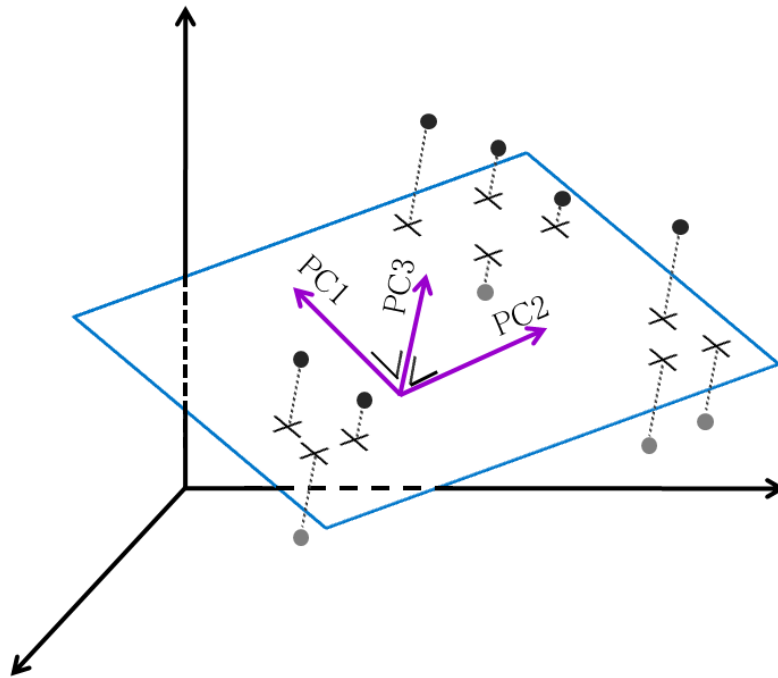


Figure 4.1 Principal components analysis (PCA); in the hyperspace of the original variables (or objects), new principal components axes are defined, which are better suited to describe the variation in the data points considered⁴.

As the original dataset contained N_{var} variables, in theory the scores matrix also contains N_{var} components. Each component contains a certain percentage of information of the dataset, which is expressed by the eigenvalue of the component λ_j :

$$\lambda_j = \frac{S_j}{S_{total}} = \frac{\sum_{i=1}^{N_{obj}} t_{ij}^2}{\sum_{i=1}^{N_{obj}} \sum_{j=1}^{N_{var}} x_{ij}^2} \quad (4.3)$$

Where S_j = sum of squares of the j^{th} PC (the j^{th} score vector)

S_{total} = sum of squares of the entire set

The first principal component has the highest eigenvalue and the eigenvalues further decrease with increasing number of the components. The dataset can now be reduced by preserving N_{PCs} selected principal components. The selection of N_{PCs} is mostly determined by studying the eigenvalues. Due to this selection PCA has reduced the data matrix (N_{obj}, N_{var}) to a scores matrix (N_{obj}, N_{PCs}):

$$\begin{array}{ccc} \text{data matrix} & & \text{scores} \\ & N_{var} & N_{PCs} \\ N_{obj} \begin{array}{|c|} \hline \mathbf{X} \\ \hline \end{array} & \longrightarrow & N_{obj} \begin{array}{|c|} \hline \mathbf{T} \\ \hline \end{array} \end{array} \quad (4.4)$$

To present the data visually, scores plots can be constructed using two principal components. Most interesting is to use the two principal components (PC1 and PC2) that contain the most information of the data. However, in this research we choose to plot PC3 versus PC2 because PC1 seems to be dominated by the size of

the objects. Analogously, a loadings plot, which shows the relation between the original variables, of these two principal components can be constructed. For the comparison between the scores and the loadings plots, a selection of variables which are characteristic for certain objects is made. In this way, spectra (objects) can be related to variables (Raman bands or XRF peaks), so information on their relative composition can be obtained.

In this work the Raman and XRF spectra underwent 2 data pre-processing steps before performing PCA: normalisation and ROI standardisation.

Normalisation increases the influence of the small intensities of some signals in the data. Because both detectors are multichannel detectors, the standard deviation is found by the Poisson distribution. Therefore, the standard deviation of the intensity (s_I) is equal to the square root of the intensity (I):

$$s_I = \frac{I}{\sqrt{I}} = \sqrt{I} \quad (4.5)$$

Where I = intensity of the signal

s_I = standard deviation of the intensity

In a second step ROI standardisation⁵ is performed. ROI standardisation is in fact mean centring of the variables of the data matrix $X(i,j)$:

$$stand_{ROI}(x_{ij}) = \frac{x_{ij} - \bar{x}_j}{\sqrt{\frac{\sum_{i=1}^{N_{obj}} (x_{ij} - \bar{x}_j)^2}{I}}} \quad (4.6)$$

Where \bar{x}_j = average value of the variables j

N_{obj} = number of spectra

4.2 K-means cluster analysis

All clustering methods aim to calculate the degree of similarity between two of the spectra (objects) to be clustered. The K-means clustering algorithm^{6,7} is an iterative procedure that obtained its name from the fact that it assumes the final number of object classes to be known a priori and equal to K. After selection of the desired number of clusters, each spectrum (object) i has to be assigned to one of the K clusters in order to minimize a measure of dispersion within the K clusters.

$$Dispersion [Clrs(K)] = \sum_k \sum_{i \in k} d_{ik}^2 \quad (4.7)$$

Where d_{ik} is the measure of similarity between the spectrum i and the cluster center k to which the spectrum i belongs for a given clustering Clrs (K). Suppose that there are N (spectra) vectors $s_1, s_2, \dots, s_j, \dots, s_n$ falling into K clusters with $K < N$, then can the mean vector m_k of the vectors in cluster k been described as follows:

$$m_{kj} = \frac{1}{N_k} \sum_{i \in k} s_{ij} \quad (4.8)$$

Where N_k = total number of vectors

The following criterion can be used to assign a spectrum to a cluster:

$$d_{ik} = \sqrt{\frac{\sum_j w_j (s_{ij} - m_{kj})^2}{\sum_j w_j}} \quad (4.9)$$

Where w_j = weight of the j^{th} coordinate.

In practice the K-means clustering algorithm has to be run with different values for K near the number of clusters one expects to exist in the dataset.

Normally, the value of K is equal to the number of meaningful principal components⁶. In practice, it is difficult to define the number of meaningful principal components. Therefore, for practical considerations, a K -means cluster analysis with $K=15$, a somewhat arbitrarily and too high value, was chosen. The K -means algorithm was already successfully used to investigate XRF data⁶. In this work, K -means cluster analysis was used to construct images of the porcelain cards, based on XRF data (Chapter 9).

In chapter 2, 3 and 4 some theoretical considerations concerning Raman spectroscopy and XRF spectroscopy, the in-house developed software, and multivariate statistical techniques were described. These 3 chapters contain the information necessary to understand the results presented in the following 6 chapters.

References

1. Wold, S., Esbensen, K., Geladi, P. (1987) Principal Components Analysis. *Chemometrics and Intelligent Laboratory Systems* 2: 37–52.
2. Brereton, R.G. (2007) *Applied chemometrics for scientists*. Chapter 5 Pattern recognition. John & Wiley and Sons Ltd., Chichester, 145–190.
3. Brereton, R.G. (2003) *Chemometrics: Data analysis for the laboratory and chemical plant*. Chapter 4 Pattern recognition. John & Wiley and Sons Ltd., Chichester, 183–270.
4. Vekemans B. (2000) *Microscopische X-stralen fluorescentie analyse: instrument-bouw en methode-ontwikkeling*. PhD thesis, Universiteit Antwerpen.
5. Brereton, R.G. (2003) *Chemometrics: Data analysis for the laboratory and chemical plant*. Chapter 6 Evolutionary signals. John & Wiley and Sons Ltd., Chichester, 183–270.
6. Vekemans, B., Janssens, K., Vincze, L., Aerts, A., Adams, F., Hertogen, J. (1997) Automated segmentation of mu-XRF image sets. *X-Ray Spectrometry* 26: 333–346.
7. Vekemans, B., Vincze, L., Brenker, F.E., Adams, F. (2004) Processing of three-dimensional microscopic X-ray fluorescence data. *Journal of Analytical Atomic Spectrometry* 19: 1302–1308.

Chapter 5: The use of mobile Raman spectroscopy to compare three full-page miniatures from the Breviary of Arnold of Egmond

Annelien Deneckere, Misha Leeftang, Miranda Bloem, Claudine A. Chavannes-Mazel, Bart Vekemans, Laszlo Vincze, Peter Vandenabeele, Luc Moens

Accepted in Spectrochimica Acta Part A

In literature, a lot of information can be found on the historical details of manuscripts, but only a few references on the analytical examination of the materials used (pigments, binding media, etc.). Therefore, in this chapter, Raman spectroscopy is used as analytical technique for the identification of 3 full-page miniatures of the Breviary of Arnold of Egmond. The in situ Raman analysis was performed in a darkened room in the conservation department of Museum Het Valkhof in Nijmegen (The Netherlands). The identification of the pigments was used as an additional argument to detect differences and similarities (different hands) between the three analysed miniatures. For this study we were allowed to submit these miniatures for the first time to spectroscopic examination.

5.1 Introduction

For art historians, it is important to have knowledge of the materials (pigments, binding media, substrates, etc.) and their provenance; to understand the ancient techniques; to locate and attribute the manuscript to a particular artist or workshop; or to date a manuscript. Although several historical details of mediaeval manuscripts have been studied extensively, the examination of the materials used is still in its infancy. The investigation of manuscripts by spectroscopic techniques is important to check their conservation state, to understand the causes of degradation and to plan an accurate conservation or restoration.

In comparison with other spectroscopic techniques, Raman spectroscopy has a number of advantages: the technique is non-destructive, no pre-treatment of the sample is necessary and mixtures can be investigated. Due to these advantages Raman spectroscopy was proven to be an interesting tool for the examination of works of art¹, in particular manuscripts. The Raman spectroscopic analysis of manuscripts has been mainly concerned with pigment identification, gathering information on the pigment palette^{2,3} used for the illuminations or a pigment palette

of a specific artist⁴. As a result of the identification of the pigments, also anachronisms can be traced⁵ and information on the evolution of the pigment use⁶ can be gathered. Next to the identification of the pigments, a lot of spectroscopic researches focus on the identification of degradation products found on manuscripts, in order to protect them against further degradation. Some of these degradation processes result in a colour change of the pigment: the light-induced degradation of realgar (red) into pararealgar (yellow)⁷, the degradation of red lead into galena (grey) and degradation of an alloy of copper, lead and zinc (gold) into a copper carboxylate (green)^{8,9}. Next to the spectroscopic analysis of the pigments, also analysis of the ink^{10,11} can be performed.

In this study, a mobile Raman spectrometer (Fig. 5.1) was used to analyse three different folios. In spite of a strong fluorescence background, different pigments were identified, obtaining important information on the pigment palette used for the illumination of the different folios. The identification of the pigments was used as an additional argument to detect differences and similarities between the three analysed folios.

5.2 The Breviary Arnold of Egmond

The Breviary of Arnold of Egmond is one of the most wealthily illuminated fifteenth century manuscripts in the Northern Netherlands. The manuscript consists, in its present state, of 433 folios; containing beautifully decorated margins, consisting of thin bars, inhabited by many small flowers, animals, monsters, human figures, hybrid creatures and lush acanthus leaves¹². Illuminating this large manuscript was too much for one artist or even for a single workshop to handle; therefore the illuminations were executed by at least two different workshops: one group of artists working in the style of the Master of Zweder van Culemborg and the other group working in the style of the Masters of Otto van Moerdrecht.

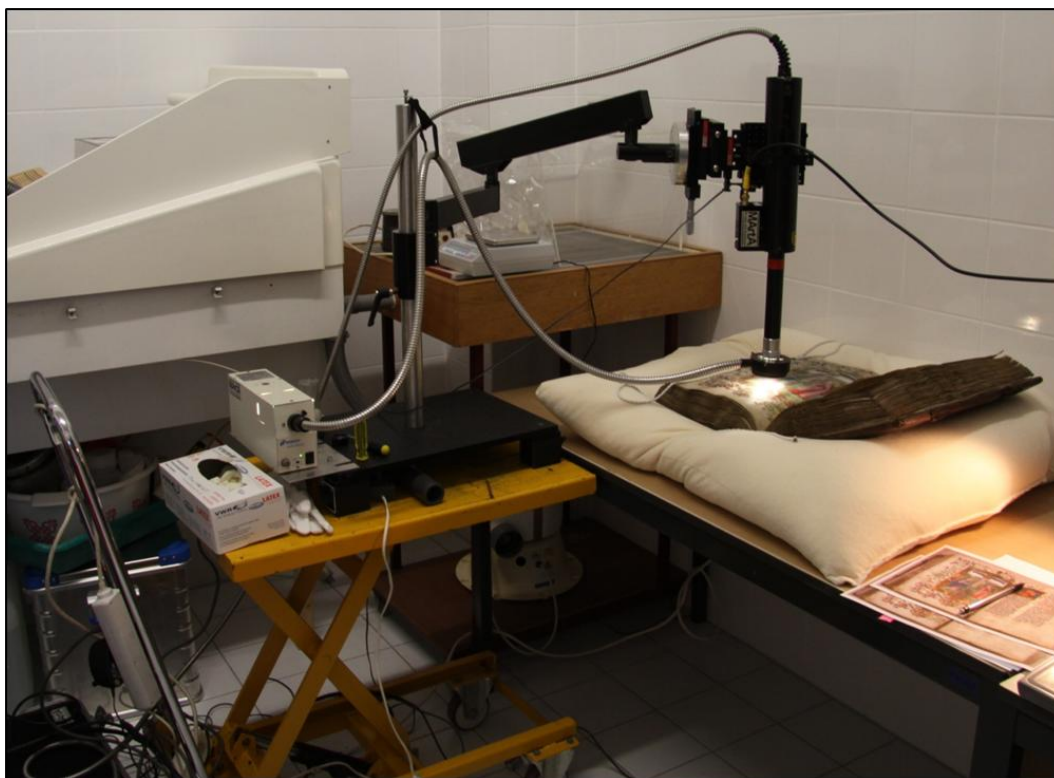


Figure 5.1 Picture of the experimental set-up of the Mobile Art Analyser (MArtA) in the conservation department of the Museum Het Valkhof.

On folio 324r in the breviary, the male commissioner of the manuscript is depicted kneeling in front of St Nicholas. For a long time nobody could identify the patron of the manuscript, except that he was a Guelders duke, because of the arms of Guelders and Jülich, implemented in the manuscript. In older literature¹², the manuscript has been dated to the period between 1420–1430. Considering this period, the patron could be: Reginald IV Duke of Guelders († 1423), Rupert von Berg († 1433) or Arnold of Egmond († 1471), the husband of Catherine of Cleves¹³. However, when looking at the miniatures made by the Zweder Masters, well developed landscapes and masterfully applied fine brush strokes suggest a matured style. Furthermore, influences of the Flemish painting technique of the early 1430s can be detected, making a date around 1435 more likely¹³.

The manuscript originally contained a number of full-page miniatures, which were all removed at an unknown date before 1902. Three of them resurfaced and are the subject of this study.

5.3 Experimental

5.3.1 The analysed folios

The three analysed folios belong to different institutions: the Fitzwilliam Museum in Cambridge (UK) (Fig. 5.2(a)), the University Library of Utrecht (The Netherlands) (Fig. 5.2(b)) and the London British Library (UK) (Fig. 5.2(c))) and were brought together for the exhibition ‘The hours of Catherine of Cleves: devotions, demons and daily life in the fifteenth century’ (Museum Het Valkhof, Nijmegen, The Netherlands, 10/10/2009 - 4/01/2010). The examinations were performed in the conservation department of the museum (Fig. 5.1), during or shortly after the dismantling of the exhibition.

The first analysed folio (318), originally forming f. 318 in the breviary, depicts King Salomon in the Temple (Fitzwilliam Museum), the second analysed folio (202), shows The Resurrection of Christ (University Library of Utrecht) and the last analysed folio (104), presents The Stoning of Saint Stephen (British Library).



Figure 5.2 Pictures of the three analysed miniatures: (a) King Salomon in the Temple (Fitzwilliam Museum), (b) The Resurrection of the Christ (University Library of Utrecht) and (c) The Stoning of Saint Stephen (British Library).

5.3.2 Mobile Raman spectroscopy

In situ Raman spectroscopy was performed on the three selected miniatures. The positions of the analysed points were conscientiously marked on prints of the miniatures. Sampling was not allowed. The measurements were performed in a darkened room in the conservation department of the museum.

Raman spectra were obtained using the Mobile Art Analyser (MArtA)¹⁴. This spectrometer contains a portable Raman imaging microscope (Spectracode, West Lafayette, IN, United States) and a SpectraPro 150i f.15 spectrometer (Roper scientific, Princeton Instruments). More detailed information on the instrument has been described elsewhere¹⁴.

The measurements were executed using a 600-grooves/mm dispersion grating and a 785 nm diode laser. Spectra were obtained in the spectral region between 100 and 2500 cm^{-1} . A 6 \times objective lens was used, giving a clearance of approximately 5 mm above the manuscript surface. The selected measurement point of the manuscript could be observed through a digitally controlled colour camera incorporated in the probe head. Micro-positioning and focussing was achieved using the flexible arm and the manually controlled micro-positioners. Using the 6 \times objective lens, a spot size of approximately 50 μm was achieved. Extreme care was taken to avoid damaging the illumination with the laser beam: by adjusting the laser current, every measurement started with a very low laser power. When necessary, the power was carefully increased in order to improve the signal-to-noise ratio.

5.4 Results and discussion

5.4.1 Visual examination based on style

As mentioned before, the illuminations in the Breviary of Arnold of Egmond were executed by at least two different workshops¹²: the Masters of Zweder van Culemborg and the Masters of Otto van Moerdrecht. Both groups have the same idea, but the illuminations of the Moerdrecht Masters are more primitive and rigid. They also make use of uniform colour fields, which makes the figures look like puppets (Fig. 5.3(a)). In contrary, the Masters of Zweder van Culemborg use different paint layers to create depth and contrast. As a result of this, the figures look more natural and human (Fig. 5.3(b)).¹²



Figure 5.3 Pictures of two folios painted by two different styles: (a) the style of the Masters of Otto van Moerdrecht and (b) the style of the Masters of Zweder van Culemborg.

Since the full-page miniatures were removed from the manuscript a long time ago, the condition of these folios is different from the illuminations in the Breviary of Arnold of Egmond itself. The paint layers of the loose folios have suffered some damage where the surfaces are worn. Therefore the classification based only on the stylistic examination of the faces is difficult.

Based on the stylistic study, the folios with The Resurrection of Christ (Fig. 5.2(b)) and The Stoning of Saint Stephen (Fig. 5.2(c)), belong to the same workshop, as the same background is used for both miniatures and as the painting style of the plants and the build-up of the faces is similar. They are painted in the style of the Masters of Zweder van Culemborg. Opposite to this, folio 318 with King Salomon in the Temple (Fig. 5.2(a)), shows somewhat a different style: the figures at the side are rather shapeless, the form and build-up of the faces is different and there is almost no shadow in the figure. Although this miniature is also painted in the style of the Masters of Zweder van Culemborg, it could have been executed by a different hand than the two other folios.¹⁵

5.4.2 Analysis with mobile Raman spectroscopy

Table 5.1 gives an overview of the identified pigments on the three analysed folios.

5.4.2.1 White colour

The white pigment used for the three folios could be identified as lead white ($2\text{PbCO}_3 \cdot \text{Pb}(\text{OH})_2$). Figure 5.4(a) shows the Raman spectrum of lead white, with the characteristic Raman band of the symmetric stretch vibration of CO_3^- at 1050 cm^{-1} .

colour	f.104	f.202	f.318
white	lead white	lead white	lead white
yellow	lead-tin yellow type I	lead-tin yellow type I	lead-tin yellow type I
blue	lapis lazuli	/	/
green	lead-tin yellow type I + lapis lazuli	lead-tin yellow type I	/
grey	/	lead white + lead-tin yellow type I	/
brown	/	massicot	/
red	red lead, vermillion	red lead, vermillion	red lead, vermillion

Table 5.1 Overview of the identified pigments of the three analysed folios: The Stoning of Saint Stephen (104), The Resurrection of Christ (202) and King Salomon in the Temple (318).

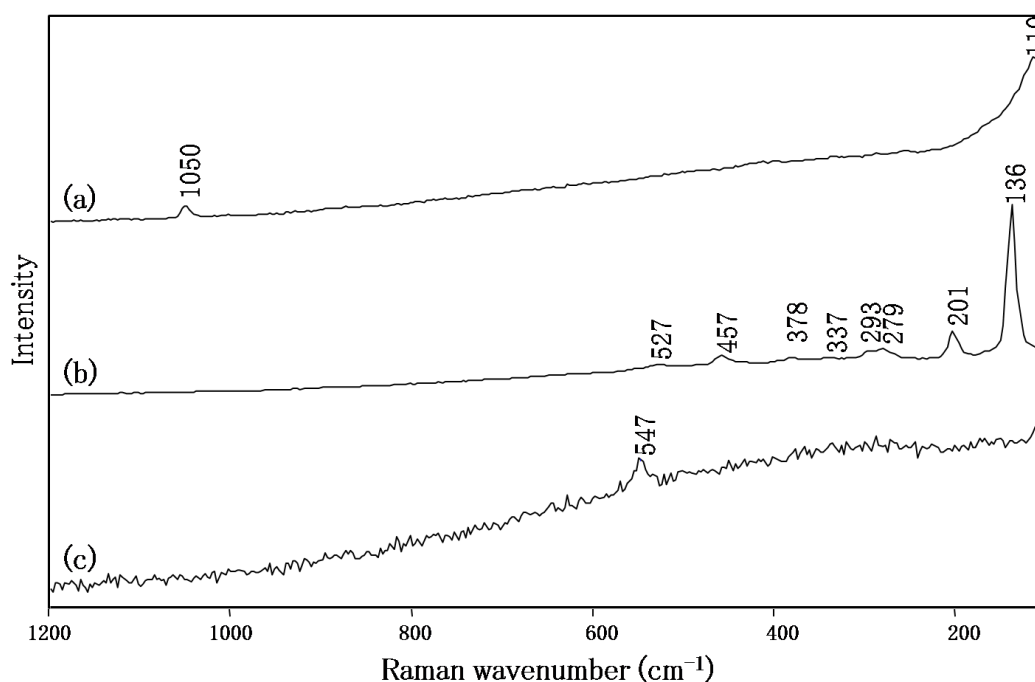


Figure 5.4 Raman spectra (6× objective, 60 s, 10% laser power) of : (a) the white pigment lead white ($2\text{PbCO}_3 \cdot \text{Pb}(\text{OH})_2$), (b) the yellow pigment lead-tin yellow type I (Pb_2SnO_4) and (c) the blue pigment lapis lazuli ($\text{Na}_{8-10}\text{Al}_6\text{Si}_6\text{O}_{24}\text{S}_{2-4}$).

Lead white has been by far the most important of the white pigments used in Europe from the Roman period till the 19th century, when it was replaced by less toxic pigments such as zinc white. Basic lead carbonate is the chemical equivalent of the natural hydrocerrusite. However, hydrocerrusite is extremely rare and consequently barely used as pigment source, which implements that already since the Roman period the synthetic equivalent was used as pigment¹⁶.

5.4.2.2 Yellow colour

Lead-tin yellow type I (Pb_2SnO_4) could be identified as the yellow pigment used in the three different folios. Figure 5.4(b) shows the Raman spectrum of lead-tin yellow type I, with the characteristic Raman bands at: 527, 457, 378, 337, 293, 279, 201 and 136 cm^{-1} . Lead-tin yellow type I is found widely in paintings throughout Europe from the 14th century until the first half of the 18th century. It does not appear to have been used in other places or cultures unless specific trade with Europe took place¹⁶.

5.4.2.3 Blue colour

Only for The Stoning of Saint Stephen, the precious pigment lapis lazuli ($\text{Na}_{8-10}\text{Al}_6\text{Si}_6\text{O}_{24}\text{S}_{2-4}$) could be identified. This pigment was found on the garment of the male figure depicted on the right side of the folio (Fig. 5.2(c) point 1). This male figure could be identified as King Saul¹⁵. The importance of this male figure is also confirmed by the presence of lapis lazuli, which was a very expensive pigment in the 15th century and was only used for important or holy figures. For all the other blue areas on the three folios we were not able to identify the blue pigment with Raman spectroscopy. Probably the pigment used for these blue areas is azurite ($2\text{CuCO}_3 \cdot \text{Cu}(\text{OH})_2$). Azurite has a similar colour as lapis lazuli, but was much

cheaper during the 15th century. Unfortunately azurite is a very weak Raman scatter and is therefore difficult to detect with Raman spectroscopy, especially during *in situ* measurements.

Figure 5.4(c) shows the Raman spectrum of lapis lazuli, with the characteristic Raman band at 547 cm⁻¹. This Raman band is caused by the $\nu(\text{S-S})^{2-}$ symmetric stretching mode. The pigment lapis lazuli is sometimes also named ultramarine, a term of historical importance used since antiquity. Additionally, this term is also used for artificially prepared pigments of similar composition. Consequently, the qualifications ‘natural’ and ‘synthetic’ are frequently used to differentiate between the two types. The pigment used for this miniature is most likely natural ultramarine, as the first commercial production of synthetic ultramarine dates from 1828. Raman spectroscopy is not able to distinguish between natural and synthetic ultramarine in paint layers¹⁶.

5.4.2.4 Green and grey colour

The green colour used on The Stoning of Saint Stephen (Fig. 5.2(c) point 2), could be identified as a mixture of lapis lazuli and lead-tin yellow type I. The Raman spectrum (Fig. 5.5(a)) shows the characteristic Raman band at 547 cm⁻¹ of lapis lazuli and the Raman bands of lead-tin yellow type I: 279, 201 and 136 cm⁻¹.

For the grey colour on The Resurrection of Christ (Fig. 5.2(b) point 1), a mixture of lead-tin yellow type I and lead white could be identified. The Raman spectrum (Fig. 5.5(b)) shows a combination of the most intense Raman band of lead-tin yellow type I (136 cm⁻¹) and the characteristic Raman bands of lead white (1050 and 110 cm⁻¹).

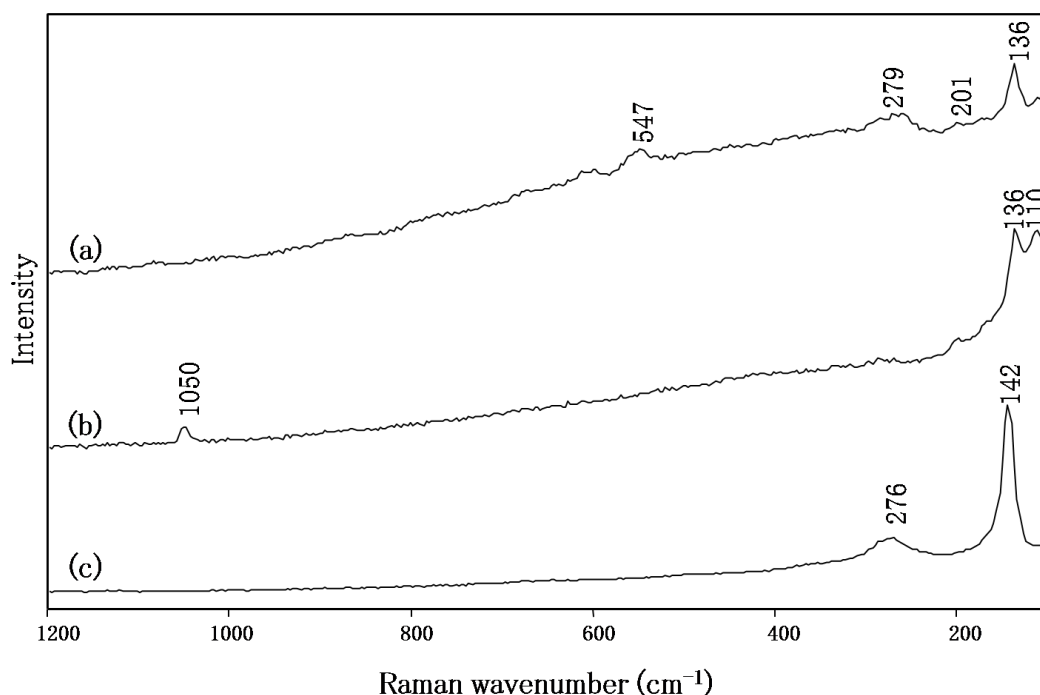


Figure 5.5 Raman spectra (6× objective, 60 s, 10% laser power) of : (a) the green colour, which is a mixture of lapis lazuli ($\text{Na}_{8-10}\text{Al}_6\text{Si}_6\text{O}_{24}\text{S}_{2-4}$) and lead-tin yellow type I (Pb_2SnO_4); (b) the grey colour, which is a mixture of lead-tin yellow type I (Pb_2SnO_4) and lead white ($2\text{PbCO}_3\cdot\text{Pb}(\text{OH})_2$); and (c) the brown colour, for which massicot (PbO) was used.

5.4.2.5 Brown colour

The pigment used for the brown colour on The Resurrection of Christ (Fig. 5.2(b) point 2), could be identified as the yellow pigment massicot (PbO). The red pigment used in the mixture to get the brown colour hue could not be identified. Massicot has characteristic Raman bands at 276 and 142 cm^{-1} (Fig. 5.5(c)). It occurs as soft yellow earthy masses in association with lead ore deposits worldwide¹⁶. Massicot is currently used to refer to the orthorhombic lead(II) oxide mineral with composition PbO . In contrary, litharge¹⁶ is used to refer to the tetragonal lead(II)oxide mineral with composition PbO . Litharge has also a yellow colour, but is in the context of painting technique mentioned as drier added to oil. Traces of litharge were also

found as impurities in red lead¹⁷. Red lead refers to the red lead(II,IV) oxide mineral with composition Pb_3O_4 (minium)¹⁶.

5.4.2.6 Red colour and incarnation

For the red colour two pigments could be identified: vermilion (HgS) (Fig. 5.6(a)) and red lead (Pb_3O_4) (Fig. 5.6(b)). Vermilion was perhaps the Romans' most valuable pigment, it was used in ambitious works and proved great wealth¹⁶. During the Middle Ages the expensive pigment vermilion was therefore sometimes replaced by a cheaper pigment, namely red lead. Red lead commonly occurs in small amounts as a bright red or orange powder or crust formed as a secondary mineral in the weathering zone around lead ore deposits. The mineral may have been used as a pigment in ancient times although the synthetic analogue was one of the first pigments to be manufactured¹⁶. The preparation of the synthetic red lead from lead white was already known in the Greek and Roman times. In the 15th century red lead was derived from lead metal in a two stage process of which litharge was the intermediate product¹⁸.

On folio 318, King Salomon in the Temple, vermilion was only found on the altar (Fig. 5.1(a) point 1). For all the other red parts of the folio, red lead was identified as red pigment. These results lead to the assumption that the more expensive vermilion was only used for the holy objects, such as the altar. On folio 202, The Resurrection of the Christ, the same assumption could be made: the more expensive vermilion was found in the wounds of Christ (mixed with lead white) (Fig. 5.2(b) points 3 & 4).

Based on this information we assumed that on folio 104, The Stoning of Saint Stephen (Fig. 5.2(c)) no traces of vermilion would be identified, because no red colour was used for the holy figures King Saul (depicted on the left) and Saint Stephen (depicted in the middle). Nevertheless, vermilion was found for the

colouring of the garment lying on the ground, which is depicted in the back of the miniature (Fig. 5.2(c) point 3). For all the other red parts red lead was identified as pigment.

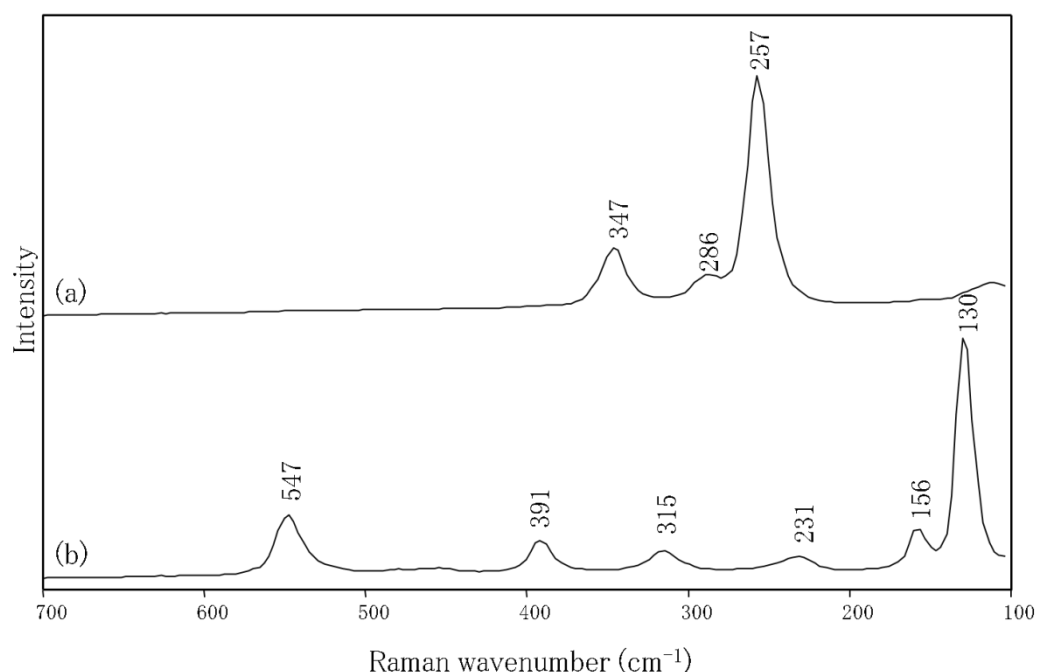


Figure 5.6 Raman spectra (6× objective, 60 s, 10% laser power) of two identified red pigments: (a) vermilion (HgS) and (b) red lead (Pb₃O₄).

The hierarchical colour use can only be found on the first two folios, while for the 3rd folio a garment laying in the back of the folio was painted with the more expensive vermilion. This information on the identification of the red pigments, may point in the direction that only King Salomon in the Temple and The Resurrection of Christ, were made by the same workshop and that The Stoning of Saint Stephen, was eventually made by another hand.

5.4.3 Interpretation of the results

Based on stylistic examination The Resurrection of Christ and The Stoning of Saint Stephen, were assigned to the same hand in the workshop, while King Salomon in the Temple probably was made by a different hand, working in the style of the

Masters of Zweder van Culemborg. However, based on the identification of the red pigments by Raman spectroscopy, King Salomon in the Temple and The Resurrection of Christ were made by the same hand, while The Stoning of Saint Stephen, might be made by another hand. Next to the hierarchical colour use of the red pigments, also hierarchical colour use of the blue pigments can be retrieved. For The Stoning of Saint Stephen, the blue pigment used for the garment of King Saul is the more expensive ultramarine. This result is in contradiction with the classification based on the identification of the red pigments and, even more important, in contradiction with the classification based on stylistic comparisons.

The possible explanation for this difference in classification could be found in a passage on the stoning of Saint Stephen in the Bible: *58 Then they cast him out of the city and stoned him. And the witnesses laid down their garments at the feet of a young man named Saul. 59 And as they were stoning Stephen, he called out, “Lord Jesus, receive my spirit.” 60 And falling to his knees he cried out with a loud voice, “Lord, do not hold this sin against him.” And when he had said this, he fell asleep. [Acts 7:54]*

In this passage, only the witnesses laid down their garment, but it could be that the garment in the back visualises the garment of the Holy Stephen, and therefore the more expensive vermilion was used.

Combining all these results leads to the following conclusion: the three folios are probably made in the same workshop, following the style of the Masters of Zweder van Culemborg, where the artists respected the hierarchical colour use. But King Salomon in the Temple shows significant stylistic differences with the two other folios. Raman spectroscopic analysis was not able to identify differences between the different hands. Further research on the pigment use in workshops has to be performed.

5.5 Conclusions

In this work, *in situ* Raman spectroscopy was used to investigate the colour palette of three different full-page miniatures from the Breviary of Arnold of Egmond. Although it is clear that once these miniatures were part of the same manuscript, at some point in the past they were separated and today, they belong to three different collections. By performing *in situ* Raman spectroscopy measurements in a darkened room in the conservation department, it was possible to identify the pigments lead white, lead-tin yellow type I, lapis lazuli, massicot, red lead and vermilion. When studying the blue and red pigments hierarchical pigment use could be demonstrated.

For the publication of this research paper only 3 folios were selected, but during this study we performed Raman spectroscopy on 22 folios of other related manuscripts, which were part of different collections: the National Library of the Netherlands (The Hague), the Bayerische Staatsbibliothek (Munich), the Museum Het Valkhof (Nijmegen), Fitzwilliam Museum (Cambridge), the British Library (London), The National Library of Belgium (Brussels), the Museum Catharijneconvent (Utrecht) and the University Library (Utrecht). All these manuscripts were brought together for an exhibition. The pigments identified with Raman spectroscopy are the ones we can expect for this period of time: red lead (Pb_3O_4), massicot (PbO), lead-tin yellow type I (Pb_2SnO_4), lead white ($2PbCO_3 \cdot Pb(OH)_2$), vermilion (HgS), chalk ($CaCO_3$), realgar (As_4S_4) and lapis lazuli ($Na_{8-10}Al_6Si_6O_{24}S_{2-4}$).

Next to mobile Raman spectroscopy also handheld XRF spectroscopy was performed on different folios. A disadvantage of handheld XRF spectroscopy on manuscripts is the penetration depth of the X-rays: all the spectra were overwhelmed by the very intense signal of Fe, coming from the gall ink on the reverse side of the folio. Another disadvantage of the handheld XRF spectrometer is the relatively large spot size of approximately 5 mm, which makes it impossible to perform analysis on the micro-level.

In the next chapter a combination of mobile Raman spectroscopy and portable XRF spectroscopy is used for the identification of pigments and degradation products of two vault paintings in the Our Lady's Cathedral in Antwerp (Belgium).

References

1. Vandenabeele, P., Edwards, H.G.M., Moens, L. (2007) A decade of Raman spectroscopy in art and archaeology. *Chemical Reviews* 107: 675–686.
2. Bioletti, S., Leahy, R., Fields, J., Meehan, B., Blau, W. (2009) The examination of the Book of Kells using micro-Raman spectroscopy. *Journal of Raman Spectroscopy* 40: 1043–1049.
3. Chaplin, T.D., Clark, R.J.H., McKay, A., Pugh, S. (2006) Raman spectroscopic analysis of selected astronomical and cartographic folios from the early 13th century Islamic 'Book of Curiosities of the Sciences and Marvels for the Eyes'. *Journal of Raman Spectroscopy* 37: 865–877.
4. Trentelman, K., Turner, N. (2009) Investigation of the painting materials and techniques of the late-15th century manuscript illuminator Jean Bourdichon. *Journal of Raman Spectroscopy* 40: 577–584.
5. Bersani, D., Lottici, P.P., Vignali, F., Zanichelli, G. (2006) A study of medieval illuminated manuscripts by means of portable Raman equipments. *Journal of Raman Spectroscopy* 37: 1012–1018.
6. Eremin, K., Stenger, J., Huang, J.F., Aspuru-Guzik, A., Betley, T., Vogt, L., Kassal, I., Speakman, S., Khandekar, N. (2008) Examination of pigments on Thai manuscripts: the first identification of copper citrate. *Journal of Raman Spectroscopy* 39: 1057–1065.
7. Burgio, L., Clark, R.J.H., Muralha, V.S.F., Stanley, T. (2008) Pigment analysis by Raman microscopy of the non-figurative illumination in 16th-to 18th-century Islamic manuscripts. *Journal of Raman Spectroscopy* 39: 1482–1493.

8. Aceto, M., Agostino, A., Boccaleri, E., Crivello, F., Garlanda, A.C. (2006) Evidence for the degradation of an alloy pigment on an ancient Italian manuscript. *Journal of Raman Spectroscopy* 37: 1160–1170.
9. Aceto, M., Agostino, A., Boccaleri, E., Crivello, F., Garlanda, A.C. (2010) Identification of copper carboxylates as degradation residues on an ancient manuscript. *Journal of Raman Spectroscopy* 41: 1144–1150.
10. Bicchieri, M., Monti, M., Piantanida, G., Sodo, A. (2008) All that is iron-ink is not always iron-gall! *Journal of Raman Spectroscopy* 39: 1074–1078.
11. Lee, A.S., Otieno-Alego, V., Creagh, D.C. (2008) Identification of iron-gall inks with near-infrared Raman microspectroscopy. *Journal of Raman Spectroscopy* 39: 1079–1084.
12. Defoer, H.L.M. (1989) *Golden Age of Dutch Manuscript painting*. George Braziller, Stuttgart.
13. Dückers, R., Priem, R. (2009) *The hours of Catherine of Cleves: Devotion, Demons and Daily life in the 15th century*. DeckersSnoeck, Antwerp.
14. Vandenabeele, P., Weis, T.L., Grant, E.R., Moens, L.J. (2004) A new instrument adapted to *in situ* Raman analysis of objects of art. *Analytical and Bioanalytical Chemistry* 379: 137–142.
15. Bloem, M. (2011) New light on three miniatures from the Egmond Breviary, *Oud Holland*, submitted.
16. Eastaugh, N., Walsh, V., Chaplin, T., Siddall, R. (2004) *Pigment compendium: a dictionary of historical pigments*. Elsevier Butterworth-Heinemann, Oxford.

17. Burgio, L., Clark, R.J.H., Gibbs, P.J. (1999) Pigment identification studies *in situ* of Javanese, Thai, Korean, Chinese and Uighur manuscripts by Raman microscopy. *Journal of Raman Spectroscopy* 30: 181–193.
18. Feller, L.F. (1986) *Artists' Pigments: A handbook of their history and characteristics volume 1*. Chapter 8: Red lead and Minium. Cambridge University Press, Cambridge, 109–140.

Chapter 6: *In situ* investigations of vault paintings in the Antwerp cathedral

Annelien Deneckere, Walter Schudel, Marina Van Bos, Helena Wouters,
Anna Bergmans, Peter Vandenabeele, Luc Moens

Spectrochimica Acta Part A, 75 (2010) 511–519

In the previous chapter, Raman spectroscopy was used to identify the pigments used in 3 full-page miniatures of a mediaeval manuscript. This chapter describes the combination of two mobile analytical techniques, Raman spectroscopy and XRF spectroscopy, for the identification of pigments and a possible deterioration product of two vault paintings in the Our Lady's Cathedral in Antwerp (Belgium). The analysis of these vault paintings had to be performed on a high scaffolding, which resulted in stability problems. These stability problems are also discussed in this chapter.

6.1 Introduction

Wall and vault paintings in churches were fairly common between the 12th and the 16th century, but only few of them survived because of the degradation over time, the reconstruction of the building, and of the 16th century iconoclastic outbreak. Fragments are occasionally discovered during structural repair works when later applications of paint or lime wash are removed. The painted scenes commonly depict lives of popular saints and are usually accompanied by geometrical patterns and decoration¹.

As by other objects of art, preservation of these paintings is indispensable. However, one of the main difficulties with mural paintings is that they have been executed as a part of a standing building and have become part of the structure. The close association between the wall painting, the substrate and the masonry attend to several problems for conservation, since air pollution², biological organism invasion³, and changes in temperature and relative humidity⁴ can have disastrous effects on the stability and integrity of the artwork. More subtle changes arising from the presence of people, e.g. soot and hydrocarbons from smoking lamps and candles, reactivity of body vapours, damp exhaled air and perspiration, and the

instability of the pigments or mixtures of pigments with time, also produces dramatic deterioration in wall paintings¹.

When performing spectroscopic analysis in the field of cultural heritage, another problem has to be taken into account: the objects for the study are very often precious and unique works of art, which cannot be destroyed or even sampled for analysis. When sampling is allowed, it is recommended that the sampling is as limited as possible, thus leaving the artistic value of the work of art untouched. In this respect, direct analysis is considered as one of the best methods to avoid damage during the analysis of artworks. If the analysis cannot be executed *in situ*, the artwork has to be transported to the laboratory or micro-sampling is a necessary step. The identification of pigments and binding media, used in mediaeval and renaissance wall paintings, provides art historians with precise information on the techniques used in the creation of the work itself, and gives conservators and restorers guidelines on the materials necessary for conservation.

This paper presents the first results of an *in situ* investigation of a 15th century and a 16th century vault painting in the Our Lady's Cathedral, Antwerp, Belgium. The aim of this research is the characterisation of the composition of the pigments present in both vault paintings. Two complementary *in situ* techniques have been used: X-ray fluorescence spectroscopy (XRF) and Raman spectroscopy. XRF yields the elemental composition of the investigated work of art. When XRF is the only research technique used for pigment identification, definite identifications can be achieved only for some pigments, such as cinnabar, thanks to the presence of specific key elements. Therefore, Raman spectroscopy⁵⁻⁷ was used, since this technique yields molecular information. The combination of these two approaches allows identifying most of the pigments. In the last decade, the combination of XRF with Raman spectroscopy was successfully used for the identification of pigments in, amongst others, mural paintings⁸⁻¹⁰, easel paintings¹¹, painted stucco fragments¹², manuscripts¹³ and wallpapers¹⁴.

6.2 The Site

Wall and vault paintings from the late-14th until the 20th century have been preserved in the Our Lady's Cathedral in Antwerp. For this research, two vault paintings in the most southern aisle have been examined. The first painting is late mediaeval and dates from the 15th century, the second is a 16th century renaissance painting¹⁵.

6.2.1 Mediaeval vault painting

The late mediaeval painting (Fig. 6.1(a)) was created on the vault of the fourth bay. This bay is part of a previous parish chapel. The church wardens paid for this painting in 1469. The vault has been decorated, around the keystone and the four pendants, with five pointed stars, which end in the finials. Along the lines of the stars, friezes composed of flower stencils run.



Figure 6.1 Overview of (a) the mediaeval vault painting, situated on the fourth bay and (b) the renaissance vault painting, situated on the fifth bay in the Our Lady's Cathedral, Antwerp (Belgium).

For this vault painting, two different techniques have been employed. All the black, red and blue areas in the triangles around the keystone and the pendants have been painted on a greyish, still more or less wet whitewash. The binder of these paints is water based. This explains why these areas are in fresco technique, although they are not intended to be, since “al fresco” painting was not known in this period in Belgium. All the other parts are painted in a pure “secco” technique. Although the binding media have not been analysed, by the naked eye the technique can easily be identified as a rather fatty. The greyish whitewash has been scratched away before painting. This could be a result of the fear of saponification that may occur during the application of a fatty paint on a caustic, fresh lime wash. The difference in painting techniques explains the differences in ageing in this vault painting.

6.1.2 Renaissance vault painting

The renaissance vault painting (Fig. 6.1(b)) is situated in the fifth bay that is part of the chapel of the Holy Sacrament. The painting was commissioned by the Brotherhood of the Holy Sacrament and bears the date 1540. On the four middle vault panels, four women in a renaissance architecture with cupids bearing banners and cornucopias, symbols of food and abundance, are depicted. The figures are identified by inscriptions of the virtues purity (puritas), piety (pietas), innocence (innocentia) and simplicity (simplicitas). Four medallions in the vault panels on the outside of the bay bear Eucharistic symbols, two with a lamb of God and two with a monstrance. On the edges of the medallions, the inscriptions of *ecce agnus dei qui tollis peccata MONDI* [sic] (see the Lamb of God that takes away the sins of the world) and *ecce panis ANGELORUM* (see the bread of the angels) can be seen. This Eucharistic iconography refers to the Brotherhood of the Holy Sacrament that used and decorated the chapel.

The painting is completely executed in oil paint. Large parts are painted with gold paint (shell gold) on tin leaf. There are strong indications that the painting has been made on another preparation than the greyish whitewash of the background. Sometimes there is a clear evidence of a red preparatory painting. The Italianising style of this painting is typical for the Southern Netherlands in the second quarter of the 16th century.

6.3 Experimental

6.3.1 XRF spectroscopy

For the *in situ* investigations of the vault paintings, a mobile micro-XRF spectrometer (ArtTAX, Bruker AXS Microanalysis, Germany) with a Tungsten tube was used (Fig. 6.2(a)). The primary X-rays are collimated by a pin-hole (200 μm). The measuring head is equipped with a thermo-electrically cooled detector (X-Flash) (energy resolution: 160 eV for the Mn-K α at 10 kcps) with preamplifier for detection of the X-ray fluorescence signal, and with a colour CCD camera which facilitates the choice of the sample area of interest and the focussing of the measuring head on the desired position. The measuring head is combined with a stepper motor based XYZ stage (range of 50 mm each) and a tripod for accurate positioning relative to the sample. The whole equipment can be placed in transport boxes and rebuilt at the site where the measurements have to be executed.

Each analysis takes 120 s (excluding positioning of the probe), which means that a large number of points can be analysed in a relatively short time, making this technique a powerful aid to get a first insight in the materials and techniques used on mural paintings. Measurements are performed in the lacunas as well as on paint layers in order to obtain information on subsequent paint layers. During the

experiments an energy of 50 kV, a current of 700 μA and a Ni 25 μm filter were used.

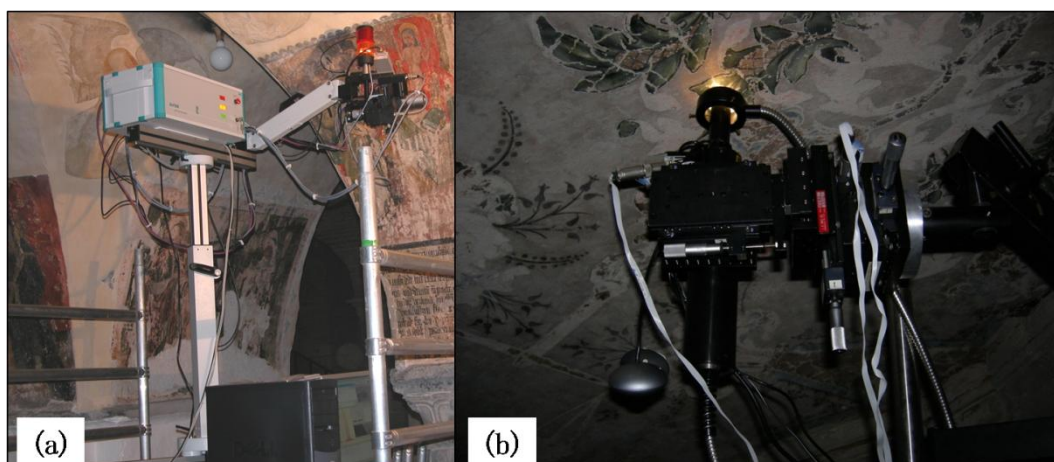


Figure 6.2 (a) The portable micro-XRF spectrometer (ArtTax, Bruker AXS Microanalysis, Germany) with a Tungsten tube and (b) the probe head of the Mobile Art Analyser (MArtA).

6.2.2 Raman spectroscopy

The Raman instrument used for this research is the Mobile Art Analyser (MArtA) (Fig. 6.2(b)). This device contains a portable Raman imaging microscope (Spectracode, West Lafayette, IN, United States) and a SpectraPro 150i f.15 spectrometer (Roper scientific, Princeton Instruments). The instrument has been described in more detail elsewhere¹⁶.

The investigations have been executed using a 600-grooves/mm dispersion grating, with a spectral resolution of about 4 cm^{-1} , and a 785 nm laser. The laser power used during the measurements was set to a few milliwatts, to avoid all possible sample damage. Spectra were obtained with a spectral region between 100 and 2500 cm^{-1} . To achieve a working distance of ca. 5 mm, a $6\times$ objective lens was used. The sample could be observed through a USB-controlled colour camera incorporated in the probe head. Micro-positioning and focussing were achieved using three

motorised and remote controlled micro-positioners (Oriel), with a working distance of 2.5 cm. During this research, more than 50 points have been examined, resulting in ca. 115 spectra.

6.4 Results and discussion

6.4.1 Conditions

Before discussing the results, some feasible problems, which occurred during the measurements, have first to be taken into account. The examined wall paintings in the Our Lady's Cathedral in Antwerp are located on the vault, 28 m above ground level. To be able to reach the wall paintings during the period of conservation treatment, a wooden platform was constructed 22 m above ground level. The instruments and their accessories had to be brought onto this platform. To achieve this, the instruments were carried by hand to the top of this platform. There, three scaffolds were placed.

For the XRF analyses, the XRF instrument with the measuring head upside down, was placed on one scaffold and the computer and one of the operators on the other scaffold. By using the stepper motor, the focussing could take place over a distance. A second operator was standing on the same scaffold as the XRF instrument, as sometimes the positioning had to be performed manually. The focus could be checked on the computer during the whole measurement.

For the Raman analyses the probe head of the MArtA instrument was placed on a scaffold, while the spectrometer and the computer were placed on the other scaffold. The distance between the probe head and the spectrometer could be bridged using optical fibres. On the third scaffold an operator was standing, to move the probe head manually.

Performing microanalysis on a platform or scaffold is associated with stability problems. Once the micro-positioning and focusing is done, the operator cannot move, because this causes vibrations in the scaffold, where the operator is standing. These vibrations are propagated in the wooden floor and the other scaffolds, and tend to bring the probe head out of focus.

For the Raman analysis, another problem has to be taken into account, namely strong interference from stray light that is entering through the stained glass windows. Therefore, the measurements had to be executed during the night. For positioning and focusing artificial light was used.

6.4.2 Pigment identification of the mediaeval vault painting

During XRF measurements, succeeding paint layers are analysed as one spot, so the resulting XRF spectra may contain elements present in different paint layers, depending on the composition, the concentration and the paint layers thicknesses. In contrast, Raman spectroscopy is a surface technique and contains only signals from one, maybe two paint layers. By carefully selecting the painted areas and by matching both techniques, so that the same area is analysed, interpretation difficulties can be overcome.

By analysing consecutively the grey whitewash, the orange ground layer and the painted layers, the analysis can be correlated with the layered structure of the paint.

6.4.2.1 Supporting layer

The material used as supporting layer in both vault paintings is calcite (CaCO_3). The Raman spectra of all analysed points show a large Raman signal at 1086 cm^{-1} . This Raman signal can be assigned as the strongest Raman band of calcium

carbonate (CaCO_3). In some Raman spectra, small amounts of gypsum ($\text{CaSO}_4 \cdot 2\text{H}_2\text{O}$) were observed (Raman bands at 414, 494, 615, 669, 1003 and 1132 cm^{-1}), along with the spectrum of CaCO_3 (Fig. 6.3(a)).

Gypsum ($\text{CaSO}_4 \cdot 2\text{H}_2\text{O}$) is a weathering product, so it tells something on the condition of the vault painting. However, it has to be taken into account that Raman spectroscopy is a surface technique. The Raman signals from CaCO_3 , showed in the Raman spectra, belong to small particles CaCO_3 , which remained after removing the plaster layer, which was put on top of these paintings during the iconoclastic outbreak.

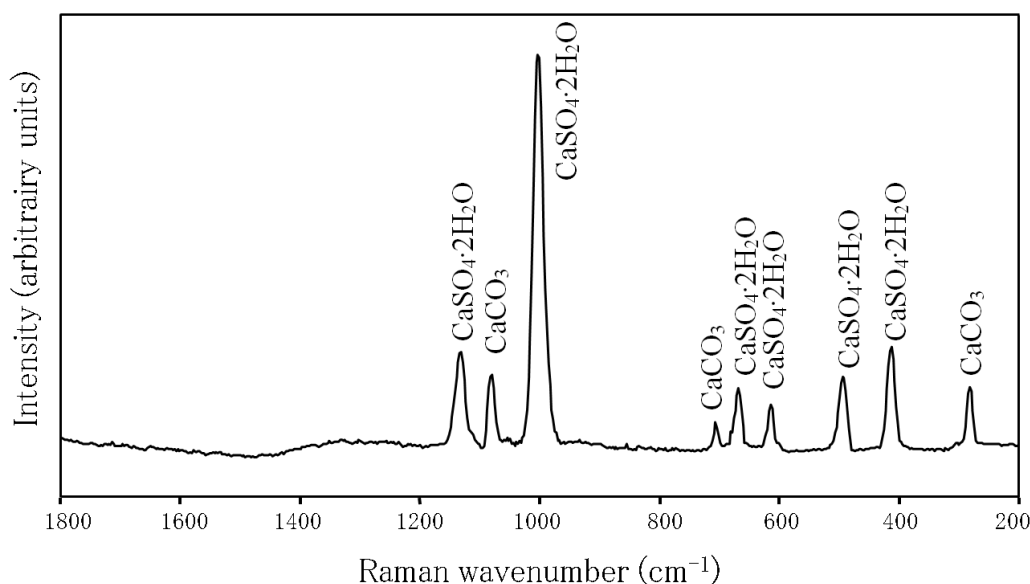


Figure 6.3 (a) Raman spectrum of the top layer of the mediaeval vault painting, showing a combined spectrum of calcite (CaCO_3) and gypsum ($\text{CaSO}_4 \cdot 2\text{H}_2\text{O}$).

6.4.2.2 Red layers

The orange ground layer is clearly present in the lacunas of the red leaves (Fig. 6.4(a)). XRF analysis of this ground layer shows the presence of calcium, iron, lead and mercury (Fig. 6.3(b)). These elements are present in relative small quantities. The spectrum of the bright red upper layer shows a large peak corresponding to mercury and small peaks for calcium, iron and lead (Fig. 6.3(c)).

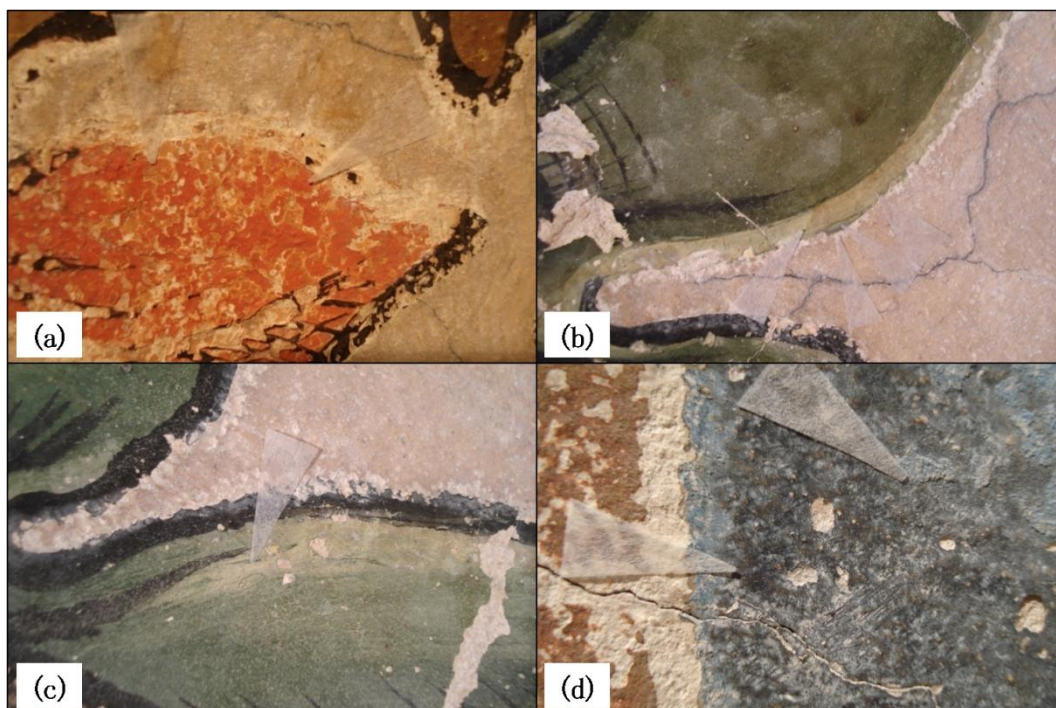


Figure 6.4 Some details of the mediaeval vault painting in the Antwerp cathedral; (a) detail of different analysed red layers; (b–c) detail of investigated green layers and (d) detail of the analysed blue layers.

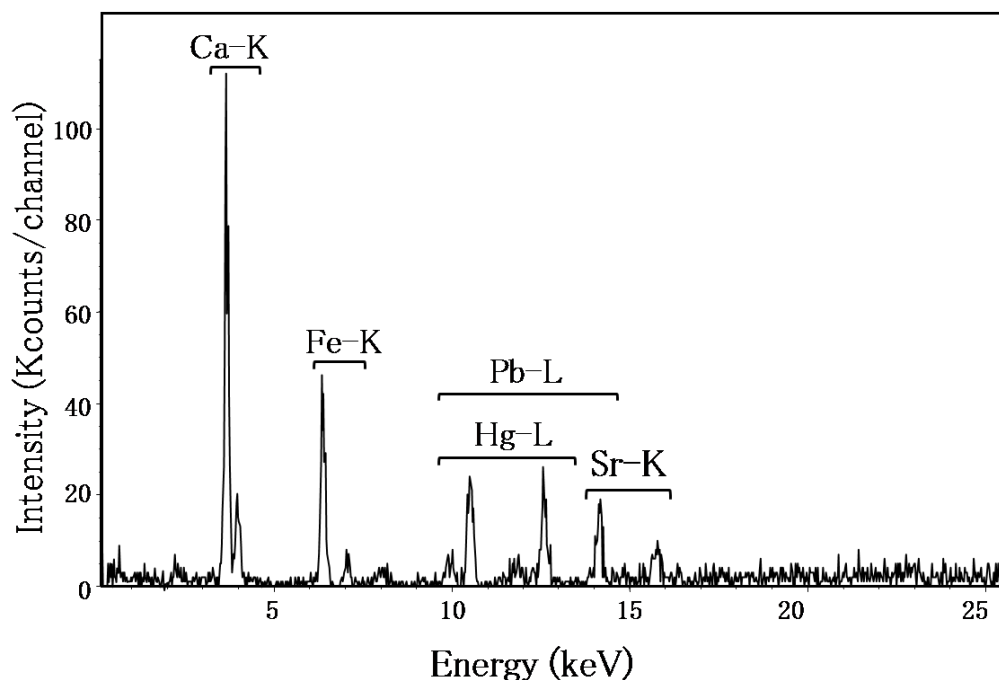


Figure 6.3 (b) XRF spectrum of the orange ground layer of the mediaeval vault painting, showing the presence of Ca, Fe, Pb and Hg.

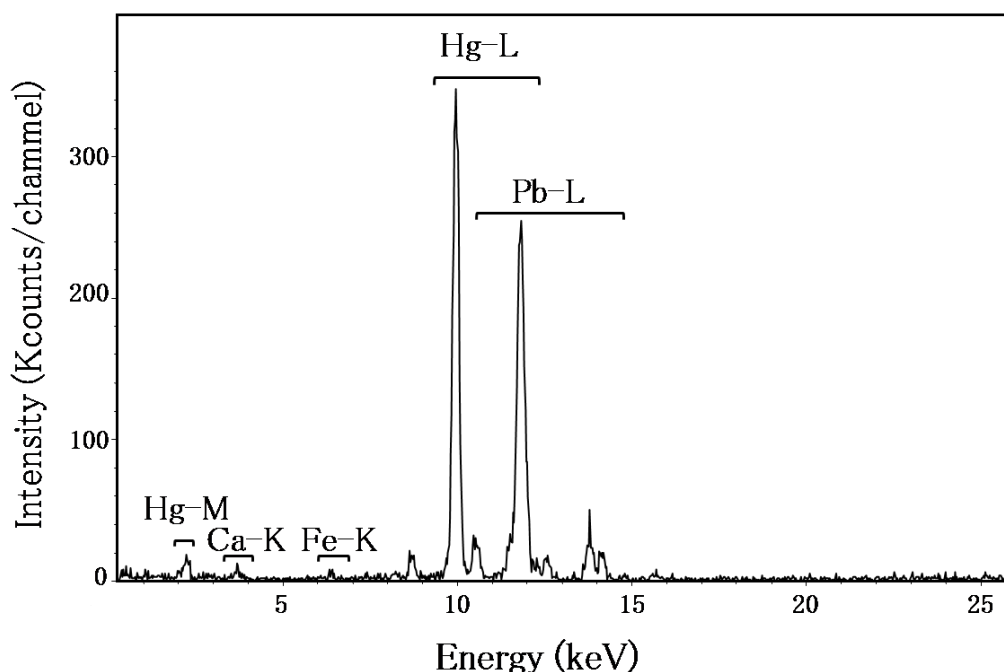


Figure 6.3 (c) XRF spectrum of the red top layer of the mediaeval vault painting, showing the presence of Ca, Fe, Pb, Hg.

These results suggest that vermilion (HgS) is applied on top of a ground layer containing small amounts of hematite (Fe_2O_3) and vermilion (HgS). With Raman spectroscopy the XRF results could only be confirmed for the red top layer. In the Raman spectrum (Fig. 6.3(d)) the Raman bands of vermilion (257 , 286 and 345 cm^{-1}) are clearly present.

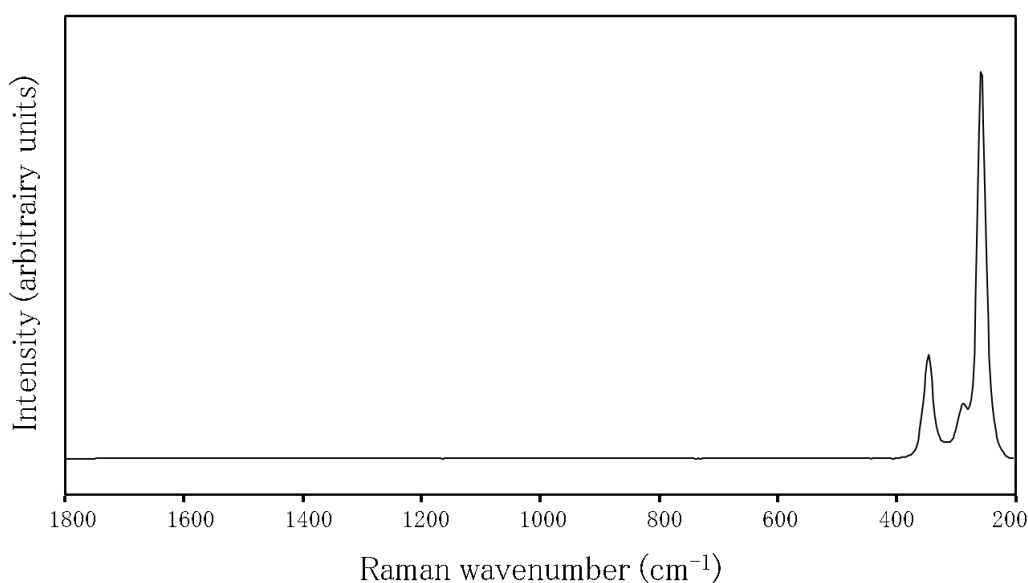


Figure 6.3 (d) Raman spectrum of the red top layer of the mediaeval vault painting, showing the spectrum of vermilion (HgS).

Vermilion (HgS) was already used as a pigment by the Chinese people 2000 years before the Romans did. This red pigment is made by crushing, washing and heating the mineral cinnabar (HgS) to give a strong red pigment. Alternatively, this compound could also be made by heating a mixture of mercury with molten sulphur (dry-process vermilion)¹⁷. During the mediaeval period those two forms of vermilion (HgS) were available, but it is difficult to distinguish between them.

Vermilion (HgS) has excellent covering power owing to its high refractive index. The pigment is stable in alkaline conditions and can be painted over a fresh lime ground. This application has been confirmed in several English mediaeval wall paintings¹⁸. In some cases the red vermilion (HgS) forms a dark pigment, metacinnabar^{19,20}. Despite of the reactivity of vermilion (HgS) with pigments such as lead white ($2\text{PbCO}_3 \cdot \text{Pb}(\text{OH})_2$) and red lead (Pb_3O_4), it appears to be fairly stable, especially when an oil-based medium is used.

6.4.2.3 Green layers

The green leaves show different colour shades present in different paint layers (Fig. 6.4(b) and (c)). The XRF results of all the different green layers (Fig. 6.5(a) and (b)) show the presence of copper, lead and tin in different relative amounts (the relative amount of lead is lower for the darker green). This result can indicate that the green colour is a mixed colour of lead white ($2\text{PbCO}_3 \cdot \text{Pb}(\text{OH})_2$), lead-tin yellow type I (Pb_2SnO_4) and a green copper pigment. Identifying the green copper pigment was not possible with Raman spectroscopy, because of the absorbance of the laser light and the overwhelming fluorescence. These problems could be solved using a laser with another wavelength, but our mobile spectrometer has only one laser.

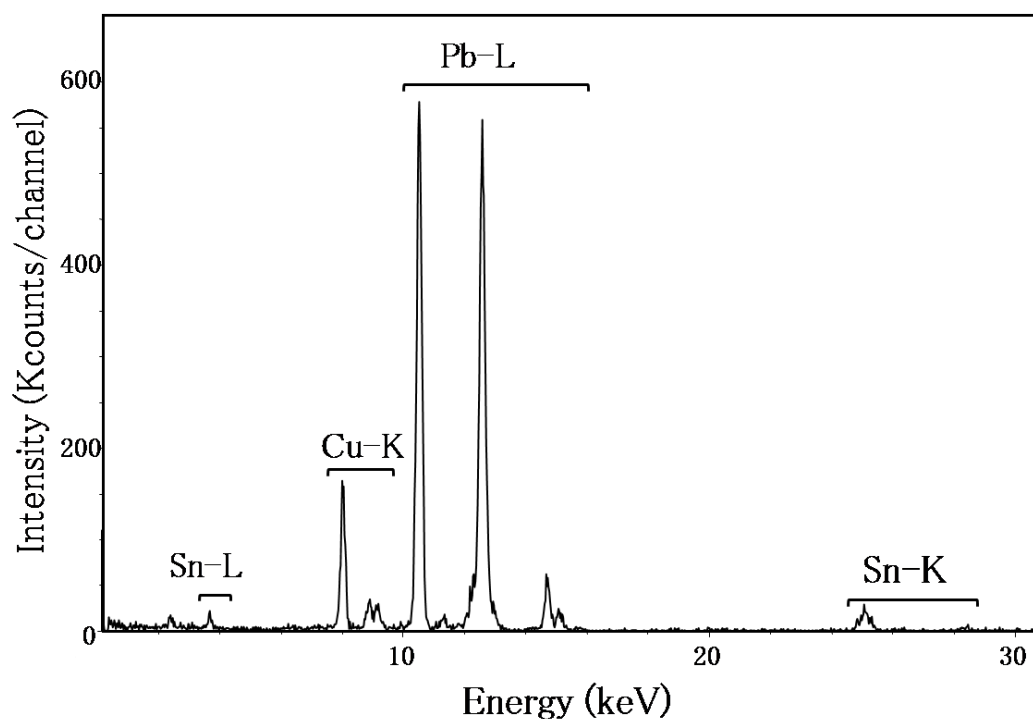


Figure 6.5 (a) XRF spectrum of the light green paint layer of the mediaeval vault painting, showing the presence of Cu, Sn, Pb.

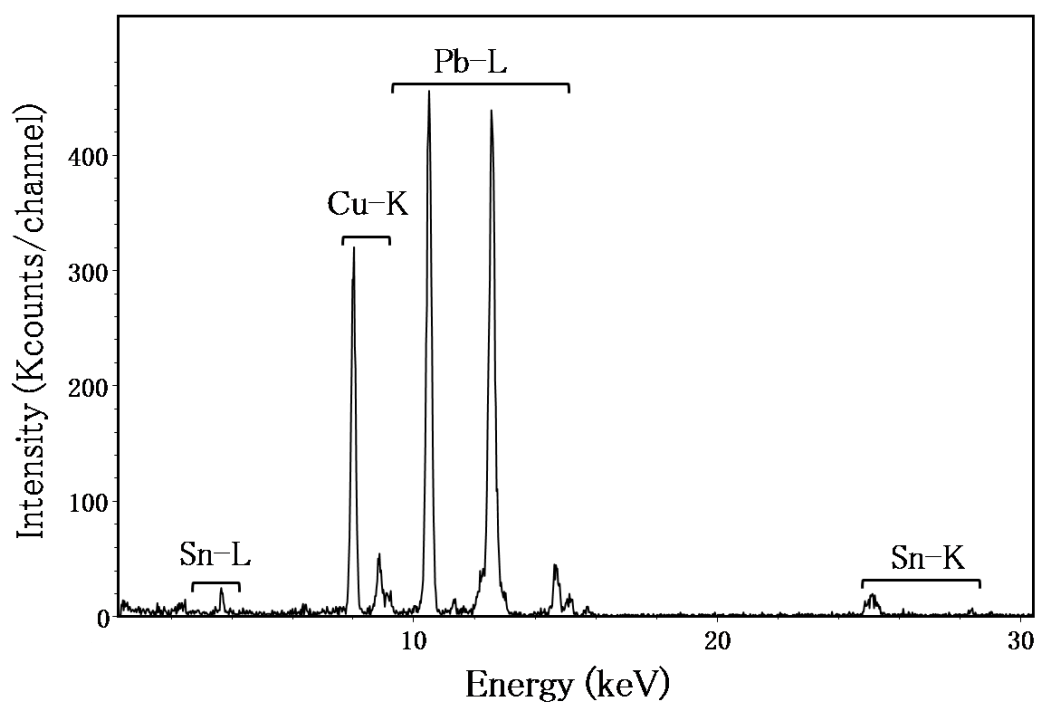


Figure 6.5 (b) XRF spectrum of the dark green paint layer of the mediaeval vault painting, showing the presence of Cu, Sn, Pb.

The XRF analysis of the white highlight (Fig. 6.5(c)) shows the same combination of elements. These results suggest lead white ($2\text{PbCO}_3 \cdot \text{Pb(OH)}_2$) on top of the mixed green colour.

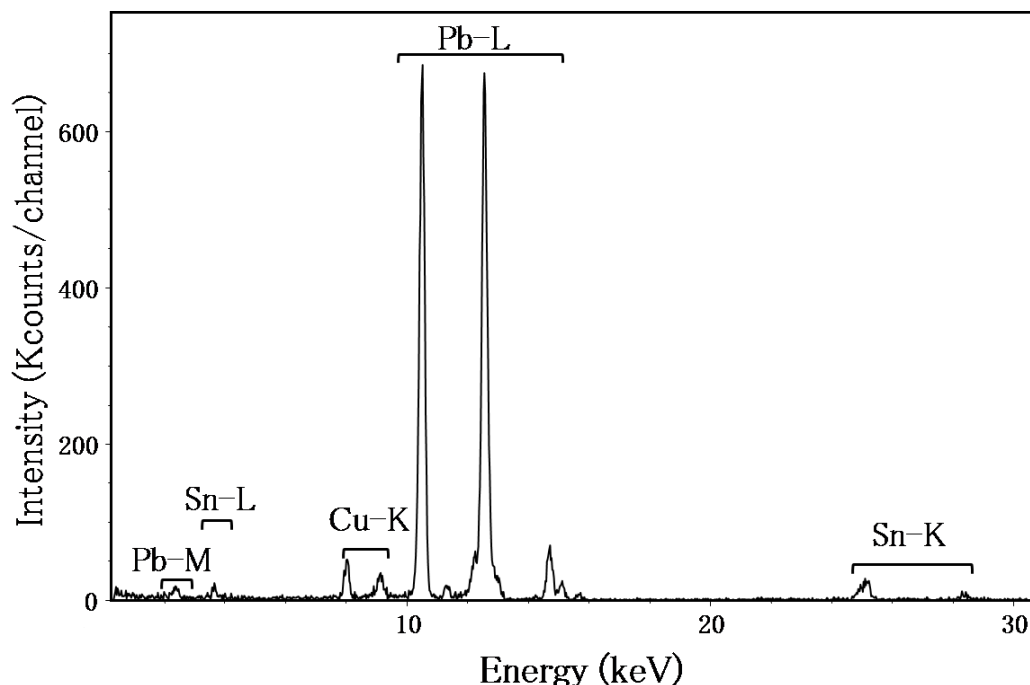


Figure 6.5 (c) XRF spectrum of a highlight of the mediaeval vault painting, showing the presence of Cu, Sn and Pb.

The Raman analysis confirms this conclusion for lead-tin yellow type I (Pb_2SnO_4) and lead white ($2\text{PbCO}_3 \cdot \text{Pb(OH)}_2$). The two forms of lead white ($2\text{PbCO}_3 \cdot \text{Pb(OH)}_2$), cerussite (PbCO_3) and hydrocerussite ($\text{Pb}_3(\text{CO}_3)_2(\text{OH})_2$) were not distinguished by Raman spectroscopy, because of the lack of reference materials. The spectrum shows Raman bands of lead-tin yellow type I (527 , 451 and 195 cm^{-1}), lead white (1052 cm^{-1}) and massicot (289 cm^{-1}). The strongest Raman band of calcite (1084 cm^{-1}) is also present in the spectrum (Fig. 6.5(d)).

During the centuries there was a widespread confusion on the identity of lead-tin yellow type I (Pb_2SnO_4). In manuscripts, lead-tin yellow type I (Pb_2SnO_4) was very often confused with massicot (PbO). However, there can be concluded that lead-tin yellow type I (Pb_2SnO_4) was used as a pigment in the Middle Ages²¹. Due to the high refractive indices of lead-tin yellow type I (Pb_2SnO_4), it has a good hiding power

when combined in oil medium. Lead–tin yellow type I (Pb_2SnO_4) is extremely stable in alkaline conditions and can be used in both, fresco and secco paintings. Exposure to soluble sulphides or hydrogen sulphide may induce darkening, with the formation of black lead sulphide (galena).

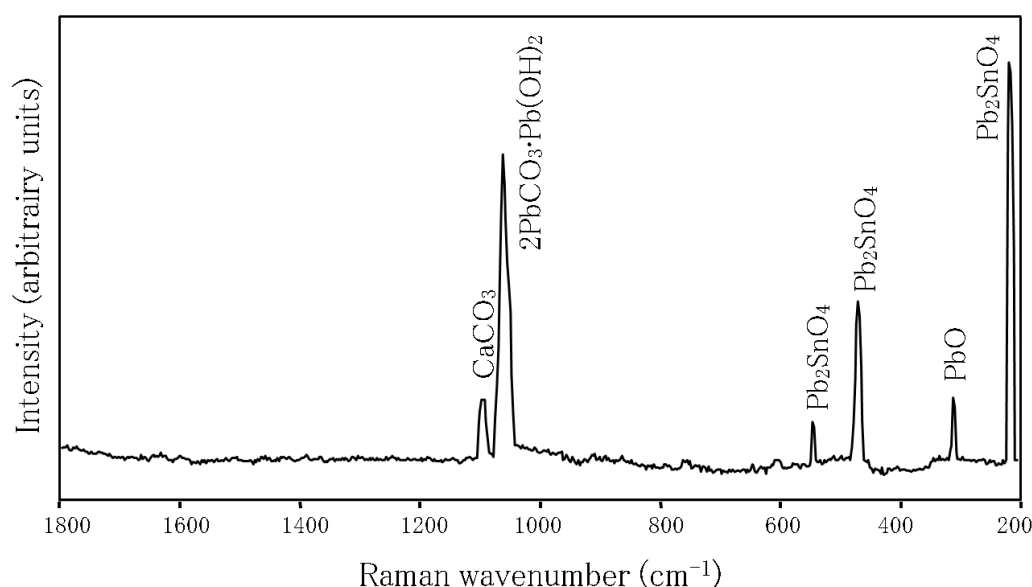


Figure 6.5 (d) Raman spectrum of the green top layer of the mediaeval vault painting, showing a combined spectrum of calcite (CaCO_3), lead white ($2\text{PbCO}_3 \cdot \text{Pb}(\text{OH})_2$), lead–tin yellow type I (Pb_2SnO_4) and massicot (PbO).

Lead white ($2\text{PbCO}_3 \cdot \text{Pb}(\text{OH})_2$) was manufactured since the Greek period. It was used by the Greco–Roman ladies as face powder with predictable effects on their health¹⁷. The pigment was manufactured by stacking lead strips in porous jars with vinegar and burying the jars in animal manure, which generated the heat necessary to speed up the reaction. The physical structure of lead white ($2\text{PbCO}_3 \cdot \text{Pb}(\text{OH})_2$) and its reaction with oil gives a very flexible, quick drying, and permanent paint film. Lead white ($2\text{PbCO}_3 \cdot \text{Pb}(\text{OH})_2$) is stable to light, but on heating to low temperatures this pigment turns yellow through the formation of massicot (PbO), while further sustained heating will produce litharge, and finally red lead (Pb_3O_4). Characteristics as alkaline conditions, high humidity and the presence of an

oxidising agent stimulate the darkening process of the lead oxide until it forms a black lead oxide. The pigment is also sensitive to sulphides through the formation of lead sulphide (black). However, in many English mediaeval wall paintings where lead white ($2\text{PbCO}_3 \cdot \text{Pb}(\text{OH})_2$) is combined with vermilion (HgS) no alteration was observed¹⁸. Lead white ($2\text{PbCO}_3 \cdot \text{Pb}(\text{OH})_2$) remained the most used white pigment until the 19th century.

Massicot (PbO) has excellent covering and colouring power. The pigment is compatible with most pigments, except for sulphides. Massicot (PbO) is frequently used as siccativ in oil paint²².

6.4.2.4 Blue layers

The blue paint is applied in two layers: a dark blue layer as supporting layer; and a light blue layer on top of it (Fig. 6.4(d)). XRF measurements on these two blue layers show a surprising result: the light blue paint (Fig. 6.6(a)) contains an important quantity of copper, probably indicating the pigment azurite ($2\text{CuCO}_3 \cdot \text{Cu}(\text{OH})_2$), while only small amounts of copper are detected in the dark blue area (Fig. 6.6(b)).

As both ultramarine ($\text{Na}_{8-10}\text{Al}_6\text{Si}_6\text{O}_{24}\text{S}_{2-4}$) and indigo (organic) cannot be detected using XRF measurements, no identification is made here. Also for the Raman measurements no conclusion could be made, because blue pigments produce a lot of severe fluorescence.

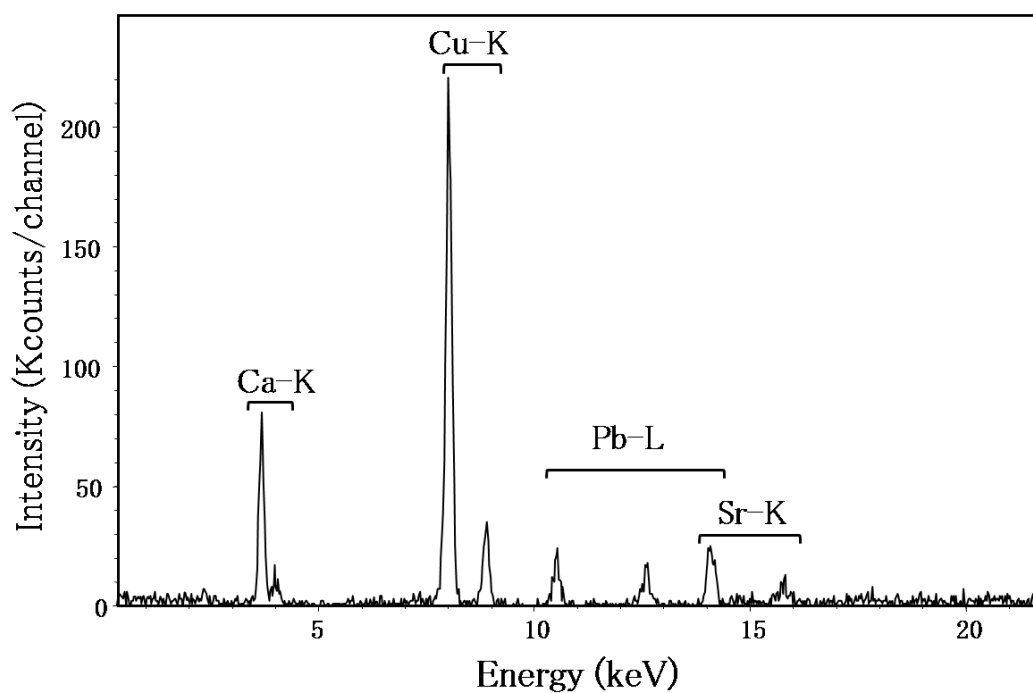


Figure 6.6 (a) XRF spectrum of the light blue paint layer of the mediaeval vault painting, showing the presence of Ca, Cu and Pb.

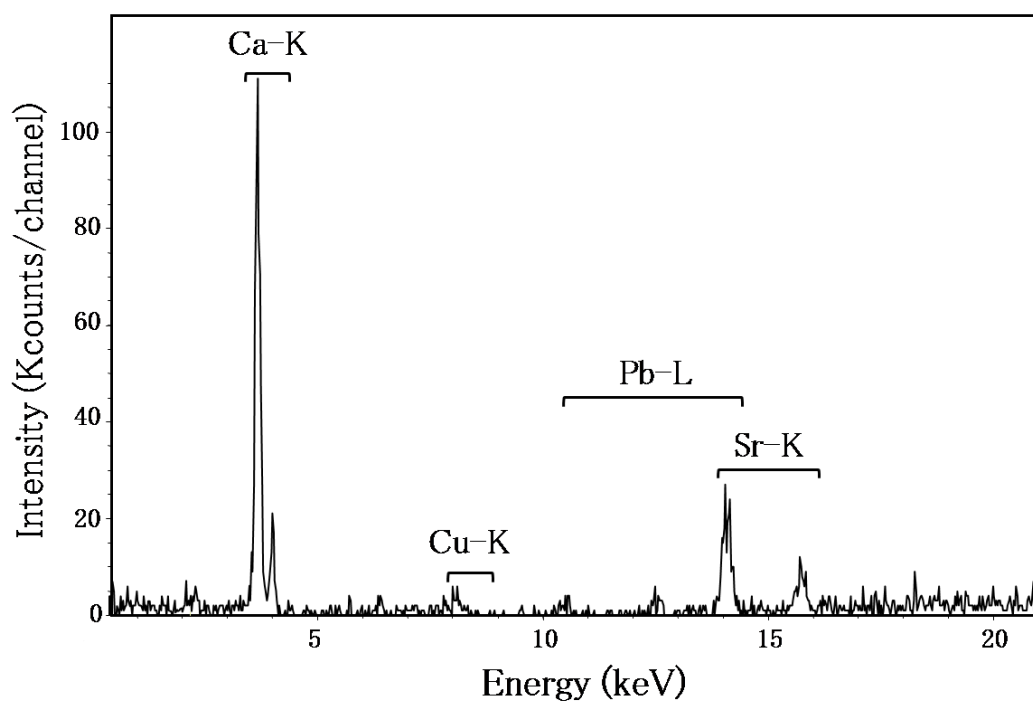


Figure 6.6 (b) XRF spectrum of the dark blue paint layer of the mediaeval vault painting, showing the presence of Ca, Cu and Pb.

6.4.3 Pigment identification of the renaissance vault painting

For the renaissance painting, more than 50 zones were selected for XRF analysis. Based on the results of the XRF analysis, 34 zones were selected to analyse with Raman spectroscopy. Due to problems with the optical fibres and filters in the probe head, it was difficult to get a good signal-to-noise ratio in the Raman spectra. However, using this multi-method approach allows identifying the most important pigments used in this vault painting.

6.4.3.1 Supporting layer

The material used as supporting layer is also calcite (CaCO_3) (Fig. 6.7(a)). But, in almost all registered XRF spectra, an important peak corresponding to lead is present (Fig. 6.6(c)).

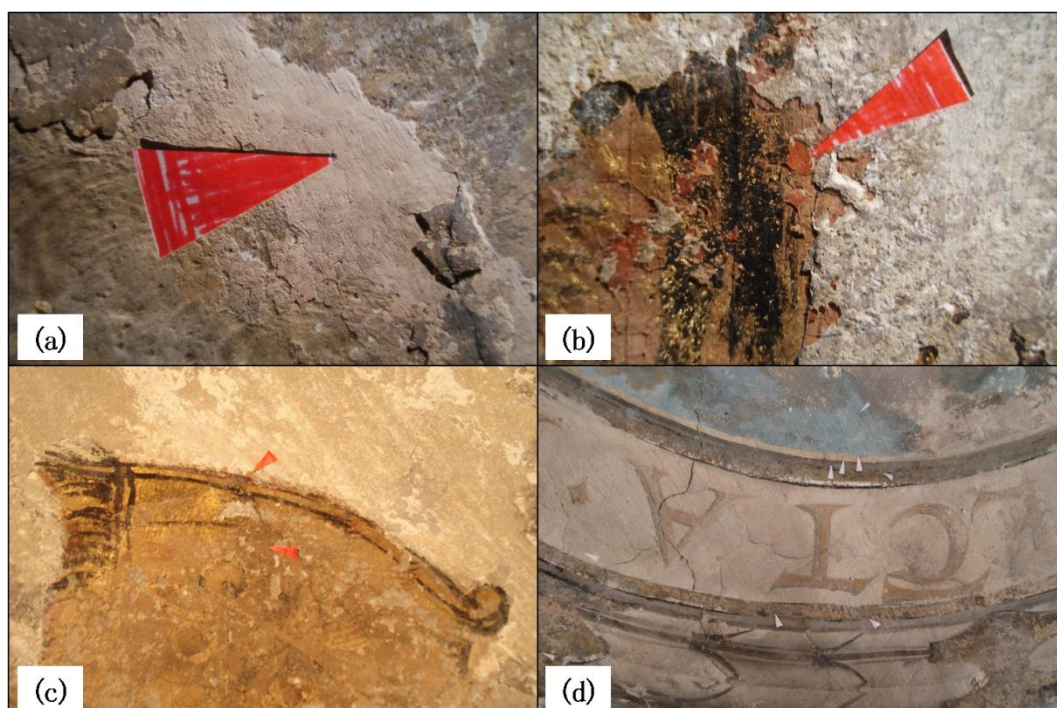


Figure 6.7 Some details of the renaissance vault painting in the Antwerp cathedral; (a) detail of the analysed ground layer; (b) detail of the different analysed red layers; (c) detail of the golden decoration and (d) detail of the analysed blue layer.

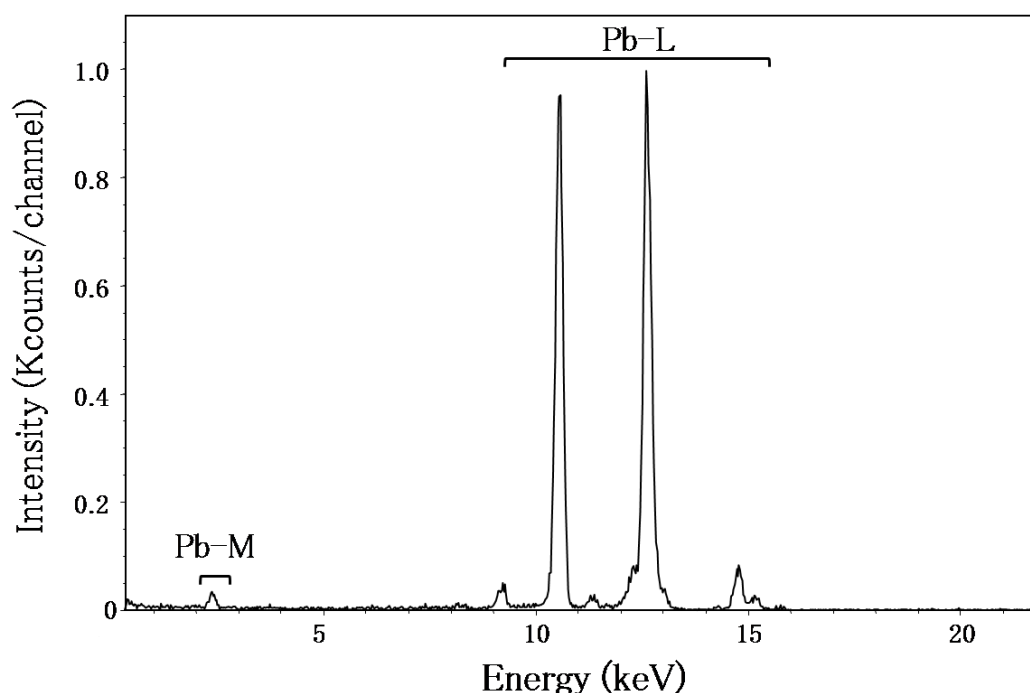


Figure 6.6 (c) XRF spectrum of the ground layer of the renaissance vault painting, showing the presence of Pb.

This is the case for grey white colours, for ‘real’ colours and for all parts in the painting (background, architectural part and figurative part). These results can indicate that lead white ($2\text{PbCO}_3 \cdot \text{Pb}(\text{OH})_2$) was used as first layer in the construction of the painting. With Raman spectroscopy the results were similar.

6.4.3.2 Red layers

The bright red paint (Fig. 6.7(b)) applied for the architecture painting does not contain any mercury, excluding the presence of vermilion (HgS). As shown in the XRF spectrum (Fig. 6.6(d)), only lead and iron are detected, suggesting that the red paint layer contains iron oxide (hematite (Fe_2O_3)). Raman spectroscopy confirms this result. In the Raman spectrum (Fig. 6.8(a)) the Raman bands of hematite (224, 290, 412 and 617cm^{-1}) are clearly present. Next to the Raman bands of hematite (Fe_2O_3), the Raman bands of red lead (312 and 552cm^{-1}) could be observed.

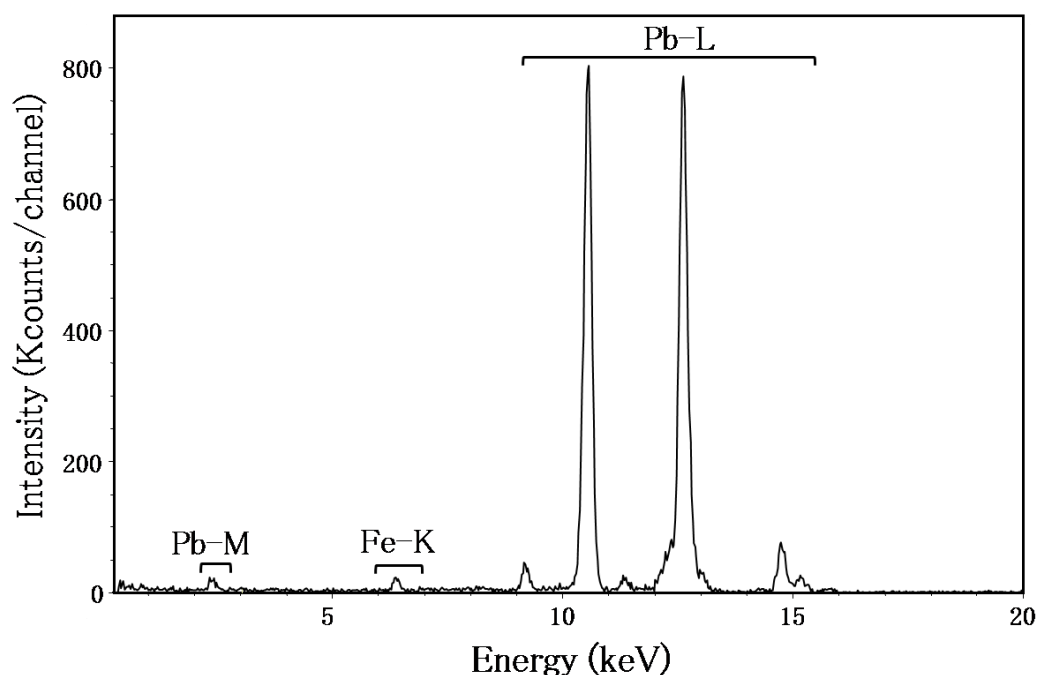


Figure 6.6 (d) XRF spectrum of the bright red paint layer of the renaissance vault painting, showing the presence of Fe and Pb.

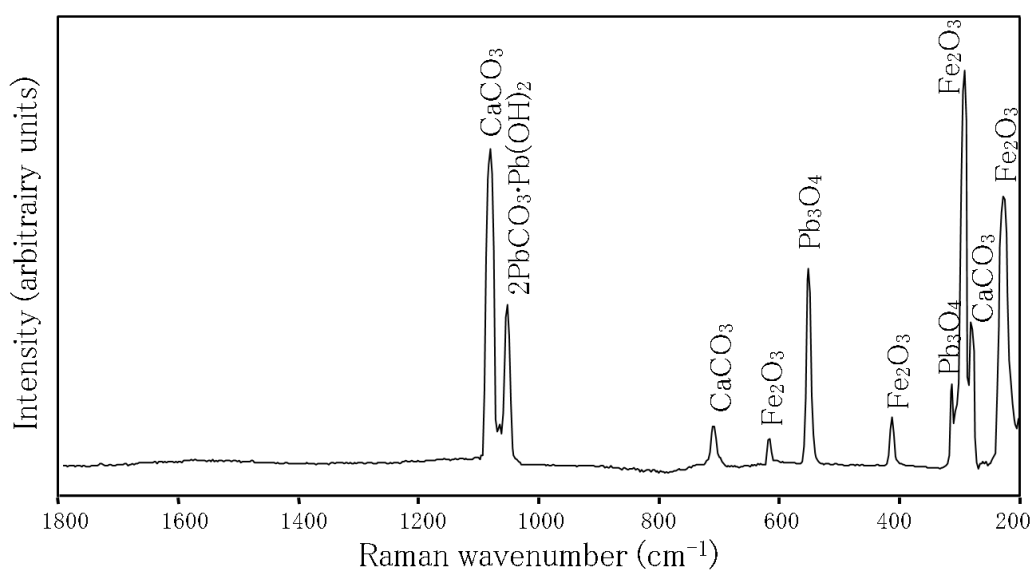


Figure 6.8 (a) Raman spectrum of the red top layer of the renaissance vault painting.

The Raman spectrum also confirms the presence of lead white (1050 cm⁻¹), painted as first layer on the calcite (CaCO₃). It is strange that no vermilion (HgS) was used for the red bright colour. Normally hematite (Fe₂O₃) is used for an underlying paint

layer and not for the top layer. The renaissance vault painting does not have this type of layered structure. To answer the question, why the artist made use of hematite (Fe_2O_3) for the red top layer, further research, where different paintings from the same artist are compared, is necessary.

Hematite (Fe_2O_3) has a high pigmenting strength and although it provides the colour of the earth pigment, it may be present in relatively low concentrations combined with a number of accessory minerals such as quartz, kaolin and other clays. Hematite (Fe_2O_3) is very stable, durable and is suitable for use both in alkaline conditions and combined with a wide range of organic binding media. However, on prolonged heating the pigment will oxidise. There are innumerable examples of the use of hematite (Fe_2O_3) in England and elsewhere in Europe throughout the Middle Ages¹⁸.

The use of red lead (Pb_3O_4) was developed by the Greeks. Red lead (Pb_3O_4) was used for priming metal in construction until it was banned in the 1990s. It is a form of lead oxide (Pb_3O_4) and is found as the mineral minium after the river Minius in the northwest of Spain. There is little evidence to suggest that the natural mineral was used as a pigment, but from the earliest times the synthetic pigment was well known and often employed.

An important characteristic of red lead (Pb_3O_4) is its drying action on oils. The pigment is not stable in alkaline condition and cannot be used on a fresh layer of lime wash or in combination with lime white. Red lead (Pb_3O_4) darkens after some time, because it forms plattnerite (PbO_2). Despite of all this limitations, red lead (Pb_3O_4) was often used in wall paintings¹⁸.

6.4.3.3 Gold and tin layer

Another feature of the renaissance paintings is the use of gold and tin. In a lacuna of the golden banner (Fig. 6.7(c)), a brown red preparation layer is visible.

XRF measurements of this layer show the presence of lead, calcium, iron and traces of gold as remaining of the upper decoration layer (Fig. 6.8(b)). Based on this analysis it is not clear whether part of the lead is present as red lead (Pb_3O_4) mixed with hematite (Fe_2O_3) in the preparation layer for the gold. Remaining of the gold is still detectable in the lacuna. Some measured areas, like the border of the medallions (Fig. 6.7(d)), reveal the presence of tin. In these cases the tin in the resulting XRF spectrum (Fig. 6.8(c)) does not indicate the use of a tin containing pigment (like lead–tin yellow type I (Pb_2SnO_4)), but confirms the presence of a metal foil (hence a tin foil). Although the use of tin foil is best known for the brocade decorations on painted wooden sculptures, its use on mural paintings was already practiced by Giotto²³.

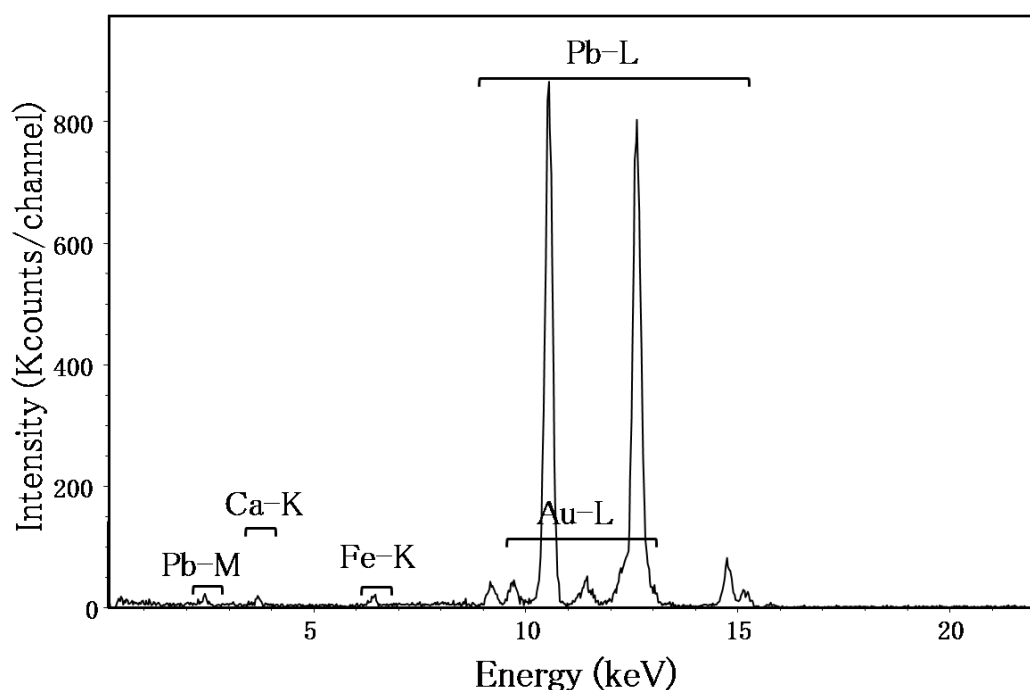


Figure 6.8 (b) XRF spectrum of the preparation layer for the gold of the renaissance vault painting, showing the presence of Ca, Au, Fe and Pb.

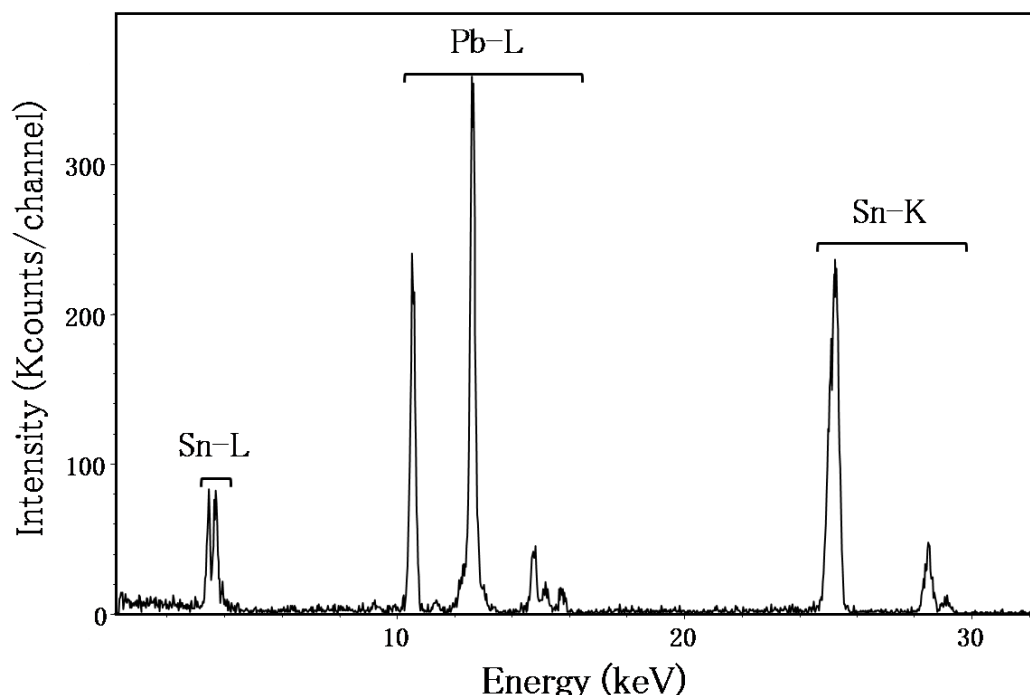


Figure 6.8 (c) XRF spectrum of the tin foil of the renaissance vault painting, showing the presence of Sn and Pb.

6.4.3.4 Blue layers

XRF analysis of the blue paint inside the medallions (Fig. 6.7(d)) shows clearly the presence of azurite ($2\text{CuCO}_3 \cdot \text{Cu}(\text{OH})_2$), as evidenced by the copper peak in the resulting spectrum (Fig. 6.8(d)). Azurite ($2\text{CuCO}_3 \cdot \text{Cu}(\text{OH})_2$) is the natural pigment of a basic copper carbonate. This pigment was used in wall paintings from antiquity till the 19th century and was in the Middle Ages, next to ultramarine ($\text{Na}_{8-10}\text{Al}_6\text{Si}_6\text{O}_{24}\text{S}_{2-4}$), the most important blue pigment. In the Middle Ages important deposits of the mineral were exploited in Hungary and France²⁴.

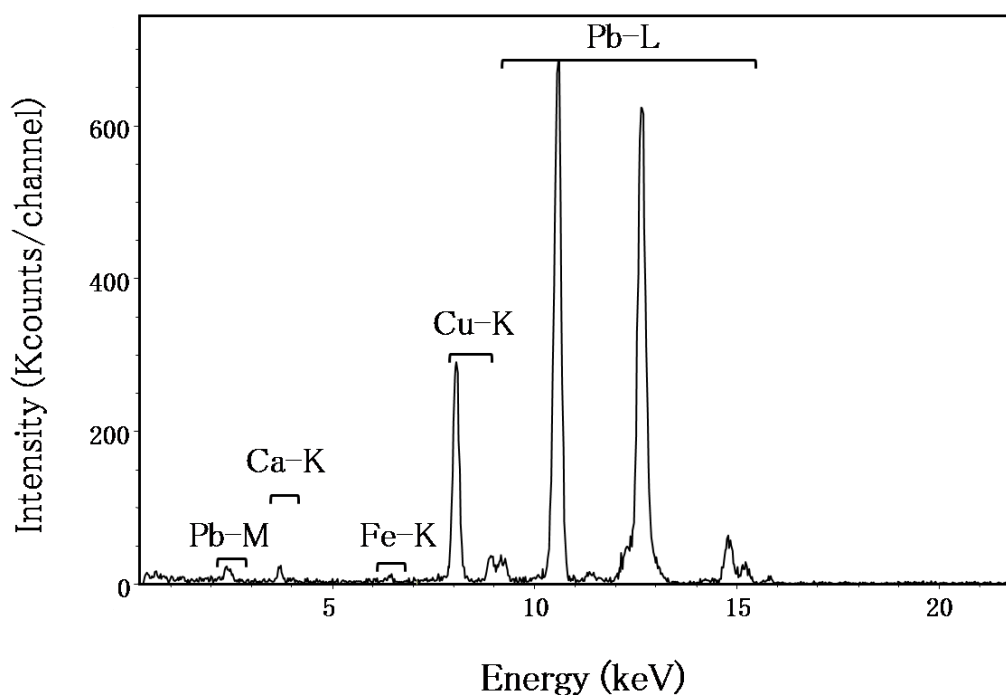


Figure 6.8 (d) XRF spectrum of the blue paint layer of the renaissance vault painting, showing the presence of Ca, Fe, Cu and Pb.

6.5 Conclusions

The results of this research show that this *in situ* multi-method approach, where a combination of X-ray fluorescence spectroscopy and Raman spectroscopy is used, provides valuable information on the composition of the vault paintings. While performing the measurements some feasible problems appear, which can easily be solved. Because XRF spectroscopy is a very fast technique, this method can be used for a preliminary research. An overview of the identified pigments of the mediaeval vault painting is summarized in table 6.1. Table 6.2 shows the identified pigments of the renaissance vault painting. The use of Raman spectroscopy, revealed the presence of calcite (CaCO_3) and gypsum ($\text{CaSO}_4 \cdot 2\text{H}_2\text{O}$). The presence of gypsum ($\text{CaSO}_4 \cdot 2\text{H}_2\text{O}$) could be related to contamination of water containing salts. In some cases, when the Raman spectrum was overwhelmed by fluorescence,

the results of the XRF measurements were unambiguous and could be used to give definite pigment identifications. This multi-method approach also revealed that the renaissance painting has a strange layered structure. It is not common to use hematite for the red top layer. The combination of XRF spectroscopy and Raman spectroscopy revealed a lot of valuable information on the vault paintings in the Our Lady's Cathedral in Antwerp (Belgium).

colour	pigment	chemical composition
white	lead white	$2\text{PbCO}_3 \cdot \text{Pb}(\text{OH})_2$
	calcite	CaCO_3
	gypsum	$\text{CaSO}_4 \cdot 2\text{H}_2\text{O}$
yellow	lead-tin yellow type I	Pb_2SnO_4
red	vermilion	HgS
green	Cu-green	not identified
blue	azurite	$2\text{CuCO}_3 \cdot \text{Cu}(\text{OH})_2$
	/(no Cu)	not identified

Table 6.1 Summary of the pigments identified in the 15th century mediaeval wall painting on the vault of the Our Lady's Cathedral, Antwerp (Belgium).

colour	pigment	chemical composition
white	lead white	$2\text{PbCO}_3 \cdot \text{Pb}(\text{OH})_2$
	calcite	CaCO_3
red	red lead	Pb_3O_4
	hematite	Fe_2O_3
blue	azurite	$2\text{CuCO}_3 \cdot \text{Cu}(\text{OH})_2$

Table 6.2 Summary of the pigments identified in the 16th century renaissance wall painting on the vault of the Our Lady's Cathedral, Antwerp (Belgium).

This study is a good example to express the complementary character of Raman spectroscopy and XRF spectroscopy. Raman spectroscopy gives molecular information, while XRF spectroscopy delivers elemental information. With Raman spectroscopy it is possible to identify the pigment immediately, because each pigment has his own unique Raman spectrum. The disadvantages of Raman spectroscopy are the weak intensity of the Raman signal and the interference of fluorescence. Especially for the green pigments fluorescence is a problem. Therefore we were not able to identify the blue and green pigments. In contrary XRF spectroscopy could identify the elemental composition of these two pigments. Due to the knowledge of the elemental composition, the blue pigment could be identified. For the green pigment no identification could be made based on the XRF results, because many green pigments contain copper.

In this study, a combined approach of two techniques was used to gather information on the pigments used and a possible deterioration product of two vault paintings. In the next chapter a combined approach is used for the analysis of the precious mediaeval manuscript Liber Floridus. In this study a combination of mobile Raman spectroscopy, laboratory Raman spectroscopy, laboratory XRF spectroscopy, UV-fluorescence photography and infrared reflectography (IRR) is used.

References

1. Edwards, H.G.M., Farwell, D.W., Perez, F.R., Villar, S.J. (1999) Spanish mediaeval frescoes at Basconcillos del Tozo: a Fourier transform Raman spectroscopic study. *Journal of Raman Spectroscopy* 30: 307–311.
2. Smith, G.D., Clark, R.J.H. (2002) The role of H₂S in pigment blackening. *Journal of Cultural Heritage* 3: 101–105.
3. Seaward, M.R.D., Edwards, H.G.M. (1997) Biological origin of major chemical disturbances on ecclesiastical architecture studied by Fourier transform Raman spectroscopy. *Journal of Raman Spectroscopy* 28: 691–696.
4. Edwards, H.G.M., Russell, N.C., Seaward, M.R.D., Slarke, D. (1995) Lichen biodeterioration under different microclimates: An FT Raman spectroscopic study. *Spectrochimica Acta Part A-Molecular and Biomolecular Spectroscopy* 51: 2091–2100.
5. Vandenabeele, P., Edwards, H.G.M., Moens, L. (2007) A decade of Raman spectroscopy in art and archaeology. *Chemical Reviews* 107: 675–686.
6. Perardi, A., Appolonia, L., Mirti, P. (2003) Non-destructive *in situ* determination of pigments in 15th century wall paintings by Raman microscopy. *Analytica Chimica Acta* 480: 317–325.
7. Perez-Alonso, M., Castro, K., Madariaga, J.M. (2006) Investigation of degradation mechanisms by portable Raman spectroscopy and thermodynamic speciation: The wall painting of Santa Maria de Lemoniz (Basque Country, North of Spain). *Analytica Chimica Acta* 571: 121–128.
8. Rosi, F., Miliani, C., Borgia, I., Brunetti, B., Sgamellotti, A. (2004) Identification of nineteenth century blue and green pigments by *in situ* x-ray

- fluorescence and micro-Raman spectroscopy. *Journal of Raman Spectroscopy* 35: 610–615.
9. Paternoster, G., Rinzivillo, R., Nunziata, F., Castellucci, E.M., Lofrumento, C., Zoppi, A., Felici, A.C., Fronterotta, G., Nicolais, C., Piacentini, M., Sciuti, S., Vendittelli, M. (2005) Study on the technique of the Roman age mural paintings by micro-XRF with Polycapillary Conic Collimator and micro-Raman analyses. *Journal of Cultural Heritage* 6: 21–28.
 10. Sawczak, M., Kaminska, A., Rabczuk, G., Ferretti, M., Jendrzewski, R., Sliwinski, G. (2009) Complementary use of the Raman and XRF techniques for non-destructive analysis of historical paint layers. *Applied Surface Science* 255: 5542–5545.
 11. Ricci, C., Borgia, I., Brunetti, B.G., Miliani, C., Sgamellotti, A., Seccaroni, C., Passalacqua, P. (2004) The Perugino's palette: integration of an extended *in situ* XRF study by Raman spectroscopy. *Journal of Raman Spectroscopy* 35: 616–621.
 12. Goodall, R.A., Hall, J., Edwards, H.G.M., Sharer, R.J., Viel, R., Fredericks, P.M. (2007) Raman microprobe analysis of stucco samples from the buildings of Maya Classic Copan. *Journal of Archaeological Science* 34: 666–673.
 13. Burgio, L., Clark, R.J.H., Muralha, V.S.F., Stanley, T. (2008) Pigment analysis by Raman microscopy of the non-figurative illumination in 16th–to 18th–century Islamic manuscripts. *Journal of Raman Spectroscopy* 39: 1482–1493.
 14. Castro, K., Perez-Alonso, M., Rodriguez-Laso, M.D., Etxebarria, N., Madariaga, J.M. (2007) Non-invasive and non-destructive micro-XRF and micro-Raman analysis of a decorative wallpaper from the beginning of the 19th century. *Analytical and Bioanalytical Chemistry* 387: 847–860.

15. Grieten, S., Bungeneers, J. (1996) Inventaris van het kunstpatrimonium van de provincie. *Antwerpen*, 3 233.
16. Vandenabeele, P., Weis, T.L., Grant, E.R., Moens, L.J. (2004) A new instrument adapted to *in situ* Raman analysis of objects of art. *Analytical and Bioanalytical Chemistry* 379: 137–142.
17. Barnett, J.R., Miller, S., Pearce, E. (2006) Colour and art: A brief history of pigments. *Optics and Laser Technology* 38: 445–453.
18. Howard H. (2003) *Pigments of English Medieval Wall Paintings*. Chapter 5 Red pigments. Archetype Publications, London, 97–140.
19. Keune, K., Boon, J.J. (2007) Analytical imaging studies of cross-sections of paintings affected by lead soap aggregate formation. *Studies in conservation* 52: 161–176.
20. Cotte, M., Susini, J., Metrich, N., Moscato, A., Gratzu, C., Bertagnini, A., Pagano, M. (2006) Blackening of Pompeian cinnabar paintings: X-ray microspectroscopy analysis. *Analytical Chemistry* 78: 7484–7492.
21. Howard H. (2003) *Pigments of English Medieval Wall Paintings*. Chapter 4 Green pigments. Archetype Publications, London, 65–96.
22. Schramm HP, Hering B. (1988) *Historische Malmaterialien und ihre identifizierung*. Chapter 4 Pigmente, Farb-und Füllstoffe. Akademische Druck- u. Verlagsanstalt, Graz, 19–78.
23. Marabelli, M., Sanopadre, P., Ioele, M., Cesareo, R., Castellano, A., Verità, M. (2005) Metal leaves utilised for decoration of Giotto's mural paintings, *Bollettino d'arte* special volume: 121–144.

24. Howard H. (2003) *Pigments of English Medieval Wall Paintings*. Chapter 3 Blue pigments. Archetype Publications, London, 27–64.

Chapter 7: The use of a multi-method approach to identify the pigments in the 12th century manuscript

Liber Floridus

Annelien Deneckere, Martine De Reu, Maximiliaan Martens, Karen De Coene,
Bart Vekemans, Laszlo Vincze, Philippe De Maeyer, Peter Vandenabeele,
Luc Moens

Spectrochimica Acta Part A, 80 (2011) 125–132

In this study a combined approach is used to analyse the precious mediaeval manuscript Liber Floridus. In a first step in situ analysis was performed using the mobile Raman spectrometer, next to UV-fluorescence photography and infrared reflectography (IRR). Due to the promising results we were allowed to take samples, which were analysed with laboratory Raman spectroscopy and laboratory XRF spectroscopy. This chapter also includes the description of a sample preparation technique that allows us to use the sample for analysis with micro-Raman spectroscopy and micro-XRF spectroscopy.

7.1 Introduction

Although several historical, codicological and iconographical details of mediaeval manuscripts in general, and of the *Liber Floridus* in particular¹⁻⁴, have been extensively studied, the examination of the materials used is still in its infancy. For art historians it is important to have knowledge of the materials (pigments, binding media, substrates, etc.) and their provenance, to understand the ancient techniques, to attribute the manuscript to a particular artist or workshop, and to date the manuscript⁵. The identification of the pigments used in manuscripts is important, both for the possible conservation and restoration of the manuscript and also for implying information regarding the availability and use of the pigments at the time of production.

For this study, a combination of imaging and analytical techniques was used. Imaging techniques provide art historical information on the painting style and result in an image of the work by using electromagnetic radiation of different wavelengths. Analytical spectroscopic techniques provide information on the painting materials and use electromagnetic radiation to produce a spectrum, which allows the identification of the material. In this case infrared reflectography (IRR)^{6,7,8} and UV-fluorescence photography^{9,10} were used as imaging techniques, while for the

analytical techniques Raman spectroscopy and X-ray fluorescence (XRF) spectroscopy were used¹¹. Because of the ability of Raman spectroscopy to perform non-destructive molecule specific analysis, it became an important tool in the examination of works of art¹².

Combining this technique with an element-specific non-destructive technique, such as X-ray fluorescence (XRF) spectroscopy¹³, gives a powerful tool that allows identifying most of the pigments. In the last decade, the combination of Raman spectroscopy with XRF was successfully used for the identification of pigments in, amongst others, mural paintings¹⁴⁻¹⁷, easel paintings^{6,18}, painted stucco fragments¹⁹, wallpapers²⁰ and illuminated manuscripts²¹⁻²⁵.

7.2 The manuscript ‘*Liber Floridus*’

The *Liber Floridus* is an early 12th century encyclopaedia kept in the Ghent University Library. The text is written on 287 numbered parchment folios of about 310 × 210 mm. On the whole, the parchment is of poor quality: several pages are re-used (palimpsest) and many leaves consist of pieces of parchment sewn together. At some point, the manuscript was cropped, causing the partial loss of marginal notes and of decoration. Despite the poor quality of the writing surface, the encyclopaedia is lavishly illustrated and some of its miniatures have been considered masterpieces of Romanesque art.

The author, scribe and illuminator of this famous work is Lambert of Saint-Omer, a canon from the collegiate church of Our Lady at Saint-Omer (nowadays in northern France, in the 12th century the city was part of the county of Flanders). Little is known on the life of Lambertus of Saint-Omer. On folio 26v and folio 43v we are informed that his father was a canon too and died on the 27th of January in 1077. By consequence, we can deduce that Lambertus of Saint-Omer was probably born

before 1077 or at the latest in 1077. He ended his book in or shortly after June 1121. Most scholars assume that the author died shortly after ending his work.

The encyclopaedia is arranged by way of association, and not in a thematic or alphabetical order. In ca. 300 chapters, the most important knowledge of the early 12th century is summarized. We find information on theology, history, (natural) sciences, astrology, geography, the interaction of the micro cosmos with the macro cosmos, etc. The author focuses on the unity of the spiritual and the material world, the connection between earth and heaven. Through his attention for historical and genealogical data he gives Flanders and even Saint-Omer a place in world history.

As pointed out previously, the manuscript is lavishly decorated with miniatures. These pictures are so intensely interwoven with the text that they often replace the text as a medium. There are a lot of diagrams representing several aspects of the cosmos, and figural paintings of real animals (e.g. the lion) or imaginary ones (e.g. the griffin, the dragon), next to religious concepts (e.g. the devil, the Antichrist, the trees of virtues and vices) or historical persons (e.g. Alexander the Great, Charles the Bald, Lambertus of Saint-Omer).

The book was written in Saint-Omer. At least since the 13th century the book was part of the library of the Saint-Bavon abbey in Ghent. After the abolition of the abbey of Saint-Bavon in 1536, the manuscript belonged to the chapter of Saint-Bavon, the successor of the famous abbey. Shortly after the French Revolution and the following annexation of the Southern Netherlands by France, the manuscript was confiscated and integrated in the library of the École centrale du département de l'Escaut. Later this library became the city library of Ghent, and after the foundation of the University in 1817 it was given in permanent loan to Ghent University together with other books.

A digital version of the manuscript can be found on the website of the Ghent University Library²⁶.

7.3 Experimental

In situ Raman spectroscopy was performed on a selection of illuminations in the *Liber Floridus*, consisting of 13 folios and 1 bifolio. The positions of the investigations were conscientiously marked on prints of the manuscript. Following the initial phase, micro-samples were taken at the exact same positions of the *in situ* analysis. These samples were analysed with confocal micro-Raman spectroscopy and energy dispersive X-ray fluorescence spectroscopy (EDXRF). The selected folios were also analysed with UV-fluorescence photography and infrared reflectography (IRR).

In the initial phase, only direct Raman analysis was performed. The results of the direct analysis give an indication of the pigments used for the different colours. Following the initial phase, samples were taken and indirect Raman analysis was performed. Because of the better spectral resolution of the laboratory spectrometer and the possibility to adapt the circumstances in the laboratory, more detailed information of the samples could be gathered, and even traces of a degradation product could be indicated. In this study taking samples allowed us also to use the complementary technique X-ray fluorescence (XRF) spectroscopy.

7.3.1 Samples and sample preparation

Samples were taken at exactly the same points as measured during the *in situ* analysis. The samples were taken with a cotton swab (Q-tip), by gently rubbing over the surface of the manuscript as described previously²⁷. In the laboratory, the samples were fixed with n-hexane on ultralene, in order to be appropriate for Raman spectroscopy as well as for X-ray fluorescence spectroscopy.

Ultralene (SPEX CertiPrep Group, Metuchen, United States) is a polymer that is appreciated by XRF spectroscopy because no impurities are seen in the XRF

spectrum. On contrary, ultralene is Raman active, but because Raman spectroscopy is a surface technique, it almost does not interfere with the Raman signal of the sample fixed on the ultralene. Also pro-analysis n-hexane (Panreac, Barcelona, Spain) was used, so that no traces of impurities could disturb the XRF signal.

To fix the sample (Fig. 7.1), first we tap the cotton swab on a thin layer of ultralene, to transfer the sample. In a next step some droplets of n-hexane are used to fix the sample on the ultralene. In a last step the sample, fixed on the thin ultralene layer is placed in a holder, to be able to work in a flexible way with the sample.

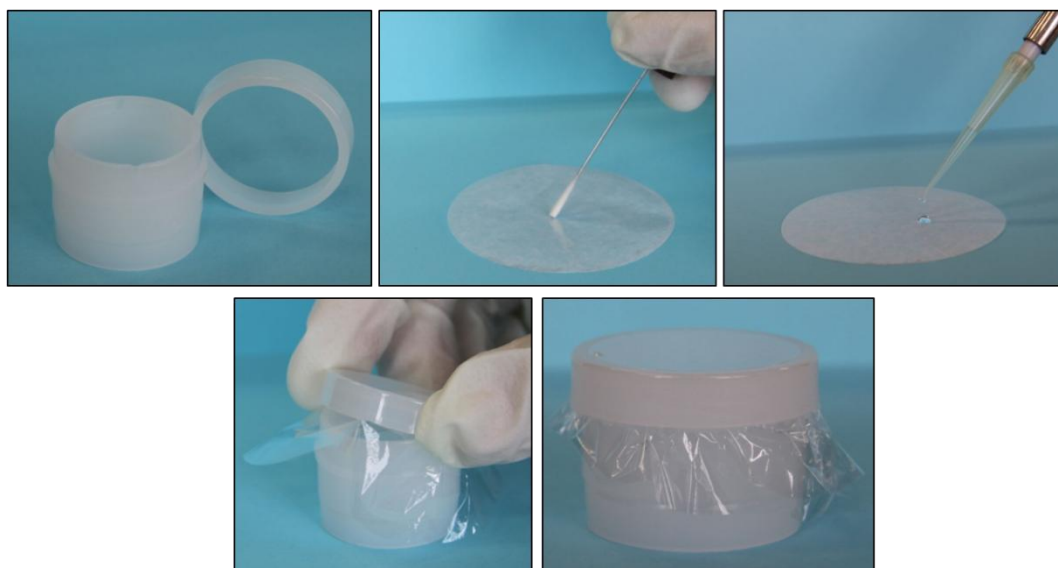


Figure 7.1 Sample preparation method: fixation with n-hexane on ultralene. After the fixation of the material on the ultralene thin film, the film itself is snapped into an X-ray cup that can be easily stored.

The collected Raman spectra were matched with a spectral library, created in-house, from inorganic and organic pigments and dyes.

During the first sampling, 64 samples were taken. During the second and third sampling we focused on folio 88r and respectively 7 and 12 new samples were taken.

7.3.2 Instrumentation

7.3.2.1 *In situ* Raman spectroscopy

Raman spectra were obtained using the Mobile Art Analyser (MArtA). This spectrometer contains a portable Raman imaging microscope (Spectracode, West Lafayette, IN, United States) and a SpectraPro 150i f.15 spectrometer (Roper Scientific, Princeton Instruments). More detailed information on the instrument has been described elsewhere²⁸.

The measurements were executed using a 600-grooves/mm dispersion grating and a 785 nm diode laser. Spectra were obtained in the spectral region between 100 and 2500 cm^{-1} . A 6 \times objective lens was used, giving a clearance of approximately 5 mm above the manuscript surface. The selected measurement point of the manuscript could be observed through a USB-controlled colour camera incorporated in the probe head. Micro-positioning and focussing was achieved using three motorised and remote-controlled micro-positioners (Oriel), with a working distance of 2.5 cm. Using the 6 \times objective lens, a spot size of approximately 50 μm was achieved. Extreme care was taken to avoid damaging the illumination with the laser beam: by adjusting the laser current, every measurement starts with a very low laser power. If necessary, the power is carefully increased in order to improve the signal-to-noise ratio.

7.3.2.2 Confocal micro-Raman spectroscopy

The laboratory Raman spectrometer used is a Bruker Optics ‘Senterra’ dispersive Raman spectrometer with a BX51 microscope. The Raman spectrometer is equipped with 532 (Nd:YAG) and 785 nm (diode) laser sources. High resolution spectra are recorded in 3 spectral windows, covering the 60–3700 cm^{-1} and 80–3500 cm^{-1} for

the 532 and 785 nm laser, respectively. The system uses a thermo-electrically cooled CCD detector, operating at -65°C . There are five software-controlled settings for the power of each laser: 100, 50, 25, 10 and 1%, i.e. up to ca. 35 mW at the sample for the 785 nm laser. The microscope has 5 \times , 20 \times and 50 \times objectives, with spot sizes of approximately 50, 10 and 4 μm , respectively. The microscope contains a joystick-controlled motorised stage and setting the analysis area is accomplished with the aid of an attached video camera. The instrument is controlled via the OPUS software version 6.5.6. Most samples were analysed using the 785 nm laser at 1–25% setting. All spectra were baseline-corrected for fluorescence.

7.3.2.3 Energy dispersive X-ray fluorescence spectroscopy (EDXRF)

A laboratory micro-XRF system (Eagle-III microprobe, EDAX, Inc., Mahwah, NJ, USA) provided elemental information of the samples. This spectrometer is equipped with a microfocus X-ray tube with a Rh anode, a polycapillary lens (X-ray Optical Systems, Inc., NY, USA) for X-ray focussing, and a 80 mm^2 energy dispersive Si-(Li) detector. The sample chamber incorporates a XYZ motorised stage for sample positioning. A high resolution microscope is used to position the sample on the desired distance from the polycapillary. To increase the sensitivity of the low Z elements, the sample chamber can be brought under vacuum. For analysing the samples a spot size of 25 μm was chosen at an operating X-ray tube voltage of 40 kV. The tube current was adapted for each sample in order to optimise the detection of X-rays corresponding to 30% detector dead time. In this work, measurements were done in vacuum typically for 1000 seconds each.

7.3.2.4 UV-fluorescence photography

The ultraviolet (UV) photographs of 13 single folios and three openings of the *Liber Floridus* were taken with a Nikon® D70 digital reflex camera with an 18–70 mm, f/3.5–4.5 lens. The object was illuminated with two commercially available UV lamps of 40 W (diameter 32, 1350 mm). Shutter times ranged between 15 and 20 seconds while a f/9.5 diaphragm and a focal length of 50 mm was used. Each folio was also photographed in the same conditions with a Cokin 85B orange filter, which sometimes allows a better clarity of the UV-image.

7.3.2.5 Infrared reflectography (IRR)

Infrared reflectograms of 14 single folios and three openings of the *Liber Floridus* were made with an OSIRIS infrared camera, operating at wavelengths from 900 to 1700 nm. The prototype of this camera was developed at the scientific department of the National Gallery London, and taken into production by Opus Instruments ltd²⁹. The OSIRIS camera has an InGaAs array sensor with an object resolution down to 0.05 mm. The 150 mm lens consists of 6 elements and has a focal length from f/5.6 to f/45. The image size is user selectable horizontally as well as vertically between 512 × 512 to 4096 × 4096 pixels. The practical advantage of this infrared camera is that it produces single, finished images rather than multiple images, which require further processing and stitching. The sharpness of the images is only enhanced by histogram correction and the application of a blurred mask in Adobe Photoshop®.

Single folios were recorded with a camera-object distance varying from 88 to 99 cm, a focal length varying from 37 to 44 mm, an f/16 diaphragm and indirectly illuminated at 2000 lx by reflectors with 2 × 300 W Tungsten Halogen Elinchrom Scanlite 300. Openings were taken with a camera-object distance varying from 108

to 111 cm, a focal length varying from 33 to 33.5 cm, a f/22 diaphragm and indirect illumination at 2200 lx.

7.4 Results and discussion

The results of the *in situ* Raman analysis, the analysis of the samples with micro-Raman spectroscopy and ED-XRF spectroscopy, and the analysis of the folios with UV-fluorescence photography are discussed by colour. Infrared reflectography was used to gather information on the underdrawing. Some examples of the investigated folios, together with the analysed points are shown in figure 7.2.



Figure 7.2 Illustration and indication of the measured points of (a) folio 25r, (b) folio 260r.



Figure 7.2 (c) Illustration and indication of the measured points of folio 88r.

7.4.1 Underdrawing

The preparatory page demarcation and lineation of some folios, executed in a dry black carbon containing material, possibly black chalk or charcoal, was revealed by infrared reflectography (IRR) on folios 6v, 13r, 20r, 25r, 52r, 88r, 222r and 260r. On some folios the lineation does not always correspond to line prickings, as on fol. 228v and on other folios the lineation is incised (e.g. fol. 58v, 231v–232).

Figurative underdrawing in the same carbon containing material was made visible on folios 6v, 13r, 231v–232, 232v, and 260r.

On fol. 6v, the contours, the facial features and the main folds of Audomarus are underdrawn. Faint lines around the globe on which he sits and besides his proper left upper arm suggest that a first drawing, perhaps in metalpoint, was reinforced by this more elaborate underdrawing.

The miniature representing Lambertus (fol. 13r) was fully underdrawn, including the architecture, the writer's chair and his working table. In executing the figure in ink, the artist just added some facial details, curls, a few drapery folds and text on his parchment. Nabucodonosor was similarly prepared in underdrawing (fol. 232v), while God the Father and the reclining woman were sparsely indicated with a few contour lines. The second representation of Audomarus (fol. 260r) (Fig. 7.3(a)) follows the same figurative underdrawing style. First, his upper part including his shoulders and halo was planned somewhat larger. In the underdrawing stage, the figure was reduced to his definitive size. He was placed originally before an irregular crucifix formed shape that included an inscription besides his head. This backdrop and the inscription were abandoned and painted over with purple paint, identified with Raman spectroscopy as hematite, and surrounded by a red border. Perhaps this was done when it was decided to identify him with a more elaborate inscription on the top of the folio. These are the only major compositional changes found during our IRR investigation of the selected folios.



Figure 7.3 (a) IR reflectograms of folio 260r.

In addition, the IRR investigation revealed the use of a compass for the circle segments. The pricked compass pigments can be distinguished: on folio 20r, in the circular motives of the labyrinth; on folio 52r, for the six circle fragments; on folio 88r, for the mandorla and the six circles; on bifolio 92v-93r, for the parallel circles of the map of Europe and on folios 228r and 228v.

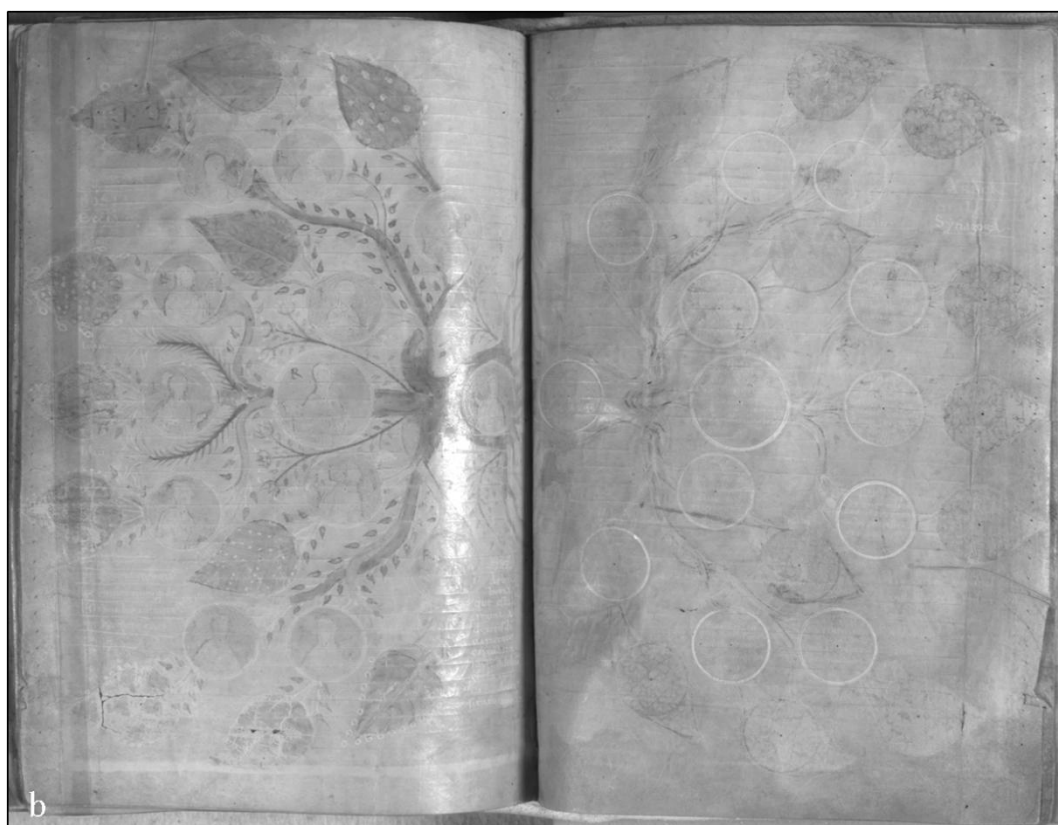


Figure 7.3 (b) IR reflectograms of bifolio 231v-232r.

Bifolio 231v-232r (Fig. 7.3(b)) is so perfectly symmetrical that it must be assumed that a copying method has been used to mirror the design of the left page of the opening onto the right one. The pink backgrounds of the virtues bear the colour indication 'R' for 'roseus'. This practise is mentioned in the famous contemporary art treatise by Theophilus³⁰. The contours of the virtues were underdrawn as well as some indications of the drapery folds of their garments. The contour of a branch or a leaf was on some places already indicated. In the leaf on the upper left of folio 231v, the trefoil-like motives were underdrawn as little triangles. The circles with

the virtues on the left side of the opening and with the texts describing the vices on the right hand side, as well as the basic circular form of the leaves were made with a compass.

7.4.2 Blue

Analysis of the blue colour was performed on illustrations of folios 6v, 13r, 24v, 25r, 58v, 88r, 88v, 89r, 222r and 259v, and on the illustration of bifolio 92v–93r. Both light and dark blue areas were analysed.

The *in situ* Raman analysis of the blue pigment showed for almost all folios and the bifolio, that ultramarine ($\text{Na}_{8-10}\text{Al}_6\text{Si}_6\text{O}_{24}\text{S}_{2-4}$) is used as blue pigment. In this case the natural form of ultramarine is used, because the first commercial production of ultramarine dates from 1828³¹⁻³⁴. Nevertheless, the first observation of local use of synthetic ultramarine in Italy, near Palermo dates from 1787³¹. Natural ultramarine is made by pulverisation and purification of the mineral lapis lazuli. Lapis lazuli contains the mineral lazurite ($\text{Na}_8[\text{Al}_6\text{Si}_6\text{O}_{24}]\text{S}_n$), which is responsible for its bright blue colour, along with a variety of other accessory minerals, of which only calcite (CaCO_3) is still present after the purification process. In mediaeval times, natural ultramarine was an extremely expensive pigment (more expensive than gold), due to the large travel distance and the labour-intensive purification process. With Raman spectroscopic analysis it is not possible to distinguish between natural or synthetic ultramarine.

The Raman bands of lazurite are clearly visible in the spectrum (Fig. 7.4(a)): a strong band centred near 543 cm^{-1} , due to the S_3^- symmetric stretching mode, and a weaker band centred between 568 and 583 cm^{-1} , due to the S_2^- symmetric stretching mode (Table 7.1)³⁵. The presence of natural ultramarine was also confirmed by performing XRF spectroscopy on the samples.

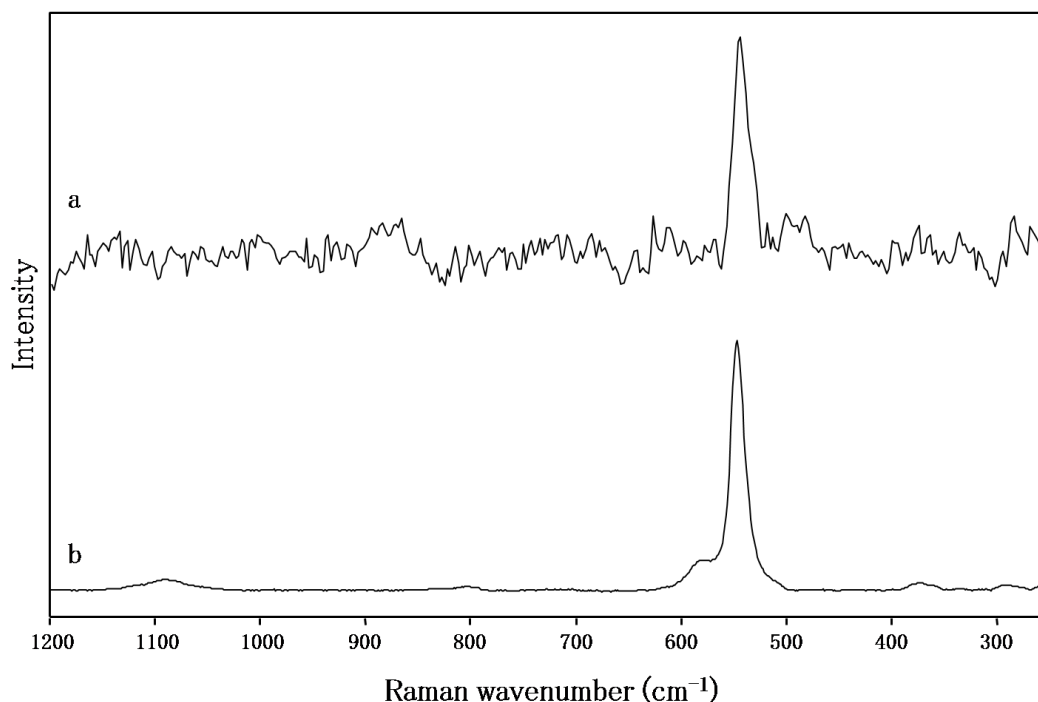


Figure 7.4 (a) *In situ* Raman spectrum of the blue pigment, showing the Raman bands of lazurite ($\text{Na}_8[\text{Al}_6\text{Si}_6\text{O}_{24}]\text{S}_n$) and (b) the reference Raman spectrum of ultramarine ($\text{Na}_{8-10}\text{Al}_6\text{Si}_6\text{O}_{24}\text{S}_{2-4}$).

While performing analysis in the laboratory on the samples, another blue pigment could be identified. For the light blue colour on folios 25r (Fig. 7.2(a) point 1) and folio 24v, the pigment azurite ($2\text{CuCO}_3 \cdot \text{Cu}(\text{OH})_2$) was used. The pigment azurite is produced by pulverisation, washing, grinding and sifting of the mineral azurite. The pigment azurite is used since antiquity, and during the Middle Ages and the Renaissance it was the most important blue pigment, in spite of the presence of the more expensive, exotic ultramarine³³. In the 18th century the use of azurite as a pigment was displaced by Prussian blue ($\text{Fe}_4[\text{Fe}(\text{CN})_6]_3$).

Figure 7.4(b) shows the Raman spectrum of azurite. The wavenumbers of the characteristic Raman bands are listed in table 7.1. The XRF spectrum (Fig. 7.4(c)) confirms the use of the pigment azurite, by the detection of copper. The Cu-K α line at 8.047 keV is clearly visible in the XRF spectrum, as also the Cu-K β line at 8.905 keV.

pigment/ polymer	composition	colour	Raman wavenumbers (cm ⁻¹)
ultramarine	Na ₈₋₁₀ Al ₆ Si ₆ O ₂₄ S ₂₋₄	blue	1086(w), 769(w), 543(vs), 251(vw)
azurite	2CuCO ₃ ·Cu(OH) ₂	blue	1578(w), 1456(w), 1428(w), 1417(w), 1330(w), 1231(w), 1094(s), 970(w), 930(w), 839(m), 809(m), 764(m), 534(w), 398(vs), 327(w), 279(w), 246(s), 178(m), 169(m), 153(m), 130(w), 122(w)
caput mortuum	Fe ₂ O ₃	purple	604(w), 404(m), 288(vs), 242(vw), 219(s)
vermilion	HgS	red	340(m), 281(w), 251(vs), 100(vw)
PR4	C ₁₆ H ₁₀ ClN ₃ O ₃	red	1589(m), 1556(vw), 1487(w), 1452(w), 1395(m), 1337(vs), 1318(w), 1266(w), 1226(w), 1190(w), 1154(vw), 1123(m), 1121(m), 1093(vw), 1042(vw), 986(w), 893(vw), 768(w), 739(vw), 709(w), 649(vw), 625(w), 591(vw), 421(w), 406(vw), 359(vw), 342(vw), 313(m), 168(w), 155(w)
PR176	C ₃₂ H ₂₄ N ₆ O ₅	red	1608(w), 1584(s), 1555(m), 1505(s), 1483(m), 1450(w), 1431(m), 1362(vs), 1328(m), 1319(m), 1288(s), 1263(w), 1224(s), 1193(m), 1141(w), 1109(m), 1093(w), 1016(w), 953(s), 838(w), 794(w), 766(w), 729(m), 706(vw), 669(vw), 635(m), 549(m), 517(m), 492(m), 425(m), 388(m), 361(m), 301(vw), 244(vw), 207(vw)
orpiment	As ₂ S ₃	yellow	383(w), 354(vs), 311(s), 293(m), 203(w), 180(vw), 15(m), 136(w)
lead white	2PbCO ₃ ·Pb(OH) ₂	white	1051 (vs), 679(vw), 414(w), 320(w), 128(w)
ultralene	polymer	/	2962(vs), 2959(vs), 2953(vs), 2923(vs), 2906(vs), 2884(vs), 2867(vs), 2839(vs), 2725(w), 2330(w), 1459(m), 1434(w), 1360(w), 1328(m), 1298(vw), 1218(w), 1168(m), 1159(w), 1153(m), 1034(m), 999(w), 972(m), 897(vw), 840(m), 809(m), 398(m), 174(vw), 138(vw), 114(w), 106(m)
gypsum	CaSO ₄ ·2H ₂ O	white	1372(vw), 1134(w), 1007(vs), 669(w), 618(w), 492(m), 413(m), 317(w), 210(w), 181(w), 122(w)

Table 7.1 List of the characteristic Raman bands of the pigments identified and the polymer ultralene.

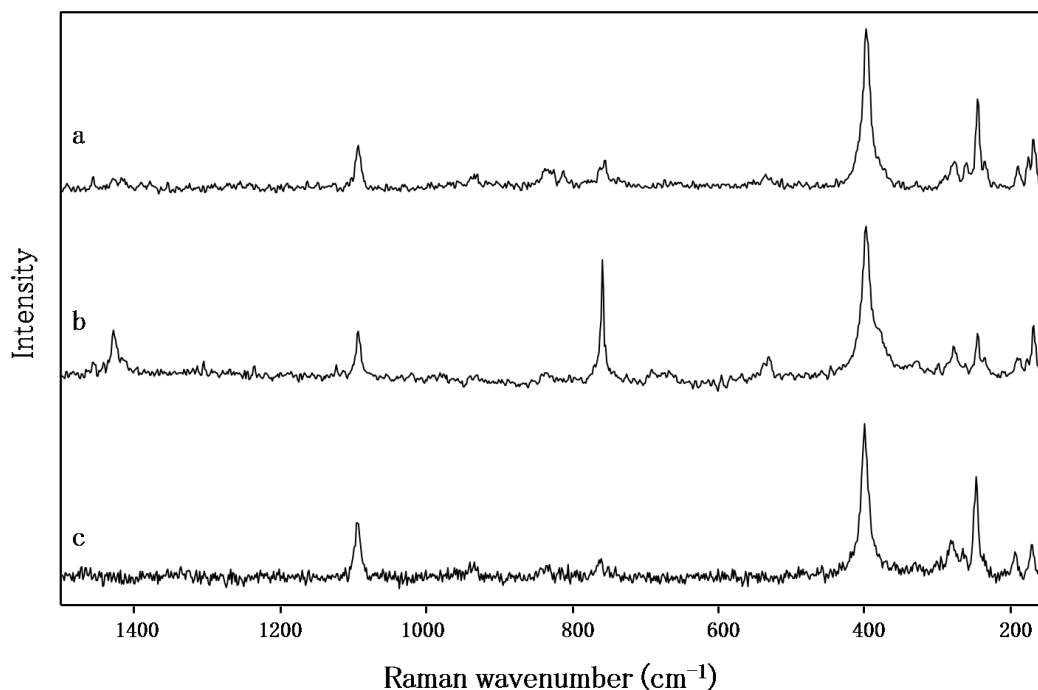


Figure 7.4 (b) (a) *In situ* Raman spectrum of the light blue pigment, showing the Raman bands of azurite ($2\text{CuCO}_3 \cdot \text{Cu}(\text{OH})_2$), (b) Raman spectrum of the darker blue pigment, showing the Raman bands of azurite ($2\text{CuCO}_3 \cdot \text{Cu}(\text{OH})_2$) and ultramarine ($\text{Na}_{8-10}\text{Al}_6\text{Si}_6\text{O}_{24}\text{S}_{2-4}$) and (c) the reference Raman spectrum of azurite ($2\text{CuCO}_3 \cdot \text{Cu}(\text{OH})_2$).

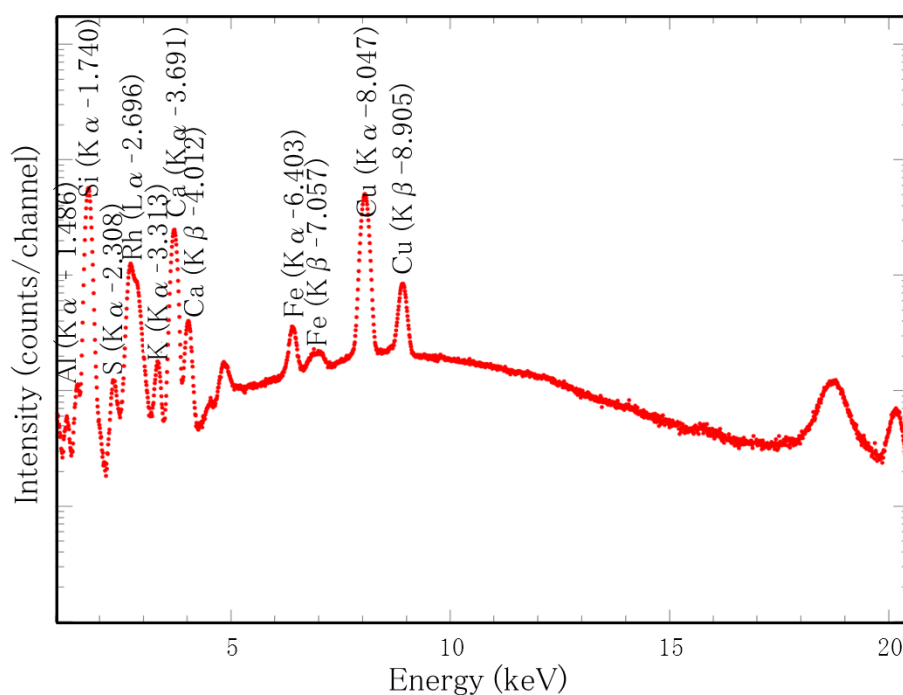


Figure 7.4 (c) X-ray fluorescence spectrum of the light blue pigment, showing the Cu-K α line at 8.047 keV and the Cu-K β line at 8.905 keV.

For the dark blue colour on folio 25r (Fig. 7.3(a) point 2) a mixture of ultramarine and azurite is used (Fig. 7.4(b)). The use of a mixture of these pigments has been observed in other mediaeval manuscripts^{36,37}. The artists diluted ultramarine with azurite, because ultramarine was too expensive or not available at the moment.

7.4.3 Green

Analysis of the green colour was performed on illustrations of folios 6v, 13r, 17r, 25r, 58v, 88r, 89r, 222r and 260r and on the illustration of bifolio 92v–93r. The pigment responsible for the green colour could not be identified with Raman or XRF spectroscopy. Looking at the sample under the microscope, it showed green, yellow and blue particles. Analysis of the blue grains with Raman spectroscopy revealed the use of ultramarine. Probably the blue pigment was mixed with a yellow lake, to produce the green colour. From our analysis, it was not possible to distinguish whether the yellow and blue pigments were mixed on the painters palette or while the paint was applied on the parchment. UV–fluorescence photography shows that the green parts of the illustrations fluoresce as deep purple; it even shows up strongly on the reverse of the folio in the UV.

7.4.4 Purple

Analysis of the purple colour was performed on the illustration of folio 260r (Fig. 7.2(b)). Probably a purple iron oxide mineral, caput mortuum, was used for the purple colour. The use of a naturally occurring and heat treated hematite-rich pigment producing a ‘violet colour’ was already identified in Roman, Byzantine and post-Byzantine art^{10,38,39}. The Raman spectrum (Fig. 7.4(d)) of the purple pigment shows the characteristic Raman bands of hematite (Fe_2O_3): 604 (E_g), 404 (E_g), 288 (E_g), 242 (E_g) and 219 (A_{1g}) cm^{-1} (Table 7.1). Figure 7.4(d) also shows the reference

spectrum of caput mortuum as purchased from Kremer⁴⁰. It is very difficult to differentiate between pure hematite and caput mortuum based on a Raman spectroscopic study^{10,39}, but because of the purple colour of the illustration on the manuscript (Fig. 7.2b), we can suggest that probably for this folio the pigment caput mortuum was used.

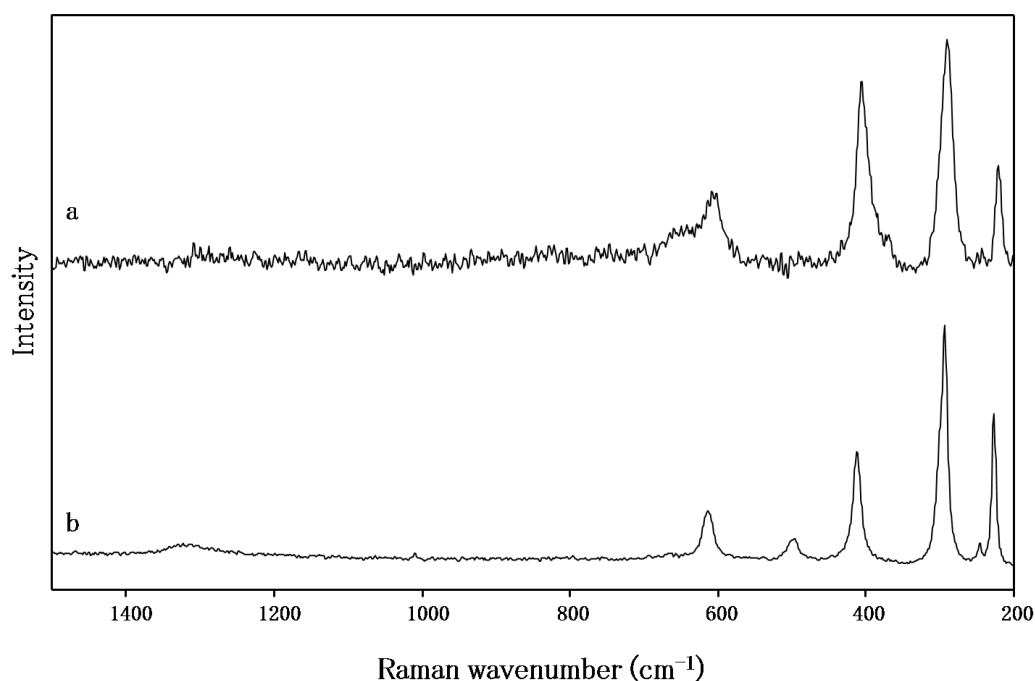


Figure 7.4 (d) (a) *In situ* Raman spectrum of the purple pigment, showing the Raman bands of caput mortuum and (b) the reference Raman spectrum of caput mortuum.

7.4.5 Red

Analysis of the red colour was performed on the illustrations of folios 6v, 13r, 17r, 24v, 25r, 37v, 58v, 88r, 88v, 222r, 259v and 260r, and on the illustration of bifolio 92v–93r. The *in situ* Raman analysis of the red pigment showed that vermilion (HgS) is used as red pigment. Vermilion is a mercury sulphide that occurs in nature as the red mineral cinnabar, but for ages it is also produced chemically. The pigment vermilion can be produced through at least three different production processes: through pulverisation and grinding of the mineral cinnabar, through a dry chemical

process (frequently used since the 14th century) and through a wet chemical process (in Europe since 1778)^{33,41–43}.

The Raman bands of vermilion are clearly visible in the spectrum (Fig. 7.5(a)): 340 (E'), 281 (E'), 251 (A1'') and 100 (E') cm^{-1} (Table 7.1)⁴⁴.

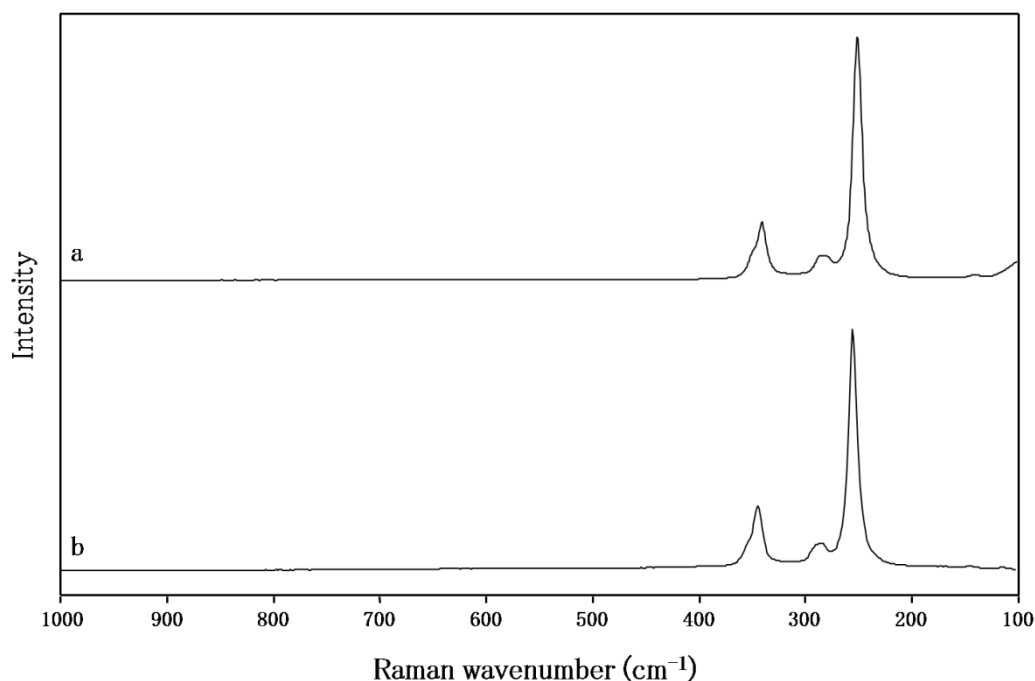


Figure 7.5 (a) (a) *In situ* Raman spectrum of the red pigment, showing the Raman bands of vermilion (HgS) and (b) the reference Raman spectrum of vermilion (HgS).

The presence of vermilion was also confirmed by performing Raman spectroscopy on the samples, combined with X-ray fluorescence spectroscopy. The signal for Hg-L α is visible at 9.989 keV and the Hg-L β line at 11.822 keV (Fig. 7.5(b)).

Next to vermilion, also two synthetic red mono-azo pigments, PR 4 and PR 176, could be identified with Raman spectroscopy. These pigments were found on folio 88r (Fig. 7.2(c), point 1). The Raman spectrum of both synthetic pigments, together with the reference spectra are displayed in figures 7.5(c) and (d). The Raman wavenumbers of both pigments are listed in table 7.1.

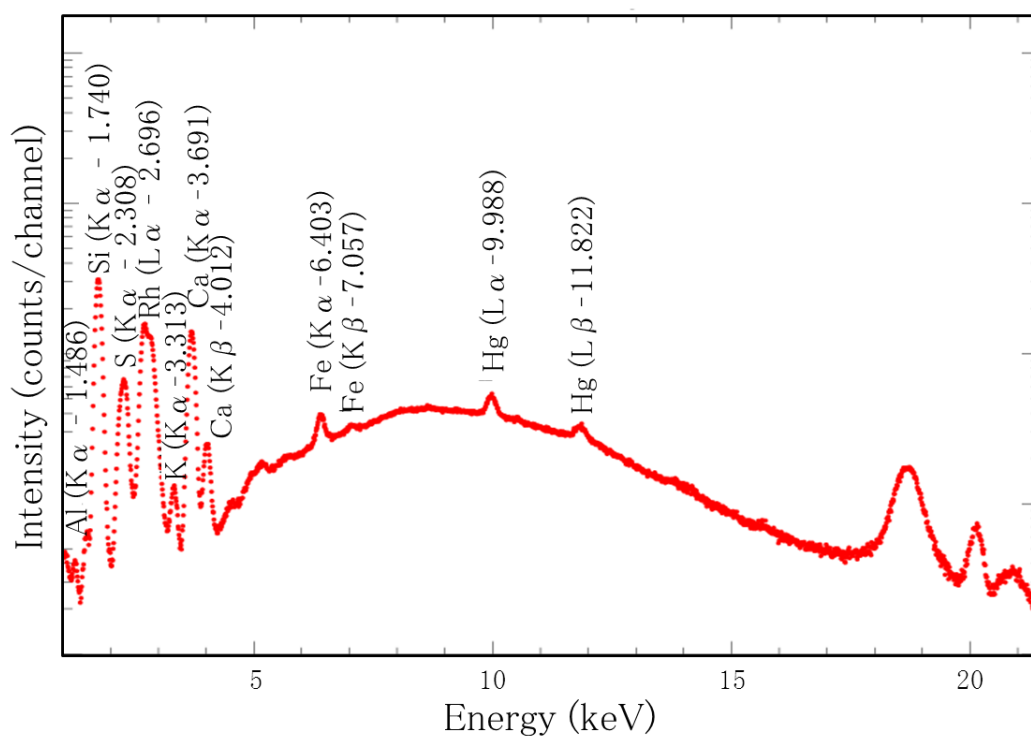


Figure 7.5 (b) X-ray fluorescence spectrum of the red pigment, showing the Hg-L α line at 9.988 keV and the Hg-L β line at 11.822 keV.

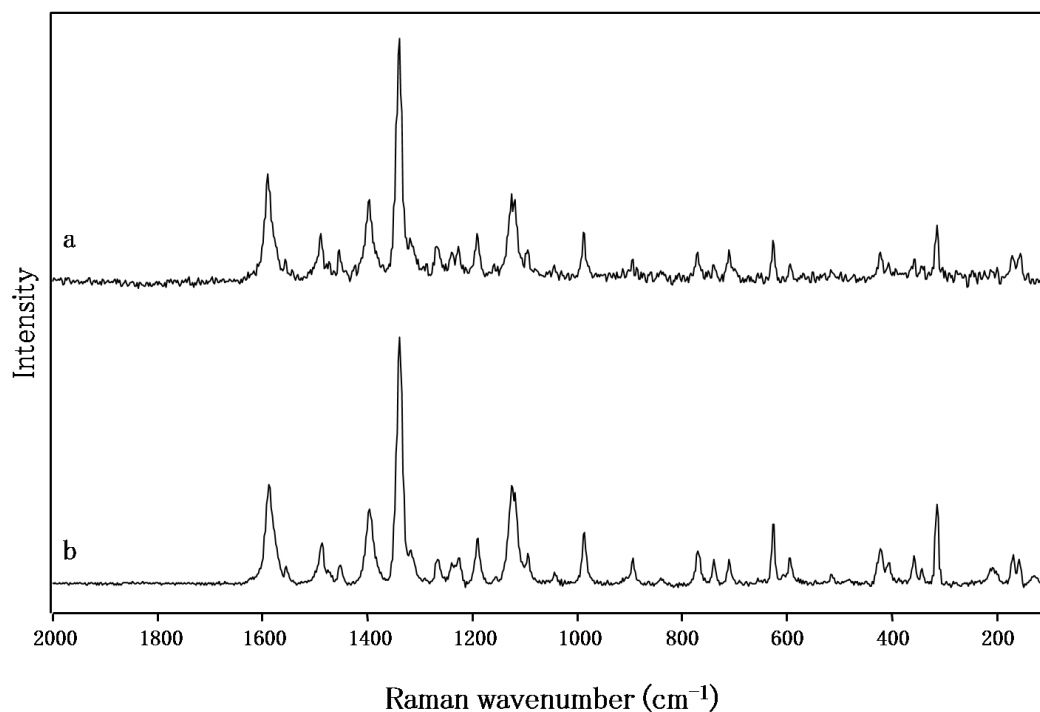


Figure 7.5 (c) (a) Raman spectrum of the organic red pigment, showing the Raman bands of Pigment Red 4 and (b) the reference Raman spectrum of Pigment Red 4.

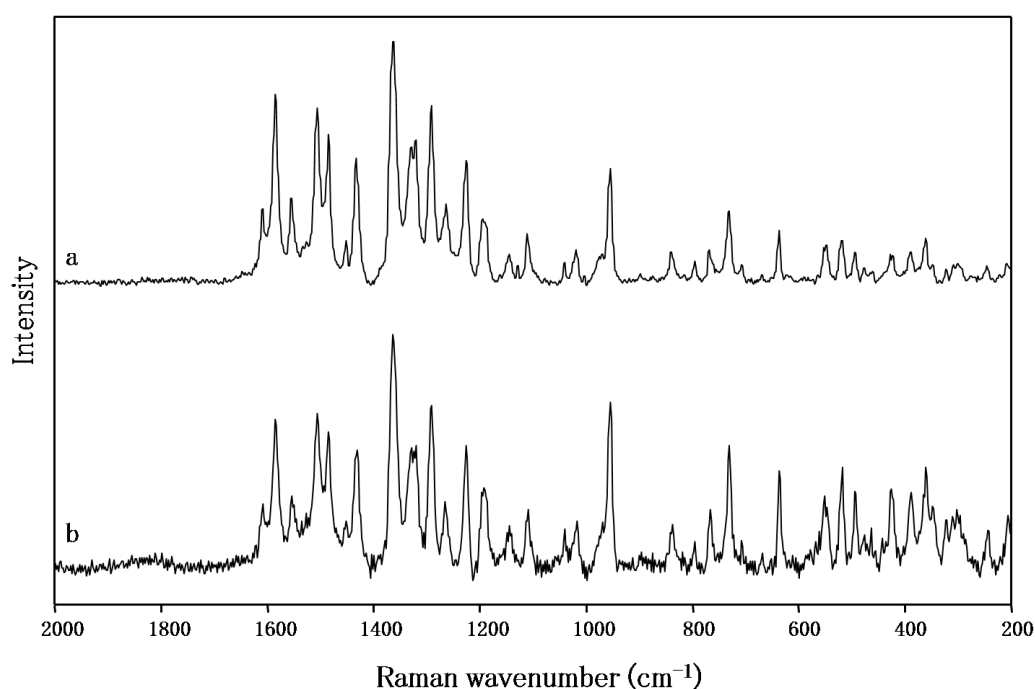


Figure 7.5 (d) (a) Raman spectrum of the organic red pigment, showing the Raman bands of Pigment Red 176 and (b) the reference Raman spectrum of Pigment Red 176.

According to the Colour Index⁴⁵ PR4 is invented in 1907, while PR 176 was even synthesised at a later date, namely around ca. 1960. So, these pigments must be later applications, as the manuscript was finished in 1120. The presence of these two organic pigment leads to the assumption that probably some restoration took place, even though no restoration is documented. Therefore, folio 88r was subject of a new research, which focussed on the red parts of the illustrations.

Seven new samples were taken, at different red parts of folio 88r (Fig 7.2(c,) points 2–8). The Raman analysis of these samples all confirmed the use of vermilion as red pigment, but no traces of synthetic pigments were found. This probably suggested that if any restoration took place, only the central illustration in the middle of the folio was restored.

7.4.6 Yellow

Analysis of the yellow colour was performed on illustrations of folios 6v, 13r, 25r, 58v, 88r, 88v, 89r and 260r. There are two different types of yellow used in this selection of folios.

The first type of yellow can be found on folio 58v, has a more golden appearance. Analysis with Raman spectroscopy shows that the pigment used to accomplish this colour is orpiment (As_2S_3). The natural pigment orpiment is produced by pulverisation and grinding of the mineral orpiment. Since the 17th century, synthetic orpiment was produced and used as painting material. In the 20th century the pigment was replaced by less toxic yellow pigments^{44,46}. The Raman spectrum of the yellow sample and the reference Raman spectrum of orpiment are shown in figure 7.7(a). The Raman wavenumbers are listed in table 7.1.

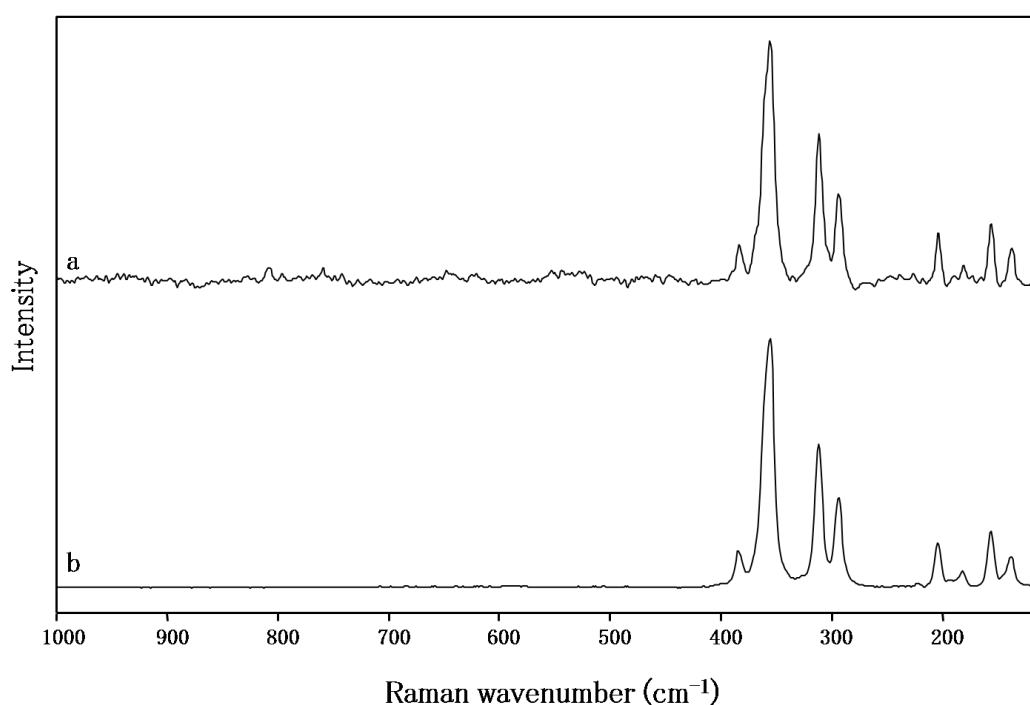


Figure 7.7 (a) (a) Raman spectrum of the yellow pigment, showing the Raman bands of orpiment (As_2S_3) and (b) the reference Raman spectrum of orpiment (As_2S_3).

A second type of yellow is a very bright light yellow. This type of yellow can be found on folios 6v, 13r, 88r, 88v, 89r and 260r. The pigment used to create this light yellow colour could not be identified with Raman spectroscopy and XRF spectroscopy. In agreement with the suggestion for the green pigment, we think that an organic yellow lake or dye is used for this type of yellow.

7.4.7 White

Analysis of the white colour was performed on illustrations of folios 58v, 88v and 260r. The pigment used for the white colour is lead white ($2\text{PbCO}_3 \cdot \text{Pb}(\text{OH})_2$). Lead white is a basic lead carbonate that occurs in nature as the rare mineral hydrocerrusite. Because the rare occurrence of the mineral, the synthetic pigment has been produced since antiquity. More details of the synthesis of lead white can be found elsewhere^{43,47}. Figure 7.7(b) shows the Raman spectrum of the white pigment: next to the characteristic Raman bands of lead white (Table 7.1), the spectrum also shows extra bands, attributed to ultralene (Table 7.1), the polymer on which the sample is fixed. The use of lead white was also confirmed by XRF spectroscopy. Figure 7.7(c) shows the XRF-spectrum of the white pigment. The Pb-K α line at 10.551 keV and the Pb-K β line at 12.613 keV are present in the spectrum.

On folio 58v traces of gypsum ($\text{CaSO}_4 \cdot 2\text{H}_2\text{O}$) were found. Figure 7.7(d) shows the Raman spectrum of the white pigment. The most intense Raman band of gypsum, 1007 cm^{-1} (Table 7.1) is clearly visible. The presence of gypsum probably points to the degradation of chalk (CaCO_3), which was used to prepare the parchment⁴⁸.

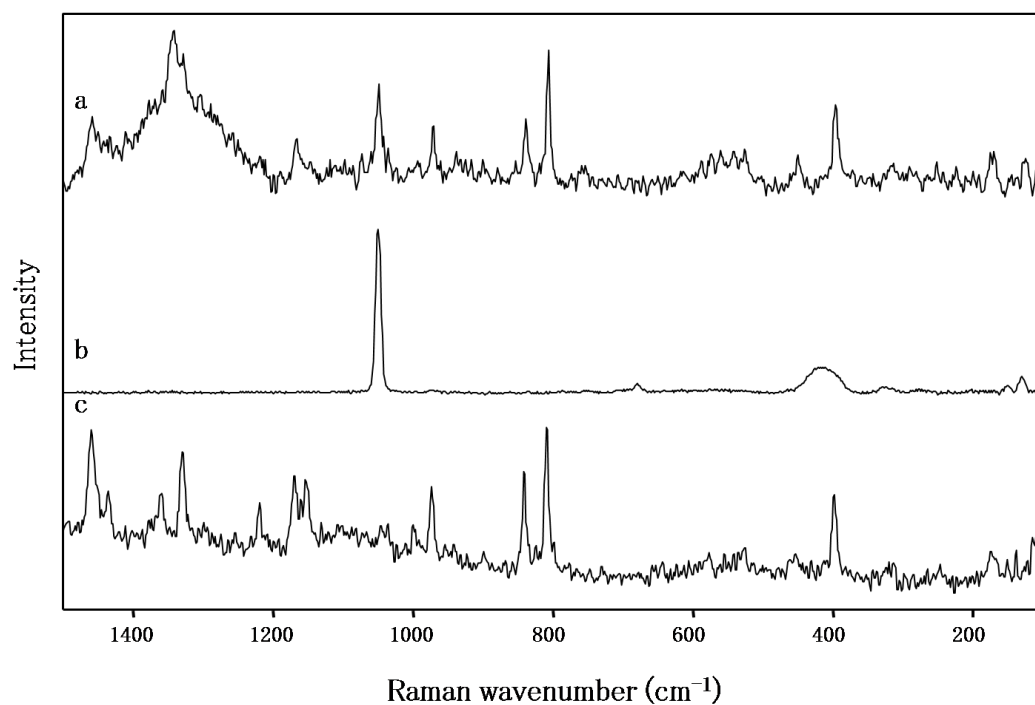


Figure 7.7(b) (a) Raman spectrum of the white pigment, showing the Raman bands of lead white ($2\text{PbCO}_3 \cdot \text{Pb}(\text{OH})_2$), (b) reference Raman spectrum of lead white ($2\text{PbCO}_3 \cdot \text{Pb}(\text{OH})_2$) and (c) the reference Raman spectrum of ultralene.

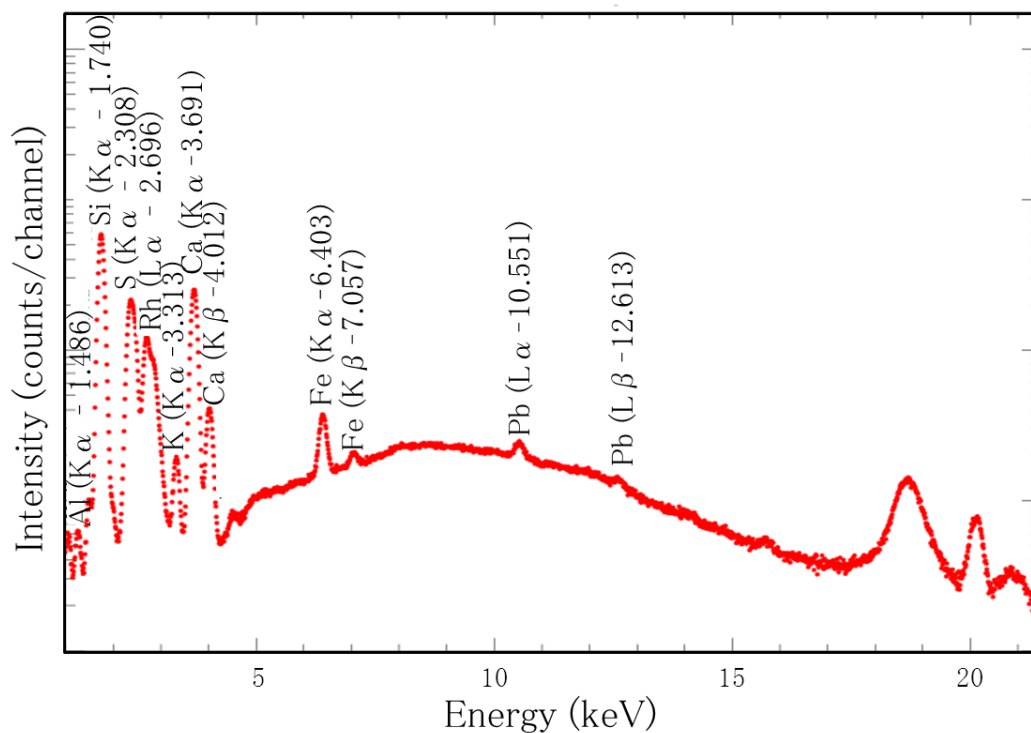


Figure 7.7(c) X-ray fluorescence spectrum of the white pigment, showing the Pb-L α line at 10.551 keV and the Pb-L β line at 12.613 keV.

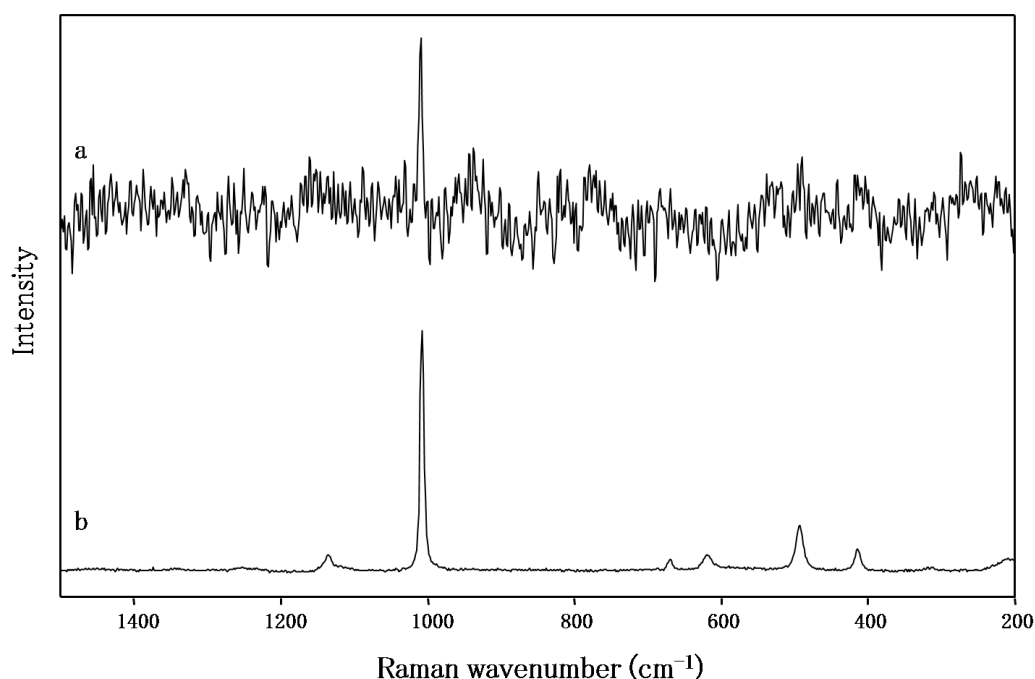


Figure 7.7(d) (a) Raman spectrum of the white pigment, showing the Raman bands of gypsum ($\text{CaSO}_4 \cdot 2\text{H}_2\text{O}$) and (b) the reference Raman spectrum of gypsum ($\text{CaSO}_4 \cdot 2\text{H}_2\text{O}$).

7.5 Conclusions

By using a combination of analytical spectroscopic techniques, such as Raman spectroscopy and X-ray fluorescence (XRF) spectroscopy, with imaging techniques, such as UV-fluorescence photography and infrared reflectography (IRR), a lot of interesting information on the underdrawing and the pigments used in the manuscript *Liber Floridus* could be gathered. IRR revealed the use of a compass to make the underdrawings of the circles on different folios, while the combination of direct and indirect Raman spectroscopy, XRF spectroscopy and UV-fluorescence spectroscopy was used to identify the pigments used, such as: ultramarine, azurite, caput mortuum, vermilion, orpiment and lead white. Moreover two synthetic azo-pigments, PR4 and PR 176, could be identified.

The presence of these two azo-pigments could indicate that some restoration of the manuscript took place, even though no restoration is documented. A challenge of this study was looking for other synthetic pigments. After a very detailed investigation of the folio, no other traces of synthetic pigments were found. Therefore, it is not certain that restoration of the illustration took place. A possible explanation for the presence of the synthetic pigments is that they are impurities of the restoration laboratory left behind during the rebinding of the manuscript.

On some folios also traces of the degradation product gypsum were identified. The presence of degradation products gives information on the best circumstances in which the manuscript must be conserved.

In this work two organic red pigments could be identified: PR 4 and PR 176. Normally the presence of organic pigments indicates that the manuscript was restored, because organic pigments were not yet synthesised during the Middle Ages. However, in literature and reports we could not find any reference of a post restoration of the manuscript. A second sampling was based on the different lightning of some parts of the miniature. The analysis of these samples could not confirm the presence of organic pigments. Also UV-fluorescence spectroscopy could not confirm that restoration took place. Therefore we concluded that the traces of organic pigments were probably left behind unintentionally during the rebinding of the manuscript.

In the next chapter, we used a combination of mobile Raman spectroscopy and mobile XRF spectroscopy to evaluate the authenticity of the so-called ‘Wyts Triptych’ after Jan van Eyck. Next to point measurements, also an XRF mapping was performed to get a better view of the restoration processes the painting underwent.

References

1. Derolez, A. (1998) *The autograph manuscript of the Liber Floridus: A key to the Encyclopedia of Lambert of Saint-Omer*. Brepols, Turnhout.
2. Derolez, A. (1978) *Lambertus qui librum fecit. Een codicologische studie van de Liber Floridus-autograaf*. Verhandeling van de Koninklijke Academie van Wetenschap. Klasse der Letteren, 40.
3. De Coene, K. (2006) *Navelnacht. Kosmologie en regeneratie in de Middeleeuwen*. Katholieke Universiteit Leuven. PhD.
4. De Coene, K. (2009) Het religieuze wereldbeeld van Lambertus van Sint-Omaars, *Trajecta* 18: 3-22.
5. Bersani, D., Lottici, P.P., Vignallil, F., Zanichelli, G. (2006) A study of medieval illuminated manuscripts by means of portable Raman equipments. *Journal of Raman Spectroscopy* 37: 1012-1018.
6. Deneckere, A., Hocquet, F.P., Born, A., Klein, P., Rakkaa, S., Lycke, S., De Langhe, K., Martens, M.P.J., Strivay, D., Vandenabeele, P., Moens, L. (2010) Direct analysis of the central panel of the so-called Wyts triptych after Jan van Eyck. *Journal of Raman Spectroscopy* 41: 1210-1219.
7. Falcone, L., Bloisi, F., Califano, V., Pagano, M., Vicari, L. (2008) An old notice board at ancient Herculaneum studied using Near Infrared Reflectography. *Journal of Archaeological Science* 35: 1708-1716.
8. Consolandi, L., Bertani, D. (2007) A prototype for high resolution infrared reflectography of paintings. *Infrared Physics & Technology* 49: 239-242.
9. Vandenabeele, P., Garcia-Moreno, R., Mathis, F., Leterme, K., Van Elslande, E., Hocquet, F.P., Rakkaa, S., Laboury, D., Moens, L., Strivay, D., Hartwig,

- M. (2009) Multi-disciplinary investigation of the tomb of Menna (TT69), Theban Necropolis, Egypt. *Spectrochimica Acta Part A-Molecular and Biomolecular Spectroscopy* 73: 546–552.
10. Daniilia, S., Bikiaris, D., Burgio, L., Gavala, P., Clark, R.J.H., Chrysoulakis, Y. (2002) An extensive non-destructive and micro-spectroscopic study of two post-Byzantine overpainted icons of the 16th century. *Journal of Raman Spectroscopy* 33: 807–814.
11. Moura, L., Melo, M.J., Casanova, C., Claro, A. (2007) A study on Portuguese manuscript illumination: The Charter of Vila Flor (Flower town), 1512. *Journal of Cultural Heritage* 8: 299–306.
12. Vandenabeele, P., Edwards, H.G.M. (2005) *Raman spectroscopy in archaeology and art history*. Chapter 11 Overview: Raman spectroscopy of artefacts. The Royal Society of Chemistry, Cambridge, 169–178.
13. Schreiner, M., Fruhmann, B., Jembrih-Simburger, D., Linke, R. (2004) X-rays in art and archaeology: An overview. *Powder Diffraction* 19: 3–11.
14. Rosi, F., Miliani, C., Borgia, I., Brunetti, B., Sgamellotti, A. (2004) Identification of nineteenth century blue and green pigments by *in situ* x-ray fluorescence and micro-Raman spectroscopy. *Journal of Raman Spectroscopy* 35: 610–615.
15. Paternoster, G., Rinzivillo, R., Nunziata, F., Castellucci, E.M., Lofrumento, C., Zoppi, A., Felici, A.C., Fronterotta, G., Nicolais, C., Piacentini, M., Sciuti, S., Vendittelli, M. (2005) Study on the technique of the Roman age mural paintings by micro-XRF with Polycapillary Conic Collimator and micro-Raman analyses. *Journal of Cultural Heritage* 6: 21–28.

16. Sawczak, M., Kaminska, A., Rabczuk, G., Ferretti, M., Jendrzewski, R., Sliwinski, G. (2009) Complementary use of the Raman and XRF techniques for non-destructive analysis of historical paint layers. *Applied Surface Science* 255: 5542–5545.
17. Deneckere, A., Schudel, W., Van Bos, M., Wouters, H., Bergmans, A., Vandenabeele, P., Moens, L. (2010) *In situ* investigations of vault paintings in the Antwerp cathedral. *Spectrochimica Acta Part A-Molecular and Biomolecular Spectroscopy* 75: 511–519.
18. Ricci, C., Borgia, I., Brunetti, B.G., Miliani, C., Sgamellotti, A., Seccaroni, C., Passalacqua, P. (2004) The Perugino's palette: integration of an extended *in situ* XRF study by Raman spectroscopy. *Journal of Raman Spectroscopy* 35: 616–621.
19. Goodall, R.A., Hall, J., Edwards, H.G.M., Sharer, R.J., Viel, R., Fredericks, P.M. (2007) Raman microprobe analysis of stucco samples from the buildings of Maya Classic Copan. *Journal of Archaeological Science* 34: 666–673.
20. Castro, K., Perez-Alonso, M., Rodriguez-Laso, M.D., Etxebarria, N., Madariaga, J.M. (2007) Non-invasive and non-destructive micro-XRF and micro-Raman analysis of a decorative wallpaper from the beginning of the 19th century. *Analytical and Bioanalytical Chemistry* 387: 847–860.
21. Burgio, L., Clark, R.J.H., Muralha, V.S.F., Stanley, T. (2008) Pigment analysis by Raman microscopy of the non-figurative illumination in 16th-to 18th-century Islamic manuscripts. *Journal of Raman Spectroscopy* 39: 1482–1493.
22. Wehling, B., Vandenabeele, P., Moens, L., Klockenkamper, R., von Bohlen, A., Van Hooydonk, G., De Reu, M. (1999) Investigation of pigments in

- medieval manuscripts by micro Raman spectroscopy and total reflection X-ray fluorescence spectrometry. *Mikrochimica Acta* 130: 253–260.
23. Trentelman, K., Turner, N. (2009) Investigation of the painting materials and techniques of the late-15th century manuscript illuminator Jean Bourdichon. *Journal of Raman Spectroscopy* 40: 577–584.
24. Hayez, V., Denoel, S., Genadry, Z., Gilbert, B. (2004) Identification of pigments on a 16th century Persian manuscript by micro-Raman spectroscopy. *Journal of Raman Spectroscopy* 35: 781–785.
25. Aceto, M., Agostino, A., Boccaleri, E., Crivello, F., Garlanda, A.C. (2006) Evidence for the degradation of an alloy pigment on an ancient Italian manuscript. *Journal of Raman Spectroscopy* 37: 1160–1170.
26. <http://www.liberfloridus.be>
27. Devos, W., Moens, L., Bohlen, A.V., Klockenkamper, R. (1995) Ultra-Microanalysis of Inorganic Pigments on Painted Objects by Total-Reflection X-Ray-Fluorescence Analysis. *Studies in conservation* 40: 153–162.
28. Vandenabeele, P., Weis, T.L., Grant, E.R., Moens, L.J. (2004) A new instrument adapted to *in situ* Raman analysis of objects of art. *Analytical and Bioanalytical Chemistry* 379: 137–142.
29. Saunders, D., Billinge, R., Cupitt, J., Atkinson, N., Liang, H. (2006) A new camera for high-resolution infrared imaging of works of art. *Studies in conservation* 51: 277–290.
30. Hawthorne, J.G., Smith, C.S. (1963) *Theophilus on divers arts: the foremost medieval treatise on painting, glassmaking and metalwork*. University Chicago Press, 61–62.

-
31. Nicolaus, K. (1980) Het schilderij; materiaal techniek-behoud. Chapter 5 De verflaag. Uitgeverij Westland nv, Schoten, 109–127.
 32. Roy, A. (1993) Artists' Pigments: A handbook of their history and characteristics volume 2. Chapter 2: Ultramarine blue, natural and artificial, Oxford University Press, New York, 37–65.
 33. Barnett, J.R., Miller, S., Pearce, E. (2006) Colour and art: A brief history of pigments. *Optics and Laser Technology* 38: 445–453.
 34. Schmidt, C.M., Walton, M.S., Trentelman, K. (2009) Characterization of Lapis Lazuli Pigments Using a Multitechnique Analytical Approach: Implications for Identification and Geological Provenancing. *Analytical Chemistry* 81: 8513–8518.
 35. Vandenabeele, P., Wehling, B., Moens, L., Dekeyser, B., Cardon, B., von Bohlen, A., Klockenkamper, R. (1999) Pigment investigation of a late-medieval manuscript with total reflection X-ray fluorescence and micro-Raman spectroscopy. *Analyst* 124: 169–172.
 36. De Reu, M., Van Hooydonk, G., Vandenabeele, P., Moens, L., Bohlen, A.V., Klockenkampfer, R. (1999) The chemical analysis of pigments used in several illuminated manuscripts. *Scriptorium* 53: 357–372.
 37. Edwards, H.G.M., Middleton, P.S., Hargreaves, M.D. (2009) Romano-British wall paintings: Raman spectroscopic analysis of fragments from two urban sites of early military colonisation. *Spectrochimica Acta Part A-Molecular and Biomolecular Spectroscopy* 73: 553–560.
 38. Bikiaris, D., Daniilia, S.X., Sotiropoulou, S., Katsimbiri, O., Pavlidou, E., Moutsatsou, A.P., Chrysosoulakis, Y. (2000) Ochre-differentiation through micro-Raman and micro-FTIR spectroscopies: application on wall paintings at

- Meteora and Mount Athos, Greece. *Spectrochimica Acta Part A-Molecular and Biomolecular Spectroscopy* 56: 3–18.
39. de Oliveira, L.F.C., Edwards, H.G.M., Frost, R.L., Klopogge, J.T., Middleton, P.S. (2002) Caput mortuum: spectroscopic and structural studies of an ancient pigment. *Analyst* 127: 536–541.
40. <http://www.kremer-pigmente.de>
41. Thompson, D.V. (1979) *The materials and techniques of medieval painting*. Chapter 3: Pigments. Dover Publications, New York, 74–189.
42. Howard, H. (2003) *Pigments of English Medieval Wall Paintings*. Chapter 5 Red pigments. Archetype Publications, London, 97–140.
43. Schramm, H.P., Hering, B. (1988) *Historische Malmaterialien und ihre identifizierung*. Chapter 4 Pigmente, Farb- und füllstoffe, Akademische Druck- und Verlagsanstalt, Graz, 19–78.
44. Frost, R.L., Martens, W.N., Klopogge, J.T. (2002) Raman spectroscopic study of cinnabar (HgS), realgar (As₄S₄), and orpiment (As₂S₃) at 298 and 77K. *Neues Jahrbuch für Mineralogie-Monatshefte* 469–480.
45. Society of Dyers and Colourists and American Association of Textile Chemists and Colourists (1971) *Colour index*. Bradford, vol. 1–4.
46. Fitzhugh, E.W. (1997) *Artists' Pigments: A handbook of their history and characteristics volume 3*. Chapter 2: Orpiment and Realgar. Oxford University Press, New York, 47–80.
47. Howard, H. (2003) *Pigments of English Medieval Wall Paintings*. Chapter 8 White pigments. Archetype Publications, London, 165–186.

48. De Hamel, C. (1992) *Medieval craftsmen: scribes and illuminators*. Chapter 1: Paper-and Parchment-Makers. British Museum Press, London, 8-26.

Chapter 8: Direct analysis of the central panel of the so-called ‘Wyts Triptych’ after Jan van Eyck

Annelien Deneckere, François-Philippe Hocquet, Annick Born, Peter Klein,
Said Rakkaa, Sylvia Lycke, Kaat De Langhe, Maximiliaan Martens,
David Strivay, Peter Vandenabeele, Luc Moens

Journal of Raman Spectroscopy, 41 (2010) 1210–1219

In this chapter the analysis of the central panel of the so-called ‘Wyts Triptych’ after Jan van Eyck is presented. For this work mobile Raman spectroscopy was combined with mobile XRF spectroscopy. This study was performed under the authority of the Bruges Groeninge Museum. Dendrochronological analysis already confirmed that the panel is dated in the period (1621) after the death of van Eyck (1441), nevertheless IRR and UV-fluorescence spectroscopy revealed that the panel underwent many restorations. Our task was to gather as much as possible information on the restored areas, by performing Raman and XRF point measurements next to XRF mappings of three of the restored areas.

8.1 Introduction

During the past decades, an increasing number of scientific investigations have been performed on different types of artworks, such as rock paintings¹⁻³, wall paintings⁴⁻⁷, panel paintings^{8,9} and polychrome objects¹⁰⁻¹³.

According to Lahanier *et al.*¹⁴, an ideal method for analysing archaeological objects should be *non-destructive*, which respects the physical integrity of the object; *fast*, so that various positions of one single object or large numbers of similar objects can be analysed; *universal*, so that many materials and objects of various shapes and dimensions can be analysed with minimum of sample preparation; *versatile*, which allows the average compositional information and local information of small areas (micrometre-sized) from heterogeneous materials to be analysed; *sensitive*, so that provenance analysis can be done through fingerprints of not only major elements but also trace elements; and *multi-elemental*, so that in a single measurement, information on different elements is simultaneously obtained.

In general, different reasons for the investigation of objects of art can be identified. There is obviously the fundamental interest in the materials and techniques that were used in the past. Art historical questions, which often concern the authenticity

or dating the artwork and placing it in a temporal context, are another reason. Other art historical questions concern the relationship between a particular work of art and similar works, and identification of new techniques and materials, e.g. the evaluation of possible trade routes. The last type of conservation questions is often related to the damage or degradation experienced by a specific art object or to identify materials in order to take optimal decisions concerning their restoration and preservation¹⁵.

In this research, an attempt is made to reconstruct a painting's material history. Apart from knowing the painting materials, art historians are often also interested in the painting style and thus they focus on specific motifs in space. A whole series of imaging techniques are available for this type of research, including macrophotography¹⁶, infrared reflectography^{17,18} and UV-fluorescence photography^{16,19}. Radiography¹⁹ is also often used to reveal underlying layers of the artwork. Analytical techniques, on the other hand, often only provide information of the selected points of analysis, and it is a complex task to recognise specific spatially resolved patterns. Therefore, mapping, combined with non-destructive analytical techniques, can provide the required analytical results, with the desired spatial distribution, for a specific point. Although this approach is quite straightforward, some drawbacks may hamper the investigation. First, stable positioning equipment and stepper motors are required for the translational stage and, second, time is usually a limiting factor.

In this work, the central panel of the 'Wyts Triptych' is examined by a combination of energy dispersive X-ray fluorescence (EDXRF) spectroscopy and Raman spectroscopy. A systematic search of case studies in literature^{4,7,16,20-23} shows the importance of combining analytical techniques in art analysis, as this strongly enhances the reliability of the results. It was possible to perform XRF mappings of three selected areas of the panel that were considered as key zones to understand the changes the painting underwent during history. XRF maps have the unique

advantage that they allow visualising the underlying paint layers and meanwhile providing analytical results of the elemental composition of all the layers together: like radiography, XRF is not capable of distinguishing between different layers. However, in some cases, where XRF is insufficient to distinguish between two pigments, Raman spectroscopy may be used to obtain additional information.

The importance of the Wyts Triptych is illustrated by the number of different studies performed, such as visual analysis, radiography, infrared photography and dendrochronological analysis²⁴⁻²⁶. The aim of our study is providing a relatively objective support to the art historical interpretation of the visual analysis and available technical documents of the painting.

8.2 The Wyts Triptych

The 16th century humanist authors, like Marcus Van Vaernewyck (1563, 1566, 1568) and Lucas de Heere (1565) have mentioned a painting by Jan van Eyck for the church of St Martin, Ypres. According to these sources, the painting remained unfinished after the painter's death in 1441²⁴. Van Vaernewyck also describes the painted wings of this triptych (1568). Art historical literature from the 19th and 20th centuries refers to this work as the *Ypres Madonna* or the *Maelbeke Madonna*, after the supposed identity of the donor, Nicolas Maelbeke, provost of St Martin's. A picture kept in successive private collections (Fig. 8.1(a)) was often, but not without controversy, identified as this last work by Jan van Eyck. Except when shown rarely in public, such as, e.g. at the exhibition 'Les Primitifs flamands' held in Bruges in 1902, only very few van Eyck scholars have had the opportunity to study the painting thoroughly; all of them reported on its precarious state of conservation. Two drawings, one in Nuremburg (Germanisches Nationalmuseum, inv. Hz. 279) and the other in Vienna (Grafische Sammlung Albertina, inv. 4841) were considered copies of the original van Eyck.

In the 1970s, when the work was offered for sale to the Belgian State, the central panel was investigated at the Royal Institute for Cultural Heritage (KIK-IRPA), Brussels. Radiographs, infrared photographs and the presence of smalt showed characteristics untypical for the 15th century painting technique²⁵. Dendrochronological analysis performed at Oxford University in 1975 suggested that the painting was a 17th century copy of the lost original painting by Jan van Eyck²⁶. Recent re-examination has confirmed that the piece of wood used for the support is Baltic oak. The earliest heartwood ring of the youngest plank of the central panel is dated 1604. Under the assumption of a median of 15 sapwood rings and 2 years for seasoning, the plausible realisation date is 1621 upwards.

That the painting is a late copy is also confirmed by the identity of the donor, which has been mistaken equally until the 1970s. The man is a canon and carries a cantor's staff and no dignitary marks of a provost. Around the presumed date of realisation, the cantor of St Martin's church at Ypres was a certain Pieter Wyts. Hence the current name for the triptych (Fig. 8.1(b)).

Older photographs of the present work, as well as radiographs, infrared reflectograms (Fig. 8.1(c)) and UV-photographs (Fig. 8.1(d)), show a very disturbed state of conservation with several retouches mainly in the donor's face, the Christ child, the Virgin and the vaults of the architecture. Indeed, documentary sources also indicate that the painting has been restored on several occasions. Some of these campaigns were very drastic: e.g. the facial features of the donor were reworked several times.

In 2007, the Bruges Goeninge Museum acquired this triptych.

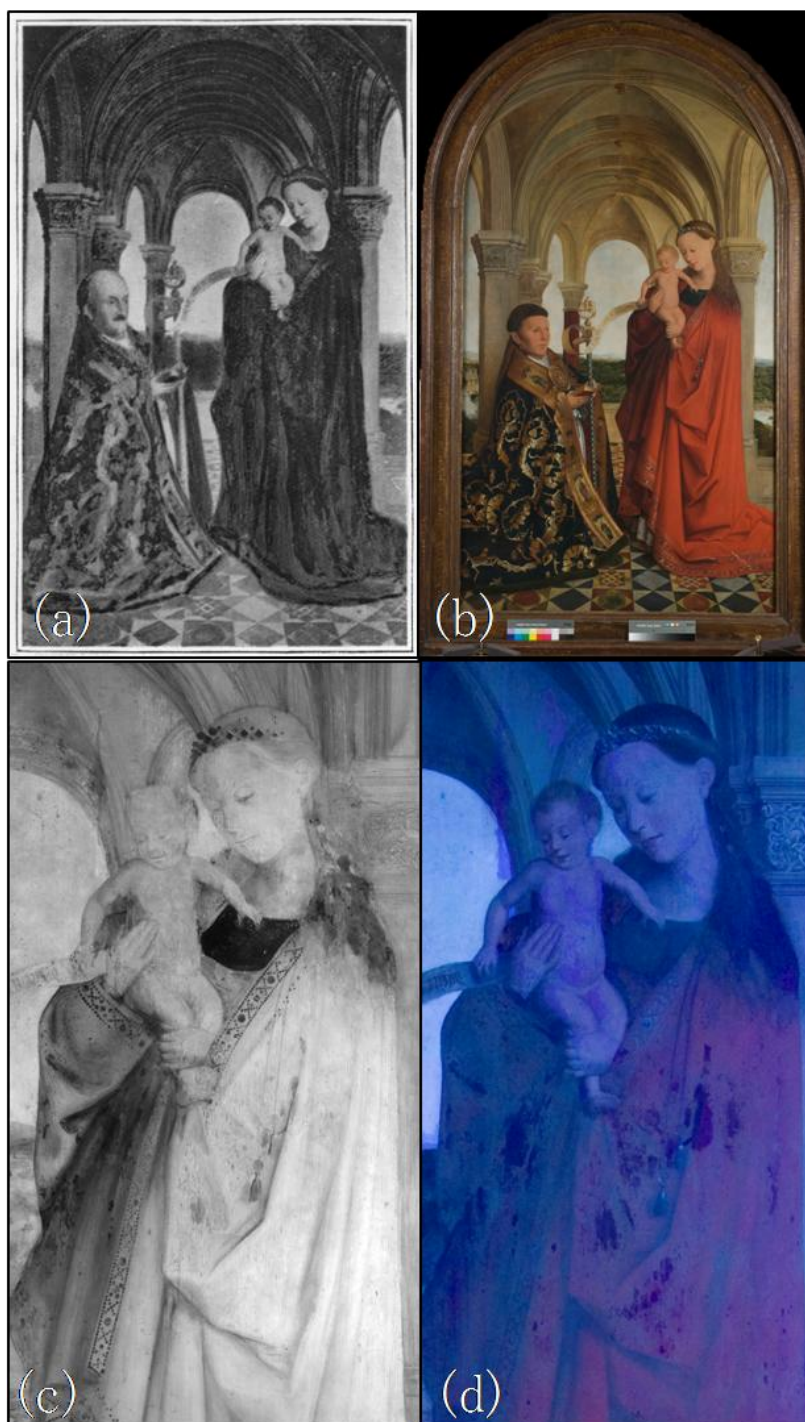


Figure 8.1 (a) State of conservation before restoration Berlin 1920–1929, taken from Fierens–Gevaert, *Histoire de la peinture flamande des origines à la fin du XV^e siècle*, Paris–Bruxelles, 1927, vol. 1, p1. LXVIII; (b) Anonymous 17th century after Jan van Eyck, *Wyts Madonna* (Bruges, Groeninge Museum) (UGent, Gica&s); (c) IRR and (d) UV detail Virgin's garment (Bruges, Groeninge Museum) (UGent, Gica&s).

8.3 Experimental

Direct XRF spectroscopy and Raman spectroscopy were performed successively. The positions of the investigations were carefully marked on a print of the painting, to allow investigation of exactly the same points.

8.3.1 Energy dispersive X-ray fluorescence spectroscopy

The EDXRF measurements of the central panel of the ‘Wyts Triptych’ were carried out with a mobile EDXRF system (Fig. 8.2(a)) from the CEA (Liège, Belgium). The EDXRF set-up is in a traditional configuration, where the miniature X-ray tube (Magnum 50 kV, Moxtek) is perpendicular to the sample, working at a distance of 21 mm, and the detector (SDD, Ketek) is placed at approximately 43° from the X-ray beam. Home-made software allows us to control the displacement system and the data acquisition. An overview of the instrumentation and the displacement system can be found in a previous article²⁷, keeping in mind that new developments, concerning the remote control system and the acquisition software, have been added recently. All spectra were recorded using the X-ray tube working at 30 kV with an acquisition time of 300 s. The X-ray spot size on the sample was about 2 mm^2 . In this case, this was not a major disadvantage, since the panel did not present details that were problematic for EDXRF analysis. Depending on the detector efficiency and EDXRF set-up, the region of interest in spectra ranges typically from around 2 to 30 keV.

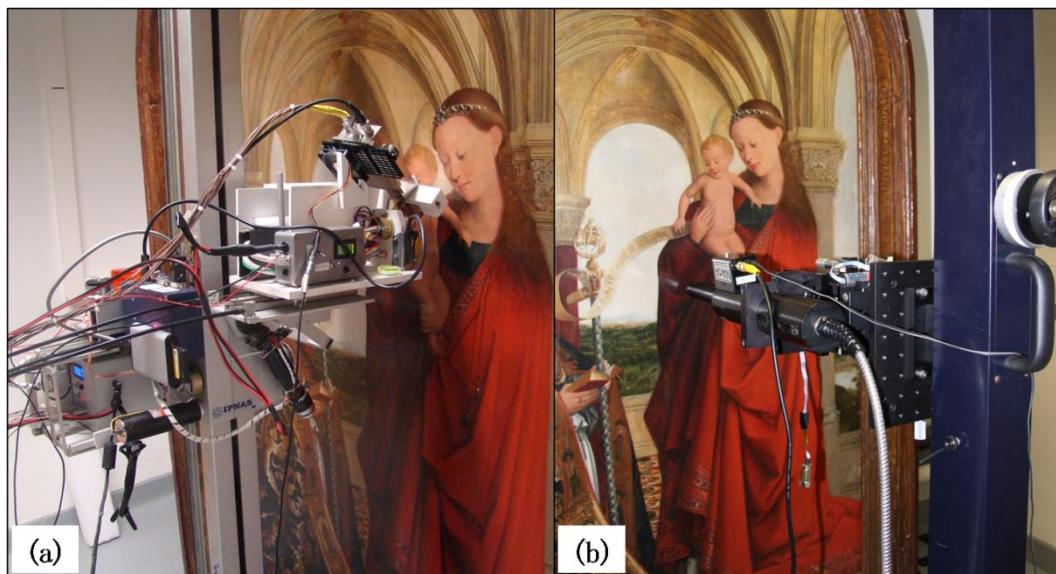


Figure 8.2 Experimental set-ups of (a) the mobile EDXRF system and (b) the Mobile Art Analyser.

8.3.2 Raman spectroscopy

The Raman instrument used for this work is the Mobile Art Analyser (Fig. 8.2(b)). This device contains a portable Raman imaging microscope (Spectracode, West Lafayette, IN, USA) and a SpectraPro 150i f.15 spectrometer (Roper Scientific, Princeton Instruments, New Jersey, USA). The instrument has been described in more detail elsewhere²⁸. The investigations were carried out using a 600 grooves/mm dispersion grating and a 785 nm laser. The laser power used during the measurements was set to a few milliwatts to avoid any possible sample damage. Spectra were obtained in the spectral region between 100 and 2500 cm^{-1} . To achieve a working distance of ca. 5 mm, a 6 \times objective lens was used. The sample could be observed through a USB-controlled colour camera incorporated into the probe head. Micro-positioning and focussing was achieved using three motorised, remote-controlled micro-positioners (Oriel), with a working distance of 2.5 cm. The spot size on the sample was about 50 μm . During this work, 60 points were examined (Table 8.1), resulting in ca. 240 spectra.

measuring point	colour	pigment	chemical composition
rim of the decorative border of the chasuble	red	vermilion	HgS
undergarment virgin	white	massicot	PbO
fold garment virgin	red	vermilion	HgS
garment Virgin	red	vermilion lead white	HgS $2\text{PbCO}_3 \cdot \text{Pb(OH)}_2$
foot christ	carnation	vermilion	HgS
groin christ	carnation	vermilion	HgS
belly Christ (navel region)	carnation	vermilion	HgS
belly Christ (Virgins hand)	carnation	vermilion	HgS
belly Christ (height Virgins hand)	carnation	vermilion	HgS
left shoulder Christ	carnation	vermilion	HgS
belly Christ (border with Virgin)	carnation	vermilion anatase	HgS TiO_2
pillar in the back of the painting	red	vermilion	HgS
left hill in the centre of the panel	blue	anatase lead white	TiO_2 $2\text{PbCO}_3 \cdot \text{Pb(OH)}_2$
middle hill in the centre of the panel	blue	anatase lead white	TiO_2 $2\text{PbCO}_3 \cdot \text{Pb(OH)}_2$
right hill in the centre of the panel	blue	anatase lead white	TiO_2 $2\text{PbCO}_3 \cdot \text{Pb(OH)}_2$
sky in the centre of the panel	blue	anatase lead white massicot	TiO_2 $2\text{PbCO}_3 \cdot \text{Pb(OH)}_2$ PbO
ribbon cantor's staff	white	anatase lead white zinc white	TiO_2 $2\text{PbCO}_3 \cdot \text{Pb(OH)}_2$ ZnO
left pillar	beige	lead white massicot	$2\text{PbCO}_3 \cdot \text{Pb(OH)}_2$ PbO
rim of the decorative border of the chasuble	brown	vermilion	HgS
collar alba priest	white	massicot/zinc white?	PbO/ZnO?
left chapter	white	massicot/zinc white?	PbO/ZnO?
bottom edge garment Virgin	red	vermilion lead white	HgS $2\text{PbCO}_3 \cdot \text{Pb(OH)}_2$
border of the decorative border of the chasuble	yellow	lead-tin yellow type I	Pb_2SnO_4

Table 8.1 Overview of the measured points and pigments identified by Raman spectroscopy.

8.4 Results and discussion

8.4.1 Direct energy dispersive X-ray fluorescence analysis

Although a number of analysis points were taken all over the Wyts panel, the main objective of the EDXRF analysis was to look at the restored parts of the painting. In total, in a compromise between time and material characterisation of this work of art, 60 EDXRF spectra were recorded, regrouping all colours as well as problematic and particular areas of investigation. From all the recorded XRF spectra, we can assume that an intermediate layer (priming layer) made of a Pb-based pigment is present. This was confirmed by X-ray radiography, because of the whitish aspect of the film. The lead white mixed with the other pigments shows more dense zones on the film.

8.4.1.1 Red, brown and flesh colour

By means of the X-ray fluorescence technique, two red pigments of the painting were identified, namely red iron oxide and vermilion (HgS). In the spectra of the red spots, where the use of iron oxides can be supposed, manganese was also identified (Fig. 8.3(a)). This could mean that the red iron oxide used in the painting was a natural iron oxide.

The intense red area on the right side of the Virgin's garment seems to be made exclusively of a Hg-based pigment (Fig. 8.3(b)). On the left side of the garment, where the colour is darker, a mixture of vermilion (HgS) with addition of red iron oxide might have been used.

Red iron oxide pigments with addition of vermilion (HgS) were also noticed in the red pillar on the background of the painting and on the inside rim of the priest's

figurative border of the chasuble. We can also observe that the colour of these areas is brownish red instead of intense, dark red.

The same combination of pigments was also present in the brown coloured areas of the painting such as the character's hair and the exterior rim of the priest's figurative border of the chasuble. For all flesh colour, vermilion (HgS) mixed with lead white ($2\text{PbCO}_3 \cdot \text{Pb}(\text{OH})_2$) was used.

The EDXRF analysis also revealed some spots where modern pigments were used, in the brown colour. Paint retouching with a Zn-based pigment was found in the left part of the Virgin's garment and in her hair. The most retouched red parts were found in the skin of the Christ child. Zinc pigments were identified in the groin of the Christ child, in his stomach and finally under his left arm.

8.4.1.2 Blue and green colour

Copper pigments were found in both blue and green areas. This is confirmed by at least one point taken in the blue priest's chasuble, in the dark blue upper Virgin's garment and finally in the green background of the painting. On the other hand, the XRF analysis indicated that the blue sky in some analysed zones contained a Co-based pigment (Fig. 8.3(c)). Traces of arsenic were found in the right part of the blue sky, but not in the centre of the panel. This result has to be taken with caution, because the Pb-L α line (10.55 keV) coincides with the As-K α line (10.54 keV) and for that reason, the difference between these two elements can only be achieved by looking at the K β line of As at about 11.7 keV, which does not present a highly intense peak. The mountains, between the green background and the sky, in the middle of the central panel suggest modern retouching, probably made with zinc and titanium white. This area seems to be completely repainted.

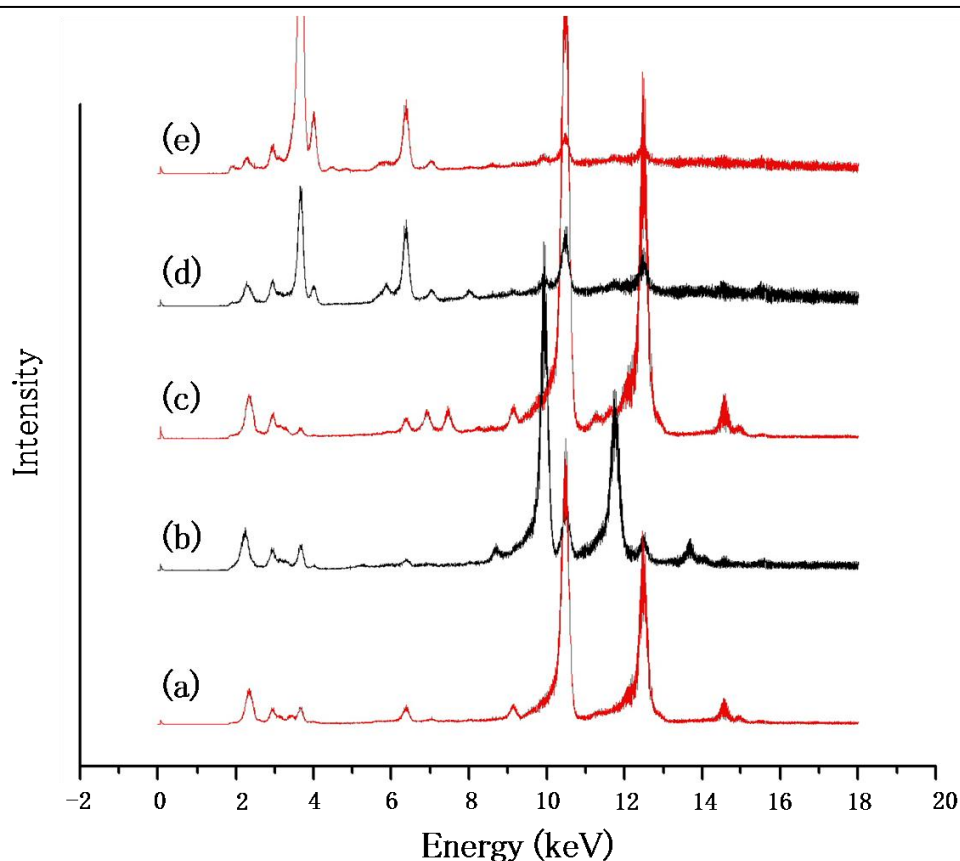


Figure 8.3 (a) XRF spectrum of red iron oxide mixed with vermilion (HgS) from the red pillar on the background of the painting; (b) XRF spectrum of vermilion (HgS) from the Virgin's red dress. $L\alpha$ of Hg is observed at 9.898 keV and $L\beta$ at 11.824 keV; (c) XRF spectrum of a Co-containing pigment from the blue mountains on the left side of the panel. The presence of Co ($K\alpha$ at 6.92 keV) and Ni ($K\alpha$ at 7.478 keV) can be observed; (d) XRF spectrum of lead-tin yellow type I ($PbSnO_4$) from the pillar on the left side of the panel. The presence of Sn ($L\alpha$ at 3.44 keV) and Pb ($L\alpha$ at 10.55 keV) can be observed. (e) XRF spectrum of probably an important restoration from the left part of the red dark garment of the Virgin. By comparing this spectrum with another one from the Virgin's red dress (b), one can see that the ratio Fe ($K\alpha$ at 6.4 keV)/Hg ($L\alpha$ at 9.989 keV) is totally different.

8.4.1.3 White colour

Lead white ($2PbCO_3 \cdot Pb(OH)_2$) was detected in the undergarment of the Virgin and in the banner crossing the middle of the central panel. Modern zinc pigments were

also discovered in the banner next to the cantor's staff. Two points were measured in the collar of the priest's alba. At least one modern white pigment was found in this area. XRF analysis showed the presence of Pb and Zn in one point and Pb and S with traces of Ca in the second point. This last point suggests the use of pure lead white ($2\text{PbCO}_3 \cdot \text{Pb}(\text{OH})_2$).

8.4.1.4 Yellow colour

There is much similarity between the results of the investigated yellow areas. All yellow points taken of the ceiling and around the rim of the priest's figurative border of the chasuble indicate lead-tin yellow type I (Pb_2SnO_4) (Fig. 8.3(d)). However, the two pillars on the left and right side have a different composition: no lead-tin yellow type I (Pb_2SnO_4) was detected. Indeed, the colour is not exactly yellow. Fe and traces of Co and Ni are found in these two areas. So it is possible that a mixture of iron oxides and a Co-containing pigment was used to paint this area, but the presence of yellow organic colorants cannot be excluded with this technique. The left vault and the low wall in the middle of the central panel do not contain Sn either. This lack of Sn suggests the use of yellow iron oxides/hydroxides for these two regions.

8.4.1.5 Restored areas and two-dimensional elemental mapping

Around the whole panel, several spectra looked totally different from all the others. Three points caught our attention. The first one is situated in the yellow rim of the priest's figurative border of the chasuble, where amending of the painting with the substrate is clearly visible. The second one is on the left part of the dark red garment of the Virgin and, finally, the third one is located in the Virgin's hair. These points all have in common an intense $\text{K } \alpha$ line coming from the Ca and nearly

no response coming from the Pb-L α line. An important restoration could have been made at these points, through which the intermediate layer (priming layer) might have been lost (Fig. 8.3(e)). According to the XRF results, Zn and Ti pigments have been used for the yellow border and in the Virgin's hair. Curiously, only traces of Ti, but no Hg, were detected in the point in the left dark red garment of the Virgin. A red iron oxide could have been used in this point.

According to the XRF results, a number repaints and restorations were identified all over the painting. Scattered points found in the dark red Virgin's garment at a level above the low wall, in the collar of the priest's alba, in the banner crossing the centre of the panel and finally in the Virgin's hair at the level of her shoulder indicate the use of Zn and Ti pigments. Areas with a large amount of restored parts were also located especially in the characters. The Christ child presents restored regions all over his body, as well as the Virgin's hair and face. The mountains and the brown line underneath, representing the beginning of the landscape in the middle of the central panel were totally repainted. This was also the case for the priest's face and its surrounding areas.

Three two-dimensional elemental maps were realised in three different sensitive regions: the priest's forehead, the Virgin's forehead and the priest's cheek. These three maps allowed us to locate, with precision, all repainting with Zn and Ti pigments in these regions. Also, by means of this elemental mapping, any particular element can be precisely positioned and a relative colour map can be made, regarding the elemental intensity in the XRF spectra. This can give information to better understand the layers' composition. Figure 8.4 shows one of the three mappings, namely in the area of the priest's forehead. First, the XRF map indicates that the paint used for the priest's hair is mainly composed of Fe and a small amount of Ca (Fig. 8.4(a)). (These Ca spots probably show that retouching was applied directly on the ground, and that the intermediate layer (priming layer) based of lead white ($2\text{PbCO}_3 \cdot \text{Pb}(\text{OH})_2$) has been lost.) This map shows also that a Pb-

containing pigment was used for the priest's skin and the sky region (Fig. 8.4(b)). Second, this map shows where the restored areas are located. Indeed, traces of Ti (Fig. 8.4(c)) and Zn (Fig. 8.4(d)) are good indicators of modern repaints.

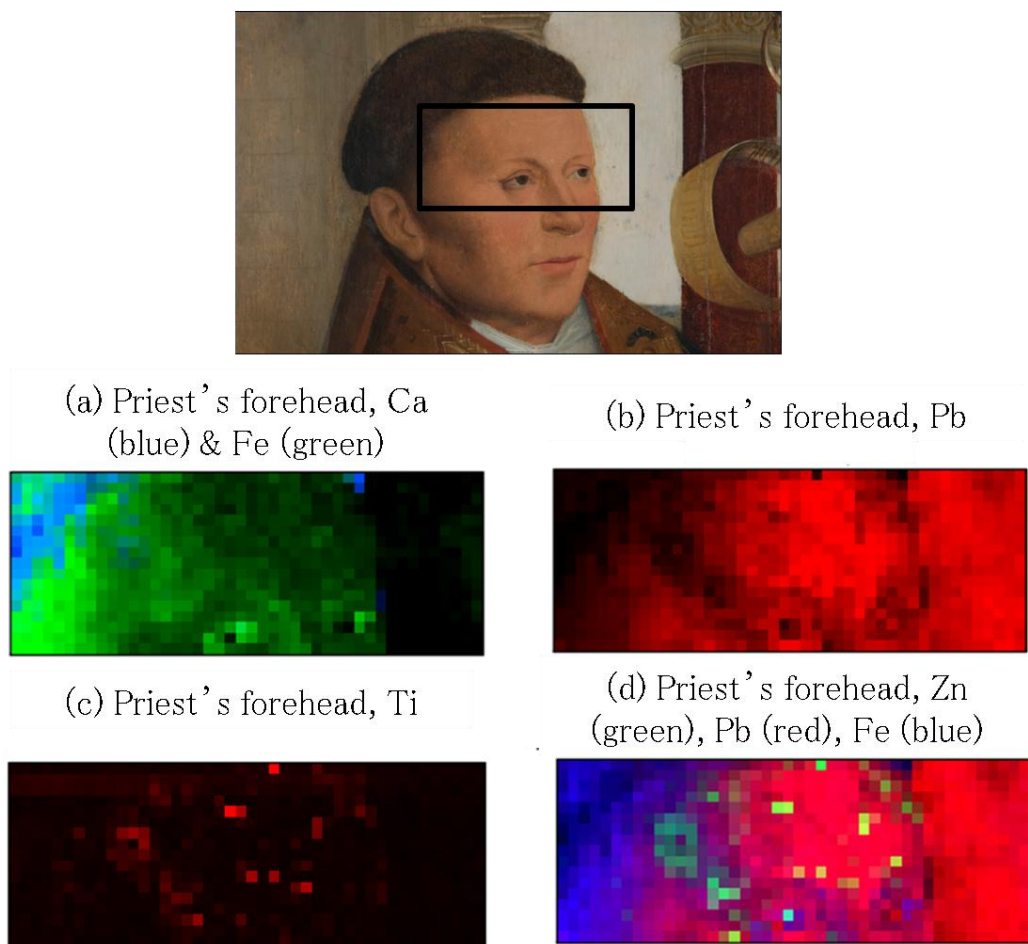


Figure 8.4 Two-dimensional elemental mapping realised by the portable EDXRF instrument with a step of 3 mm in horizontal and vertical directions in the region of the priest's forehead: (a) Ca and Fe mapping; (b) Pb mapping; (c) Ti mapping and (d) Zn, Pb and Fe mapping.

8.4.2 Direct Raman spectroscopic analysis

Because Raman spectroscopy is a surface technique, with a relatively small penetration depth, it is not obvious that Raman spectroscopy can help to reconstruct the layered structure of the central panel of the 'Wyts Triptych' unless

sampling takes place. Sampling the panel was not possible, so direct Raman analysis had to be performed. Nevertheless, Raman spectroscopy can provide much interesting information on the used pigments. Another problem that has to be taken into account is that some of the recorded Raman spectra are overwhelmed by fluorescence due to the thick varnish layer on top of the painting. Despite these difficulties, the Raman analysis yields some interesting results. An overview of the measured points and the identified pigments is listed in table 8.1.

8.4.2.1 Red, brown and flesh colour

As can be seen in table 8.1, the pigment vermilion (HgS) is used for the red, brown and flesh-coloured parts of the painting. To accomplish these three different colour tones, the pigment vermilion (HgS) (Raman bands at 256, 284 and 343 cm^{-1}) has to be mixed with another pigment.

The pigment vermilion (HgS) was used for the red and brown rim of the priest's figurative border of the chasuble. Vermilion (HgS) is a pigment used since antiquity, so it is impossible to determine, by pigment identification, whether the top layer is the original one. By looking at drawings and pictures of the painting taken before restoration and in between the different restoration processes, one can see that the decorations on the priest's figurative border of the chasuble are adapted during the years. During the restoration, it is possible that the priest's figurative border of the chasuble is overpainted or even repainted, or even that some parts were never restored.

Raman analysis of the red garment of the Virgin reveals the use of vermilion (HgS) and a small Raman band at 111 cm^{-1} (Fig. 8.5(a)). With Raman spectroscopy, it was not possible to identify this pigment. The few reports of the restorations and from the pictures taken between and during the restoration processes, implicate no restoration of the Virgin's garment. Only on the UV-pictures (Fig. 8.1(d)) one can

see that some areas are heavily repainted. However, this would be almost impossible to detect by pigment identification, because no modern pigment was used.

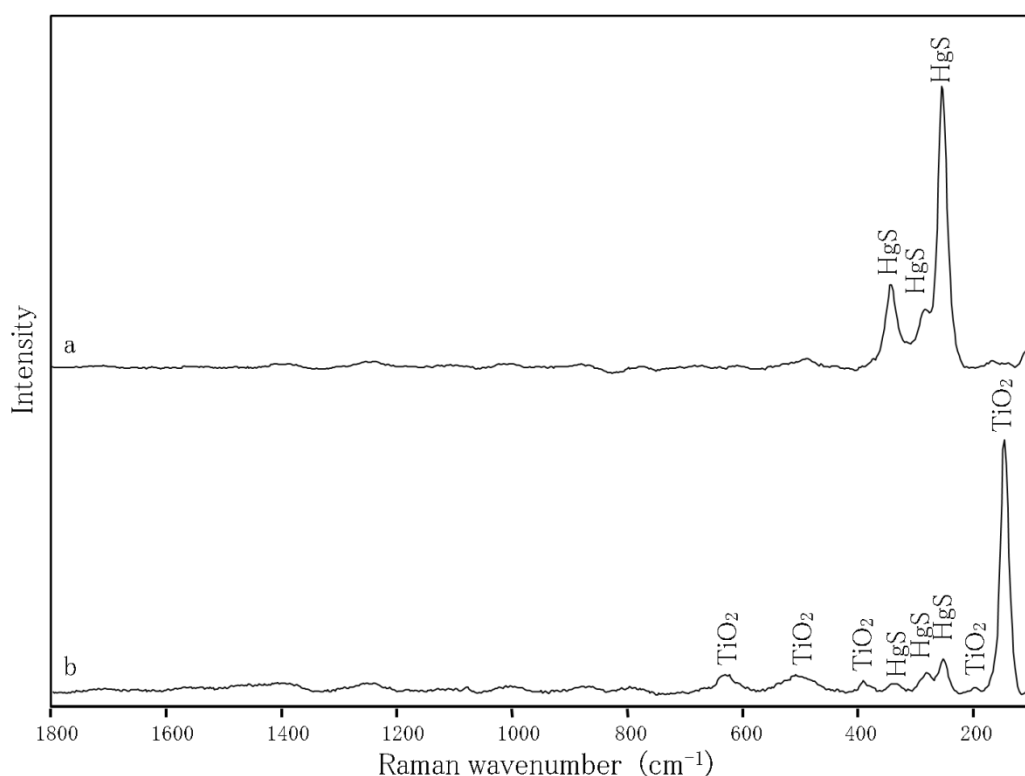


Figure 8.5 Raman spectrum of (a) the Virgin's garment, showing Raman bands of vermilion (HgS) and (b) the chest of the Christ child, showing Raman bands of vermilion (HgS) and anatase (TiO₂).

Comparing the drawings and the different pictures taken from the Wyts panel during history, it could be noticed that the figure of the Christ child underwent many adaptations. Raman analysis executed on the foot, groin and shoulder as well as on different places on the belly and chest of the Christ child shows the presence of vermilion (HgS). It looks as though during restoration vermilion (HgS) was used as a red pigment. It is possible that the original red paint used to paint the figure of the Christ child was also vermilion (HgS) and that, during restoration, the choice was made to use the original pigment. Raman analysis from the chest of the Christ child shows an intense Raman band at 149 cm⁻¹ and a smaller band at 198 cm⁻¹. This Raman band is caused by the pigment anatase (TiO₂) (Fig. 8.5(b)). Anatase (TiO₂)

was not used by the artists immediately following its industrial manufacture (around 1920)²⁹. This was partly due to the high price. The industry was also influenced by the pigment's somewhat unreliable colour, its limited supply in most countries and their reluctance to change from traditional materials. Next to the pure pigment, composite anatase (TiO_2) pigments with barium sulphate (BaSO_4) became commercially available in 1916. By 1950, barium sulphate was almost completely replaced by calcium sulphate (CaSO_4). The presence of anatase (TiO_2), which is a modern pigment, suggests that restoration took place.

8.4.2.2 Blue colour

Different Raman spectra were recorded from the middle of the central panel, such as from the left, middle and right hill, and from the sky above them. The colour of these regions is very light blue, almost white. It was not possible to identify the blue pigment because of the overwhelming Raman signals caused by the white pigments. The Raman spectra of these measured points all show a very strong Raman band at 149 cm^{-1} caused by the pigment anatase (TiO_2). The weaker Raman bands of anatase (TiO_2) (393 , 511 and 632 cm^{-1}) are also clearly visible in the spectra. Since the pigment anatase (TiO_2) is a modern pigment, this region of the Wyts panel was definitely restored.

The Raman spectra also show bands at 110 and 1050 cm^{-1} . These bands are caused by the pigment lead white ($2\text{PbCO}_3 \cdot \text{Pb}(\text{OH})_2$). There are three possibilities: lead white ($2\text{PbCO}_3 \cdot \text{Pb}(\text{OH})_2$) was used as the original paint for this region; or the restorers used a combination of lead white ($2\text{PbCO}_3 \cdot \text{Pb}(\text{OH})_2$) with anatase (TiO_2); or the pigment anatase (TiO_2) was later applied.

The Raman spectrum of the blue sky shows a strong extra band (149 cm^{-1}) (Fig. 8.6(a)). This band is caused by zinc white (ZnO) or massicot (PbO). Massicot

(PbO) is a pigment used since antiquity, and has a yellow colour. Although zinc white (ZnO) is known since antiquity, it was not considered as an artists' pigment until the end of the 18th century. Today many manufactures incorporate zinc white (ZnO) as a supplementary pigment in titanium white (TiO_2) and lead white ($2\text{PbCO}_3 \cdot \text{Pb(OH)}_2$) oil paints, to improve the performance particularly for use outdoors²⁹. To give a decisive answer on the used pigment, the Raman results have to be compared with the XRF results.

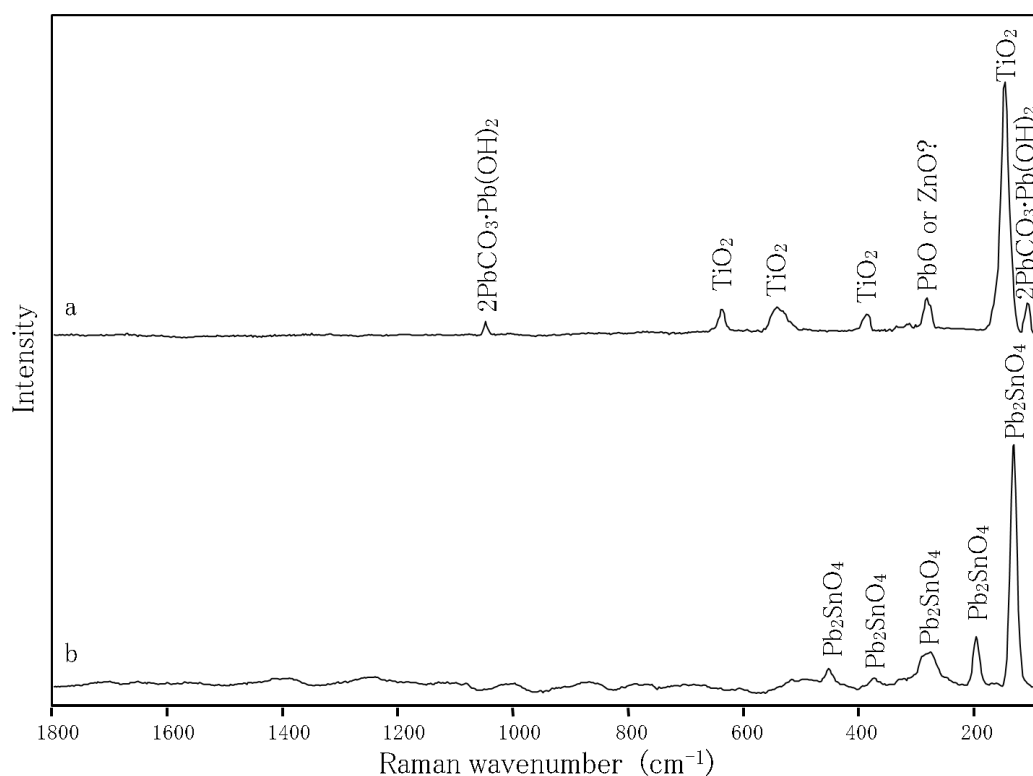


Figure 8.6 Raman spectrum of (a) the sky in the centre of the panel, showing bands of lead white ($2\text{PbCO}_3 \cdot \text{Pb(OH)}_2$), anatase (TiO_2) and massicot (PbO) and (b) the rim of the priest's figurative border of the chasuble showing the spectrum of lead-tin yellow type I (Pb_2SnO_4).

8.4.2.3 White colour

The Raman spectra of the ribbon of the cantor's staff show Raman bands of anatase (TiO_2), lead white ($2\text{PbCO}_3 \cdot \text{Pb}(\text{OH})_2$) and zinc white (ZnO) or massicot (PbO) (285 cm^{-1}). The presence of anatase (TiO_2) indicates that this part of the panel is probably also restored. The Raman spectrum of the left pillar, which has a beige colour, shows bands of lead white ($2\text{PbCO}_3 \cdot \text{Pb}(\text{OH})_2$) and massicot (PbO) or zinc white (ZnO) (285 cm^{-1}). In both the above-mentioned cases, the Raman results have to be compared with the XRF results to give a decisive answer.

8.4.2.4 Yellow colour

The Raman spectrum of the yellow rim of the priest's figurative border of the chasuble shows bands caused by lead-tin yellow type I (Pb_2SnO_4) ($135, 200, 279, 295, 377$ and 455 cm^{-1}) (Fig. 8.6(b)). The pigment lead-tin yellow type I is also used since antiquity, so no judgement could be made on the original paint layer.

8.4.2.5 Discussion

By studying the Raman spectra, we conclude that most of the identified pigments cannot be used to collect information on the original paint layers and the layered structure of the paint. The use of a modern pigment, anatase (TiO_2), proves that some parts of the painting were restored. By comparing the Raman analysis with the XRF analysis, a decisive answer can be given on the use of zinc white (ZnO) or massicot (PbO) for the light blue and white colour.

8.4.3 Integration of the results

By comparing the results of both complementary techniques, some conclusions could be made on the used pigments, the layered structure and the restored areas of the painting. Visual analysis of the triptych already confirmed that the investigated panel is a copy of van Eyck; comparing, for example, the meticulous decorations on the boarder of the Virgin's garment with other known works of van Eyck, shows that the decorations painted by van Eyck are much more refined.

8.4.3.1 Red, brown and flesh colour

XRF spectroscopy and Raman spectroscopy confirmed that the pigment used for these three different colours is Hg-based, namely vermilion (HgS). With Raman spectroscopy it was not possible to identify the other pigments of the mixture. In contrast, the XRF results show that a red iron-based oxide is used to make the different colour tones. By using other proportions of both pigments, shifting colour tones were produced. For the bright red colours, such as for various areas of the Virgin's garment, the intensity of the $K\alpha$ line of Hg is much higher than the $K\alpha$ line of Fe, meaning that for this colour the relative amount of the Hg-based pigment is much higher than the amount of Fe-based pigment. For the brown colour, the opposite is detected. Here, the quantity of the iron-based pigment is higher in comparison with the amount of Hg-based pigment.

For the flesh colour, XRF spectroscopy as well as Raman spectroscopy confirms the use of vermilion (HgS) with titanium dioxide (TiO_2) for the restored parts, such as for the chest of the Christ child (Raman spectroscopy could confirm the use of anatase). Moreover, XRF also confirms the presence of a Pb-based pigment, probably lead white ($2PbCO_3 \cdot Pb(OH)_2$). The combination of vermilion (HgS) and a

Pb-based pigment can be found in different areas of the Christ child, such as on the foot, groin, belly and shoulder.

Both techniques confirm the use of vermilion (HgS) as the main pigment for the garment of the Virgin, except for one point on the left part of the dark red area. The UV-picture (Fig. 8.1(d)) of this point shows overpainting. Because of the thick fluorescent varnish layer, it was not possible to obtain a Raman spectrum of this point. However, if we take a closer look at the XRF results, we see almost no response from the Pb-L α line. This could suggest that a big restoration took place, where even the intermediate layer (priming layer) was scraped away and the retouching was applied immediately on the ground layers made of Ca. The red pigment used was probably Fe-based. Because there are only 3 of the 60 analysed points that show this composition, we believe that the painting was unintentionally damaged in these regions.

8.4.3.2 Blue and green colour

By using a red diode laser (785 nm) for Raman spectroscopy, it is almost impossible to identify green pigments because of the fluorescence. A solution to this problem is the use of a green laser, or the use of a complementary technique, as XRF spectroscopy, which gives information on the elemental composition. This was the case for the green as well as for the blue areas. Cu-based pigments were found both for the blue and green areas of the painting. The XRF results also show that the blue sky was partly overpainted by a Co-based pigment.

For the mountains, between the green background and the sky, in the centre of the painting both techniques found traces of anatase (TiO₂), suggesting that this part of the painting was repainted. The XRF spectrum shows traces of Zn, suggesting that zinc white (ZnO) was mixed with the Co-containing pigment. This interpretation supports the fact that this part of the painting was restored.

8.4.3.3 White and yellow colour

When taking a closer look to the ribbon of the cantor's staff, one can see that two parts can be distinguished in the ribbon: the left part, which has a darker colour and is not very smooth; and the right part, which has a lighter colour and is very smooth. XRF measurements of the left part show the presence of Pb as the major element. The Raman spectrum of this part shows only bands of lead white ($2\text{PbCO}_3 \cdot \text{Pb}(\text{OH})_2$), suggesting that no restoration took place. For the right part, XRF measurements found traces from Ti and Zn, suggesting that this part was definitely restored. The presence of Zn in the XRF spectra points to the use of zinc white (ZnO). So the Raman band at 285 cm^{-1} is, in this case, caused by zinc white (ZnO). For the left pillar, which has a beige colour, the XRF spectrum only shows the presence of lead. This information can be used to interpret the Raman results. The Raman band at 285 cm^{-1} in the spectrum of the beige pillar is caused by massicot (PbO).

For the yellow colour, both techniques agree with the use of lead-tin yellow type I (Pb_2SnO_4). The XRF spectra in some points (left vault and low wall in the middle of the central panel) do not contain Sn. This lack of Sn could suggest that yellow oxides/hydroxides or even yellow organic colorants were used.

8.5 Conclusions

This research shows that, when a combination of EDXRF spectroscopy and Raman spectroscopy is used, all the characteristics of an ideal method for analysing archaeological objects, according to Lahanier *et al.* are present.

We can conclude that the intermediate layer (priming layer) of the painting is painted with a Pb-based pigment, probably lead white ($2\text{PbCO}_3 \cdot \text{Pb}(\text{OH})_2$). This was confirmed by X-ray radiography. The main pigment used for the red and brown

areas is vermilion (HgS) mixed with different amounts of iron oxide to obtain different colour shades. For the flesh colour, a combination of vermilion (HgS) and lead white ($2\text{PbCO}_3 \cdot \text{Pb}(\text{OH})_2$) or anatase (TiO_2) was used, depending whether the area of the painting was restored or not.

For the blue and green areas, the pigment used is Cu-based, except that in the blue sky traces of Co were found. The presence of anatase (TiO_2) and zinc white (ZnO) suggests that also some parts of the painting were restored. The yellow pigment used is lead-tin yellow type I (Pb_2SnO_4). Another yellow pigment could not be identified, but the results point in the direction of a yellow oxide/hydroxide or a yellow organic colorant.

Three of the investigated areas showed a totally different XRF spectrum: no signal of lead was present. This suggests that for these points the original intermediate layer (priming layer) was lost. Some other points also show signs of restoration, but here lead white ($2\text{PbCO}_3 \cdot \text{Pb}(\text{OH})_2$) was still present. This suggests that only the top layers of the painting were scrapped away.

By producing XRF maps, we got an idea of the changes the painting underwent during history. The restored parts could easily be identified on the basis of the XRF maps.

It was not possible to obtain much information on how the painting looked during history, as too many restorations took place. It is impossible to know which parts of the painting are still original, since the different restorations are not (well) documented.

The mapping of the restored area with XRF spectroscopy, as described in this chapter, gave a very precise image of the distribution of the elements in the mapped zone. The presence of some traces of Zn and Ti indicates that restoration took

place. Performing point measurements with Raman spectroscopy and XRF spectroscopy resulted in the identification of the modern pigments: anatase (TiO_2) and zinc white (ZnO). Point measurements do not result in an image of the restored area, but show the presence of anachronisms, which indicate a possible restoration. For this research, it was not possible to perform mappings on the central panel of the Wyts Triptych with the mobile Raman spectrometer (MArtA). Nevertheless we wanted to explore the possibilities of combining Raman mapping and XRF mapping. In the next chapter porcelain cards are used as subject to explore the different possibilities of laboratory Raman and laboratory XRF mapping.

References

1. Smith, D.C., Bouchard, M., Lorblanchet, M. (1999) An initial Raman microscopic investigation of prehistoric rock art in caves of the Quercy District, S. W. France. *Journal of Raman Spectroscopy* 30: 347–354.
2. Zoppi, A., Signorini, G.F., Lucarelli, F., Bachechi, L. (2002) Characterisation of painting materials from Eritrea rock art sites with non-destructive spectroscopic techniques. *Journal of Cultural Heritage* 3: 299–308.
3. Hernanz, A., Gavira-Vallejo, J.M., Ruiz-Lopez, J.F. (2006) Introduction to Raman microscopy of prehistoric rock paintings from the Sierra de las Cuerdas, Cuenca, Spain. *Journal of Raman Spectroscopy* 37: 1054–1062.
4. Rosi, F., Miliani, C., Borgia, I., Brunetti, B., Sgamellotti, A. (2004) Identification of nineteenth century blue and green pigments by in situ x-ray fluorescence and micro-Raman spectroscopy. *Journal of Raman Spectroscopy* 35: 610–615.
5. Paternoster, G., Rinzivillo, R., Nunziata, F., Castellucci, E.M., Lofrumento, C., Zoppi, A., Felici, A.C., Fronterotta, G., Nicolais, C., Piacentini, M., Sciuti, S., Vendittelli, M. (2005) Study on the technique of the Roman age mural paintings by micro-XRF with Polycapillary Conic Collimator and micro-Raman analyses. *Journal of Cultural Heritage* 6: 21–28.
6. Vandenabeele, P., Lambert, K., Matthys, S., Schudel, W., Bergmans, A., Moens, L. (2005) In situ analysis of mediaeval wall paintings: a challenge for mobile Raman spectroscopy. *Analytical and Bioanalytical Chemistry* 383: 707–712.
7. Deneckere, A., Schudel, W., Van Bos, M., Wouters, H., Bergmans, A., Vandenabeele, P., Moens, L. (2010) In situ investigations of vault paintings in

- the Antwerp cathedral. *Spectrochimica Acta Part A-Molecular and Biomolecular Spectroscopy* 75: 511–519.
8. Ortega-Aviles, M., Vandenabeele, P., Tenorio, D., Murillo, G., Jimenez-Reyes, M., Gutierrez, N. (2005) Spectroscopic investigation of a 'Virgin of Sorrows' canvas painting: A multi-method approach. *Analytica Chimica Acta* 550: 164–172.
 9. Burgio, L., Clark, R.J.H., Theodoraki, K. (2003) Raman microscopy of Greek icons: identification of unusual pigments. *Spectrochimica Acta Part A-Molecular and Biomolecular Spectroscopy* 59: 2371–2389.
 10. Castillejo, M., Martin, M., Oujja, M., Silva, D., Torres, R., Domingo, C., Garcia-Ramos, J.V., Sanchez-Cortes, S. (2001) Spectroscopic analysis of pigments and binding media of polychromes by the combination of optical laser-based and vibrational techniques. *Applied Spectroscopy* 55: 992–998.
 11. Bruni, S., Ciariati, F., Guglielmi, V. (2005) *Raman spectroscopy in archaeology and art history*. Chapter 9 Case study: field and in situ identification of pigments in works of art by micro-Raman and visible-NIR reflectance spectroscopies: a polychrome 16th century Italian fresco and black-coloured Etruscan pottery. The Royal Society of Chemistry, Cambridge, 142–151.
 12. Centeno, S.A., Mahon, D., Wypyski, M.T. (2004) Examination of a Spanish medieval processional crucifix substantially reworked in the 20th century. *Journal of Raman Spectroscopy* 35: 774–780.
 13. Edwards, H.G.M., Villar, S.E.J., Eremin, K.A. (2004) Raman spectroscopic analysis of pigments from dynastic Egyptian funerary artefacts. *Journal of Raman Spectroscopy* 35: 786–795.

14. Lahanier, Ch., Preusser, F.D. Van zelst L. (1986) *Nuclear instruments and Methods in Physics Research*. North-Holland Physics publishing division, Amsterdam.
15. Vandenabeele, P., Edwards, H.G.M. (2005) *Raman spectroscopy in archaeology and art history*. Chapter 11 Overview: Raman spectroscopy of artefacts. The Royal Society of Chemistry, Cambridge, 169–178.
16. Vandenabeele, P., Garcia-Moreno, R., Mathis, F., Leterme, K., Van Elslande, E., Hocquet, F.P., Rakkaa, S., Laboury, D., Moens, L., Strivay, D., Hartwig, M. (2009) Multi-disciplinary investigation of the tomb of Menna (TT69), Theban Necropolis, Egypt. *Spectrochimica Acta Part A-Molecular and Biomolecular Spectroscopy* 73: 546–552.
17. Falcone, L., Bloisi, F., Califano, V., Pagano, M., Vicari, L. (2008) An old notice board at ancient Herculaneum studied using Near Infrared Reflectography. *Journal of Archaeological Science* 35: 1708–1716.
18. Consolandi, L., Bertani, D. (2007) A prototype for high resolution infrared reflectography of paintings. *Infrared Physics & Technology* 49: 239–242.
19. Daniilia, S., Bikiaris, D., Burgio, L., Gavala, P., Clark, R.J.H., Chrysoulakis, Y. (2002) An extensive non-destructive and micro-spectroscopic study of two post-Byzantine overpainted icons of the 16th century. *Journal of Raman Spectroscopy* 33: 807–814.
20. Sawczak, M., Kaminska, A., Rabczuk, G., Ferretti, M., Jendrzewski, R., Sliwinski, G. (2009) Complementary use of the Raman and XRF techniques for non-destructive analysis of historical paint layers. *Applied Surface Science* 255: 5542–5545.

-
21. Fremout, W., Saverwyns, S., Peters, F., Deneffe, D. (2006) Non-destructive micro-Raman and X-ray fluorescence spectroscopy on pre-Eyckian works of art – verification with the results obtained by destructive methods. *Journal of Raman Spectroscopy* 37: 1035–1045.
 22. Ricci, C., Borgia, I., Brunetti, B.G., Miliani, C., Sgamellotti, A., Seccaroni, C., Passalacqua, P. (2004) The Perugino's palette: integration of an extended in situ XRF study by Raman spectroscopy. *Journal of Raman Spectroscopy* 35: 616–621.
 23. Castro, K., Perez-Alonso, M., Rodriguez-Laso, M.D., Etxebarria, N., Madariaga, J.M. (2007) Non-invasive and non-destructive micro-XRF and micro-Raman analysis of a decorative wallpaper from the beginning of the 19th century. *Analytical and Bioanalytical Chemistry* 387: 847–860.
 24. Jones, S.F. (2006) New evidence for the date, function and historical significance of Jan van Eyck's 'Van Maelbeke Virgin'. *Burlington Magazine* 148: 73–81.
 25. KIK-IRPA (1975) Triptyque Van Maelbeke: Conclusions générales de l'examen fait à l'IRPA du 6 mars au 26 juillet 1974 (dossier 2l/43. 74/613).
 26. KIK-IRPA (1975) Letter and report by Fletcher, J.M, Research Laboratory for Archaeology and the History of Art, Oxford University, to R. Lefevre KIK-IRPA (dossier L3/13/311320).
 27. Hocquet, F.P., Garnir, H.P., Marchal, A., Clar, M., Oger, C., Strivay, D. (2008) A remote controlled XRF system for field analysis of cultural heritage objects. *X-Ray Spectrometry* 37: 304–308.

28. Vandenabeele, P., Weis, T.L., Grant, E.R., Moens, L.J. (2004) A new instrument adapted to in situ Raman analysis of objects of art. *Analytical and Bioanalytical Chemistry* 379: 137–142.
29. Fitzhugh, E.W. (1997) *Artists' Pigments: A handbook of their history and characteristics volume 3*. Chapter 10: Titanium dioxide whites. Oxford University Press, New York, 295–343.

Chapter 9: Feasibility study of the application of micro-Raman imaging as complement to micro-XRF imaging

Annelien Deneckere, Bart Vekemans, Lien Van de Voorde, Paul de Paepe,
Laszlo Vincze, Luc Moens, Peter Vandenabeele

Submitted for the Special Issue of Applied Physics A on
“Optical Technologies in Art and Archaeology.”

In the previous case studies (Chapters 5,6 &7) only point measurements were used to analyse the different art objects, except for Chapter 8, where XRF mappings were performed on the central panel of the ‘Wyts Triptych’ to get an image of the restored areas. In this chapter the possibilities of Raman and XRF mapping are explored using porcelain cards as subjects. Micro-XRF mapping is already a routine analytical imaging method because of the well-established spectrum evaluation methodology enabling specific data handling procedures. These include multivariate statistical analysis procedures such as principal components analysis (PCA) in order to explore and describe the acquired data, and clustering techniques in order to find similar pixels (or areas) in the obtained images. In the case of micro-Raman, however, the usual approach is to perform a single spot analysis of only a few selected positions in order to ultimately identify the material on the basis of the comparison with Raman spectra obtained from reference materials. However, when samples are heterogeneous, imaging is still to be preferred in order to deal with the problem of sampling. One of the most important aspects of imaging is the time needed for the analysis. Therefore, the influence of different instrumental parameters, such as resolution (low or high) and measuring time per pixel, on the quality of Raman spectra and images was investigated in order to evaluate the possibility of performing fast Raman mappings because of the need to identify the regions of interest on the art object in a more systematic manner.

In the first part of this chapter, an overview of the developments in Raman spectroscopy and XRF spectroscopy and the combination of both techniques for the analysis of art objects is given.

9.1 Introduction

During the last decade Raman mapping has proved to be a basic tool to gain insight into, amongst others: the composition of multi-layered structures, by investigating

stratigraphic samples removed from art objects¹, the deterioration process of pigments in frescos², the painting technique of 16th century artists³, rust scales on archaeological iron artefacts⁴ and the penetration depth of conservation treatment on cultural heritage⁵. Non-destructive Raman mapping can be performed using a motorised x-y stage system that allows moving the objects in a plane. When the stage additionally also moves in the z direction, depth profiling can take place. Performing Raman mappings with the conventional experimental set-up may have two limitations: only objects which fit under the microscope can be analysed, and due to the fact that the surfaces of art objects are usually not flat, the analysis is time consuming because of the optimisation of the focal distance that is necessary for each point¹. Ropret et al.¹ suggested an alternative experimental set-up to exclude the limitation of the dimensions of the objects: a Raman mapping based on a set of scanning mirrors that direct the laser beam in two spatial directions, vertically through a horizontal exit on the Raman spectrometer. In this approach, when the beam is directed through the microscope objective, the size of the object remains the limiting factor, but when the mirrors are placed at the spectrometer's horizontal exit, considerably larger works of art can be studied, keeping the advantages of full confocality and the possibility to use multiple excitation lines.

In this research, a Raman spectrometer with a conventional experimental set-up is used to perform Raman mappings on a selected area of a porcelain card. Porcelain cards are 19th century art objects, printed by a lithographic process, and are due to their dimensions excellent test-cases for mapping experiments. Next to the Raman mappings also XRF mappings using a conventional set-up were performed on a similar area of the porcelain card. The availability of the microscopic type of XRF spectroscopy allows to perform a fast mapping to select the regions of interest and afterwards performing long point measurements or mappings with a long measurement time in the selected regions of interest⁶. In this work, the possibility of performing fast maps with Raman spectroscopy on a selected area of the porcelain

card is evaluated by changing different parameters, such as the measurement time and the resolution.

Porcelain cards are cardboards covered with a layer of lead white, printed with text and brightened with decorations. They represent the modern business cards or announcements of the 19th century. Historical details of these cards are described elsewhere⁷. Previous research⁷ showed that the identification of the pigments used is straightforward, even when analysing with a short measuring time. Therefore a porcelain card was used as object to evaluate the influence of Raman mapping in high or low resolution mode and measuring for a short or long time.

Before presenting the results of the XRF maps and discussing the influence of the different parameters on the Raman maps, an overview of the development and applications in the field of archaeometry of Raman spectroscopy, XRF spectroscopy and the combination of both techniques is given.

9.2 Techniques

9.2.1 Raman spectroscopy

During the last 15 years Raman spectroscopy has increasingly been applied for the analysis of art objects^{8,9}. In 1979 Dhamelincourt et al.¹⁰ described the coupling of a microscope to the Raman spectrometer and the application for the analysis of art objects. The earliest papers focused in general on instrumental improvements and explored the suitability of the approach for the investigation of art objects^{11,12}, focusing mainly on pigment identification. The identification of pigments in art objects can provide information on the manufacture date¹³, can help to decide on future restoration actions¹⁴, or can be useful to expose forgeries^{13,15}. Pigment analysis with Raman spectroscopy has been performed to study different types of art objects¹⁶.

A small number of studies were carried out on antique polychrome objects, such as on dynastic Egyptian funerary artefacts¹⁷ and wooden crucifixes¹⁵.

Panel paintings¹⁸⁻²⁰, rock paintings²¹⁻²³ and wall paintings²⁴⁻²⁶ are also common objects to analyse with Raman spectroscopy. When investigating art objects the focus is often not only on the identification of pigments, but also on the identification of deterioration products²⁷, such as salts²⁸ that are formed by weathering processes. Identification of deterioration products can provide conservators information on the future protection of the object.

Raman spectroscopic analysis of manuscripts has mainly been concerned with pigment investigation of European mediaeval books of loose parchment leaves²⁹⁻³¹, but also extends to other periods. Next to pigment identification, Raman spectroscopic analysis of manuscripts can give insight in relations between manuscripts and scriptoria³². An extended research of different manuscripts can lead to an overview of pigments used over a wider period or region.

Research was done on works of paper such as lithographs³³⁻³⁵, drawings³⁶ and wallpapers³⁷⁻³⁹. Analysis of these works of art should be undertaken with special care, since these art objects are extremely vulnerable to damage.

For Raman spectroscopy, and similar to all other analytical techniques, the evolution in applications is directly linked to the improvements in instrument technology. One of the most important instrumental improvements is the presence of the capability to measure different layers in confocal mode, and the resulted effective spatial resolution achieved in the instruments¹⁶.

Using standard micro-Raman equipment, the direct analysis of large art objects is difficult since focussing the laser beam on the surface of the artwork is not easy. An elegant solution for this problem is using fibre optics to send the laser beam to the artefact and to collect the backscattered radiation⁴⁰. Due to the development of mobile equipment⁴¹, *in situ* analysis, where the instrument is transported to the location of the art object, could be executed.

During the last decade motorised stages were introduced, which can move an object point by point in three dimensions. Due to this instrumental development, Raman spectroscopy can be used as a mapping technique. Mapping an art object consists of performing point measurements for scanning the art object in two or three dimensions. The most important disadvantage of mapping is that it is very time consuming, because of the sequential analysis. A solution for this problem is performing Raman imaging. With this technique a larger area of the sample is illuminated and the spectral information is gathered on different places of the detector. The disadvantage of this technique is that only the total intensity within a certain wavelength region is recorded. As a consequence, no background correction can be made and apart of the total intensity no other variables, such as band position or band width, could be plotted.

In 1990, Bowden et al⁴² presented a new approach: line scanning. In this approach a line is illuminated on the sample instead of a single point. This approach increases the speed of data acquisition, while good spectral quality is maintained. In 2008, Renishaw⁴³ developed a commercial Raman spectrometer based on this approach, the Streamline plus. The instrument uses optics within the inVia Raman microscope to illuminate a line on the sample. The inVia's motorised microscope stage moves the sample beneath the objective lens so that the line is rastered across the region of interest. Data are swept synchronously across the detector as the line moves across the sample, and are read out simultaneously.

Micro-Raman mapping results in a multivariate dataset. Information on the chemical composition of a sample can be obtained by multivariate analysis^{3,44,45}. The most commonly used techniques for multivariate analysis are: principal components analysis (PCA), partial least squares regression (PLSR), hierarchical cluster analysis (HCA), K-means cluster analysis (KCA) and fuzzy cluster analysis (FCA). PCA reduces the number of variables condensing all the spectral information of a large number of spectra into a few latent variables (principle components). For PLSR a

reference dataset consisting of spectra with known analyte concentrations is used to build a calibration model. In cluster analysis, HCA, KCA and FCA, spectra are segmented in groups (clusters) according to their similarity, so that all spectra belonging to one cluster have similar characteristics. The difference between HCA and KCA is that for KCA the number of clusters should be known in advance. In “hard” clustering methods such as HCA, a spectrum exclusively belongs to one cluster, whereas “soft” methods such as FCA allow one spectrum to belong to more than one cluster at the same time.

9.2.2 X-ray fluorescence (XRF) spectroscopy

The first application of XRF in the field of archaeology was in 1967, when Vilnat et al⁴⁶ compared different XRF methods for the analysis of enamel. During the next 20 years the use of XRF spectroscopy for the analysis of art objects was only for a few cases reported in scientific literature, amongst others: for the analysis of Etruscan gold objects (1973)⁴⁷, pigments of Minoan painted pottery (1979)⁴⁸, online analysis of china clays (1982)⁴⁹, quantitative analysis of traces of barium in porcelains (1985)⁵⁰ and archaeological pottery (1987)⁵¹. The small number of applications is probably due to instrumental drawbacks.

Starting from the nineties, the number of applications of XRF spectroscopy for the analysis of art increases exponentially because of instrumental developments. In 1976 Cesareo et al⁵² already mentioned the use of portable units for analysis with XRF spectroscopy. This was followed by the discussion to use different probes for the analysis of art objects by Vaughan⁵³ in 1982. In 1998 Longoni et al⁵⁴ introduced a portable XRF spectrometer for non-destructive analysis in archaeometry. Until now, the detectors used in conventional XRF spectrometers were the classical high-resolution cryogenic detectors, like Si(Li) and HPGe detectors (whose resolution is in the order of 140 eV FWHM at 6 keV). These detectors are not completely

suitable for portable instrumentation because of the necessary cooling with liquid N₂. To compensate this disadvantage, non-cryogenic detectors, like Peltier cooled Si PIN diodes, have been developed, with a big improvement in terms of size and weight of the instrumentation⁵⁵. The energy resolution of this type of detectors of the order of 250 eV FWHM at 6 keV, is nevertheless sometimes unsatisfactory. This type of portable XRF spectrometer was used for the analysis of metal alloys, pottery and pigment identification in paintings⁵⁶. A same type of instrument was used for the analysis of Egyptian statues in the Museum Vleeshuis (Antwerp, Belgium)⁵⁷. This instrument has in addition a mini-focus side window X-ray tube, which implies the use of a small beam with a spot size of approximately 0.5 mm².

Williams–Thorpe et al⁵⁸ introduced the use of a HgI detector for the analysis of British Stone Axe. Nevertheless, the developed portable XRF spectrometers use detectors that need cooling: a liquid N₂ cooled Si(Li) detector (X-art⁵⁹), a Peltier cooled Si-PIN X-ray detector (semi-micro XRF spectrometer⁶⁰) or a Peltier cooled Si drift detector (Lab-view controlled portable XRF spectrometer⁶¹). The selection of the detector for the analysis of art objects depends on the nature of the object and the characteristics of the environment⁶².

These instrumental developments made portable XRF spectroscopy an appropriate technique for qualitative (*in situ*) analysis of art objects, such as pigment analysis of Spanish artworks⁶³, enamels⁶⁴ and rock art⁶⁵.

Performing quantitative analysis requires the use of an excitation beam with a very stable energy and intensity. This is essential for the determination of elemental concentrations since it simplifies the calibration procedures. A portable XRF spectrometer was introduced for this purpose: the BSC-XRF system⁶⁶ (beam stability-controlled XRF spectrometer). This spectrometer is equipped with a system to monitor the energy and stability of the beam emitted by the X-ray tube. The control of the system is obtained by a direct intervention on the beam through suitable parameters. In order to operate under stable conditions, the system was

accurately calibrated. This spectrometer was used for the quantitative analysis of archaeological pottery⁶⁷.

In the last decade, many instrumental analytical techniques have developed microscopic equivalents. The drive for this development is twofold: the need to improve the techniques to be able to investigate the higher degree of material complexity, and the growing need to investigate local changes in properties of materials. For this reason, portable micro-XRF spectrometers^{68,69} were introduced for the analysis of art objects. Bunzanich et al^{70,71} reported the use of a portable micro-X-ray fluorescence spectrometer with polycapillary optics and vacuum chamber for archaeometrical and other applications. When working in vacuum, the detection of low Z elements is possible. This instrument was used for the identification of Egyptian blue ($\text{CaCuSi}_4\text{O}_{10}$) in art objects of the Egyptian collection of the Kunsthistorisches Museum in Vienna, Austria⁷². Normally the detection of Ca and Si is difficult, but with this device also the presence of Si (low Z element) can be easily detected. The presence of Si is important to distinguish between the blue pigments azurite ($2\text{CuCO}_3 \cdot \text{Cu}(\text{OH})_2$) and Egyptian blue ($\text{CaCuSi}_4\text{O}_{10}$).

In all the above mentioned applications of XRF spectroscopy for the analysis of art or archaeological objects, the microscopic X-ray beam has been used to perform local analysis by point measurements, 2D elemental mapping^{73,74} or line-scanning on the sample surface, but not to perform investigations in depth. In 2003, a 3D micro-XRF analysis set-up was introduced to perform depth sensitive investigations of paint layers in ancient Indian Mughal miniatures⁷⁵. Successive paint layers could be distinguished with a depth resolution of about 10 μm . This set-up was also used for the depth resolved investigation of corrosion layers of historical glass objects⁷⁶. Until now monochromatic 3D micro-XRF is only reported using synchrotron radiation, as X-ray tube radiation in combination with state-of-the-art monochromatising optics does not yield enough flux on the sample. Using a polychromatic set-up in combination with a conventional X-ray tube results in an

increase of the flux on the sample. By using this set-up compact XRF spectrometers are developed for archaeometric applications⁷⁷.

9.2.3 Combined techniques

Using a combination of analytical techniques has the advantage that complementary information can be gathered. In this research, Raman spectroscopy gives molecular information, while XRF spectroscopy provides elemental information on the pigments used.

Hunter et al⁷⁸ describe the first application of a combined approach for the analysis of archaeological art objects in 1993. They used a combination of XRF spectroscopy, Raman spectroscopy, electron spin resonance, infrared spectroscopy, thermogravimetric analysis, scanning electron microscopy and X-radiography. During the last decade, such very extended approaches were used for the analyses of: sienese ‘archaic’ majolica⁷⁹, Byzantine wall paintings⁸⁰ and the tomb of Menna, Theban Necropolis, Egypt⁸¹. Nevertheless, typically many archaeometric analysis were performed using a combination of only three techniques: (a) combination of infrared (IR), Raman and XRF spectroscopy for the analysis of inks^{82,83}, English polychrome alabaster sculptures⁸⁴, ancient pottery⁸⁵ and ancient polychrome prints⁸⁶; (b) combination of scanning electron microscopy, Raman and XRF spectroscopy for the analysis of Perugino’s palette⁸⁷, an ancient Italian manuscript⁸⁸, a painted leather screen⁸⁹ and for the identification of 19th and 20th century pigments⁹⁰; (c) combination of Nuclear Magnetic Resonance (NMR), Raman and XRF spectroscopy for the analysis of coloured maps^{91,92}, and (d) combination of X-ray diffraction, Raman and XRF spectroscopy for the analysis of Chinese celadon shards⁹³ and illuminated manuscripts⁹⁴.

The current research focuses on the combination of Raman spectroscopy with XRF spectroscopy, because both instruments are readily available in the UGent Department of Analytical Chemistry.

During the last decade the combination of these two techniques was applied for the analysis of different art objects, such as: mural paintings⁹⁵⁻⁹⁷, Byzantine icons⁹⁸, wallpaper⁹⁹, canvas painting¹⁸, Spanish stamps¹⁰⁰, Islamic manuscripts¹⁰¹ and blue glaze¹⁰².

A combination of a portable Raman spectrometer with a portable XRF spectrometer was used to monitor the influence of nitrate on historical building materials^{103,104}. Depending the nature of the materials and the nitrate compound impacting them, several nitrate salts can be formed: NaNO_3 , $\text{Mg}(\text{NO}_3)_2$, $\text{Ca}(\text{NO}_3)_2$ and $\text{Ba}(\text{NO}_3)_2$. Because with Raman spectroscopy only the strongest band of the nitrates ($1060\text{--}1035\text{ cm}^{-1}$) is detectable, XRF spectroscopy helps to distinguish between the different nitrates, based on the detectable elements present in these salts (Na, Mg, Ca, Ba).

Ramos et al¹⁰⁵ reported the use of a special data treatment for the classification of ochre pigments, where Raman and XRF data are fused. If different spectroscopic techniques are used, the spectra need to be balanced in order to perform a correct data sensor association. Several methods could be used, but in this case study they make use of partial least square discriminant analysis (PLS-DA).

All the above mentioned analyses were based on point measurements. In many cases there is also an interest to make maps of the analysed object. In an earlier study⁷³ we already reported the use of a two dimensional XRF mapping to get a better insight in the restoration processes the painting underwent during history.

9.3 Experimental

The porcelain card (Fig. 9.1) selected for this research represents a typical business card: Frans Claes, manufacturer of chemical products in Ghent, Belgium. This card was produced at a local lithographic shop: G. Jacqumain and R. Basse. The dimensions of the card are: 133 x 89 x 1 mm.

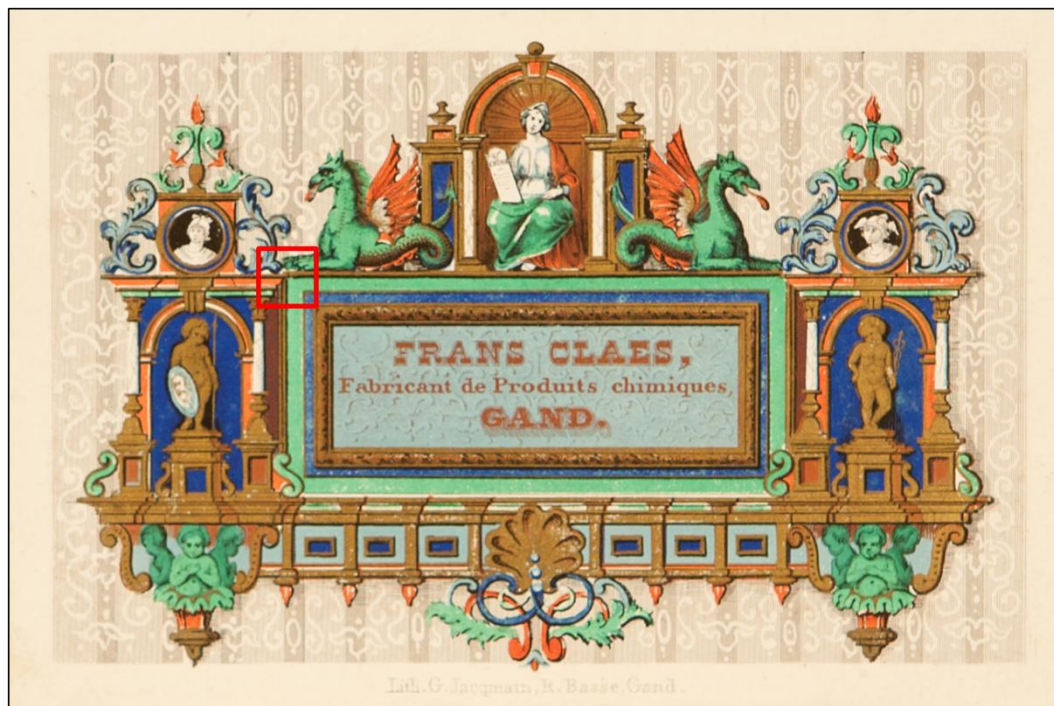


Figure 9.1 Picture of the analysed porcelain card (133 × 89 × 1 mm), with selected region of interest.

9.3.1 Confocal micro-Raman spectroscopy

The laboratory Raman spectrometer used is a Bruker Optics ‘Senterra’ dispersive Raman spectrometer with a BX51 microscope. The Raman spectrometer is equipped with 532 (Nd:YAG) and 785 nm (diode) laser sources. High resolution spectra are recorded in 3 spectral windows, covering the 60–3700 cm^{-1} and 80–3500 cm^{-1} for the 532 and 785 nm laser, respectively. The system uses a thermo-electrically cooled CCD detector, operating at -65°C . Five software-controlled settings for

the power of each laser are available: 100, 50, 25, 10 and 1%, i.e. up to ca. 35 mW on the sample for the 785 nm laser. The microscope has 5 \times , 20 \times and 50 \times objectives, with spot sizes of approximately 50, 10 and 4 μm , respectively. The microscope contains a joystick-controlled motorised stage and setting the analysis area is accomplished with the aid of an attached video camera. The instrument is controlled via the OPUS software version 6.5.6. Mapping the selected area of the porcelain card was performed using the 785 nm laser at 1% power setting, to avoid any possible sample damage.

9.3.2 Energy dispersive X-ray fluorescence (EDXRF) spectroscopy

A laboratory micro-XRF system (Eagle-III microprobe, EDAX, Inc, Mahwah, NJ, USA) provided elemental information of the mapped area. This spectrometer is equipped with a microfocus X-ray tube with a Rh anode, a polycapillary lens (X-ray Optical Systems, Inc., NY, USA) for X-ray focussing, and a N₂ cooled 80 mm² energy dispersive Si-(Li) detector. The sample chamber incorporates an XYZ motorised stage for sample positioning. A high resolution microscope is used to position the sample on the desired distance from the polycapillary. Operating in vacuum allows the use of the Rh-L photons originating from the X-ray tube to improve the investigation of low Z-elements down to sodium. Mapping of the selected area of the porcelain card was performed at an operating X-ray tube voltage of 40 kV, a tube current of 80 μA to optimise the detection of X-rays corresponding to ca. 30% detector dead time, and a spot size of 100 μm on the sample.

9.4 Results and discussion

9.4.1 *X-ray fluorescence (XRF) spectroscopy*

In the first step of this research the possibility to identify the different pigments used was explored performing a fast map with XRF spectroscopy. The resulting images were used to select an area on the card to perform a second map with a longer measurement time. On this second map principal components analysis (PCA) and K-means cluster analysis were performed.

9.4.1.1 Identification of the pigments

For the first map an area of 18923 by 13563 μm was mapped. In this area, respectively 128×100 single points were measured in vacuum for a very short time (0.5 s). Although a short measurement time of 0.5 s was chosen approximately 2 hours were needed to acquire these data. This preliminary map was performed to select the area of interest of the porcelain card.

The results of this map are presented in figure 9.2. This fast mapping already provides a lot of information on the elements of the pigments used. The maps of Al-K and Si-K lines (Fig. 9.2) are very similar. The most intense regions of both lines cover the blue zones of the selected area. The presence of Al and Si may indicate that ultramarine blue ($\text{Na}_{8-10}\text{Al}_6\text{Si}_6\text{O}_{24}\text{S}_{2-4}$) was used as blue pigment. The maps of Hg-L,M and S-K are also very similar. This implies that for the red regions, vermilion (HgS) was used as red pigment. If we take a closer look to the X-ray map of Pb-L and Pb-M, we can recognise the whole structure of the selected area in the map. This probably means that the whole cardboard is covered with a layer of lead white. For the green zones of the card, the X-ray signal of Cu-K is the most intense. This suggests that a Cu-based pigment was used as green pigment. The

XRF results of this fast map already give some information of the elements used for the golden, brown colour: a mixture of Cu and Zn.

These first results allowed the selection of a sub area of 8 by 8 mm (red raster in Fig. 9.2) for a next imaging experiment. For this, each of the 64×64 single points were measured for 10 s. The total map of the area took approximately 17 hours. On this XRF dataset some multivariate statistical techniques were performed, to look if even better XRF maps could be obtained.

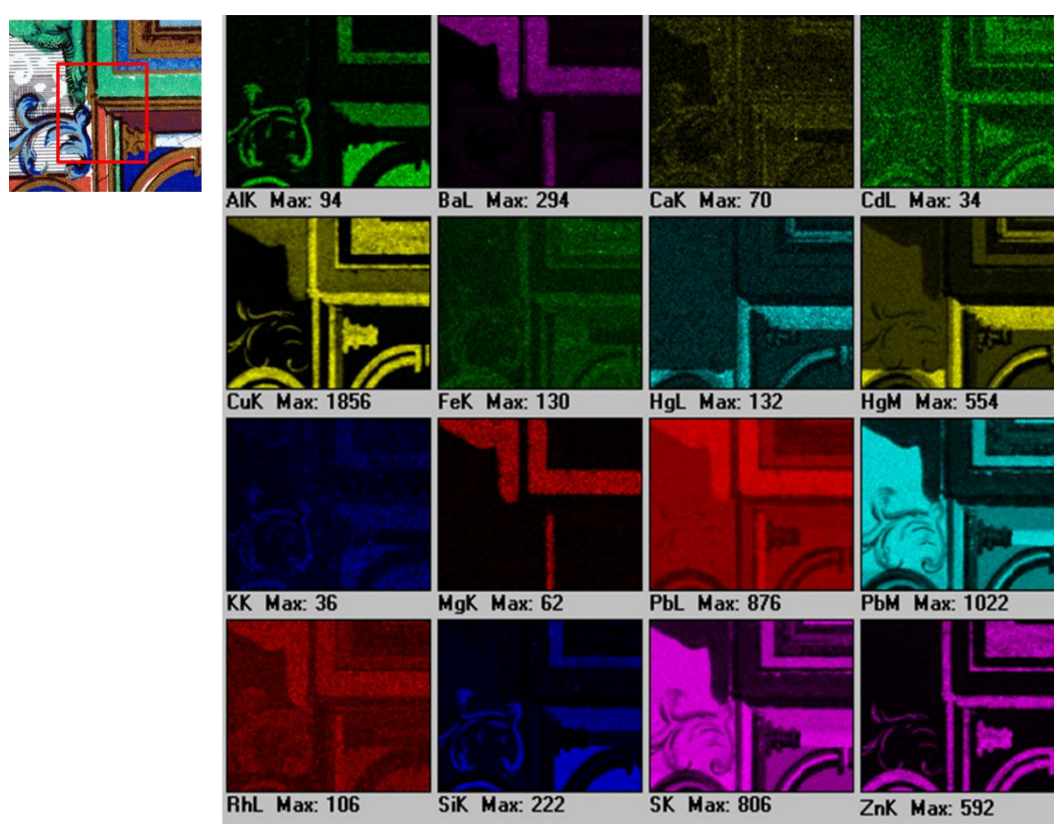


Figure 9.2 μ -XRF elemental maps obtained by scanning the selected area of the porcelain card using a $100\ \mu\text{m}$ X-ray beam derived from a Rh anode operated at 40 kV. Step size, $0.149 \times 0.137\ \text{mm}$, image size 128×100 pixels, or $18.923 \times 13.563\ \text{mm}$; spectrum collection time per pixel, 0.5 s. (2 hours)

9.4.1.2 Chemometrical data processing

9.4.1.2.1 Principal components analysis (PCA)

This XRF dataset, which consists of series of X-ray maps, each corresponding to one chemical element, may contain maps which are highly correlated (e.g. Fig. 9.3, Hg and S maps).

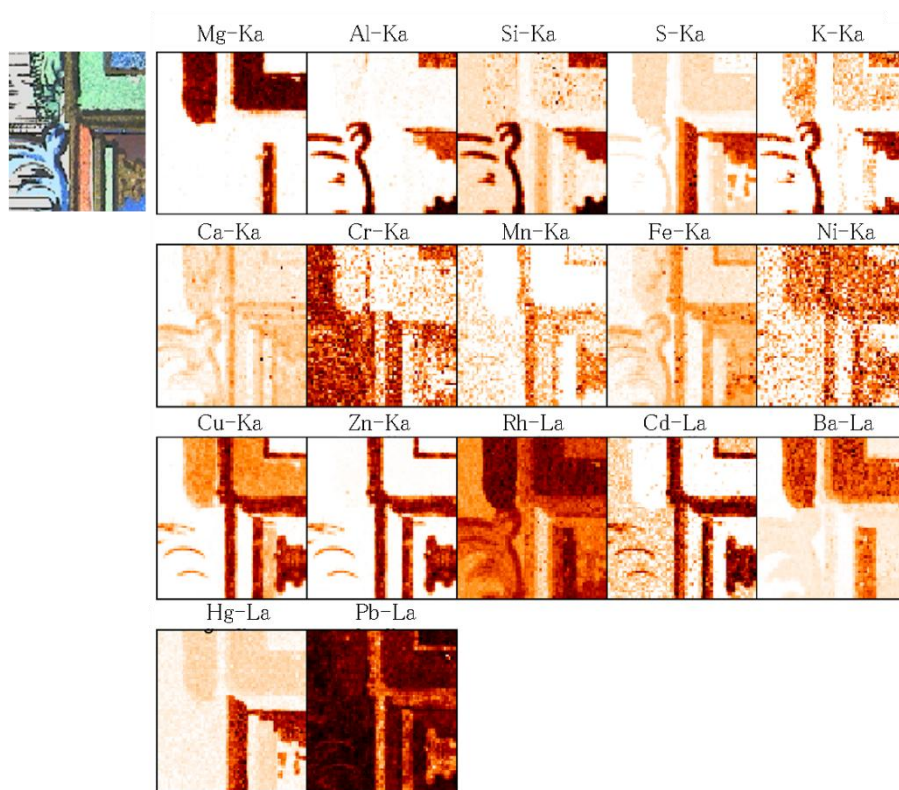


Figure 9.3 μ -XRF elemental maps obtained by scanning the selected area of the porcelain card using a 100 μ m X-ray beam derived from a Rh anode operated at 40 kV. Step size, 0.125×0.125 mm, image size 65×65 pixels, or 8×8 mm; spectrum collection time per pixel, 10 s. (17 hours)

Figure 9.4 shows the scores images resulting from the PCA of the dataset presented in figure 9.3. Principal components analysis (PCA) is a multivariate statistical technique which aims to detect similarities between experimental multivariate datasets, essentially through reduction of the dimensionality of the data.

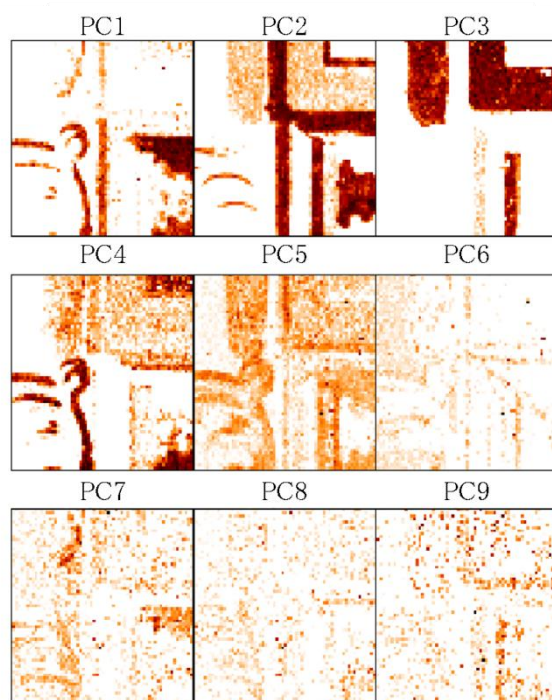


Figure 9.4 Scores images obtained by PCA of the X-ray maps in Fig. 9.3.

In figure 9.5(a) the contribution to the variance (CVE) of each PC is plotted; clearly the first 6 PCs explain 90% of the total variance in the dataset. Figure 9.5(b) shows the PC2–PC3 loadings plot of the original variables, i.e. the chemical elements. In the loadings plot the presence of vermilion is clearly visible (correlation between Hg–La and S–Ka). The loadings plot also shows a correlation between Al–Ka, Si–Ka and K–Ka. This correlation may indicate the presence of ultramarine blue. For the correlation between Mg–Ka and Ba–La on the one side, and between Fe–Ka and Zn–Ka on the other side, we don't have a plausible explanation. Perhaps the correlation between Fe–Ka and Zn–Ka is due to the lithographical process: for the ink a combination of Fe and Zn was often used. Mg and Ba are chemical related and therefore appear often together.

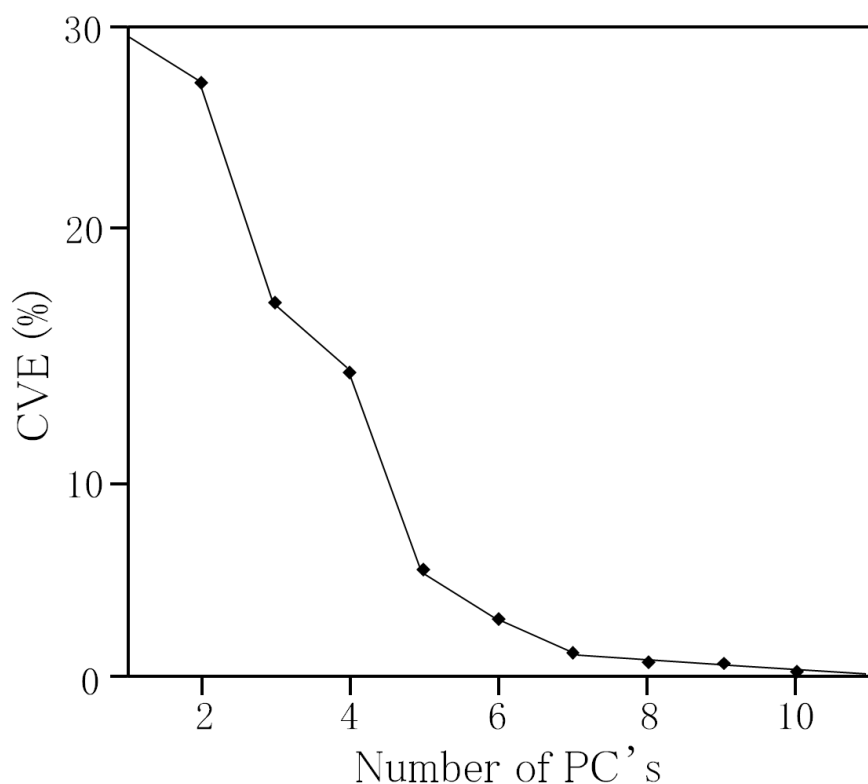


Figure 9.5 (a) Contribution of the variance explained (CVE) as function of the number of principal components for the data shown in figure 9.4.

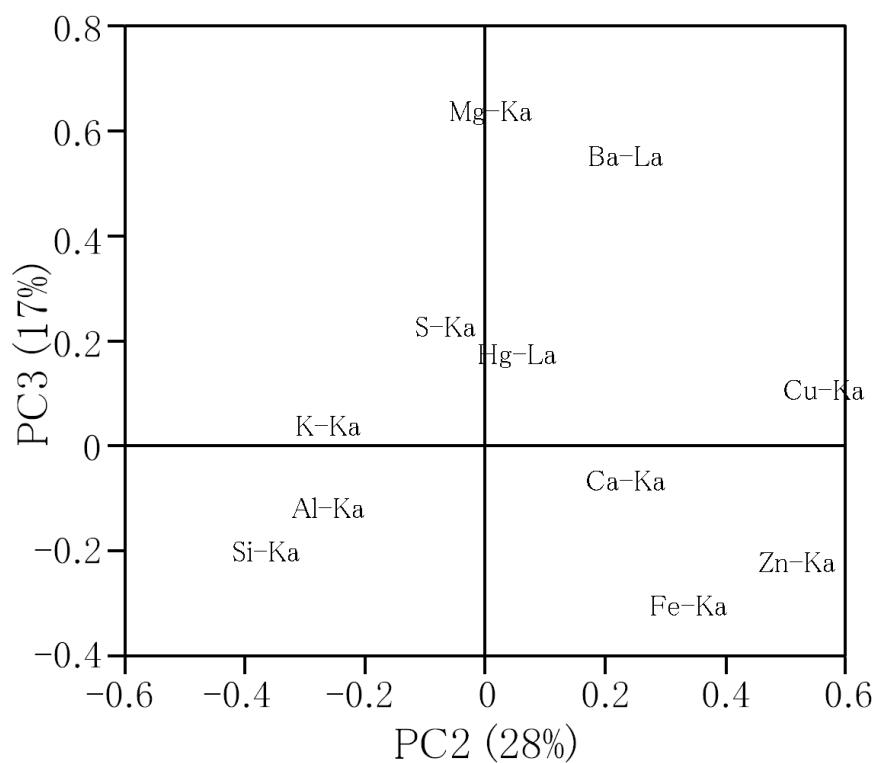


Figure 9.5 (b) Loadings plot in the PC2-PC3 plane for the data shown in figure 9.4.

9.4.1.2.2 K-means cluster analysis

All clustering methods are based on measuring the degree of similarity between two of the objects to be clustered. The K-means cluster algorithm is an iterative procedure that derives its name from the fact that it assumes the final number of object classes to be known a priori and equal to K. It would be straightforward that K is equal to the number of meaningful principal components. However, in practice it is difficult to define the number of important principal components.

Therefore, for practical considerations, a K-means clustering with $K = 15$, a somewhat arbitrarily and too high value, was chosen. The resulting clusters represent sub-areas of the obtained image. Comparing these cluster images with the optical image (picture) of the selected area, gives elemental information on the pigments used. The clusters obtained by applying the K-means algorithm to the original data are shown in figure 9.6.

Figure 9.7(a) shows the sum spectrum and the cluster image of the white zones of the analysed area. The presence of the intense Pb-L lines in the sum spectrum indicate that lead white ($2\text{PbCO}_3 \cdot \text{Pb(OH)}_2$) was used for the covering layer of the cardboard. The sum spectrum of figure 9.7(b) shows intense Cu-K lines, suggesting that a Cu based pigment was used for the green zones. For the blue pigment (Fig. 9.7(c)), the Al-K, Si-K and the S-K lines can be observed in the sum spectrum. Also for the red pigment (Fig. 9.7(d)), the intense Hg-L and S-K lines are clearly visible in the sum spectrum. Performing K-means cluster analysis on the XRF dataset delivers additional information on the different types of brown colors used. Figure 9.7(e) shows intense Hg-L and Cu-K lines. This suggests that a mixture of vermilion and a Cu-based pigment was used for the dark brown color. The brown, bronze color is also a mixture of vermilion and a Cu-based pigment (Fig. 9.7(f)), but some Zn was also applied to the mixture.

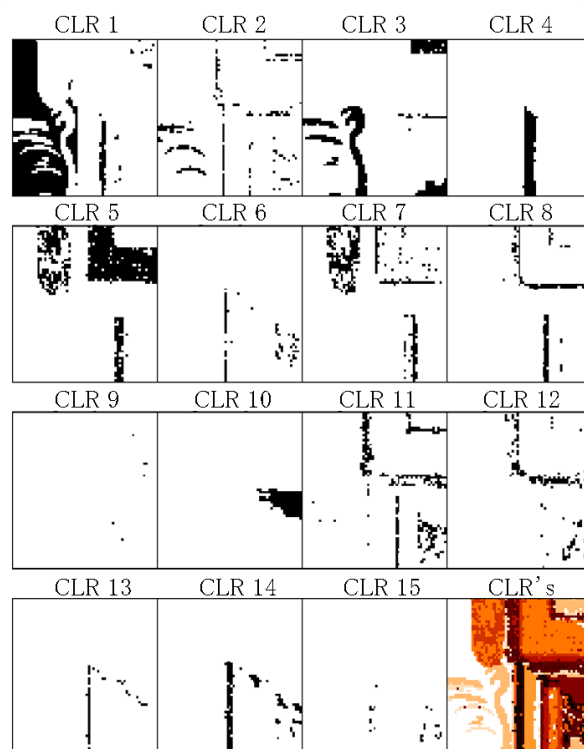


Figure 9.6 Compound segmentation masks obtained by K-means cluster analysis of the original data.

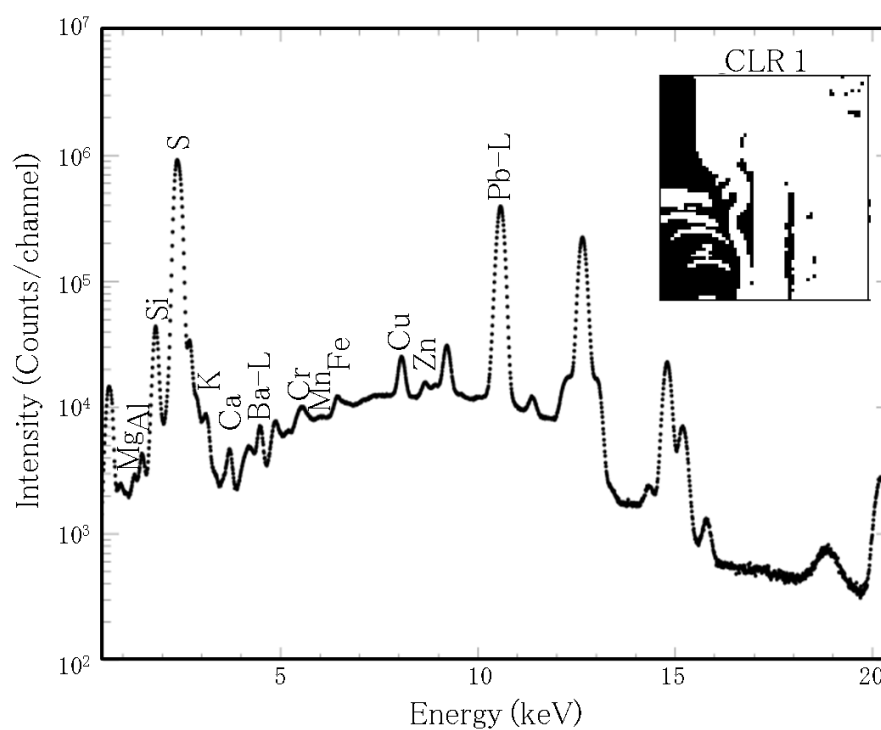


Figure 9.7 (a) Sum spectrum of the first cluster showing the presence of lead white ($2\text{PbCO}_3 \cdot \text{Pb}(\text{OH})_2$) for the white colour.

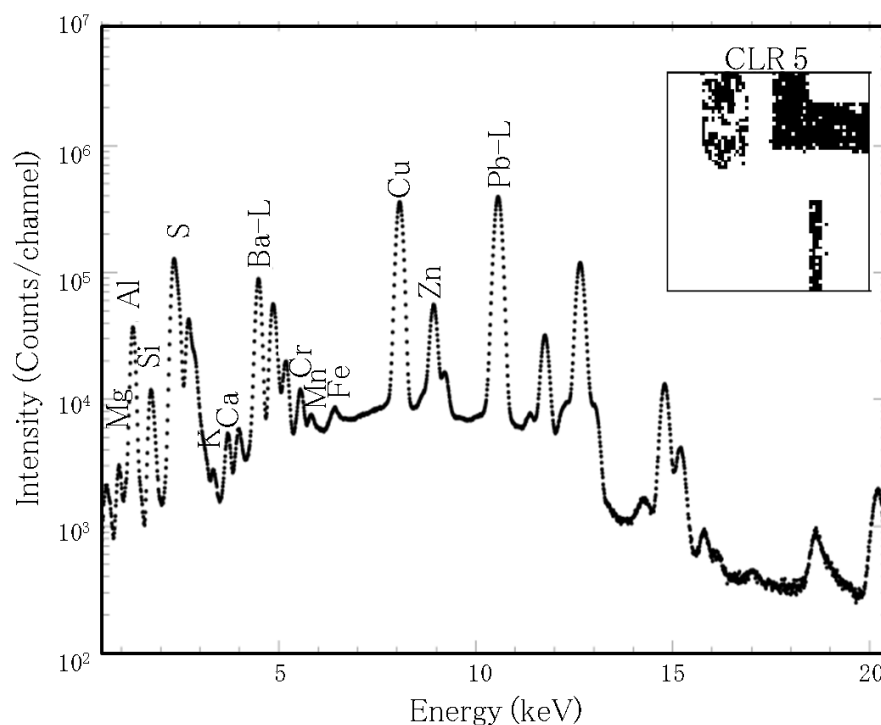


Figure 9.7 (b) Sum spectrum of the 5th cluster showing the presence of a Cu-based pigment for the green colour.

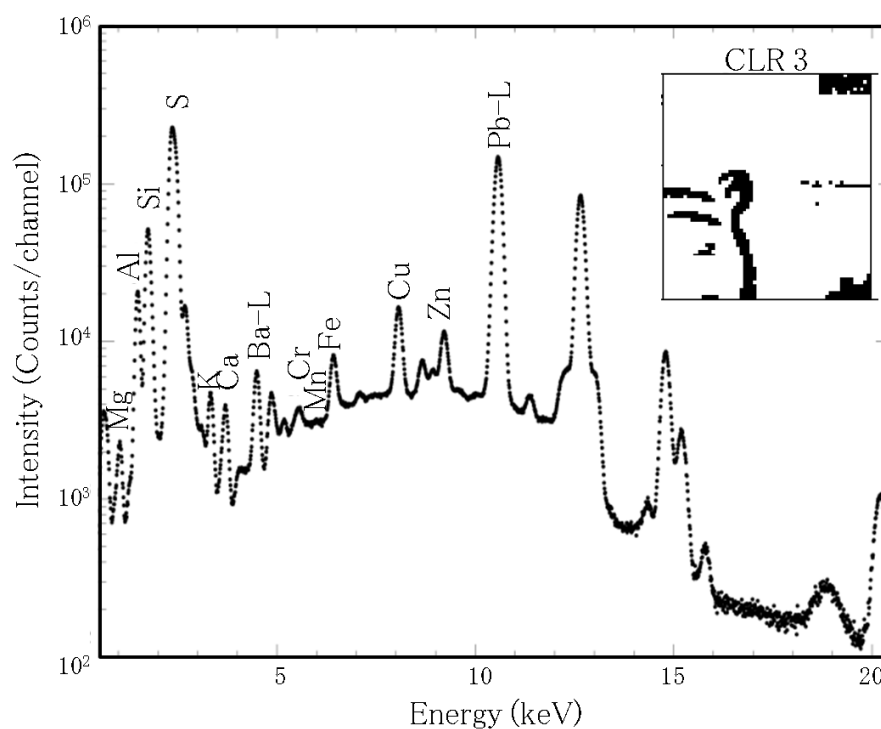


Figure 9.7 (c) Sum spectrum of the 3th cluster showing the presence of ultramarine ($\text{Na}_{8-10}\text{Al}_6\text{Si}_6\text{O}_{24}\text{S}_{2-4}$) for the dark blue colour.

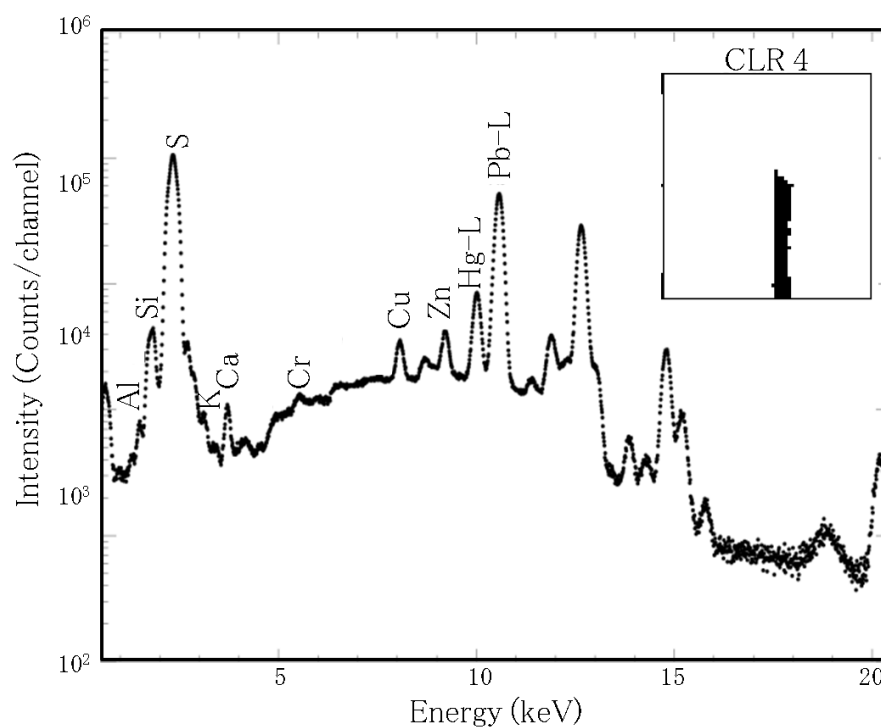


Figure 9.7 (d) Sum spectrum of the 4th cluster showing the presence of vermillion (HgS) for the red colour.

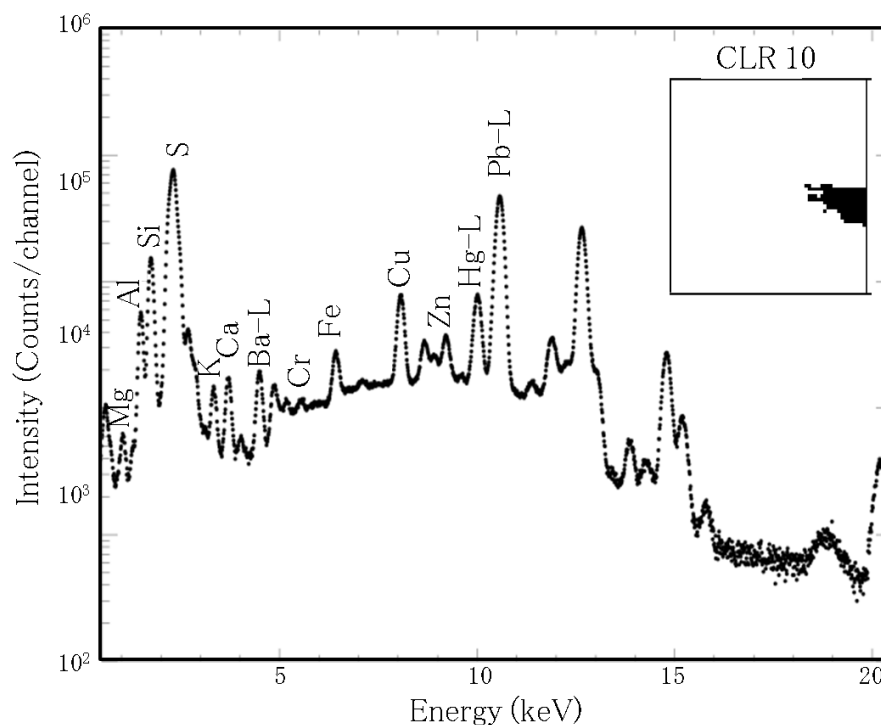


Figure 9.7 (e) Sum spectrum of the 10th cluster showing the presence of a mixture of vermillion (HgS) and a Cu-based pigment for the dark brown colour.

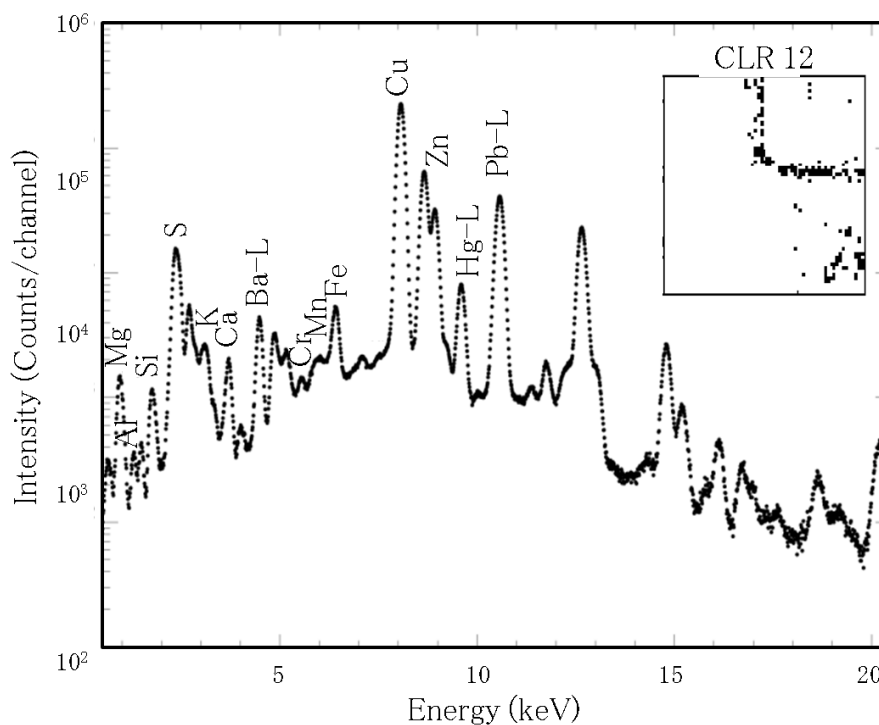


Figure 9.7 (f) Sum spectrum of the 12th cluster showing the presence of a mixture of vermilion (HgS), a Cu-based and a Zn-based pigment for the light brown, bronze colour.

Due to the penetrative character of the X-rays, XRF spectroscopy delivers spectral data that contains information of all layers in case of multilayer samples. Additional XRF spectroscopy only delivers elemental information, which makes in some cases identification of the pigments impossible.

9.4.2 Raman spectroscopy

For the Raman analysis of the porcelain cards, approximately the same area was mapped as during the XRF analysis. In a first step of the Raman analysis point measurements (60 s, 10 acc.) were performed in order to identify the different pigments used. This first step was necessary to select the Raman wavenumbers specific for each identified pigment. These wavenumbers are necessary to create an

image of the selected area of the porcelain card. In a second step of the Raman analysis the influence of the measuring time and measuring in high and low resolution mode, on the intensity of the selected Raman wavenumbers was evaluated, in order to decide whether a fast mapping can be used to select the region of interest of art objects.

9.4.2.1 Identification of the pigments

For the identification of the pigments used, point measurements were performed in the same area which was mapped with XRF spectroscopy. Table 9.1 gives an overview of the identified pigments with Raman spectroscopy and the identified elements with XRF spectroscopy for each colour.

colour	XRF results	Raman results
white	Pb	lead white ($2\text{PbCO}_3 \cdot \text{Pb}(\text{OH})_2$)
red	Hg,S	vermilion (HgS)
blue	Al, Si, S	ultramarine blue ($\text{Na}_{8-10}\text{Al}_6\text{Si}_6\text{O}_{24}\text{S}_{2-4}$)
green	Cu	malachite ($\text{CuCO}_3 \cdot \text{Cu}(\text{OH})_2$)
black	/	carbon black (C)
brown, gold	Cu, Hg, S, Zn	/
	Cu, Hg, S	/

Table 9.1 Overview of the pigments identified with Raman spectroscopy and the elements identified with XRF spectroscopy for each colour.

After the selection of the Raman wavenumbers of interest a selected area of 8.031×5.658 mm (81×56 points) (Fig 9.8(a)) was mapped with the red laser (785 nm), with a laser power of 1% (0.63 mW). A 5x objective lens was used, resulting in a spot size of ca. $50 \mu\text{m}$ on the card. The measurement time of all the single points of the

mapping was 60 s (20 s, 3 acc.), resulting in a total time of almost 7 days for the whole mapped area. These 7 days are the accumulated result of the measurements, the movement of the sample, the movement of the grating to record different spectral regions, and the automatic background correction of the used Raman spectrometer. The control software OPUS 6.5.6 (Bruker) is not able to switch off the automatic background correction, which results in a doubling of the measurement time.

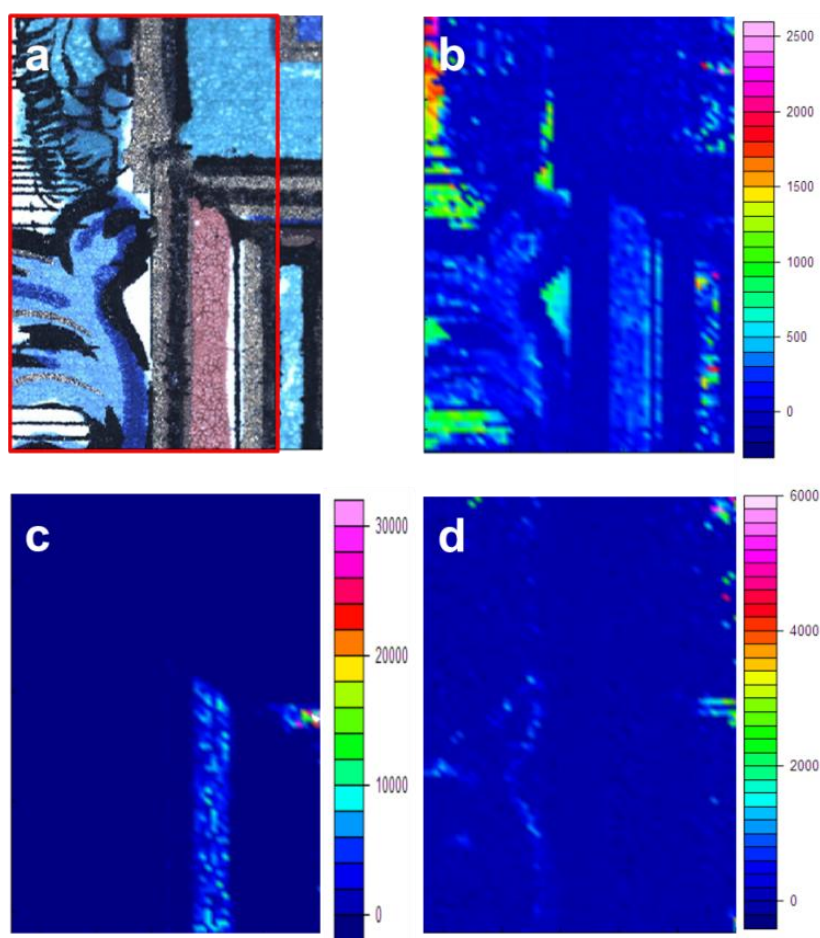


Figure 9.8 (a) Optical microscope image of the analysed area of the porcelain card, integration of the Raman band at (b) 1050 cm^{-1} (lead white), (c) 257 cm^{-1} (vermilion) and (d) 545 cm^{-1} (ultramarine). (785 nm, $5\times$ objective, 20 s, 3 acc., high spectral resolution, 1% laser power)

To construct the maps of the different pigments, the data were processed with OPUS 6.5.6. A selection of the most intense bands was made for the identified pigments: lead white (1050 cm^{-1}), vermilion (254 cm^{-1}) and ultramarine blue (545 cm^{-1}). The Raman signal for malachite (218 cm^{-1}) and carbon black (1297 cm^{-1}) were too weak to give a clear image. A possible solution for this problem could be performing the same mapping with the green laser (532 nm). Next, all the selected bands were integrated one by one. For this, first the baseline is constructed before integration of the surface area of the Raman band above the baseline. The results of this integration are presented in figure 9.8.

Figure 9.8(b) shows the integration of the most intense band of lead white (1050 cm^{-1}). One can see that lead white is detected over the whole mapped area, which implies that the first step in the manufacturing process was covering the cardboard with a layer of lead white. The different intensities of the Raman signal of lead white on the different coloured areas are also clearly visible. The maps, made by the integration of the bands of vermilion (Fig. 9.8(c)) and ultramarine blue (Fig. 9.8(d)), show obviously the red and blue coloured zones of the mapped area.

9.4.2.2 The influence of spectral resolution and measurement time

To evaluate the dependency of the resolution on the intensity of the Raman signal, a similar area of the porcelain card (the red frame in Fig. 9.8(a)) was mapped two times with the same experimental parameters (20 s, 3 acc., $5\times$ objective lens), except for the spectral resolution. The first map was performed using the high spectral resolution mode ($3\text{--}5\text{ cm}^{-1}$), while the second map was recorded in low spectral resolution mode ($9\text{--}18\text{ cm}^{-1}$). Changing to lower resolution results for the used Raman spectrometer in a significantly shorter measurement time, because the spectra are recorded using one grating over a range of $90\text{--}3500\text{ cm}^{-1}$. When measuring in high resolution mode the grating has to turn during the measurement,

because the two spectral ranges ($80\text{--}1525\text{ cm}^{-1}$ and $1520\text{--}2660\text{ cm}^{-1}$) are measured separately and stitched together. This results in a much longer measurement time, especially because after each movement of the grating the spectrometer performs a new calibration. The total mapping time of the map with low resolution was ca. 22 hours, while for the map with high resolution the total mapping time was ca. 7 days. As part of the interpretation of the Raman data, an in-house written software was developed. This program automatically removes the spectral background using the SNIP method¹⁰⁶. Next, the sum spectrum of all the spectra is made and the Raman bands are selected. In a following step the selected bands are integrated for all spectra. Details of this in-house written software will be published elsewhere¹⁰⁷. By selection of one band, the distribution of the Raman intensity over the selected area can be shown as a map. Figure 9.9 compares different Raman maps with high and low resolution. Figures 9.9(a) and 9.9(b) show the Raman intensity of the band of lead white at ca. 1050 cm^{-1} , with respectively high (9.9(a)) and low (9.9(b)) spectral resolution. The Raman map with low spectral resolution gives a better view of the whole structure of the porcelain card than measuring in high resolution mode. The same comparison is made for the Raman band of vermilion at 254 cm^{-1} . The Raman map with low spectral resolution (Fig. 9.9(d)) is again more obvious than the one with high spectral resolution (Fig. 9.9(c)). When measuring in low spectral resolution mode, the amount of light which enters the detector is higher, corresponding in a higher sensitivity. By measuring at low spectral resolution, the same information on the pigments is obtained in a shorter period. In this particular example the measurement time was reduced with a factor of ca. 7. This reduction of the measurement time is, when measuring with the Senterra Raman spectrometer, important because of the instability of the stage.

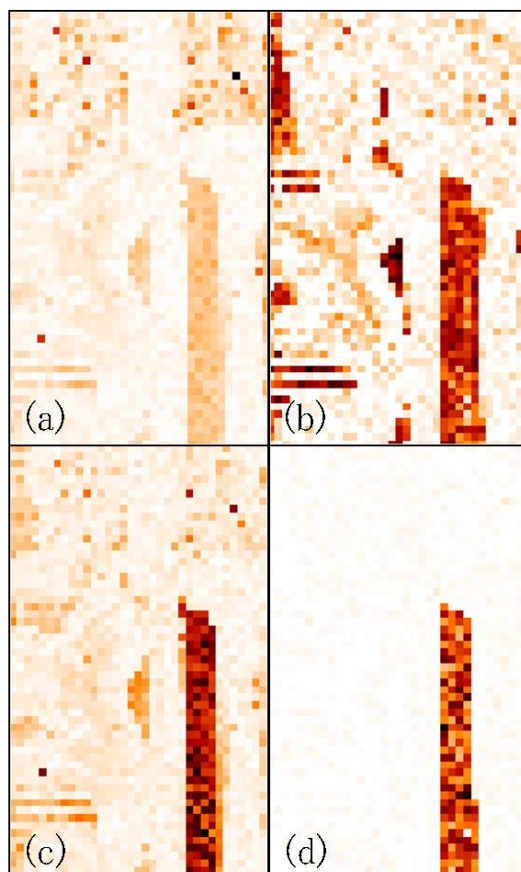


Figure 9.9 Map of the Raman intensity of: lead white at 1050 cm^{-1} for (a) high and (b) low spectral resolution; and vermilion at 254 cm^{-1} for (c) high and (d) low spectral resolution. (785 nm, $5\times$ objective, 20 s, 3 acc., 1% laser power)

The same procedure was followed to evaluate the influence of the measurement time on the quality of the map. The same area of the porcelain card was twice mapped with the same experimental parameters ($5\times$ objective lens, low resolution), but with different measurement times. For the first map the measurement time of a single point spectrum was 60 s (20 s, 3 acc.), while for the second map the measurement time only was 6 s (3 s, 2 acc.). The total time of the long measurement was ca. 22 hours and for the short measurement ca. 6 hours. Figure 9.10 shows the different Raman maps: the intensity of the Raman band of lead white at 1050 cm^{-1} for a long (Fig. 9.10(a)) and a short measurement (Fig. 9.10(b)); and the intensity of the Raman band of vermilion at 254 cm^{-1} for a long (Fig. 9.10(c)) and a short

measurement (Fig. 9.10(d)). Only the Raman maps of lead white and vermilion are showed, because for the other pigments there is no clear difference between the maps under different circumstances. This is because of the low signal-to-noise ratio of the Raman data, due to the instability of the stage system for long measurements. The instability of the stage is a drawback in this research. It is obvious that with a stable stage, longer measurements would lead to better Raman maps.

The Raman maps of the long measurements (Fig. 9.10(a) and (c)) are sharper than the ones of the short measurement. We can conclude that we have to select a (longer) measurement time, which gives a more obvious Raman signal. Choosing a shorter measurement time has in this case no advantages.

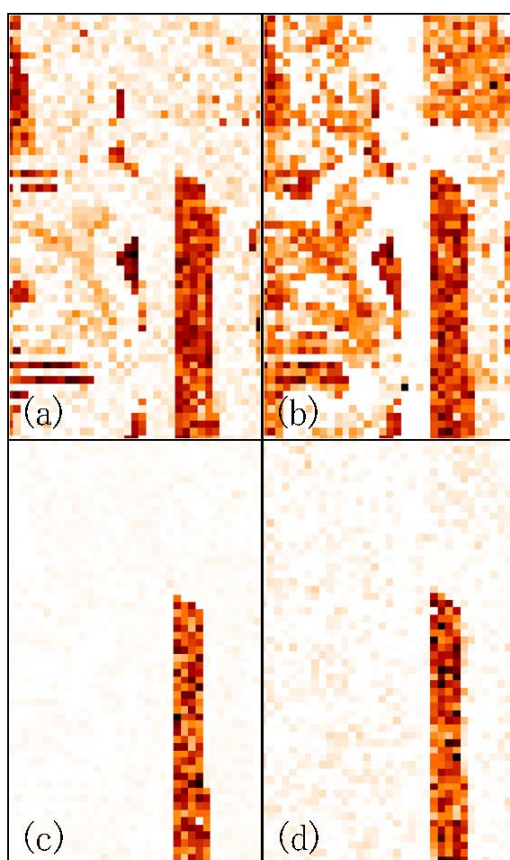


Figure 9.10 Raman map of the Raman intensity of: lead white at 1050 cm^{-1} for (a) a long (20 s, 3 acc.) and (b) a short (3 s, 2 acc.) measurement time ; and vermilion at 254 cm^{-1} for (c) a long and (d) a short measurement time. (785 nm, $5\times$ objective, low resolution , 1% laser power)

Due to the weak Raman signal, noisy Raman images were obtained. These noisy images result, after performing multivariate statistical analysis such as PCA and K-means cluster analysis, in noisy results. To improve these results Raman images with better signal-to-noise ratio have to be obtained.

9.5 Conclusions

This paper shows that by mapping an art object with Raman spectroscopy and XRF spectroscopy, molecular and elemental images could be produced containing information on the pigments used: ultramarine blue, vermilion, malachite, carbon black and lead white.

By using the obtained XRF dataset, the possibility of using principal components analysis (PCA) and K-means cluster analysis for gathering information on the pigments used, has been explored. After performing K-means cluster analysis on the dataset, the resulting sum spectra associated with each image segment give additional information and simplify the interpretation of the measurements.

It was also indicated that by recording Raman maps at low spectral resolution a similar image was obtained as by measuring at high resolution. This results in a shorter time needed for analysing the art object.

In the future, we intend to examine if the total measurement time for the Raman analysis could be diminished by using a stable stage and the new control software is mandatory to allow auto-focussing without the automatic calibration, in order to improve the quality and reduce the time.

In this chapter, the possibilities of Raman and XRF mapping were explored using laboratory spectrometers. In all the previously discussed case studies the Raman results and XRF results are first interpreted separately and afterwards compared with each other. Because of the stability problems with the Senterra Raman spectrometer, analysis of art objects was performed using point measurements. In the next chapter the possibilities of fused Raman and XRF data are explored. The “fused” data consists of combining the Raman data and the XRF data in a single data matrix, before performing principal components analysis (PCA) on the data. Because porcelain cards are very colourful, also PCA was performed on the RGB values. The fused Raman–XRF data was evaluated comparing the different scores and loadings plots, with the scores and loadings plots of performing PCA on the Raman data and XRF data separately. Identification of the pigments used for the porcelain cards was not possible performing PCA on the fused data. Therefore, an attempt was made to develop an identification procedure using the fused Raman and XRF data. The details of this attempt are described extensively in the next chapter.

References

1. Ropret, P., Miliani, C., Centeno, S.A., Tavzes, C., Rosi, F. (2010) Advances in Raman mapping of works of art. *Journal of Raman Spectroscopy* 41: 1172–1177.
2. Aze, S., Vallet, J.M., Baronnet, A., Grauby, O. (2006) The fading of red lead pigment in wall paintings: tracking the physico-chemical transformations by means of complementary micro-analysis techniques. *European Journal of Mineralogy* 18: 835–843.
3. Lau, D., Villis, C., Furman, S., Livett, M. (2008) Multispectral and hyperspectral image analysis of elemental and micro-Raman maps of cross-sections from a 16th century painting. *Analytica Chimica Acta* 610: 15–24.
4. Neff, D., Bellot-Gurlet, L., Dillmann, P., Reguer, S., Legrand, L. (2006) Raman imaging of ancient rust scales on archaeological iron artefacts for long-term atmospheric corrosion mechanisms study. *Journal of Raman Spectroscopy* 37: 1228–1237.
5. Conti, C., Colombo, C., Matteini, M., Realini, M., Zerbi, G. (2010) Micro-Raman mapping on polished cross sections: a tool to define the penetration depth of conservation treatment on cultural heritage. *Journal of Raman Spectroscopy* 41: 1254–1260.
6. Vekemans, B., Janssens, K., Vincze, L., Aerts, A., Adams, F., Hertogen, J. (1997) Automated segmentation of mu-XRF image sets. *X-Ray Spectrometry* 26: 333–346.

7. Vandenabeele, P., De Paepe, P., Moens, L. (2008) Study of the 19th century porcelain cards with direct Raman analysis. *Journal of Raman Spectroscopy* 39: 1099–1103.
8. Vandenabeele P, Moens L. Overview: Raman spectroscopy of pigments and dyes. CAMBRIDGE: ROYAL SOC CHEMISTRY, 2005.
9. Smith, G.D., Clark, R.J.H. (2004) Raman microscopy in archaeological science. *Journal of Archaeological Science* 31: 1137–1160.
10. Dhamelincourt, P., Wallart, F., Leclercq, M., Nguyen, A.T., Landon, D.O. (1979) Laser Raman Molecular Microprobe (Mole). *Analytical Chemistry* 51: A414-&.
11. Guineau, B. (1984) Microanalysis of Painted Manuscripts and of Colored Archaeological Materials by Raman Laser Microprobe. *Journal of Forensic Sciences* 29: 471–485.
12. Guineau, B., Vezin, J. (1992) A Technical Study of Paintings in the Manuscript 'de Laudibus Sanctae Crucis' in the Amiens Municipal Library (Ms-Amiens-223) + Rabanus-Maurus. *Scriptorium* 46: 224–237.
13. Saverwyns, S. (2010) Russian avant-garde ... or not? A micro-Raman spectroscopy study of six paintings attributed to Liubov Popova. *Journal of Raman Spectroscopy* 41: 1235–1242.
14. Martinez-Arkarazo, I., Sarmiento, A., Maguregui, M., Castro, K., Madariaga, J.M. (2010) Portable Raman monitoring of modern cleaning and consolidation operations of artworks on mineral supports. *Analytical and Bioanalytical Chemistry* 397: 2717–2725.

15. Centeno, S.A., Mahon, D., Wypyski, M.T. (2004) Examination of a Spanish medieval processional crucifix substantially reworked in the 20th century. *Journal of Raman Spectroscopy* 35: 774–780.
16. Vandenabeele, P., Edwards, H.G.M., Moens, L. (2007) A decade of Raman spectroscopy in art and archaeology. *Chemical Reviews* 107: 675–686.
17. Edwards, H.G.M., Villar, S.E.J., Eremin, K.A. (2004) Raman spectroscopic analysis of pigments from dynastic Egyptian funerary artefacts. *Journal of Raman Spectroscopy* 35: 786–795.
18. Borgia, I., Brunetti, B.G., Miliani, C., Ricci, C., Seccaroni, C., Sgamellotti, A. (2007) The combined use of lead–tin yellow type I and II on a canvas painting by Pietro Perugino. *Journal of Cultural Heritage* 8: 65–68.
19. Vandenabeele, P., Castro, K., Hargreaves, M., Moens, L., Madariaga, J.M., Edwards, H.G.M. (2007) Comparative study of mobile Raman instrumentation for art analysis. *Analytica Chimica Acta* 588: 108–116.
20. Marano D, Marniontelli M, De Benedetto GE, Catalano IM, Sabbatini L, Vona F. Pigment identification on "The Ecstasy of St. Theresa" painting by Raman microscopy. BERLIN: SPRINGER-VERLAG BERLIN, 2007.
21. Smith, D.C., Bouchard, M., Lorblanchet, M. (1999) An initial Raman microscopic investigation of prehistoric rock art in caves of the Quercy District, S. W. France. *Journal of Raman Spectroscopy* 30: 347–354.
22. Goodall, R.A., David, B., Kershaw, P., Fredericks, P.M. (2009) Prehistoric hand stencils at Fern Cave, North Queensland (Australia): environmental and chronological implications of Raman spectroscopy and FT-IR imaging results. *Journal of Archaeological Science* 36: 2617–2624.

-
23. Prinsloo, L.C., Barnard, W., Meiklejohn, I., Hall, K. (2008) The first Raman spectroscopic study of San rock art in the Ukhahlamba Drakensberg Park, South Africa. *Journal of Raman Spectroscopy* 39: 646–654.
 24. Maguregui, M., Knuutinen, U., Castro, K., Madariaga, J.M. (2010) Raman spectroscopy as a tool to diagnose the impact and conservation state of Pompeian second and fourth style wall paintings exposed to diverse environments (House of Marcus Lucretius). *Journal of Raman Spectroscopy* 41: 1110–1119.
 25. Cristini, O., Kinowski, C., Turrell, S. (2010) A detailed micro-Raman spectroscopic study of wall paintings of the period AD 100–200: effect of atmospheric conditions on the alteration of samples. *Journal of Raman Spectroscopy* 41: 1120–1127.
 26. Edwards, H.G.M., Middleton, P.S., Hargreaves, M.D. (2009) Romano-British wall paintings: Raman spectroscopic analysis of fragments from two urban sites of early military colonisation. *Spectrochimica Acta Part A-Molecular and Biomolecular Spectroscopy* 73: 553–560.
 27. Perez-Alonso, M., Castro, K., Martinez-Arkarazo, I., Angulo, M., Olazabal, M.A., Madariaga, J.M. (2004) Analysis of bulk and inorganic degradation products of stones, mortars and wall paintings by portable Raman microprobe spectroscopy. *Analytical and Bioanalytical Chemistry* 379: 42–50.
 28. Zehnder, K. (2007) Long-term monitoring of wall paintings affected by soluble salts. *Environmental Geology* 52: 395–409.
 29. Bioletti, S., Leahy, R., Fields, J., Meehan, B., Blau, W. (2009) The examination of the Book of Kells using micro-Raman spectroscopy. *Journal of Raman Spectroscopy* 40: 1043–1049.

-
30. Bersani, D., Lottici, P.P., Vignali, F., Zanichelli, G. (2006) A study of medieval illuminated manuscripts by means of portable Raman equipments. *Journal of Raman Spectroscopy* 37: 1012–1018.
31. Villar, S.E.J., Edwards, H.G.M., Medina, J., Perez, F.R. (2006) Raman spectroscopic analysis of mediaeval wall paintings in the Palencia region, Spain. *Journal of Raman Spectroscopy* 37: 1078–1085.
32. Van Hooydonk, G., De Reu, M., Moens, L., Van Aelst, J., Milis, L. (1998) A TXRF and micro-Raman spectrometric reconstruction of palettes for distinguishing between scriptoria of related medieval manuscripts. *European Journal of Inorganic Chemistry* 639–644.
33. Castro, K., Vandenabeele, P., Rodriguez-Laso, M.D., Moens, L., Madariaga, J.M. (2004) Micro-Raman analysis of coloured lithographs. *Analytical and Bioanalytical Chemistry* 379: 674–683.
34. Otieno-Alego, V., Hodgeman, J., Creagh, D.C. (2001) Micro-Raman identification of bloom formed on a historical print artifact. *Journal of the American Institute for Conservation* 40: 35–41.
35. Baraldi, P., Fagnano, C., Bensi, P. (2006) Raman study of a 'Tabula Colorum Physiologica' in a 1686 printed journal. *Journal of Raman Spectroscopy* 37: 1104–1110.
36. Wise, D., Wise, A. (2004) Application of Raman microspectroscopy to problems in the conservation, authentication and display of fragile works of art on paper. *Journal of Raman Spectroscopy* 35: 710–718.
37. Frausto-Reyes, C., Ortiz-Morales, M., Bujdud-Perez, J.M., Magana-Cota, G.E., Mejia-Falcon, R. (2009) Raman spectroscopy for the identification of

- pigments and color measurement in Duges watercolors. *Spectrochimica Acta Part A-Molecular and Biomolecular Spectroscopy* 74: 1275–1279.
38. Castro, K., Vandenabeele, P., Rodriguez-Laso, M.D., Moens, L., Madariaga, J.M. (2005) Improvements in the wallpaper industry during the second half of the 19th century: Micro-Raman spectroscopy analysis of pigmented wallpapers. *Spectrochimica Acta Part A-Molecular and Biomolecular Spectroscopy* 61: 2357–2363.
39. Castro, K., Perez-Alonso, M., Rodriguez-Laso, M.D., Madariaga, J.M. (2004) Pigment analysis of a wallpaper from the early 19th century: Les Monuments de Paris. *Journal of Raman Spectroscopy* 35: 704–709.
40. Vandenabeele, P., Verpoort, F., Moens, L. (2001) Non-destructive analysis of paintings using Fourier transform Raman spectroscopy with fibre optics. *Journal of Raman Spectroscopy* 32: 263–269.
41. Vandenabeele, P., Weis, T.L., Grant, E.R., Moens, L.J. (2004) A new instrument adapted to in situ Raman analysis of objects of art. *Analytical and Bioanalytical Chemistry* 379: 137–142.
42. Bowden, M., Gardiner, D.J., Rice, G., Gerrard, D.L. (1990) Line-Scanned Micro Raman-Spectroscopy Using A Cooled Ccd Imaging Detector. *Journal of Raman Spectroscopy* 21: 37–41.
43. <http://resources.renishaw.com>
44. Bonifacio, A., Beleites, C., Vittur, F., Marsich, E., Semeraro, S., Paoletti, S., Sergo, V. (2010) Chemical imaging of articular cartilage sections with Raman mapping, employing uni- and multi-variate methods for data analysis. *Analyst* 135: 3193–3204.

-
45. Mobili, P., Londero, A., De Antoni, G., Gomez-Zavaglia, A., Araujo-Andrade, C., Avila-Donoso, H., Ivanov-Tzonchev, R., Moreno, I., Frausto-Reyes, C. (2010) Multivariate analysis of Raman spectra applied to microbiology Discrimination of microorganisms at the species level. *Revista Mexicana de Fisica* 56: 378–385.
 46. Vilnat, J., Bourgois, D., Dubois, M. (1967) Comparison of Spectrochemical and Xrf Methods of Enamel Analysis. *Applied Spectroscopy* 21: 408–&.
 47. Cesareo, R., Hase, F.W.V. (1973) Nondestructive Radioisotope Xrf Analysis of Early Etruscan Gold Objects. *Kerntechnik* 15: 565–569.
 48. Stosfertner, Z., Hedges, R.E.M., Evely, R.D.G. (1979) Application of the Xrf-Xrd Method to the Analysis of the Pigments of Minoan Painted Pottery. *Archaeometry* 21: 187–194.
 49. Hogg, C.S., Burr, K.J. (1982) Automatic Particle-Size Measurement and Online Xrf Analysis of China Clays. *Transactions and Journal of the British Ceramic Society* 81: 129–129.
 50. Yap, C.T., Tang, S.M. (1985) Quantitative Xrf Analysis of Trace Barium in Porcelains by Source Excitation. *Applied Spectroscopy* 39: 1040–1042.
 51. Radamacher, D., Shimotake, T., Bower, N., Peckham, S. (1987) Preliminary-Analysis of Archaeological Pottery Using Sem-Xrf. *Abstracts of Papers of the American Chemical Society* 193: 29–CHED.
 52. Cesareo, R., Frazzoli, F.V., Sciuti, S. (1976) Sensitivity of Radioisotope Xrf Technique with Particular Reference to Portable Units. *Journal of Radioanalytical Chemistry* 34: 157–170.

-
53. Vaughan, D. (1982) Xrf Spectroscopy Probes Art Objects and Routine Samples. *Industrial Research & Development* 24: 144–147.
54. Longoni, A., Fiorini, C., Leutenegger, P., Sciuti, S., Fronterotta, G., Struder, L., Lechner, P. (1998) A portable XRF spectrometer for non-destructive analyses in archaeometry. *Nuclear Instruments & Methods in Physics Research Section A-Accelerators Spectrometers Detectors and Associated Equipment* 409: 407–409.
55. Cesareo, R., Gigante, G.E., Canegallo, P., Castellano, A., Iwanczyk, J.S., Dabrowski, A. (1996) Applications of non-cryogenic portable EDXRF systems in archaeometry. *Nuclear Instruments & Methods in Physics Research Section A-Accelerators Spectrometers Detectors and Associated Equipment* 380: 440–445.
56. Leutenegger, P., Longoni, A., Fiorini, C., Struder, L., Kemmer, J., Lechner, P., Sciuti, S., Cesareo, R. (2000) Works of art investigation with silicon drift detectors. *Nuclear Instruments & Methods in Physics Research Section A-Accelerators Spectrometers Detectors and Associated Equipment* 439: 458–470.
57. Vittiglio, G., Janssens, K., Vekemans, B., Adams, F., Oost, A. (1999) A compact small-beam XRF instrument for in-situ analysis of objects of historical and/or artistic value. *Spectrochimica Acta Part B-Atomic Spectroscopy* 54: 1697–1710.
58. Williams–Thorpe, O., Potts, P.J., Webb, P.C. (1999) Field-portable non-destructive analysis of lithic archaeological samples by X-ray fluorescence instrumentation using a mercury iodide detector: Comparison with

- wavelength-dispersive XRF and a case study in British stone axe provenancing. *Journal of Archaeological Science* 26: 215–237.
59. Serebryakov, A.S., Demchenko, E.L., Koudryashov, V.I., Sokolov, A.D. (2004) Energy dispersive X-ray fluorescent (ED XRF) analyzer X-Art for investigation of artworks. *Nuclear Instruments & Methods in Physics Research Section B-Beam Interactions with Materials and Atoms* 213: 699–702.
60. Zarkadas, C., Karydas, A.G. (2004) A portable semi-micro-X-ray fluorescence spectrometer for archaeometrical studies. *Spectrochimica Acta Part B-Atomic Spectroscopy* 59: 1611–1618.
61. Desnica, V., Schreiner, M. (2006) A LabVIEW-controlled portable x-ray fluorescence spectrometer for the analysis of art objects. *X-Ray Spectrometry* 35: 280–286.
62. Ferretti, M. (2004) Fluorescence from the collimator in Si-PIN and Si-drift detectors: problems and solutions for the XRF analysis of archaeological and historical materials. *Nuclear Instruments & Methods in Physics Research Section B-Beam Interactions with Materials and Atoms* 226: 453–460.
63. Ferrero, J.L., Roldan, C., Juanes, D., Rollano, E., Morera, C. (2002) Analysis of pigments from Spanish works of art using a portable EDXRF spectrometer. *X-Ray Spectrometry* 31: 441–447.
64. Rohrs, S., Stege, H. (2004) Analysis of Limoges painted enamels from the 16th to 19th centuries by using a portable micro x-ray fluorescence spectrometer. *X-Ray Spectrometry* 33: 396–401.

-
65. Newman, B., Loendorf, L. (2005) Portable X-ray fluorescence analysis of rock art pigments. *Plains Anthropologist* 50: 277–283.
66. Romano, F.P., Calvi, G., Furia, E., Garraffo, S., Marchetta, C., Pappalardo, G., Pappalardo, L., Rizzo, F., Rovelli, A. (2005) A new portable XRF spectrometer with beam stability control. *X-Ray Spectrometry* 34: 135–139.
67. Romano, F.P., Pappalardo, G., Pappalardo, L., Garraffo, S., Gigli, R., Pautasso, A. (2006) Quantitative non-destructive determination of trace elements in archaeological pottery using a portable beam stability-controlled XRF spectrometer. *X-Ray Spectrometry* 35: 1–7.
68. Vittiglio, G., Bichhneier, S., Klinger, P., Heckel, J., Fuzhong, W., Vincze, L., Janssens, K., Engstrom, P., Rindby, A., Dietrich, K., Jembrih-Simburger, D., Schreiner, M., Denis, D., Lakdar, A., Lamotte, A. (2004) A compact mu-XRF spectrometer for (in situ) analyses of cultural heritage and forensic materials. *Nuclear Instruments & Methods in Physics Research Section B-Beam Interactions with Materials and Atoms* 213: 693–698.
69. Papadopoulou, D.N., Zachariadis, G.A., Anthemidis, A.N., Tsirliganis, N.C., Stratis, J.A. (2006) Development and optimisation of a portable micro-XRF method for in situ multi-element analysis of ancient ceramics. *Talanta* 68: 1692–1699.
70. Buzanich, G., Wobrauschek, P., Streli, C., Markowicz, A., Wegrzynek, D., Chinea-Cano, E., Bamford, S. (2007) A portable micro-X-ray fluorescence spectrometer with polycapillary optics and vacuum chamber for archaeometric and other applications. *Spectrochimica Acta Part B-Atomic Spectroscopy* 62: 1252–1256.

-
71. Buzanich, G., Wobrauschek, P., Streli, C., Markowicz, A., Wegrzynek, D., Chinea-Cano, E., Griesser, M., Uhlir, K. (2010) PART II (Portable ART analyzer) – development of a XRF spectrometer adapted for the study of artworks in the Kunsthistorisches Museum, Vienna. *X-Ray Spectrometry* 39: 98–102.
72. Uhlir, K., Griesser, M., Buzanich, G., Wobrauschek, P., Streli, C., Wegrzynek, D., Markowicz, A., Chinea-Cano, E. (2008) Applications of a new portable (micro) XRF instrument having low-Z elements determination capability in the field of works of art. *X-Ray Spectrometry* 37: 450–457.
73. Deneckere, A., Hocquet, F.P., Born, A., Klein, P., Rakkaa, S., Lycke, S., De Langhe, K., Martens, M.P.J., Strivay, D., Vandenabeele, P., Moens, L. (2010) Direct analysis of the central panel of the so-called Wyts triptych after Jan van Eyck. *Journal of Raman Spectroscopy* 41: 1210–1219.
74. Dik, J., Janssens, K., van der Snickt, G., van der Loeff, L., Rickers, K., Cotte, M. (2008) Visualization of a lost painting by Vincent van Gogh using synchrotron radiation based X-ray fluorescence elemental mapping. *Analytical Chemistry* 80: 6436–6442.
75. Kanngiesser, B., Malzer, W., Reiche, I. (2003) A new 3D micro X-ray fluorescence analysis set-up – First archaeometric applications. *Nuclear Instruments & Methods in Physics Research Section B-Beam Interactions with Materials and Atoms* 211: 259–264.
76. Kanngiesser, B., Mantouvalou, I., Malzer, W., Wolff, T., Hahn, O. (2008) Non-destructive, depth resolved investigation of corrosion layers of historical glass objects by 3D Micro X-ray fluorescence analysis. *Journal of Analytical Atomic Spectrometry* 23: 814–819.

-
77. Mantouvalou, I., Lange, K., Wolff, T., Grotzsch, D., Luhl, L., Haschke, M., Hahn, O., Kanngiesser, B. (2010) A compact 3D micro X-ray fluorescence spectrometer with X-ray tube excitation for archaeometric applications. *Journal of Analytical Atomic Spectrometry* 25: 554–561.
78. Hunter, F.J., McDonnell, J.G., Pollard, A.M., Morris, C.R., Rowlands, C.C. (1993) The Scientific Identification of Archaeological Jet-Like Artifacts. *Archaeometry* 35: 69–89.
79. Fortina, C., Barbone, A.S., Memmi, I.T. (2005) Sienese 'archaic' majolica: A technological study of ceramic bodies and coatings. *Archaeometry* 47: 535–555.
80. Sotiropoulou, S., Daniilia, S., Miliani, C., Rosi, F., Cartechini, L., Papanikola-Bakirtzis, D. (2008) Microanalytical investigation of degradation issues in Byzantine wall paintings. *Applied Physics A-Materials Science & Processing* 92: 143–150.
81. Vandenabeele, P., Garcia-Moreno, R., Mathis, F., Leterme, K., Van Elslande, E., Hocquet, F.P., Rakkaa, S., Laboury, D., Moens, L., Strivay, D., Hartwig, M. (2009) Multi-disciplinary investigation of the tomb of Menna (TT69), Theban Necropolis, Egypt. *Spectrochimica Acta Part A-Molecular and Biomolecular Spectroscopy* 73: 546–552.
82. Zieba-Palus, J., Kunicki, M. (2006) Application of the micro-FTIR spectroscopy, Raman spectroscopy and XRF method examination of inks. *Forensic Science International* 158: 164–172.
83. Bicchieri, M., Monti, M., Piantanida, G., Sodo, A. (2008) All that is iron-ink is not always iron-gall! *Journal of Raman Spectroscopy* 39: 1074–1078.

-
84. Castro, K., Sarmiento, A., Maguregui, M., Martinez-Arkarazo, I., Etxebarria, N., Angulo, M., Barrutia, M.U., Gonzalez-Cembellin, J.M., Madariaga, J.M. (2008) Multianalytical approach to the analysis of English polychromed alabaster sculptures: μ Raman, μ EDXRF, and FTIR spectroscopies. *Analytical and Bioanalytical Chemistry* 392: 755–763.
85. Akyuz, S., Akyuz, T., Basaran, S., Bolcal, C., Gulec, A. (2008) Analysis of ancient potteries using FT-IR, micro-Raman and EDXRF spectrometry. *Vibrational Spectroscopy* 48: 276–280.
86. Striova, J., Coccolini, G., Micheli, S., Lofrumento, C., Galeotti, M., Cagnini, A., Castellucci, E.M. (2009) Non-destructive and non-invasive analyses shed light on the realization technique of ancient polychrome prints. *Spectrochimica Acta Part A-Molecular and Biomolecular Spectroscopy* 73: 539–545.
87. Ricci, C., Borgia, I., Brunetti, B.G., Miliani, C., Sgamellotti, A., Seccaroni, C., Passalacqua, P. (2004) The Perugino's palette: integration of an extended in situ XRF study by Raman spectroscopy. *Journal of Raman Spectroscopy* 35: 616–621.
88. Aceto, M., Agostino, A., Boccaleri, E., Crivello, F., Garlanda, A.C. (2006) Evidence for the degradation of an alloy pigment on an ancient Italian manuscript. *Journal of Raman Spectroscopy* 37: 1160–1170.
89. Chaplin, T.D., Clark, R.J.H., Martinon-Torres, M. (2010) A combined Raman microscopy, XRF and SEM-EDX study of three valuable objects – A large painted leather screen and two illuminated title pages in 17th century books of ordinances of the Worshipful Company of Barbers, London. *Journal of Molecular Structure* 976: 350–359.

-
90. Aibeo, C.L., Goffin, S., Schalm, O., van der Snickt, G., Laquiere, N., Eyskens, P., Janssens, K. (2008) Micro-Raman analysis for the identification of pigments from 19th and 20th century paintings. *Journal of Raman Spectroscopy* 39: 1091–1098.
 91. Castro, K., Pessanha, S., Proietti, N., Princi, E., Capitani, D., Carvalho, M.L., Madariaga, J.M. (2008) Noninvasive and nondestructive NMR, Raman and XRF analysis of a Blaeu coloured map from the seventeenth century. *Analytical and Bioanalytical Chemistry* 391: 433–441.
 92. Castro, K., Proietti, N., Princi, E., Pessanha, S., Carvalho, M.L., Vicini, S., Capitani, D., Madariaga, J.M. (2008) Analysis of a coloured Dutch map from the eighteenth century: The need for a multi-analytical spectroscopic approach using portable instrumentation. *Analytica Chimica Acta* 623: 187–194.
 93. Prinsloo, L.C., Wood, N., Loubser, M., Verryyn, S.M.C., Tiley, S. (2005) Re-dating of Chinese celadon shards excavated on Mapungubwe Hill, a 13(th) century iron age site in South Africa, using Raman spectroscopy, XRF and XRD. *Journal of Raman Spectroscopy* 36: 806–816.
 94. van der Snickt, G., De Nolf, W., Vekemans, B., Janssens, K. (2008) mu-XRF/mu-RS vs. SR mu-XRD for pigment identification in illuminated manuscripts. *Applied Physics A-Materials Science & Processing* 92: 59–68.
 95. Paternoster, G., Rinzivillo, R., Nunziata, F., Castellucci, E.M., Lofrumento, C., Zoppi, A., Felici, A.C., Fronterotta, G., Nicolais, C., Piacentini, M., Sciuti, S., Vendittelli, M. (2005) Study on the technique of the Roman age mural paintings by micro-XRF with Polycapillary Conic Collimator and micro-Raman analyses. *Journal of Cultural Heritage* 6: 21–28.

-
96. Deneckere, A., Schudel, W., Van Bos, M., Wouters, H., Bergmans, A., Vandenabeele, P., Moens, L. (2010) In situ investigations of vault paintings in the Antwerp cathedral. *Spectrochimica Acta Part A-Molecular and Biomolecular Spectroscopy* 75: 511–519.
 97. Sawczak, M., Kaminska, A., Rabczuk, G., Ferretti, M., Jendrzewski, R., Sliwinski, G. (2009) Complementary use of the Raman and XRF techniques for non-destructive analysis of historical paint layers. *Applied Surface Science* 255: 5542–5545.
 98. Andrikopoulos, K.S., Daniilia, S.X., Roussel, B., Janssens, K. (2006) In vitro validation of a mobile Raman–XRF micro-analytical instrument’s capabilities on the diagnosis of Byzantine icons. *Journal of Raman Spectroscopy* 37: 1026–1034.
 99. Castro, K., Perez-Alonso, M., Rodriguez-Laso, M.D., Etxebarria, N., Madariaga, J.M. (2007) Non-invasive and non-destructive micro-XRF and micro-Raman analysis of a decorative wallpaper from the beginning of the 19th century. *Analytical and Bioanalytical Chemistry* 387: 847–860.
 100. Castro, K., Abalos, B., Martinez-Arkarazo, I., Etxebarria, N., Madariaga, J.M. (2008) Scientific examination of classic Spanish stamps with colour error, a non-invasive micro-Raman and micro-XRF approach: The King Alfonso XIII (1889–1901 “Pelón”) 15 cents definitive issue. *Journal of Cultural Heritage* 9: 189–195.
 101. Burgio, L., Clark, R.J.H., Muralha, V.S.F., Stanley, T. (2008) Pigment analysis by Raman microscopy of the non-figurative illumination in 16th-to 18th-century Islamic manuscripts. *Journal of Raman Spectroscopy* 39: 1482–1493.

-
102. Sendova, M., Kaiser, B., Scalera, M., Zhelyaskov, V. (2010) Della Robbia blue glaze: micro-Raman temperature study and X-ray fluorescence spectroscopy characterization. *Journal of Raman Spectroscopy* 41: 469–472.
 103. Maguregui, M., Sarmiento, A., Martinez-Arkarazo, I., Angulo, M., Castro, K., Arana, G., Etxebarria, N., Madariaga, J.M. (2008) Analytical diagnosis methodology to evaluate nitrate impact on historical building materials. *Analytical and Bioanalytical Chemistry* 391: 1361–1370.
 104. Maguregui, M., Martinez-Arkarazo, I., Angulo, M., Castro, K., Fernandez, L.A., Madariaga, J.M. (2008) *Lasers in the Conservation of Artworks*. Chapter 27 Portable spectroscopic analysis of nitrates affecting to cultural heritage materials. Talor and Francis Group, London, 177–182.
 105. Ramos, P.M., Ruisanchez, I., Andrikopoulos, K.S. (2008) Micro-Raman and X-ray fluorescence spectroscopy data fusion for the classification of ochre pigments. *Talanta* 75: 926–936.
 106. Vekemans, B., Janssens, K., Vincze, L., Adams, F., Vanespen, P. (1994) Analysis of X-Ray-Spectra by Iterative Least-Squares (Axil) – New Developments. *X-Ray Spectrometry* 23: 278–285.
 107. Deneckere, A., De Vries, L., Vekemans, B., Van de Voorde, L., Ariese, F., Vincze, L., Moens, L., Vandenabeele, P. (2011) Identification of inorganic pigments used in porcelain cards based on fusing Raman and XRF data. *Applied Spectroscopy*, accepted.

**Chapter 10: Identification of inorganic pigments
used in porcelain cards based on
fusing Raman and XRF data**

Annelien Deneckere, Lieke de Vries, Bart Vekemans, Lien Van de Voorde,
Freek Ariese, Laszlo Vincze, Luc Moens, Peter Vandenabeele

Accepted in Applied Spectroscopy

In the previously discussed case studies (Chapters 5–9) the Raman results and XRF results are first interpreted separately and afterwards compared with each other. In this chapter, the possibilities of fusing Raman and XRF data are explored. The first part of this chapter describes the fusion for the classification of the different measured points on 4 copies of a similar porcelain card using principal components analysis (PCA). In the second part an attempt is made to develop a procedure for the identification of the pigments used in the porcelain cards based on the fused Raman–XRF data.

10.1 Introduction

Raman spectroscopy and X-ray fluorescence (XRF) spectroscopy are particularly well suited for the analysis of ancient art objects in cultural heritage studies because both techniques are fast, sensitive, non-destructive and measurements can take place *in situ*^{1,2}. Raman spectroscopy provides molecular information of the material, while XRF spectroscopy provides the elementary composition. Moreover, the penetration depth of the X-rays is larger than the penetration depth of the laser light, resulting in combined information of different layers.

Using complementary methods maximises the amount of information obtained. In cultural heritage studies, one should always try to maximise the amount of information that is obtained, while minimising the (risk on) damage to the artefact³. In recent literature, several examples of research in the field of cultural heritage can be found, where Raman spectroscopy is combined with XRF spectroscopy. One of these studies expressing the complementary characteristics of both techniques is the monitoring of the influence of nitrates on historical building materials. Different nitrate salts can be formed (e.g. NaNO_3 , $\text{Mg}(\text{NO}_3)_2$, $\text{Ca}(\text{NO}_3)_2$ and $\text{Ba}(\text{NO}_3)_2$), depending the nature of the materials and the impacting nitrate compound. Whereas Raman spectroscopy mainly detect the strongest band of the nitrates

(νNO_3^- , 1060–1035 cm^{-1}), XRF spectroscopy, together with thermodynamical modelling and ion chromatography, is used to identify counter ions and possible nitrate combinations^{4,5}. The combination of Raman spectroscopy and XRF spectroscopy was also used in several studies on the identification of pigments used for different art objects, amongst others, Byzantine icons⁶, mural^{7–9} and easel^{10,11} paintings, manuscripts^{12–14}, Egyptian tombs¹⁵ and burial masks³.

Van der Snickt¹⁶ et al mentioned also the use of a combined Raman–XRF spectrometer, PRAXIS. The analytical possibilities of this combined instrument were evaluated analysing illuminated manuscripts. The advantage of this approach is that exactly the same spot size is measured with both techniques.

When combining different spectroscopic techniques, as in case of performing analyses on same material with separate XRF and Raman spectrometers, there is the obvious request to develop methods that are based on “joined” data.

For all the previously mentioned studies, both techniques were used separately, in a sense that the spectra were obtained and processed independently and single conclusions are obtained, by expert analysts, considering both results. The aim of the current research is to merge the spectra and process the fused data together. Ramos et al^{2,17} proposed a mid-level data fusion system to process Raman and XRF spectra obtained from a combined micro–Raman–XRF instrument. In the first step of their data fusion system wavelet transformation is used to split each spectrum set in blocks, according to their frequency. Next, the blocks which contain background and noise signals are removed and variable selection is performed on the remaining blocks to extract those variables with the most power of classification. Then, the variables are concatenated and form a Raman–XRF meta-signal ensemble. Finally, dual-domain signal ensembles from references and samples are classified using partial least squares discriminant analysis (PLS-DA). This data fusion system was already successful for the classification of different ochre pigments. The advantage of this data fusion system is that the fusion is suitable for automated processing of

large amounts of data and can be applied to an individual data source or n data sources to achieve data fusion. The main drawback of this approach is the complex data processing, requiring quite some computing power (e.g. the use of wavelet transformation). Therefore, we propose here a less complex approach.

This current paper describes another attempt to develop methods for pigment identification that are based on joining or fusion of Raman data with XRF data. The experimental data are obtained from point measurements with both spectroscopic techniques of selected positions on a set of porcelain cards (Fig. 10.1).



Figure 10.1 (a) Picture of copy A of the porcelain card, with an overview of the analysed points.

Each point was measured with Raman spectroscopy and XRF spectroscopy. As part of the evaluation of the method, principal components analysis (PCA) results calculated from the fused data are compared with PCA results obtained from the data acquired with only one of the spectroscopic techniques. Eventually, the aim is

to provide a new tool that may help the researcher in the pigment identification process on the basis of fused data from inorganic pigments.



Figure 10.1 (b) Picture of copy B of the porcelain card.

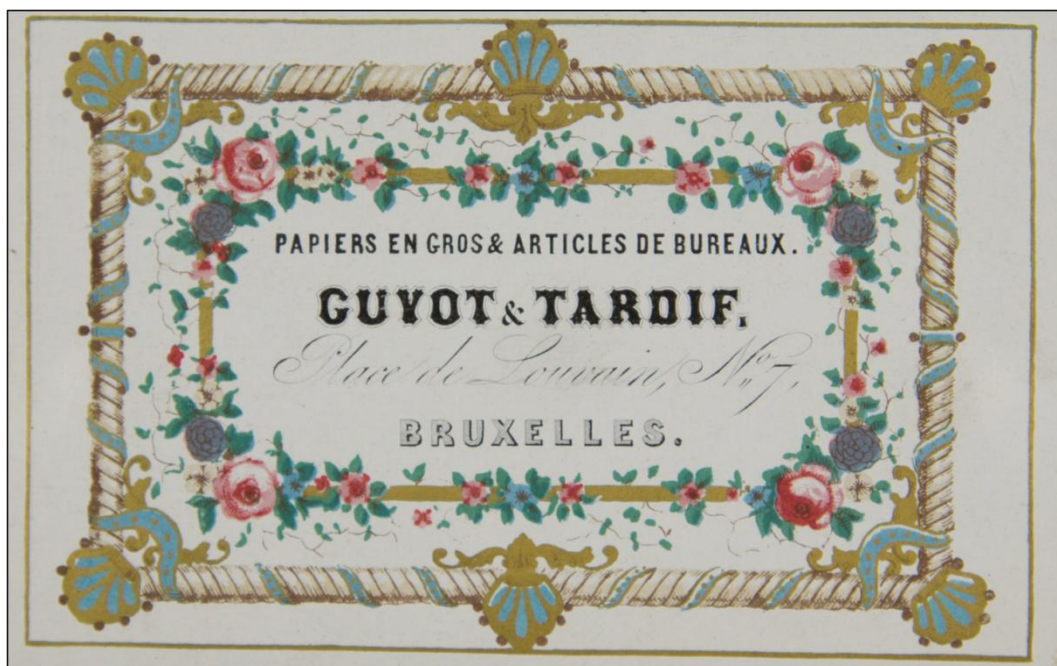


Figure 10.1 (c) Picture of copy C of the porcelain card.



Figure 10.1 (d) Picture of copy D of the porcelain card.

10.2 Experimental

10.2.1 Samples

As test-case for the development of the data fusion system porcelain cards were analysed, because these cards are very colourful and easy to handle. In the 19th century, porcelain cards were used as visiting cards, New year greetings, menus, calendars, labels, certificates, funeral notices,... These cards were not only printed with text, but also brightened with decorations and illustrations of professions, workshops, products and production machines. Typical dimensions of porcelain cards range from 10 × 8 cm to even 28 × 18 cm, for luxurious cards, and ca. 1 mm thickness¹⁸. The porcelain card (Fig. 10.1) selected for this research represents a typical business card for the company Guyot & Tardif, wholesale business in paper and office supplies in Brussels, Belgium. During this research, 4 copies of this card were analysed. A selection of different colours was made: white,

gold, brown, blue, pink, red, green, purple, black, light blue and beige. The 11 measured points (Fig. 10.1) were meticulously reported for each card, in order to achieve the best possible correspondence between the position of the Raman measurement and the XRF measurement.

The proposed identification procedure uses a small database of reference pigments. Therefore, a selection of reference pigments was made. For the XRF analysis a small amount of the reference pigment was fixed as a powder with n-hexane on ultralene as described before¹³, whereas Raman spectroscopy was performed on a small amount of pigment grains on a microscope slide. Table 10.1 gives an overview of the selected reference pigments. The pigments were selected from our collection, to cover materials with a diverse chemical composition.

10.2.2 Instrumentation

10.2.2.1 Micro-Raman spectroscopy

Raman spectra were recorded with a Bruker Optics ‘Senterra’ dispersive Raman spectrometer coupled with an Olympus BX51 microscope. The Raman spectrometer is equipped with 532 (Nd:YAG) and 785 nm (diode) laser sources. High resolution spectra are recorded in 3 spectral windows, covering 60–3700 cm^{-1} and 80–3500 cm^{-1} for the 532 and 785 nm laser, respectively. The system uses a thermo-electrically cooled CCD detector, operating at -65°C . Five software-controlled settings for the power of each laser are available: 100, 50, 25, 10 and 1%, i.e. up to 35 mW at the sample for the 785 nm laser. The microscope has 5 \times , 20 \times and 50 \times objectives, with spot sizes of approximately 50, 10 and 4 μm , respectively. The instrument is controlled via the OPUS 6.5.6 software.

pigment	colour	chemical structure	supplier
azurite	blue	$2\text{CuCO}_3 \cdot \text{Cu}(\text{OH})_2$	Kremer Pigmente
cerulean blue	blue	$\text{CoO} \cdot n\text{SnO}_2$	Winsor & Newton
cobalt blue	blue	$\text{CoO} \cdot \text{Al}_2\text{O}_3$	Kremer Pigmente
Prussian blue	blue	$\text{Fe}_4(\text{Fe}[\text{CN}]_6)_3$	Kremer Pigmente
ultramarine	blue	$\text{Na}_{8-10}\text{Al}_6\text{Si}_6\text{O}_{24}\text{S}_{2-4}$	Kremer Pigmente
malachite	green	$\text{Cu}_2\text{CO}_3(\text{OH})_2$	Kremer Pigmente
green earth	green	$\text{FeSiO}_3 \cdot n\text{H}_2\text{O}$	Gerin
chrysocolla	green	$\text{CuSiO}_3 \cdot n\text{H}_2\text{O}$	Kremer Pigmente
viridian	green	$\text{Cr}_2\text{O}_3 \cdot 2\text{H}_2\text{O}$	Winsor & Newton
verdigris	green	$\text{Cu}(\text{CH}_3\text{COO})_2 \cdot n\text{Cu}(\text{OH})_2$	Kremer Pigmente
cadmium red	red	$\text{CdS}(\text{Se})$	Winsor & Newton
vermilion	red	HgS	Kremer Pigmente
hematite	red	Fe_2O_3	Kremer Pigmente
red ochre	red	$\text{Fe}_2\text{O}_3 + \text{silicate} + \text{clay}$	Winsor & Newton
lead white	white	$2\text{PbCO}_3 \cdot \text{Pb}(\text{OH})_2$	Kremer Pigmente
chalk	white	CaCO_3	Sigma Aldrich
gypsum	white	$\text{CaSO}_4 \cdot 2\text{H}_2\text{O}$	Sigma Aldrich
lithopone	white	$\text{BaSO}_4 + \text{ZnS}$	Kremer Pigmente
zinc white	white	ZnO	Kremer Pigmente
orpiment	yellow	As_2S_3	Kremer Pigmente
lead-tin yellow type I	yellow	Pb_2SnO_4	Kremer Pigmente
massicot	yellow	PbO	Delvigne
chrome yellow	yellow	PbCrO_4	Kremer Pigmente
cadmium yellow	yellow	CdS	Sennelier Paris

Table 10.1 Overview of the selected reference pigments.

10.2.2.2 Energy dispersive X-ray fluorescence (EDXRF) spectroscopy

A laboratory micro-XRF system (Eagle-III microprobe, EDAX, Inc, Mahwah, NJ, USA) provided elemental information of the analysed samples. This spectrometer is equipped with a microfocus X-ray tube with a Rh anode, a polycapillary lens (X-ray Optical Systems, Inc., NY, USA) for X-ray focussing, and a liquid N₂ cooled 80 mm² energy dispersive Si-(Li) detector. The sample chamber incorporates a XYZ motorised stage for sample positioning. A high resolution microscope is used to position the sample on the desired distance from the polycapillary. Operation in vacuum allows the use of the Rh-L photons originating from the X-ray tube to improve the investigation of low Z-elements down to sodium. For all XRF experiments a beam size of 100 μ m was chosen, a voltage of 40 kV, and a tube current of 100 μ A was selected to reach 30% detector dead time.

10.3 Results and discussion

10.3.1 Fusion of the data: proposed methodology

Ramos et al^{2,17} suggest two different strategies to fuse spectral data: data level fusion or low-level fusion on the one hand and feature level fusion or mid-level fusion on the other hand. When using low-level fusion the raw spectral data are fused, whereas when using mid-level fusion the fusion is done ideally over the most relevant features, so variable selection is performed before the fusion. In this research, mid-level fusion was selected to fuse Raman and XRF data (Fig. 10.2).

Figure 10.2 shows the proposed method of fusing the data of the different spectroscopic methods. Each of the spectrometers has, next to their specific instrument controlling software, specialised data evaluation software that helps the

researcher to interpret the acquired technique-specific data. In case of the EDAX Eagle-III micro-XRF spectrometer the spectroscopic data are evaluated with the dedicated spectrum evaluation routine of the AXIL software package^{19,20} to identify the detected elements, and to extract the areas of the peaks of the identified elements. Application of this dedicated software is necessary in order to compensate for the spectral background, peak overlap, and artefacts such as escape peaks and sum peaks that may appear in X-ray spectra. Following the proposed method in figure 10.2, as a first step, raw spectroscopic data should be processed with dedicated software. In case of XRF data, the fitting module of the AXIL software package converts the raw spectra into a list of elements (XRF variables) with corresponding peak areas for each point measurement (object).

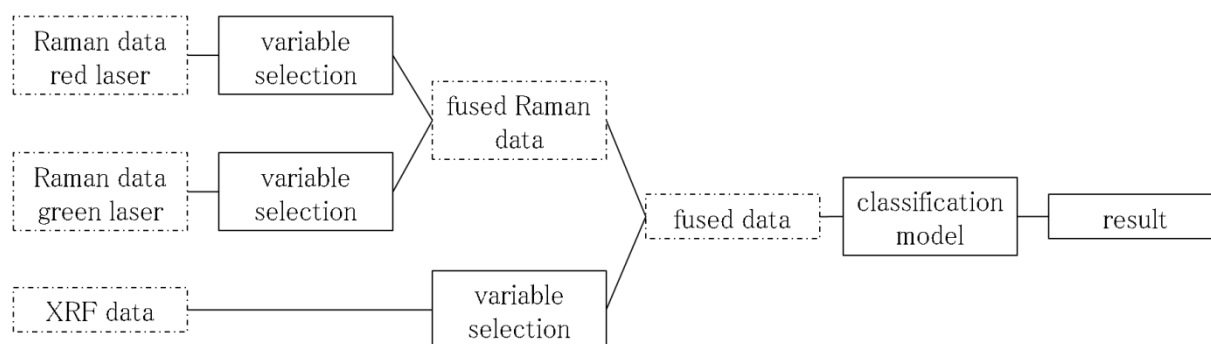


Figure 10.2 Schematic overview of the proposed mid-level fusion.

In the case of the Senterra micro-Raman spectrometer commercial software such as OPUSTM can be used to analyse the acquired Raman spectral data. However, although this software is mature and contains many features, it lacks typically methods for tasks such as processing and classification. Therefore, different research groups started the development of software, specially dedicated for spectral evaluation of Raman data^{21,22}. In analogy with the data processing of the XRF spectra, and to allow all data processing in a simple software package, for the Raman data processing, new routines were written to extract automatically Raman band positions and the corresponding band areas from the Raman spectra.

In the first step of the Raman spectrum evaluation, the SNIP²⁰ background estimation procedure was used so that, in a next step, the determination of the Raman band positions and the calculation of the corresponding band areas could be performed after Raman background subtraction. The estimation of the background also allows us to decide whether a signal is significantly higher than its background or not. The band positions were determined on the basis of simple calculations of the first and second derivatives of the Raman spectrum. In contrast to XRF data processing of series of XRF spectra, when book-keeping of the Raman band information, processing a large number of Raman spectra may lead to an overwhelming number of Raman bands. This situation was avoided by making first a Raman sum spectrum of the dataset from which the positions of the significant Raman bands were determined and the areas were calculated for the individual Raman spectra as described above. This working method is commonly used when processing XRF data constituting XRF maps. Using the above described Raman spectrum evaluation procedure allows obtaining results with a minimum of effort in a completely automated manner. This approach has the advantage of drastically reducing the dataset and focussing on the molecular spectra that are commonly present in the dataset. However, the importance of inhomogeneity's or outlier spectra is reduced.

Since the Senterra Raman spectrometer is a dual laser system equipped with of a red laser (785 nm) and a green laser (532 nm), as a general procedure, all sample positions were measured with both lasers. The “red” laser data and the “green” laser data can be considered as whether they were obtained from different techniques as indicated in figure 10.2. Therefore, each of these Raman datasets was processed separately as described above. In a next step, the selected variables (Raman band positions) of the red laser data and the green laser data were compared. If the same Raman band positions are significantly present in both

datasets, the data of the “green” laser are omitted. Indeed, from our general experience in Raman spectroscopy, we consider the 785 nm (red) laser as the most versatile for Raman spectroscopy of pigments, due to the probably lower occurrence of fluorescence overwhelming the spectrum. In some cases, however, the green (532 nm) laser may introduce extra information, e.g. in cases where the red laser is seriously absorbed by the pigment. Therefore, if the same band is present in both Raman spectra, we consider the information of the green spectrum as redundant, whereas in the other case the data of that band are included in the new dataset. In order to be able to compare the data in a convenient way, the Raman data were scaled to a measuring time of 300 s. Finally the variables (Raman band positions and corresponding band areas) were organised in a single data matrix.

For the same reason as for the Raman data, the XRF data were scaled to a measurement time of 100 s and a tube current of 100 μ A. After scaling the Raman and the XRF datasets, the variables (Raman band positions + XRF elements), together with the corresponding band and peak areas, were fused into a single data matrix.

Next to the measurement of the porcelain cards, a dataset of reference pigments was subjected to the same methodology as described above. In this way, there are different datasets for the porcelain cards and the reference pigments: datasets for each spectroscopic method, and the fused dataset. To prepare for the identification process, the above described procedure was followed again including all point measurements, i.e. processing all porcelain card spectra together with the reference pigments spectra.

The development of the software tools was done in the high-level software environment of IDL (ITT Visual Information Solutions). This greatly simplified the programming task of making this prototype of the pigment identification method as

the IDL programming language is optimised for array calculations and provides access to numerous sets of routines for mathematical calculations.

10.3.2 Identification procedure applied on the fused data

Until now, the results of the Raman data and the XRF data were first evaluated separately, most often by different researchers, possibly experienced in only one of the applied spectroscopic techniques. In the next steps, the complementary information of both techniques is joined and interpreted together in the attempt to formulate answers on the sample that are consistent to the results of both techniques. In this way, table 10.2 shows the pigment identification of the different points of porcelain card A. Similar results were obtained from the other porcelain cards B, C and D, as expected since similar positions on the cards were investigated. Figure 10.3 shows the resulting Raman and XRF spectra of the red analysed point A6. In figure 10.3(a) the characteristic Raman bands of vermilion (HgS) are clearly visible (343, 280, 254 cm^{-1}). The characteristic lines of Hg and S are clearly visible in the XRF spectrum (Fig. 10.3(b)), suggesting that the unknown red pigment could be identified as vermilion (HgS). One must take into account that the XRF method gives information of all the layers together because of the penetration character of the X-rays. E.g. the signal of Pb, that is clearly visible in the spectrum, is caused by the covering layer (lead white ($2\text{PbCO}_3 \cdot \text{Pb}(\text{OH})_2$)) on top of the paper or cardboard. The Raman band of lead white at 1050 cm^{-1} is also clearly visible in the Raman spectrum (Fig. 10.3(a)).

analysed point	colour	identification, based on Raman spectroscopy
1	white	lead white ($2\text{PbCO}_3 \cdot \text{Pb}(\text{OH})_2$)
2	gold	/
3	brown	vermilion (HgS) + carbon black (C)
4	blue	Prussian blue ($\text{Fe}_4(\text{Fe}[\text{CN}]_6)_3$)
5	pink	vermilion (HgS) + lead white ($2\text{PbCO}_3 \cdot \text{Pb}(\text{OH})_2$)
6	red	vermilion (HgS) + traces of carbon black (C)
7	green	Prussian blue ($\text{Fe}_4(\text{Fe}[\text{CN}]_6)_3$) + chrome yellow (PbCrO_4)
8	purple	Prussian blue ($\text{Fe}_4(\text{Fe}[\text{CN}]_6)_3$) + vermilion (HgS)
9	black	carbon black (C)
10	light blue	Prussian blue ($\text{Fe}_4(\text{Fe}[\text{CN}]_6)_3$)
11	beige	lead white ($2\text{PbCO}_3 \cdot \text{Pb}(\text{OH})_2$)

Table 10.2 Identification of the analysed points of copy A of the porcelain card, based on the interpretation of the Raman spectra and the XRF spectra separately.

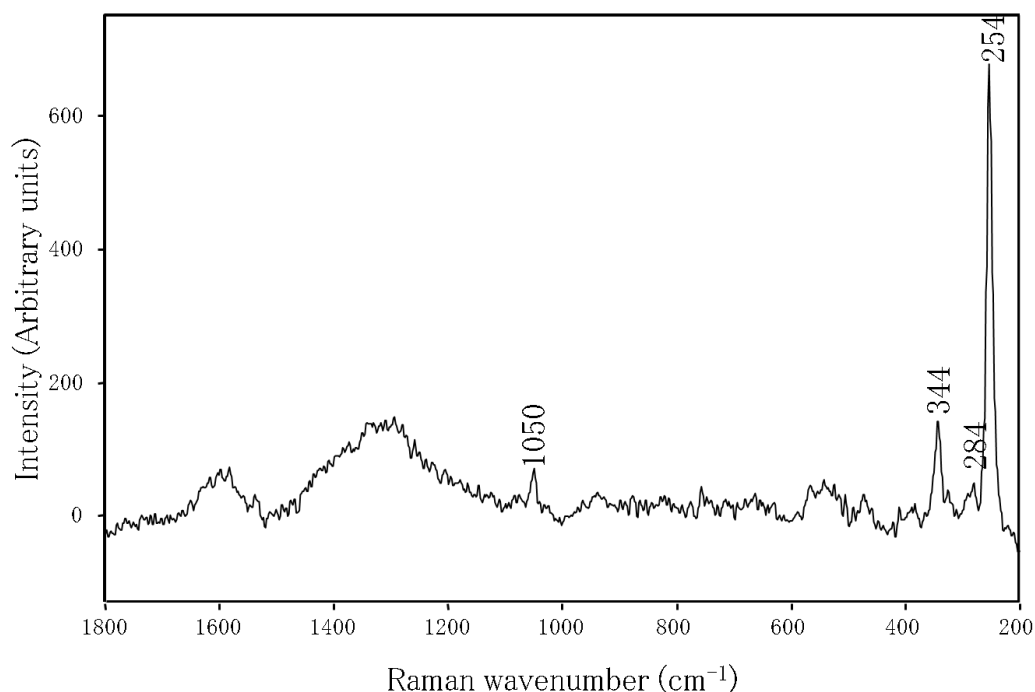


Figure 10.3 (a) Raman spectrum of point A6 (red), showing the Raman bands of vermilion (343, 283, 254 cm⁻¹) (785 nm, 20× objective, 300 s, 1% laser power).

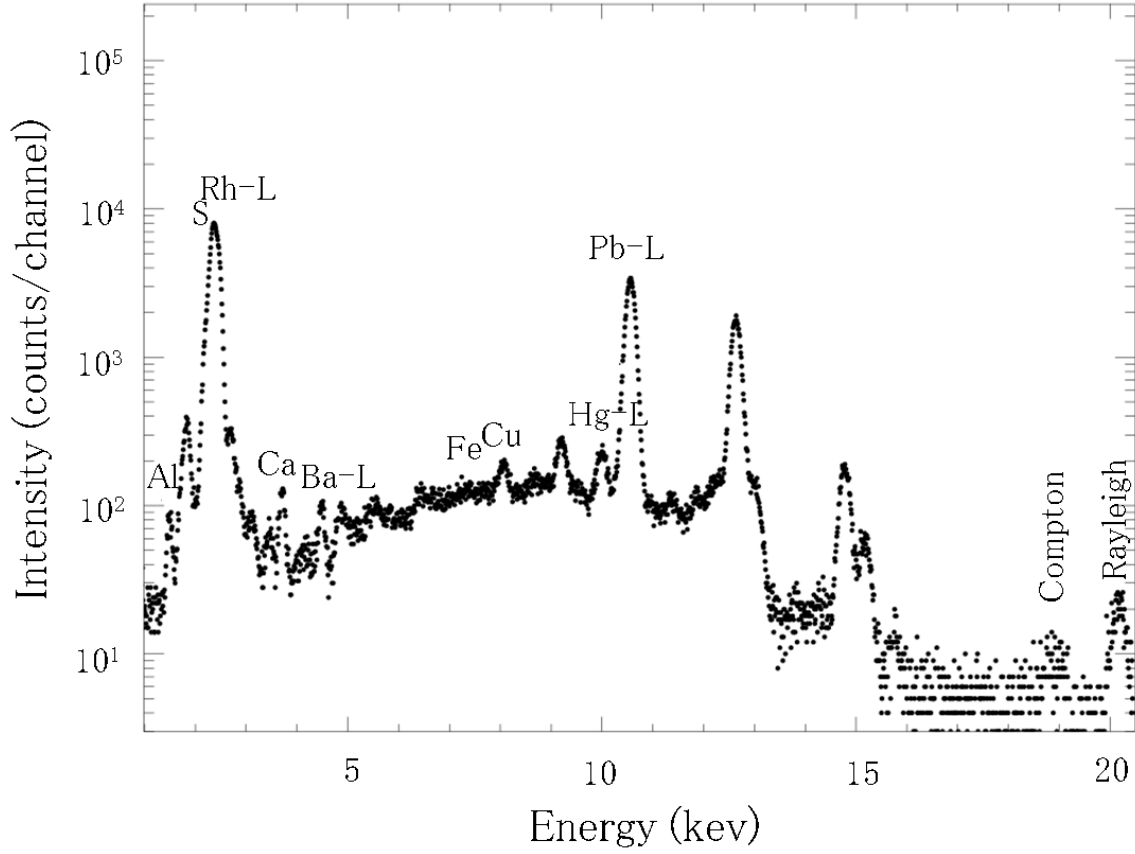


Figure 10.3 (b) XRF spectrum of point A6, peak identification is done with the dedicated XRF spectrum evaluation AXIL.

The availability of fused data that contain information from both techniques enables the possibility to develop tools that may help in the quest of obtaining answers on the samples. In case of the porcelain cards, the questions are related to the identification of pigments as shown in table 10.2. Therefore, a very simple software tool was implemented on the basis of comparing the presence of peaks in the fused data (i.e. presence of peaks in the Raman spectra and XRF spectra). Mathematically we may present the fused data objects of the porcelain cards \mathbf{f}_i as follows:

$$\mathbf{f}_i = (a_{i1}, a_{i2}, \dots, a_{ik}, \dots, a_{iN_{\text{Raman}}}, a_{iN_{\text{Raman}}+1}, a_{iN_{\text{Raman}}+2}, \dots, a_{iN_{\text{Raman}}+N_{\text{XRF}}}) \quad (10.1)$$

where a_{ik} ($k=1, 2, \dots, N_{\text{Raman}}$) is the value of the k^{th} Raman variable (band position), and a_{ik} ($k=N_{\text{Raman}}+1, N_{\text{Raman}}+2, \dots, N_{\text{Raman}}+N_{\text{XRF}}$) is the value of the $(k-N_{\text{Raman}})^{\text{th}}$ XRF

variable (element). The dataset consisting of fused objects of reference pigments \mathbf{f}_j is constructed in a similar way.

The availability of these vectors \mathbf{f}_i and \mathbf{f}_j allows a visual comparison of a porcelain card object's profile \mathbf{f}_i with reference pigment profiles \mathbf{f}_j . Preparing for a working method similar to the conventional way of comparing Raman bands, where distinction is made between very weak, weak, medium, strong and very strong Raman signals, the data of each spectroscopic technique are scaled in such a way that the highest peak is set to 100%. An example of this working method is graphically presented in figure 10.4.

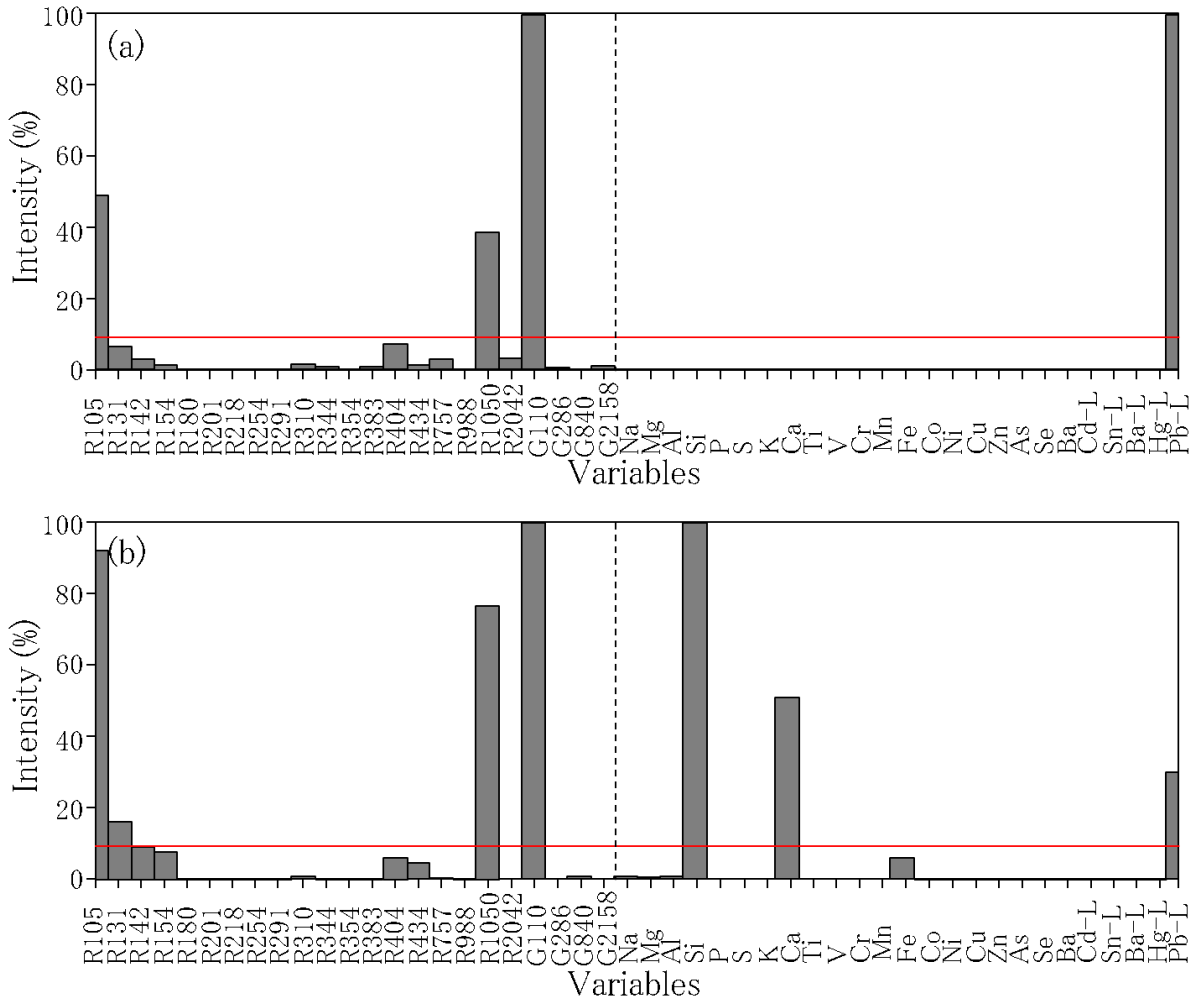


Figure 10.4 Graphic plots of the intensity (%) as function of the variables for (a) the first analysed point A1 and (b) lead white.

In order to reduce the influence of small bands, we choose to exclude Raman bands that are lower than 10%. This is probably similar to the exclusion of weak and very weak bands. However, the amount of profiles to look at, actually pairs of \mathbf{f}_i with \mathbf{f}_j is uncomfortably high, so that the visual inspection of the graphical comparison is preferably done after the book-keeping of the presence of peaks proposed here.

It should be noted that the values a_{ik} (or a_{jk}) for the k^{th} variable are non-zero if that peak is significantly present. Therefore, we may define the presence of peak $p_{ij,k}$ as:

$$p_{ij,k} = \begin{cases} 1 & (\text{if } a_{ik} \times a_{jk} > 0) \\ 0 & (\text{if } a_{ik} \times a_{jk} = 0) \end{cases} \quad (10.2)$$

With $i = 1, \dots, N_{\text{unknowns}}$, and $j = 1, \dots, N_{\text{refpigments}}$. I.e., $p_{ij,k}$ is equal to 1 or 0, depending whether the peak related to the k^{th} variable is significantly present or not in both, the i^{th} data object of the porcelain card and the j^{th} reference pigment object.

For each object (i.e. porcelain card i , and reference pigment j) the number of bands or peaks (i.e. number of non-zero a_{ik} values and number of non-zero a_{jk} values) can be obtained, so that there can be calculated how many of the bands or peaks of the porcelain card i are present in the spectra of the reference pigment j , and vice versa. This book-keeping can also be done separately for each of the spectroscopic techniques (i.e. $k=[1, 2, \dots, N_{\text{raman}}]$ for Raman and $k=[N_{\text{Raman}+1}, N_{\text{Raman}+2}, \dots, N_{\text{Raman}+\text{XRF}}]$ for XRF). As an example, in table 10.3(a) it is shown that porcelain card measurement A1 contains 3 Raman band values and 1 XRF peak value (i.e. in total 4 fused data), while for the cerulean blue 1 Raman band value and 2 XRF peak values (i.e. in total 3 fused data values) are considered. The book-keeping procedure indicates that the porcelain card measurement and the cerulean blue

have the presence of only 1 Raman data value in common. This corresponds with 33% of the Raman information or 25% of the fused data information, when considering the totals of the card A1.

object	# peaks			# common peaks in A1 and ref. pigment			% common peaks in A1 and ref. pigment		
	Raman	XRF	Total	Raman	XRF	Total	Raman	XRF	Total
A1	3	1	4						
cerulean blue	1	2	3	1	0	1	33	0	25
cobalt blue	4	4	8	1	0	1	33	0	25
Prussian blue	9	4	13	2	0	2	66	0	50
ultramarine	6	4	10	1	0	1	33	0	25
azurite	11	3	14	2	0	2	66	0	50
malachite	15	1	16	1	0	1	33	0	25
viridian	8	3	11	1	0	1	33	0	25
green earth	1	3	4	0	0	0	0	0	0
chrysocolla	5	2	7	2	0	2	66	0	50
verdigris	3	3	6	1	0	1	33	0	25
cadmium red	5	3	8	0	0	0	0	0	0
vermilion	2	4	6	0	0	0	0	0	0
hematite	3	3	6	0	0	0	0	0	0
red ochre	3	2	5	0	0	0	0	0	0
orpiment	6	4	10	0	0	0	0	0	0
massicot	3	2	5	0	0	0	0	0	0

Table 10.3 (a) The output of the identification procedure to identify the first analysed point on porcelain card A (A1). For the identification the fused Raman–XRF dataset of the reference pigments was used.

10.3.3 Porcelain cards

10.3.3.1 Raman classification

For the classification of the Raman data with PCA, the following Raman wavenumbers were selected as variables: 2157, 2095, 2042, 1993, 1820, 1654, 1614, 1370, 1351, 1280, 1050, 970, 757, 556, 542, 535, 411, 385, 344, 284, 254 and 105 cm^{-1} . These variables are projected in the loadings plot (Fig. 10.5(a)). Combinations of different Raman band positions, suggest a possible identification of the pigments: Raman band positions at 344, 284, 254 cm^{-1} represent for instance the characteristic Raman bands of the red pigment vermilion. However, the Raman bands at 2095 and 2157 cm^{-1} are expected to be related to each other, because they are both characteristic Raman bands of Prussian blue. Nevertheless, Raman wavenumber 2042 cm^{-1} is also characteristic for Prussian blue, but according to the loadings plot it is not related to the other two wavenumbers. Also for the other variables it is difficult to explain the mutual correlation.

The scores plot of PC2 versus PC3 (Fig. 5b) shows that with Raman spectroscopy it is not possible to distinguish between all the different colours of the analysed objects. The blue and green objects (A4-D4, A7-D7, A8-D8 and A10-D10) form one group which is related with the variables 2157 and 2095 cm^{-1} , suggesting that the blue pigment used is Prussian blue. For the green objects the Prussian blue was probably mixed with a yellow pigment, but identification of this pigment is not possible when studying the loadings plot. The different red objects are spread out over the whole scores plot, which makes identification of the red pigment impossible. Only the white objects (A1-D1 and A11-D11) form a separate group, but relating with the correlated variables (1050 and 105 cm^{-1}) is not possible.

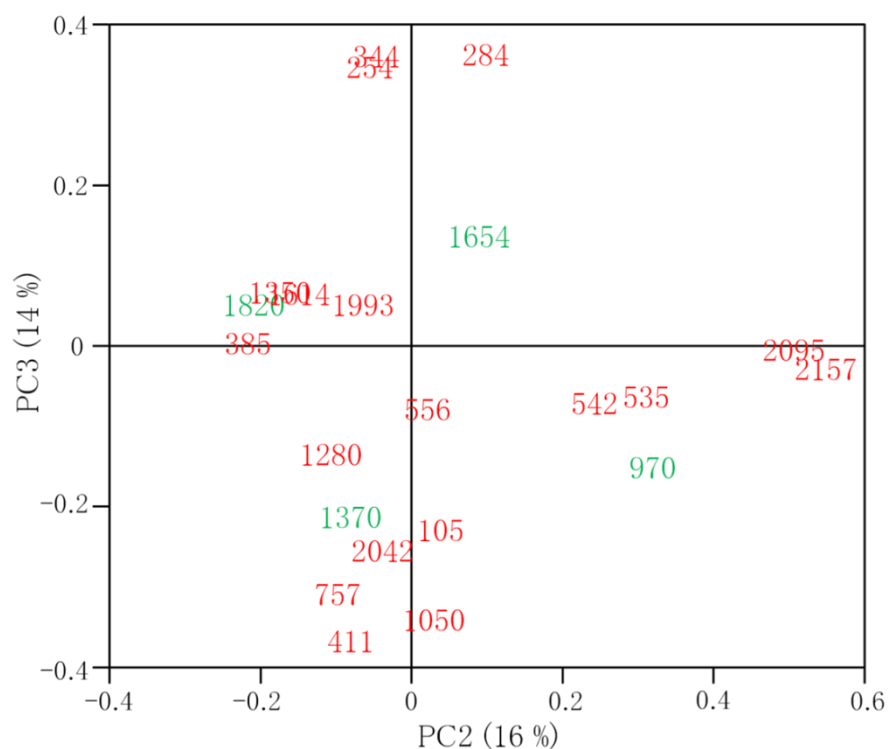


Figure 10.5 (a) Loadings plot of PC2 versus PC3 created by performing PCA on the Raman dataset.

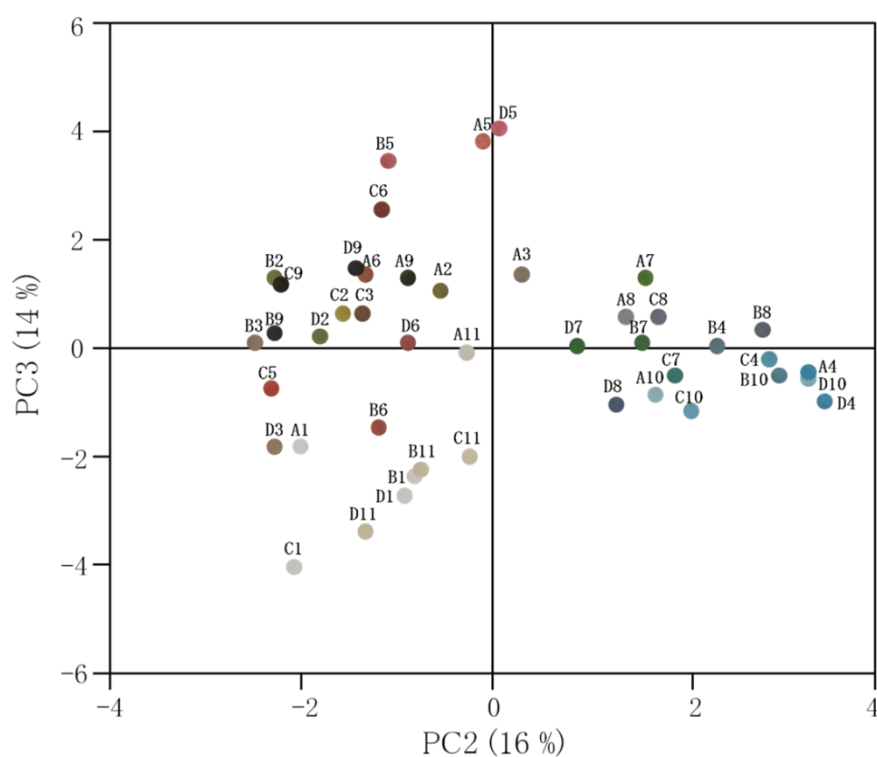


Figure 10.5 (b) Scores plot of PC2 versus PC3 created by performing PCA on the Raman dataset.

10.3.3.2 XRF classification

For the classification of the XRF data with PCA, the following elements were selected as variables: Al, S, Ca, Cr, Fe, Ni, Cu, Zn, Ba, Hg and Pb. The loadings plot (Fig. 10.6(a)) shows the distribution of the variables. Looking at the mutual correlation between the elements leads to a possible identification of the pigments. The correlation between Hg-L and S suggest the presence of the red pigment vermilion (HgS). The presence of Fe shows that Prussian blue ($\text{Fe}_4(\text{Fe}[\text{CN}]_6)_3$) was used. The signal of Pb shows the presence of lead white ($2\text{PbCO}_3 \cdot \text{Pb}(\text{OH})_2$). The correlation between the Zn, Ni and Cr can be explained by the presence of these elements in the XRF spectra of the golden analysed points (A2-D2). The presence of Cr suggests also that chrome yellow (PbCrO_4) was used. The scores plot of PC2 versus PC3 (Fig. 10.6(b)) shows that no classification of the objects is possible based on the XRF dataset. All the objects are centralised in the middle of the plot and mixed. The red objects are spread to the bottom left corner of the plot, which correlates with Hg-L and S, suggesting that vermilion (HgS) was used as red pigment.

10.3.3.3 Raman and XRF data fusion

The scores and loadings plots of PC2 versus PC3 of the fused data are displayed in figure 10.7. In the loadings plot (Fig. 10.7(a)) the correlation between the Raman band positions and the elements is shown. The correlation between the bands at 344 and 254 cm^{-1} , and the elements Hg and S, indicates the use of the pigment vermilion. The distance to the other characteristic Raman band of vermilion (284 cm^{-1}) is also relatively small.

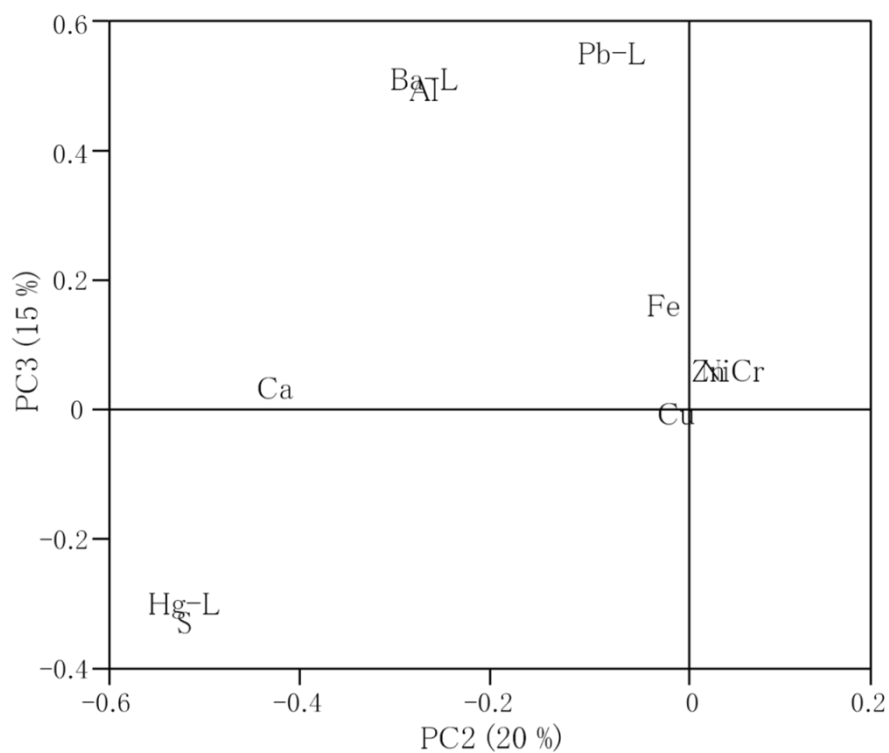


Figure 10.6 (a) Loadings plot of PC2 versus PC3 created by performing PCA on the XRF dataset.

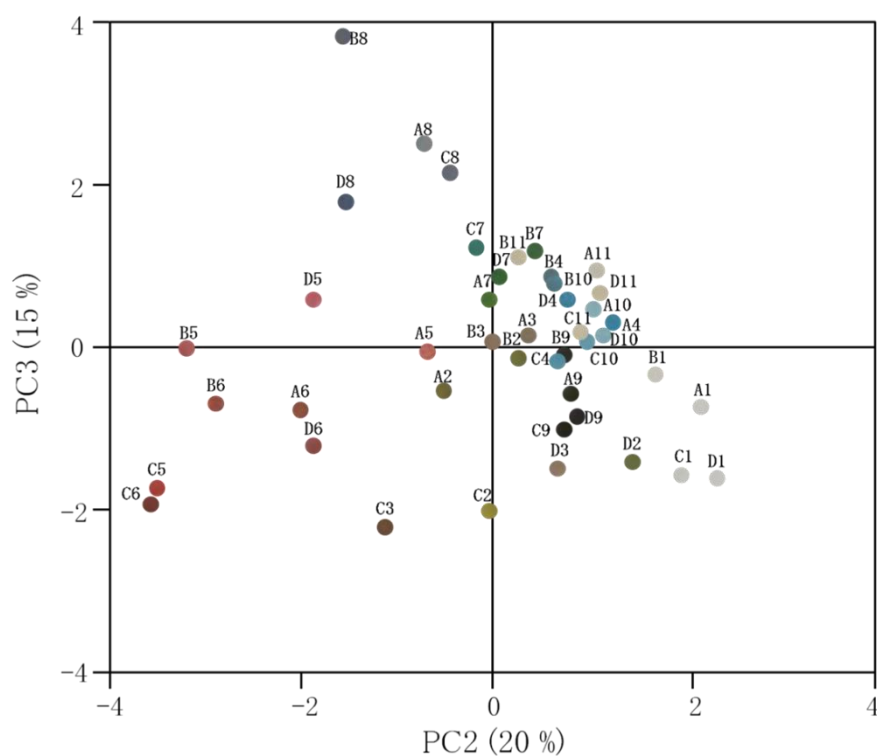


Figure 10.6 (b) Scores plot of PC2 versus PC3 created by performing PCA on the XRF dataset.

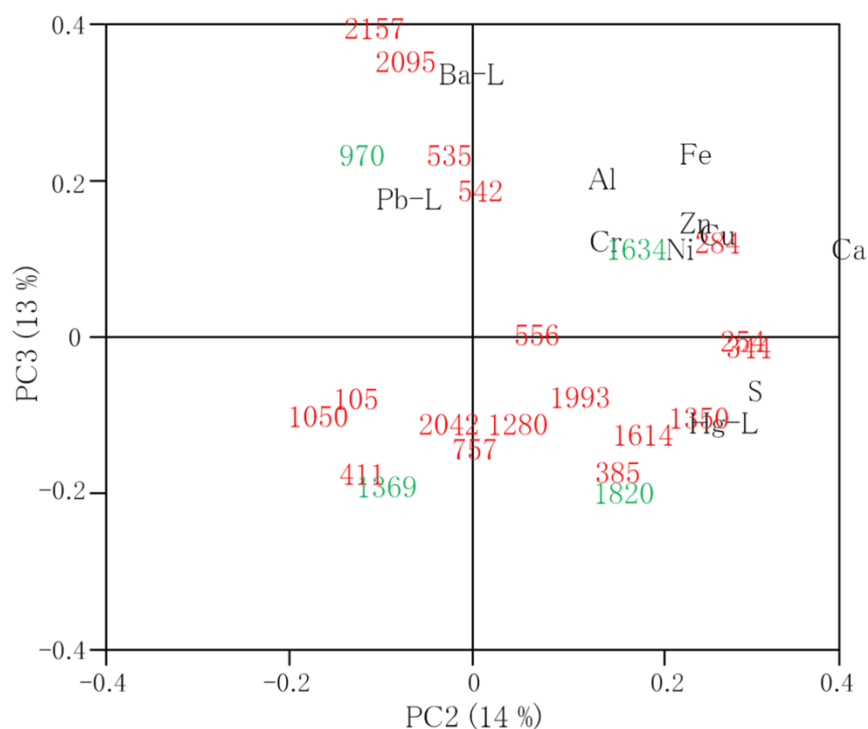


Figure 10.7 (a) Loadings plot of PC2 versus PC3 created by performing PCA on the Raman-XRF dataset.

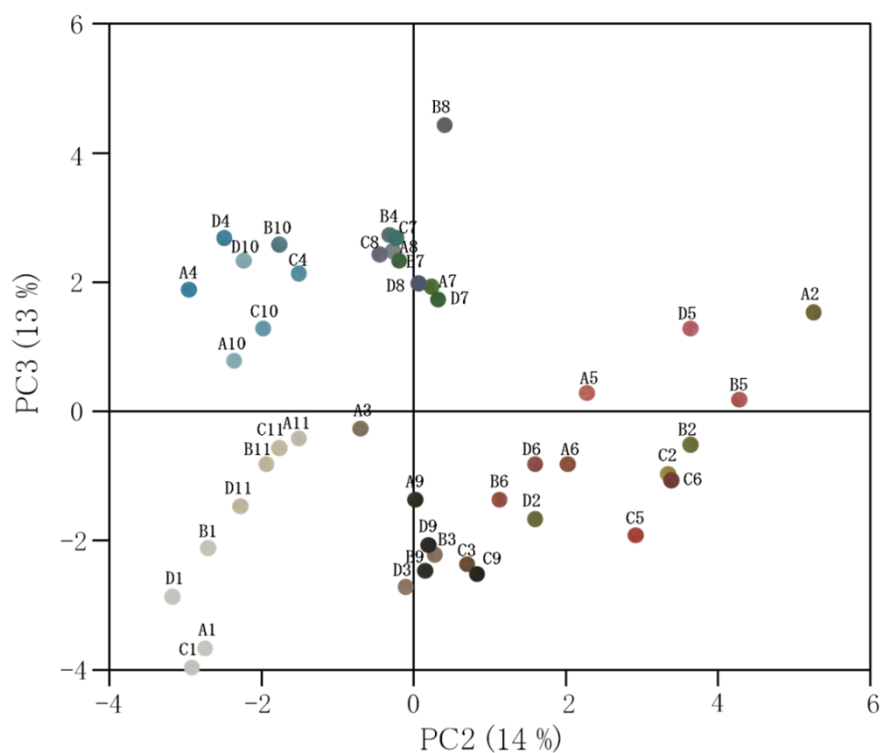


Figure 10.7 (b) Scores plot of PC2 versus PC3 created by performing PCA on the Raman-XRF dataset.

The characteristic Raman bands of lead white (1050 and 105 cm^{-1}) are, in contrary with the loadings plot of the Raman data, correlated to each other. The signal of Pb normally has to be correlated with these two Raman bands, but this is not shown in the loadings plot of PC2 versus PC3. Two of the three characteristic Raman bands of Prussian blue (2157 , 2095 and 2042 cm^{-1}) are again correlated, but are not correlated with Fe. The other correlations between the Raman and XRF variables are not very clear, but looking at the scores plot (Fig. 10.7(b)), a good classification of the objects is performed. The objects are divided into groups, according to their colour: the white group, the blue-green-purple group, the grey-black group and the gold-pink-red group. The blue-green-purple group can be divided into two subgroups, the blue group and the green-purple group. The green and purple objects are plotted together. For the purple objects a mixture of Prussian blue and vermilion was used, while for the green objects chrome yellow was mixed with Prussian blue. The variables responsible for vermilion (344 , 284 and 254 cm^{-1} ; S and Hg-L) and chrome yellow (Cr) are plotted close to each other in the loadings plot, resulting in grouping of the purple and green objects. The explanation of the black-grey group is very obvious: the grey objects contain carbon black mixed with lead white. This group is correlated to one of the broad characteristic Raman bands of carbon black (around 1369 cm^{-1}), but the correlation with the other broad band (1634 cm^{-1}) is not visible in the plots of PC2 versus PC3. The mixture of the red and golden objects is probably due to the similar direction in which the variables of the red objects (Hg and S) and the variables of the golden objects (Fe, Zn, Cr, Ni) are plotted.

The fact that certain variables (Raman band positions and elements) are unexpectedly not correlated in the loadings plot, can be understood when considering that the presence of a specific element (e.g. Fe) can be associated with

different materials (e.g. Prussian blue, hematite, limonite, etc.). Similarly, different pigments may have a Raman band at the same position.

Comparing the plots of the three different datasets, the classification of the porcelain card measurement (objects) is the best for the fused data. Raman spectroscopy also gives a good classification, while classification with XRF spectroscopy is more difficult probably because XRF spectroscopy obtains information of the different layers together, so more mixture of pigments can be expected. In the following, the same working method was repeated for a set of 24 reference pigments.

10.3.4 Reference pigments

10.3.4.1 Raman and XRF data fusion

PCA was performed on a fused dataset of 24 reference pigments. After performing analysis with Raman spectroscopy, 24 Raman band positions were selected as variables: 1050, 1017, 988, 837, 457, 434, 405, 403, 382, 353, 348, 344, 310, 291, 286, 254, 218, 201, 180, 169, 153, 142, 130 and 105 cm^{-1} . For the variables related to XRF, the following 23 elements were selected: Na, Mg, Al, Si, P, S, K, Ca, Ti, V, Cr, Mn, Fe, Co, Cu, Zn, As, Se, Cd, Sn, Ba, Hg and Pb. The plot of the principal components (PCs) in function of the contribution to the variance explained (Fig. 10.8) shows that probably at least 15 PCs are needed to explain the variance, resulting in 105 scores plots ($C_n^m = \frac{n!}{m!(n-m)!}$) and 105 loadings plots.

Therefore, in practice, it is difficult to use the classification of the reference pigments to identify an unknown sample, especially when the unknown sample represents a mixture of pigments.

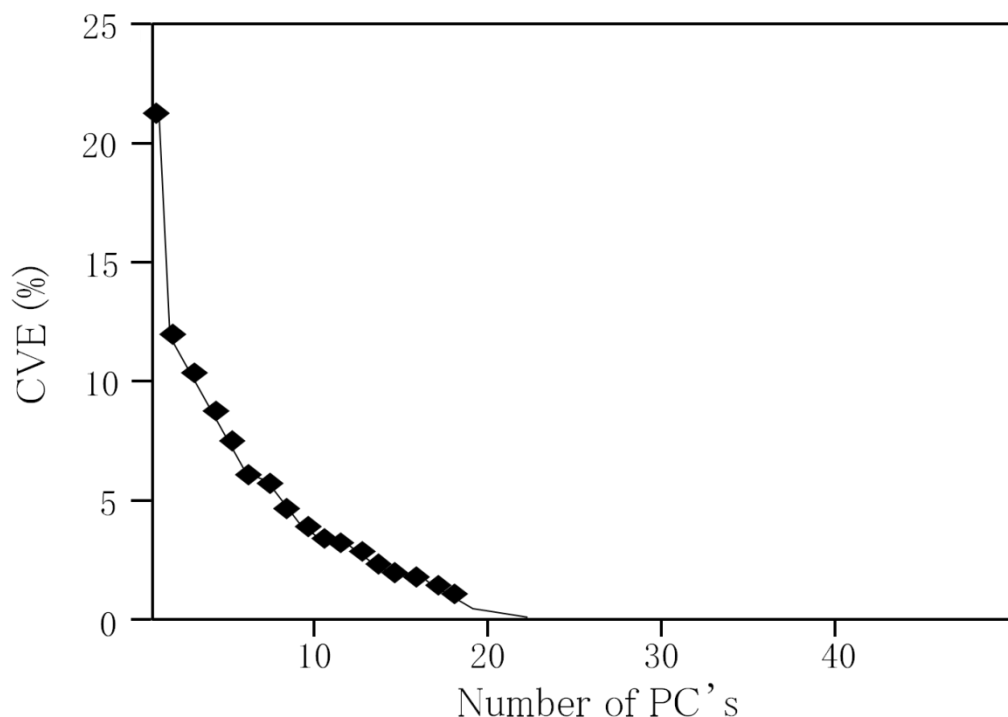


Figure 10.8 The number of principal components (PCs) as a function of contribution of the variance explained (CVE) after performing PCA on the fused dataset of the reference pigments.

10.3.4.2 Identification procedure

This identification procedure was applied for the identification of the pigments used in the different copies of the porcelain card. Interpretation of the Raman spectra and XRF spectra independently of points A1, B1, C1 and D1, showed the presence of lead white. Table 10.3(a) presents the results of the identification procedure for A1. Similar results were obtained for B1, C1 and D1, as expected since similar positions on the card were investigated. According to this table the percentage of peaks retrieved in A1 and the reference pigment lead white is 100%.

This identification procedure was performed for all the analysed points of the 4 copies of the porcelain card. Table 3b shows the highest percentage of peaks found back in the measurement points and the reference pigments of the first copy of the

porcelain card. The black analysed point (A9) was removed from the table, because in the reference pigments no black pigment is present.

Table 10.3(b) shows that a lot of the analysed points are often wrongly identified as lead white after applying the identification procedure. This is due to the high signal of Pb present in the XRF spectra (XRF spectroscopy obtains elemental information of all the layers together). The presence of the dominant signal of Pb is problematic, because the peak areas of all the other lines are scaled to the area of Pb. Due to the minimum limit of 10% a lot of the XRF signals are excluded from the identification procedure.

analysed point	pigment standard	% _{Raman}	% _{XRF}	% _{Total}
A1 (white)	lead white	100	100	100
A2 (gold)	azurite/malachite	66	33	55
A3 (brown)	Prussian blue	100	0	80
A4 (blue)	lead white	75	100	80
A5 (pink)	vermilion	100	0	66
A6 (red)	vermilion	50	50	50
A7 (green)	azurite/malachite	66	33	55
A8 (purple)	lead white	60	100	66
A10 (light blue)	lead white	75	100	80
A11 (beige)	Lead white	100	100	100

Table 10.3 (b) Identification of 10 of the analysed points of porcelain card A, after performing the identification procedure on the fused Raman–XRF data.

In order to correct for this, in a next step, the signal of Pb and the characteristic Raman band of lead white at 105 cm^{-1} were set to zero, resulting in, after normalisation, a different number of peaks present in the Raman and XRF spectra.

Table 10.4 shows the results of performing the adapted identification method. The identification of the unknown pigments is much better with this dataset.

analysed point	pigment standard	% _{Raman}	% _{XRF}	% _{Total}
A1 (white)	lead white	75	100	80
A2 (gold)	Prussian blue	80	0	47
A3 (brown)	Prussian blue	38	50	41
A4 (blue)	Prussian blue	66	33	50
A5 (pink)	vermilion	100	33	50
A6 (red)	vermilion	100	100	100
A7 (green)	chrysocolla	100	16	37
	Prussian bleu	100	16	37
	chrome yellow	50	33	37
A8 (purple)	azurite	71	33	53
A10 (light blue)	chrysocolla	100	25	57
	Prussian blue	66	50	57
	lead white	66	25	42
A11 (beige)	lead white	75	100	80

Table 10.4 Identification of 10 of the analysed points of porcelain card A, after performing the identification procedure on the fused Raman–XRF data, without taken into account the signal of Pb and the Raman band at 105 cm^{-1} .

Table 10.4 shows that in 50% of the cases (A1, A4, A5, A6 and A11) the identification is correct. For 20% of the cases (A7 and A10) the identification is not straightforward, but by looking at the Raman spectra and XRF spectra separately the correct identification can be made. For the green sample (A7) a mixture of Prussian blue (37% match) and chrome yellow (37% match) was used, while for the light blue sample (A10) Prussian blue (57%) was mixed with lead white (42%). Only in

30% of the cases the identification was wrong. This is probably due to the presence of impurities as trace elements in the reference pigments and due to the ability of gathering only the data characteristic to the pigment and not the information of the different layers together, when analysing an unknown sample.

10.4 Conclusions

The combination of two complementary techniques, Raman spectroscopy and XRF spectroscopy, is a powerful tool for the characterisation of pigments in art objects. For the combination of data originating from different spectroscopic techniques a robust methodology is necessary. In this work mid-level data fusion was presented for the characterisation of pigments used in porcelain cards. Mid-level fusion implements the selection of variables, before applying the classification method. For the Raman data, the Raman band positions of the sum spectrum were chosen as variables, while for the XRF data the elements present in the single files were selected. The classification with PCA of the pigments used in the porcelain cards based on the fused data was remarkably better than the classification based on the Raman data and XRF data separately. The procedure proposed here to identify pigments in the sample based on book-keeping of presence of bands and peaks gives satisfying results: in 50% of the cases the automated identification was straightforward, in 20% of the cases the identification could be performed using additional data, such as the single Raman and XRF spectra and only in 30% of the cases no identification was possible.

In the future, different improvements of the identification procedure have to be implemented. One improvement could be the inclusion of the colour information (RGB) of the references and the samples in the identification procedure. If the colour info is included a restriction of the list with all the reference pigments to a list of reference pigments with a particular colour can be made. The critical step for

this improvement is the availability of a colour card on the microscopic level, because we only have small amounts of the reference pigment available, as well as the influence of the grain size on the colour of the pigments. Another improvement would be using a linear combination of the reference pigments fused data to describe the fused data of the samples, because in practice, we may expect that the measurements are related to mixtures of pigments. Also the use of the recorded peak ratios could lead to an improvement of the identification procedure. As a last suggestion to improve the identification procedure, it would be perhaps more appropriate to perform Raman spectrum evaluation on the individual spectra, similar to XRF. However, the currently proposed method, based on sum spectra does not require any user input.

This research shows that performing the proposed mid-level data fusion of the Raman and XRF data results in a more accurate classification of the measured points on the porcelain cards, using PCA, than the classification based on the spectral data of one of the two techniques. This fused Raman-XRF dataset was also used as test dataset to develop a procedure for the identification of pigments, which is based on a simple vector multiplication of the fused data of an unknown pigment and the fused data of 24 reference pigments. According to the results presented in this chapter, this attempt to develop an identification procedure is relatively successful. Nevertheless, an extensive study has to be performed to optimise this proposed identification procedure.

Additionally to the evaluation on the basis of spectroscopic data, a special effort was made to describe the pigment samples on the basis of colour. For this, pictures of the 4 copies of the porcelain card were taken using a Canon EOS 50D camera, with an EFS 17-85 mm lens. Afterwards, the pictures were calibrated in Adobe Photoshop Lightroom 3, using an X-rite colour checker passport. For each analysed

point the RGB values were determined and stored in a file. PCA was performed to classify the different analysed points according to their RGB values.

Figure 10.9 shows the loadings and scores plots of PC2 versus PC3. Different groups are presented, according to the colour: the red group (point measurements A5–D5 and A6–D6), the blue group (A4–D4 and A10–D10), the green group (A7, B7 and D7) and the golden group (A2–D2). Point C7 falls in the middle of the green and blue group, suggesting that the colour of object C7 is somewhere in between blue and green. The two other groups present in the scores plot are mixtures of two different colours. For PC2 versus PC3 no distinction can be made between the white (A1–D1 and A11–D11) and the purple objects (A3–D3). The same conclusion is made for the black (A9–D9) and grey objects (A8–D8). Comparing the scores plot with the loadings plot shows that the green objects are linked to the variable G, the red objects to the variable R and the blue objects to the variable B. This confirms the choice of PCA for the classification according to the RGB values.

No RGB information of the pigment reference materials could be obtained because in the lab only small amounts are present of each pigment reference material. In order to perform a conventional calibration of the pictures taken, a colour card on the micro-level is necessary. These cards are not commercially available. Moreover, the appearance (colour) of pigment grains is different from the macroscopic view and is also strongly influenced by the grain size as well as by the method of applying pigments on the cards.

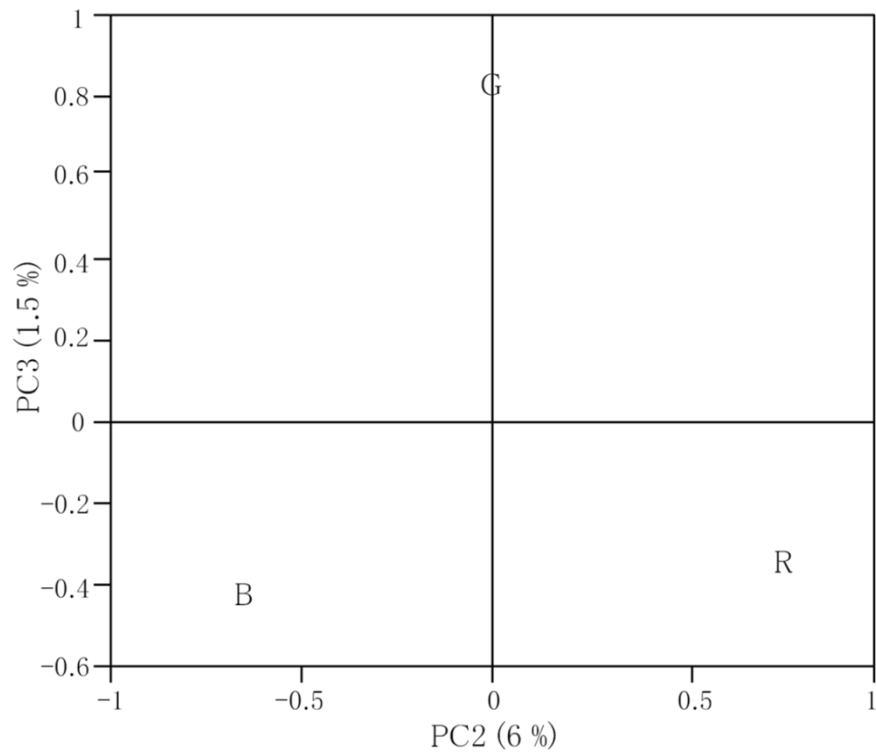


Figure 10.9 (a) Loadings plot of PC2 versus PC3 created by performing PCA on the RGB dataset.

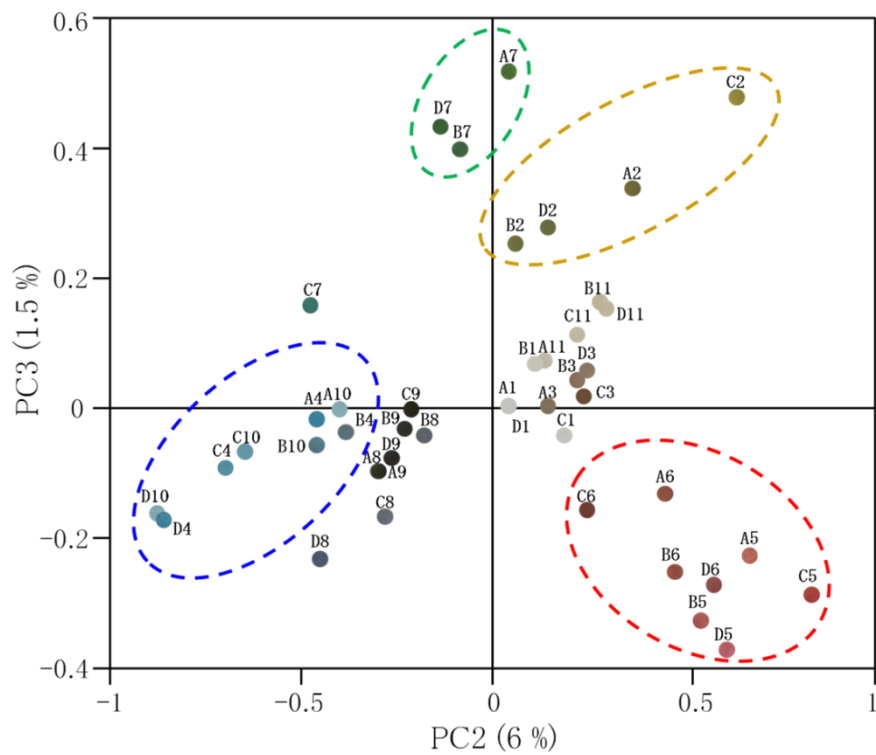


Figure 10.9 (b) Scores plot of PC2 versus PC3 created by performing PCA on the RGB dataset.

References

1. Lahanier, C., Preusser, F.D., Vanzelst, L. (1986) Study and Conservation of Museum Objects – Use of Classical Analytical Techniques. *Nuclear Instruments & Methods in Physics Research Section B-Beam Interactions with Materials and Atoms* 14: 1–9.
2. Ramos, P.M., Ruisanchez, I. (2006) Data fusion and dual-domain classification analysis of pigments studied in works of art. *Analytica Chimica Acta* 558: 274–282.
3. Vandenabeele, P., von Bohlen, A., Moens, L., Klockenkamper, R., Joukes, F., Dewispelaere, G. (2000) Spectroscopic examination of two Egyptian masks: A combined method approach. *Analytical Letters* 33: 3315–3332.
4. Maguregui, M., Martinez-Arkarazo, I., Angulo, M., Castro, K., Fernandez, L.A., Madariaga, J.M. (2008) *Lasers in the Conservation of Artworks*. Chapter 27 Portable spectroscopic analysis of nitrates affecting to cultural heritage materials. Talor and Francis Group, London, 177–182.
5. Maguregui, M., Knuutinen, U., Castro, K., Madariaga, J.M. (2010) Raman spectroscopy as a tool to diagnose the impact and conservation state of Pompeian second and fourth style wall paintings exposed to diverse environments (House of Marcus Lucretius). *Journal of Raman Spectroscopy* 41: 1110–1119.
6. Andrikopoulos, K.S., Daniilia, S.X., Roussel, B., Janssens, K. (2006) In vitro validation of a mobile Raman-XRF micro-analytical instrument's capabilities on the diagnosis of Byzantine icons. *Journal of Raman Spectroscopy* 37: 1026–1034.

-
7. Deneckere, A., Schudel, W., Van Bos, M., Wouters, H., Bergmans, A., Vandenabeele, P., Moens, L. (2010) In situ investigations of vault paintings in the Antwerp cathedral. *Spectrochimica Acta Part A-Molecular and Biomolecular Spectroscopy* 75: 511–519.
 8. Sawczak, M., Kaminska, A., Rabczuk, G., Ferretti, M., Jendrzewski, R., Sliwinski, G. (2009) Complementary use of the Raman and XRF techniques for non-destructive analysis of historical paint layers. *Applied Surface Science* 255: 5542–5545.
 9. Paternoster, G., Rinzivillo, R., Nunziata, F., Castellucci, E.M., Lofrumento, C., Zoppi, A., Felici, A.C., Fronterotta, G., Nicolais, C., Piacentini, M., Sciuti, S., Vendittelli, M. (2005) Study on the technique of the Roman age mural paintings by micro-XRF with Polycapillary Conic Collimator and micro-Raman analyses. *Journal of Cultural Heritage* 6: 21–28.
 10. Deneckere, A., Hocquet, F.P., Born, A., Klein, P., Rakkaa, S., Lycke, S., De Langhe, K., Martens, M.P.J., Strivay, D., Vandenabeele, P., Moens, L. (2010) Direct analysis of the central panel of the so-called Wyts triptych after Jan van Eyck. *Journal of Raman Spectroscopy* 41: 1210–1219.
 11. Borgia, I., Brunetti, B.G., Miliani, C., Ricci, C., Seccaroni, C., Sgamellotti, A. (2007) The combined use of lead–tin yellow type I and II on a canvas painting by Pietro Perugino. *Journal of Cultural Heritage* 8: 65–68.
 12. Burgio, L., Clark, R.J.H., Muralha, V.S.F., Stanley, T. (2008) Pigment analysis by Raman microscopy of the non-figurative illumination in 16th–to 18th–century Islamic manuscripts. *Journal of Raman Spectroscopy* 39: 1482–1493.
 13. Deneckere, A., De Reu, M., Martens, M.P.J., De Koene, K., Vekemans, B., Vincze, L., De Mayer, Ph., Vandenabeele, P., Moens, L. (2011) The use a

- multi-method approach to identify the pigments in the 12th century manuscript Liber Floridus. *Spectrochimica Acta Part A* 80: 125–132.
14. Vandenabeele, P., Wehling, B., Moens, L., Dekeyzer, B., Cardon, B., von Bohlen, A., Klockenkamper, R. (1999) Pigment investigation of a late-medieval manuscript with total reflection X-ray fluorescence and micro-Raman spectroscopy. *Analyst* 124: 169–172.
 15. Vandenabeele, P., Garcia-Moreno, R., Mathis, F., Leterme, K., Van Elslande, E., Hocquet, F.P., Rakkaa, S., Laboury, D., Moens, L., Strivay, D., Hartwig, M. (2009) Multi-disciplinary investigation of the tomb of Menna (TT69), Theban Necropolis, Egypt. *Spectrochimica Acta Part A-Molecular and Biomolecular Spectroscopy* 73: 546–552.
 16. van der Snickt, G., De Nolf, W., Vekemans, B., Janssens, K. (2008) mu-XRF/mu-RS vs. SR mu-XRD for pigment identification in illuminated manuscripts. *Applied Physics A-Materials Science & Processing* 92: 59–68.
 17. Ramos, P.M., Ruisanchez, I., Andrikopoulos, K.S. (2008) Micro-Raman and X-ray fluorescence spectroscopy data fusion for the classification of ochre pigments. *Talanta* 75: 926–936.
 18. Vandenabeele, P., De Paepe, P., Moens, L. (2008) Study of the 19th century porcelain cards with direct Raman analysis. *Journal of Raman Spectroscopy* 39: 1099–1103.
 19. Vanespen, P., Janssens, K., Nobels, J. (1986) Axil-Pc, Software for the Analysis of Complex-X-Ray Spectra. *Chemometrics and Intelligent Laboratory Systems* 1: 109–114.

20. Vekemans, B., Janssens, K., Vincze, L., Adams, F., Vanespen, P. (1994) Analysis of X-Ray-Spectra by Iterative Least-Squares (Axil) – New Developments. *X-Ray Spectrometry* 23: 278–285.
21. Reisner, L.A., Cao, A., Pandya, A.K. (2011) An integrated software system for processing, analyzing, and classifying Raman spectra. *Chemometrics and Intelligent Laboratory Systems* 105: 83–90.
22. De Gussem, K., De Gelder, J., Vandenabeele, P., Moens, L. (2009) The Biodata toolbox for MATLAB. *Chemometrics and Intelligent Laboratory Systems* 95: 49–52.

Chapter 11: Conclusions and future prospects

When performing spectroscopic analysis of art objects information is gathered which can answer different types of questions concerning, amongst others, dating the art object, identification of new materials, manufacturing processes, the authenticity of the artwork, conservation and remediation of the object, relationships between a particular work and similar works, trade routes, etc. Because of the (economical and artistic) value of the artworks, the selected spectroscopic technique has to be non-destructive, fast, universal, versatile and sensitive. The term universal points to the possibility of analysing materials and objects of various shapes with a minimum of sample preparation, while the term versatile indicates the possibility to gather average compositional information and local information of micrometre-sized areas.

Raman spectroscopy and X-ray fluorescence (XRF) spectroscopy are both analytical spectroscopic techniques with the above mentioned characteristics. Both techniques already proved to be very useful for the spectroscopic analysis of art objects. In this work, a combination of Raman spectroscopy and XRF spectroscopy was used, as both approaches provide complementary information; Raman spectra contain molecular information, while XRF spectra give the elemental composition.

When analysing precious objects of art, it is of great importance to gather as much as possible information with a minimum of (or preferably no) damage to the art object. When artworks have to be moved to the laboratory, the integrity can be affected unintentionally during transport. Therefore, mobile, portable and handheld Raman and XRF spectrometers were developed to perform *in situ* analysis.

In the first part of this work (Chapters 5, 6, 7 & 8) the focus lays on performing *in situ* analysis with mobile Raman and XRF instruments. The large amount of identified pigments, binding media and degradation products show that the combination of Raman spectroscopy and XRF spectroscopy is a very effective tool for *in situ* analysis in the field of cultural heritage. While performing these *in situ*

measurements, we observed also some drawbacks. Analysing manuscripts with the handheld XRF spectrometer was impossible. This was due to the overwhelming signal of Fe in the XRF spectra. This signal is caused by the gall ink that was used to write the text between the miniatures. Due to the large penetration depth of the X-rays, also the signals caused by the ink and the pigments on the back of the folio are present in the XRF spectrum. A possible solution to this problem would be the use of total reflection X-ray fluorescence (TXRF) spectroscopy after micro-sampling. The main advantages of TXRF spectroscopy regard to conventional energy dispersive XRF spectroscopy are: very low detection limits (pg), reduction of the matrix effects due to smaller penetration depth of the X-rays. The biggest drawback for TXRF analysis is that sampling is necessary to fulfil the conditions of total reflection.

Another drawback of performing *in situ* analysis is sometimes the environment in which the measurements have to take place. An example of this is given in Chapter 6 for the *in situ* analysis of two vault paintings in the Our Lady's Cathedral in Antwerp (Belgium). To reach the vault paintings, the instruments had to be brought on a scaffolding 22 m above ground level. Performing measurements on scaffoldings is affected by stability problems: because of the vibrations the laser beam and X-ray beam can be brought out of focus. Another problem for Raman spectroscopy is the interference of stray light, entering through the stained glass windows.

Because of these drawbacks, we choose to perform the measurements in the laboratory when sampling is allowed or if the dimensions of the artwork are not too large. Using laboratory instruments allows a careful optimisation of the experimental parameters when acquiring the data.

Performing point measurements provides the analyst with information of a very small region (<50µm), therefore mappings can be used to gather information of a larger area. In the second part of this thesis (Chapters 8 and 9) the possibilities of

performing Raman and XRF mappings with as well mobile XRF as laboratory Raman and XRF instruments were evaluated. From the case study presented in Chapter 8, we can conclude that performing an XRF mapping results in element images, which give information on the different restoration processes. According to the results in Chapter 9, the images of the Raman maps measured in low resolution mode are already of sufficient quality. Measuring in low resolution mode decreases the measurement time for the Senterra Raman spectrometer. No conclusions on the quality as function of the time could be made, because the stage of the Senterra Raman spectrometer is insufficiently stable. As a result of this instability, the object moved out of focus during the measurements. For the XRF maps, a multivariate statistical technique, K-means cluster analysis, was used to increase the quality of the element images and to show the presence of different colour clusters.

When a combination of Raman spectroscopy and XRF spectroscopy is used, the critical step is measuring with both techniques on exactly the same position. Therefore, the measured spots were meticulously marked on a printed copy of the analysed art object. This was done for the case study described in Chapter 10, where the fusion of Raman and XRF data is presented for the identification of pigments in porcelain cards. For this case study, we tried to measure with both techniques on the same spot of the sample. Fusion of Raman and XRF data results in a better classification of the pigments, using principal components analysis (PCA), compared to the classification based on the results of only one spectroscopic technique. Because of the promising results these fused Raman–XRF data were used as a test dataset for the first attempt to develop an identification procedure based on the fused Raman–XRF data. Although this identification procedure is based on a rather simple vector multiplication, good results were obtained.

Using a combination of Raman spectroscopy and XRF spectroscopy for the analysis of art objects has some drawbacks, which leads to some ideas for future research.

First of all some instrumental improvements would make *in situ* analysis of art objects more successful. The possibility of performing Raman analysis with a mobile or portable spectrometer containing two lasers with a different wavelength would lead to more successful identifications. Especially the blue and green pigments are hard to identify because of the absorbance of the red laser light (785 nm) and the interference of fluorescence. Having the possibility to switch to a laser with another wavelength would make the identification of green and blue pigments easier. Also the possibility of performing measurements using auto-focussing would result in more successful identifications.

Another instrumental improvement is performing *in situ* analysis with a combined Raman-XRF spectrometer. Combined Raman and XRF spectrometers were developed, but are not commercially available. They offer the advantage of measuring with both techniques on exactly the same spot, but the main challenge is the data processing. Until now the Raman spectra and XRF spectra are processed independently/separately. In this work, a first attempt was made to fuse Raman and XRF data, but there are still some parameters of the proposed identification procedure that could be improved. One possible improvement would be using a linear combination of the reference pigments fused data to describe the fused data of the samples, as in practise we may expect that the measurements are related to pigment mixtures and to mixtures of pigments and binding media. Therefore, an extensive study has to be performed including datasets of different types of materials (binding media, minerals,...) to improve the identification procedure.

Summary / Samenvatting

Summary

Using a combination of Raman spectroscopy and X-ray fluorescence (XRF) spectroscopy is an attractive tool for the analysis of art objects in cultural heritage studies, because of the non-destructive character of both spectroscopic techniques. The success of this combination is also based on the complementary character of both techniques: Raman spectroscopy delivers molecular information, while XRF spectroscopy provides the analyst with elemental information. Another reason why both techniques are attractive is the availability of mobile and portable Raman and XRF spectrometers, which makes *in situ* analysis possible. Especially in the field of cultural heritage this is a major advantage, because performing analysis *in situ* does not affect the integrity of the artwork. Therefore, the aim of this work is identification of pigments used for different types of art objects using a combination of both techniques, the optimisation of both techniques for mapping and developing methodology for data processing of fused Raman–XRF data.

In Chapter 2 the basic theory of both techniques is described. Special attention was given to the characterisation of the recently acquired Senterra Raman spectrometer. In this chapter, also a comparison is made between the different Raman spectrometers used in this work: the Mobile Art Analyser (MArtA) spectrometer and the laboratory Senterra Raman spectrometer; as well as between the different XRF spectrometers that were used: the laboratory EDAX Eagle–III spectrometer, the mobile ArtTAX spectrometer and the mobile EDXRF spectrometer of the University of Liège.

Chapter 3 describes the details of the spectrum evaluation of the Raman and XRF spectra. In the first part of this chapter the spectrum evaluation software package AXIL is described for the study of XRF spectra. For the Raman analysis, an

in-house spectrum evaluation program was developed. The different functions of this software are automated background subtraction and automatic band identification based on first and second derivatives.

The last chapter of the theoretical considerations (Chapter 4) describes into detail two multivariate statistical techniques, namely principal components analysis (PCA) and K-means cluster analysis. In the next four chapters (5–8) the theory was implemented in different case studies where a combination of laboratory, mobile and portable spectrometers is used for the identification of pigments, binding media and degradation products.

Chapter 5 describes the *in situ* analysis of 3 loose folios of the Breviary of Arnold of Egmond with mobile Raman spectroscopy. Combination with XRF spectroscopy was not possible because of the overwhelming signal of Fe due to the ink on the back of the folio. As an additional technique to visual analysis, *in situ* Raman spectroscopy was used to differentiate between different hands or workshops. The results of the Raman spectroscopic analysis show that on each of the folios a hierarchical colour use is present: the precious pigment vermillion (HgS) was only used for the holy figures (probably the blue pigment ultramarine ($\text{Na}_{8-10}\text{Al}_6\text{Si}_6\text{O}_{24}\text{S}_{2-4}$) also).

A combination of mobile Raman spectroscopy and portable XRF spectroscopy was used for the *in situ* analysis of two vault paintings in the Our Lady's Cathedral in Antwerp (Belgium) (Chapter 6). The measurements had to be performed on a scaffolding, 22 m above ground level. Performing analysis on a scaffolding results in stability problems: because of vibrations the laser beam or X-ray beam could be brought out of focus. Moreover, the Raman analysis had to be performed during the night because of the interference of stray light entering through the stained glass windows during the day. Nevertheless, many pigments could be identified, such as:

lead white ($2\text{PbCO}_3 \cdot \text{Pb}(\text{OH})_2$), calcite (CaCO_3), lead-tin yellow type I (Pb_2SnO_4), vermilion (HgS), red lead (Pb_3O_4), hematite (Fe_2O_3) and azurite ($2\text{CuCO}_3 \cdot \text{Cu}(\text{OH})_2$). Next to the identification of pigments also information on the structure of the different paint layers was gathered and the presence of a possible degradation product, gypsum ($\text{CaSO}_4 \cdot 2\text{H}_2\text{O}$), was indicated.

In Chapter 7, a combination of mobile Raman spectroscopy, laboratory Raman spectroscopy, laboratory XRF spectroscopy, UV-fluorescence photography and infrared reflectography (IRR) was used for the analysis of the precious mediaeval manuscript *Liber Floridus*. In a first step *in situ* analysis with the MArtA spectrometer was performed. Because of the promising results, sampling was allowed. These micro-samples were taken using a cotton swab and in the laboratory fixed with n-hexane on ultralene, in order to be able to use the samples for both spectroscopic techniques. Next to inorganic pigments, also two modern pigments were identified, suggesting that some restorations took place. After performing an extensive study, based on the UV-fluorescence photos, we concluded that the manuscript was not restored before and that the two modern pigments are impurities probably left behind unintentionally during the renovation of the band.

Chapter 8 presents the results of the direct analysis of the central panel of the so-called ‘Wyts Triptych’ after Jan van Eyck with mobile Raman spectroscopy and mobile XRF spectroscopy. Earlier analysis already showed that the analysed painting is a copy after the original work. Nevertheless, this copy already underwent a lot of restoration processes. The aim of this study was to get a better insight in the different restoration steps the painting underwent over time. After performing point measurements with both techniques, a few modern pigments could be

identified, such as zinc white (ZnO) and anatase (TiO₂). Also XRF mappings were performed, resulting in element images of the restored areas.

Because of the promising results of the XRF mapping with the mobile XRF spectrometer, an extensive study was performed evaluating the possibilities of Raman and XRF mappings (Chapter 9). For this study 19th century colourful porcelain cards were mapped. The first part of this chapter gives an extensive overview of the use of Raman spectroscopy, XRF spectroscopy and the combination of both techniques in the field of cultural heritage. Recording maps implies that both spectrometers have a very stable XYZ stage. The stability of the stage is especially a problem for the Raman mappings, because a tiny movement of the stage already brings the sample out of focus. Therefore, in this chapter the stability of the stage of the Senterra Raman spectrometer was evaluated. In addition, the quality of the resulting images was evaluated measuring in low and high resolution mode. The XRF maps already give a good quality image of the mapped area, but by performing multivariate statistical techniques, such as PCA and K-means cluster analysis, the quality of the different images could be improved.

In Chapter 10 data fusion of Raman and XRF data is presented. Until now, the spectra of both techniques were interpreted separately and afterwards brought together for the identification of pigments, binding media, degradation products, etc. In this chapter a mid-level fusion, which is based on the selection of variables before the actual fusion, is presented. The Raman variables are Raman band positions selected using the in-house developed spectrum evaluation program. For the XRF variables, the elements present in the spectra after performing the spectrum evaluation using the software package AXFIT were selected. After fusing the data, in a first step PCA was performed on the dataset, created by performing point measurements on different copies of a similar porcelain card. PCA resulted in the classification of the different analysed points. Interpretation of the loadings and

scores plots show that for each copy of the card, the same pigments or mixture of pigments was used. For the identification of the pigments, a set of reference pigments was selected and analysed with both techniques. A first attempt was made to develop a procedure for the identification of the pigments used, based on a simple vector multiplication.

In conclusion, Raman spectroscopy and XRF spectroscopy form a powerful combination for the identification of pigments in the field of cultural heritage. Both techniques are non-destructive and provide complementary information. As well for Raman spectroscopy as for XRF spectroscopy mobile or portable spectrometers are available, which makes both techniques suitable for *in situ* analysis. Fusion of Raman and XRF data leads to a more accurate identification of the pigments than identification based on the spectra of one of these techniques. In future research the possibilities of the automatic identification procedure based on the fused Raman–XRF data should be further explored, which would result in improving the identification procedure.

Samenvatting

De combinatie van Ramanspectroscopie en X-straal fluorescentiespectroscopie (XRF) is erg aantrekkelijk voor de analyse van kunstobjecten omdat beide spectroscopische technieken niet destructief zijn. Het succes van deze combinatie is gebaseerd op de complementariteit van beide technieken: Ramanspectroscopie geeft moleculaire informatie, terwijl XRF spectroscopie de elementsamenstelling weergeeft. Een andere reden waarom deze technieken zo aantrekkelijk zijn, is de beschikbaarheid van mobiele en draagbare Raman en XRF spectrometers, wat *in situ* analyse mogelijk maakt. Dit is een belangrijk voordeel voor kunstanalyse, aangezien bij het uitvoeren van *in situ* analyse de integriteit van het kunstwerk niet beschadigd wordt. Het doel van dit werk is de identificatie van pigmenten van verschillende kunstobjecten gebruikmakend van een combinatie van beide technieken, optimalisatie van het uitvoeren van mappings met beide technieken en het ontwikkelen van een methodiek voor de dataverwerking van gecombineerde Raman-XRF data.

In het tweede hoofdstuk wordt de theoretische basis van beide technieken besproken. Er wordt ook veel aandacht besteed aan de recent aangekochte Senterra Ramanspectrometer. Tenslotte wordt in dit hoofdstuk een vergelijking gemaakt tussen de verschillende Ramanspectrometers die hier ingezet worden: de Mobile Art Analyser (MArtA) en the laboratorium Senterra Ramanspectrometer. Daarnaast worden de verschillende XRF spectrometers die hier gebruikt werden, besproken: de laboratorium EDAX Eagle-III spectrometer, de mobiele ArtTAX spectrometer en de mobiele energie dispersieve XRF spectrometer van de universiteit van Luik.

Hoofdstuk 3 beschrijft gedetailleerd de spectrumevaluatie van de Raman en XRF spectra. In het eerste deel van dit hoofdstuk wordt een beschrijving gegeven van

het softwarepakket AXFIT, gebruikt voor de evaluatie van de XRF spectra. Voor de evaluatie van de Ramanspectra werd intern een spectrumevaluatie programma ontwikkeld. Het doel van dit programma is het verwijderen van de achtergrond en de automatische aanduiding van de karakteristieke Ramanbanden gebaseerd op de eerste en tweede afgeleiden.

Het laatste hoofdstuk van het deel ‘theoretical considerations’ beschrijft gedetailleerd twee multivariabele statistische technieken, namelijk principale componentenanalyse (PCA) en K-means clusteranalyse. De daarop volgende vier hoofdstukken (5–8) behandelen verschillende case studies, waarbij een combinatie van laboratorium, mobiele en draagbare spectrometers is gebruikt voor de identificatie van pigmenten, bindmiddelen en degradatieproducten.

Hoofdstuk 5 beschrijft de *in situ* analyse van 3 losse folios uit het Breviarium van Arnold van Egmond met behulp van mobiele Ramanspectroscopie. De combinatie met mobiele XRF spectroscopie is niet mogelijk door het overheersende signaal voor ijzer, veroorzaakt door de inkt op de achterkant van het folio. Naast visuele analyse werd *in situ* Ramanspectroscopie gebruikt als extra techniek om een onderscheid te maken tussen verschillende handen en ateliers. De resultaten van de Ramanspectroscopische analyse tonen aan dat voor elk van de onderzochte folio's hiërarchisch kleurgebruik kan teruggevonden worden: het kostbaar pigment vermiljoen (HgS) werd enkel gebruikt voor de heilige figuren, alsook waarschijnlijk het blauwe pigment ultramarijn ($\text{Na}_{8-10}\text{Al}_6\text{Si}_6\text{O}_{24}\text{S}_{2-4}$).

Een combinatie van mobiele Ramanspectroscopie en XRF spectroscopie werd gebruikt voor de *in situ* analyse van twee gewelfschilderijen in de Onze-Lieve-Vrouwekathedraal in Antwerpen (België) (Hoofdstuk 6). De metingen hiervoor werden uitgevoerd op een stelling van 22 m hoog. Het meten op een stelling gaat

gepaard met stabiliteitsproblemen: door de vibraties kan de laserbundel of de X-straalbundel uit focus gebracht worden. Daarnaast werden de Ramanmetingen gedurende de nacht uitgevoerd, omdat overdag interferentie optrad met het licht dat invalt via de grote glasramen. Desondanks konden toch veel pigmenten geïdentificeerd worden zoals: loodwit ($2\text{PbCO}_3 \cdot \text{Pb}(\text{OH})_2$), calciumcarbonaat (CaCO_3), loodtingeel type I (Pb_2SnO_4), vermiljoen (HgS), loodrood (Pb_3O_4), hematiet (Fe_2O_3) en azuriet ($2\text{CuCO}_3 \cdot \text{Cu}(\text{OH})_2$). Naast de identificatie van de pigmenten werd ook informatie verzameld over de structuur van de verschillende lagen en werden sporen van een mogelijk degradatieproduct, gips ($\text{CaSO}_4 \cdot 2\text{H}_2\text{O}$), teruggevonden.

In hoofdstuk 7, werd een combinatie van mobiele Ramanspectroscopie, laboratorium Ramanspectroscopie, laboratorium XRF spectroscopie, UV-fluorescentiefotografie en infraroodreflectografie (IRR) gebruikt voor de analyse van het kostbaar middeleeuws handschrift *Liber Floridus*. In een eerste fase van het onderzoek werd *in situ* analyse uitgevoerd met de MArtA spectrometer. Omdat deze eerste resultaten veelbelovend waren, werd staalname toegelaten. Deze micro-staaltjes werden genomen met een wattenstaafje en in het labo gefixeerd met n-hexaan op ultraleen, zodat dezelfde staaltjes gebruikt konden worden voor beide spectroscopische technieken. Naast de identificatie van anorganische pigmenten, werden ook twee moderne pigmenten teruggevonden. De aanwezigheid van deze moderne pigmenten suggereert dat de miniaturen werden gerestaureerd. Na een uitgebreide studie, gebaseerd op UV-fluorescentiefoto's, kon geconcludeerd worden dat het manuscript niet werd gerestaureerd, maar dat deze onzuiverheden waarschijnlijk per ongeluk zijn achtergebleven tijdens de vernieuwing van de boekband.

In hoofdstuk 8 worden de resultaten van de directe analyse van het middenpaneel van het zogenaamde Wyts drieluik naar Jan van Eyck, met mobiele Ramanspectroscopie en mobiele XRF spectroscopie beschreven. Vroegere analyses

hadden al aangetoond dat het onderzochte paneel een kopie is van het origineel. Verschillende foto's lieten echter zien dat deze kopie al vaak werd gerestaureerd. Het doel van dit onderzoek is een beter inzicht krijgen in de verschillende restauratieprocessen dat het middenpaneel onderging. Door puntanalyses met beide technieken konden enkele moderne pigmenten geïdentificeerd worden, zoals zinkwit (ZnO) en anataas (TiO₂). Daarnaast werden ook XRF mappings uitgevoerd. Deze mappings geven per element een beeld van de gerestaureerde zone en geven dus informatie over de verschillende restauratieprocessen.

Doordat de resultaten van de XRF mappings, die uitgevoerd werd met de mobiele XRF spectrometer, veelbelovend waren, werd een uitgebreide studie uitgevoerd met als doel de verschillende mogelijkheden van Raman en XRF mappings te evalueren (Hoofdstuk 9). Voor deze studie werd een mapping uitgevoerd op kleurrijke porseleinkaarten van de 19^e eeuw. In het eerste deel van dit hoofdstuk wordt een overzicht gegeven van het gebruik van Ramanspectroscopie, XRF spectroscopie en de combinatie van beide technieken voor cultureel erfgoedstudies. Een noodzaak voor het uitvoeren van mappings is de aanwezigheid van een stabiele XYZ microscooptafel. De stabiliteit van deze tafel is vooral van belang bij het uitvoeren van Ramananalyses, omdat een minuscule verplaatsing van de tafel ervoor kan zorgen dat het object uit focus wordt gebracht. Om deze reden wordt in dit hoofdstuk de stabiliteit van de microscooptafel van de Senterra Ramanspectrometer geëvalueerd bij verschillende meettijden. Bijkomend werd ook de kwaliteit van de verzamelde beelden geëvalueerd bij metingen met lage en hoge resolutie. De beelden afkomstig van de XRF mapping geven al beelden van voldoende kwaliteit, maar door gebruik te maken van multivariabele statistische technieken, zoals PCA en K-means clusteranalyse, kan de kwaliteit van de beelden nog verbeterd worden.

In hoofdstuk 10 wordt de fusie van de Raman en XRF data voorgesteld. Tot nu toe werden de spectra van beide technieken onafhankelijk van elkaar geïnterpreteerd, vooraleer de resultaten samen gebracht werden voor de identificatie van pigmenten, bindmiddelen, degradatieproducten,... Dit hoofdstuk presenteert een fusie op het middenniveau, waarbij eerst een variabele selectie doorgevoerd wordt, vooraleer de echte fusie plaatsvindt. De Raman variabelen zijn Ramangolfgetallen die geselecteerd werden door gebruik te maken van het intern ontwikkeld spectrumevaluatie programma. Voor de XRF variabelen werden de elementen geselecteerd door gebruik te maken van het spectrumevaluatie software pakket AXFIT. Na de fusie werd in de eerste fase PCA uitgevoerd op een dataset die bestaat uit puntmetingen van verschillende kopieën van een gelijkaardige porseleinkaart. Het toepassen van PCA op de dataset zorgt voor een classificatie van de verschillende geanalyseerde punten. Interpretatie van de ladinggrafieken en scoregrafieken tonen aan dat voor elke kopie van de kaart dezelfde pigmenten of een mengsel van dezelfde pigmenten werd gebruikt. Voor de identificatie van de pigmenten werd een set van referentiematerialen geselecteerd en geanalyseerd met beide technieken. Een eerste poging voor het ontwikkelen van een identificatieprocedure werd ondernomen, gebaseerd op een vectorvermenigvuldiging.

We kunnen besluiten dat Ramanspectroscopie en XRF spectroscopie een krachtige combinatie vormen voor de identificatie van pigmenten in cultureel erfgoedstudies. Beide technieken zijn niet destructief en voorzien de onderzoeker van complementaire informatie. Zowel voor Ramanspectroscopie als voor XRF spectroscopie zijn er mobiele en draagbare spectrometers beschikbaar, die beide technieken geschikt maken voor *in situ* analyse. De fusie van de Raman en XRF data zorgt voor een meer accurate identificatie van de pigmenten in vergelijking met de identificatie gebaseerd op één van beide technieken. In de toekomst moeten de mogelijkheden van de automatische identificatieprocedure gebaseerd op de

gecombineerde Raman-XRF data verder onderzocht worden. Dit zal ongetwijfeld leiden tot een verder verbetering van de identificatieprocedure.

Dankwoord

Ik wil beginnen met het bedanken van de vakgroepvoorzitter Prof. Karel Strijckmans en mijn team van promotoren voor de directe ondersteuning van dit werk. Prof. Luc Moens, bedankt om dit werk te promoten. Ondanks het feit dat het niet mogelijk was om elkaar vaak te ontmoeten, bleef je steeds geïnteresseerd in mijn werk. Telkens een artikel gepubliceerd werd, kreeg ik een mail met daarin felicitaties voor het geleverde werk.

Peter, ik wil je bedanken voor de vele mogelijkheden die ik via jou toedoen verkregen heb om op verschillende locaties metingen te gaan uitvoeren. Voor vele van deze metingen buitenshuis waren we samen op pad en ik heb mij steevast goed geamuseerd! Verder wil ik je ook bedanken voor de wetenschappelijke ondersteuning en het feit dat je steeds paraat stond (al was dit vaak telefonisch of per mail) indien ik vragen of problemen had.

Bart, jij hebt het team van promotoren pas in het laatste jaar vervoegd en ik heb zeker geen spijt van deze beslissing. Jij was thuis in de wereld van XRF spectroscopie, ik in de wereld van Ramanspectroscopie; maar toch zijn we samen tot een boeiende combinatie van beide werelden gekomen. Bedankt voor de vele uren programmeerwerk en natuurlijk ook de taartjes af en toe. Doordat je zoveel vragen stelde over de techniek en het onderzoek, kreeg ik een betere, meer kritische kijk op mijn onderzoek.

Prof. Laszlo Vincze, bedankt om het Eagle labo ter beschikking te stellen.

Naast het team van promotoren zijn er natuurlijk ook de vele mensen waarmee ik samengewerkt heb, vooreerst binnen het labo analytische chemie.

Sylvia, bedankt voor de vele hulp met de metingen en de steun tijdens mijn doctoraat. We zijn begonnen met 5 collega's, toen nog op het INW. Na het eerste

jaar bleven enkel wij nog over. Ook al waren we maar met twee en afgezonderd van de rest van de vakgroep, toch hebben we samen veel plezier beleefd!

Jolien en Lieke bedankt voor de vele leuke gesprekken en de steun tijdens het schrijven van mijn doctoraat. Jullie stonden altijd klaar om mij te helpen als ik een probleem had.

Verder wil ik ook nog Lucien, Marc en Roger bedanken voor de vele leuke praatjes op de gang. Ook als het even niet goed ging, slaagden jullie er steeds in om mij op te vrolijken.

Als laatste wil ik ook nog Sien en Kenny bedanken voor de vele steun. We zijn samen afgestudeerd en konden ook samen bij de vakgroep Analytische Chemie beginnen. Samen hebben we ons door de jaren heen een weg gebaand doorheen de vele artikels die moesten gelezen worden, de vele metingen die uitgevoerd moesten worden,...

I would like to express my gratitude to a number of people with whom I worked during the different projects, who helped in the research or provided access to interesting art objects: Anna, Annick, Claudine, David, Helena, Helena Wouters François-Philippe, Kaat, Karen, Lien, Marina, Miranda, Misha, Martine, Max, Paul, Peter Klein, Philippe, Saïd en Walter.

I would like to thank the BELSPO Interuniversity Attraction Pole Program (P6/16) for the financial support of this work.

Verder wil ik ook mijn mama, zus en broer bedanken voor alle steun.

Jeroen, het zou belachelijk zijn om ook maar proberen onder woorden te brengen waarvoor ik je allemaal zou willen bedanken. Bedankt om steeds voor 100% achter mij te staan!

Appendix A: Idl routines *read_jcamp_dx.pro* and *calc_jcamp_dx_parameters.pro*

A.1 read_jcamp_dx.pro

The file `read_jcamp.pro` contains a set of IDL routines that are used to import the so-called “*.dx” or “*.jdx” Raman spectral data as the step before the actual processing of these data. The `read_jcamp_dx` routine is able to return a table of spectral data in case the *filemask* represents more than one file, or the single file contains more than one Raman spectrum (e.g. data of Raman map). The extended routine `read_jcamp_dx_files` is able to import multiple Raman data (files) and returning the data of the common Raman wavelength interval (in case Raman spectra were recorded with different wavelength intervals).

```
SYNTAX      read_jcamp_dx[, filemask, x, y, info, [/show]]

RETURN VALUES      x          vector or array (wave number, spectrum)

                   y          vector or array (intensity, spectrum)

                   info        vector or array (info, spectrum)

SUBROUTINES      read_jcamp_dx_spectrumbody

                  import the data of an individual Raman spectrum

                  calc_jcamp_dx_spectrum

                  convert the data imported from the file to intensities and

                  wavelength numbers so that plotting a Raman spectrum

                  is as simple as executing "plot, x, y"

EXAMPLES

read_jcamp_dx          (reading without plotting and returning data)

read_jcamp_dx, /show   (only plotting the data)

read_jcamp_dx, '*.dx', x, y, info, /show (importing *.dx data returning x, y and info)
```

Listing of read_jcamp_dx.pro

```

; read_jcamp_dx.pro
;
; how to call:
; (i) read_jcamp_dx      -> reading without plotting and returning data
; (ii) read_jcamp_dx, /show -> only plotting
; (iii) read_jcamp_dx, '%dx', x, y, info, /show
;                                -> plotting: plot, x, y
;                                -> returning data: x, y, info
;
; note: if mask is given, only the first file found is read

;-----
;=====
PRO read_jcamp_dx_spectrumbody, unit, headerline, t_firstx, t_lastx, t_spectraldata

emptystr = ' '

; reading file
; read first header
line = emptystr
i = 0
WHILE(STRPOS(line,'##XYDATA=') NE 0) DO BEGIN
    READF, unit, line
    IF(i EQ 0) THEN BEGIN
        headerline = [line]
    ENDIF ELSE BEGIN
        headerline = [headerline, line]
    ENDELSE
    i = i + 1
ENDWHILE
;PRINT, headerline

; read data
i = 0
READF, unit, line
REPEAT BEGIN ; ((STRPOS(line,'##END') GE 0) OR EOF(unit))
    t_line = strjoin(strsplit(line,/extract), '+')
    sublines = STRSPLIT(t_line,'[+-]',/extract,/regex) ; extract different words separated by '+' or '-'
    ;sublines = STRSPLIT(t_line,'\+',/extract,/regex) ; extract different words separated by '+'
    IF(sublines(0) NE '##END=') THEN BEGIN
        ;PRINT, sublines
        nwords = N_ELEMENTS(sublines)
        IF(i EQ 0) THEN BEGIN
            t_firstx = FLOAT(sublines(0))
            t_spectraldata = LONG(sublines(1:nwords-1))
        ENDIF ELSE BEGIN
            ;PRINT, t_line
            ;PRINT, sublines
            t_lastx = FLOAT(sublines(0))
            t_spectraldata = [t_spectraldata, LONG(sublines(1:nwords-1))]
        ENDELSE
    ENDIF
    i = i + 1
    READF, unit, line
ENDREPEAT UNTIL ((STRPOS(line,'##END') GE 0) OR EOF(unit))
END

;-----
;=====
; calculate spectrum
PRO calc_jcamp_dx_spectrum, spefile, headerline, t_firstx, t_lastx, t_spectraldata, spectraldata_x, spectraldata_y,
info, show=show

;-----
emptystr = ' '
floatnr = 0.0
longnr = 0L
title = emptystr ; !
jcampver = emptystr
data_type = emptystr
date_exp = emptystr ; !
xunits = emptystr ; !
yunits = emptystr ; !
resolution = floatnr
xfirst = longnr ; !
xlast = longnr ; !
;xdelta = floatnr ; could be non-existing
ymax = floatnr
ymin = floatnr
xfactor = floatnr
yfactor = floatnr
npoints = longnr
yfirst = floatnr
xydata = emptystr
;-----
;-----
; decoding header
;help, headerline
nheaderline = N_ELEMENTS(headerline)
FOR i = 0, nheaderline - 1 DO BEGIN
    sublines = STRSPLIT(headerline(i),'=',/extract,/regex) ; extract different words separated by '='
    CASE sublines(0) OF '##TITLE': title = sublines(1)

```

```

        '##JCAMP-DX': jcampver = sublines(1)
        '##DATA TYPE': data_type = sublines(1)
        '##DATE': BEGIN
                    IF (N_ELEMENTS(date_exp) EQ 0) THEN BEGIN
                        date_exp = sublines(1)
                    ENDIF ELSE BEGIN
                        date_exp = sublines(1) + ' ' + date_exp
                    ENDELSE
                    END
        '##TIME': BEGIN
                    IF (N_ELEMENTS(date_exp) EQ 0) THEN BEGIN
                        date_exp = sublines(1)
                    ENDIF ELSE BEGIN
                        date_exp = date_exp + ' ' + sublines(1)
                    ENDELSE
                    END
        '##ORIGIN': origin = sublines(1)
        '##OWNER': owner = sublines(1)
        '##RESOLUTION': resolution = sublines(1)
        '##NPOINTS': npoints = sublines(1)
        '##XUNITS': xunits = sublines(1)
        '##FIRSTX': xfirst = sublines(1)
        '##LASTX': xlast = sublines(1)
        '##MINX': xmin = sublines(1)
        '##MAXX': xmax = sublines(1)
        '##XFACTOR': xfactor = sublines(1)
        '##DELTAX': xdelta = sublines(1)
        '##YUNITS': yunits = sublines(1)
        '##YFACTOR': yfactor = sublines(1)
        '##FIRSTY': yfirst = sublines(1)
        '##MINY': ymin = sublines(1)
        '##MAXY': ymax = sublines(1)
        '##XYDATA': xydata = sublines(1)
    ELSE:
    ENDCASE
ENDFOR

;-----
; calculate spectraldata

; X
IF (N_ELEMENTS(xdelta) EQ 0) THEN BEGIN
    xdelta = (FLOAT(xlast)-FLOAT(xfirst))/(npoints-1.)
    PRINT, 'xdelta', xdelta
ENDIF
spectraldata_x = LINDGEN((FLOAT(xlast)-FLOAT(xfirst))/FLOAT(xdelta)+1) * FLOAT(xdelta))
spectraldata_x = spectraldata_x + FLOAT(xfirst)
nx = N_ELEMENTS(spectraldata_x)
; Y
spectraldata_y = t_spectraldata(0:nx-1) * FLOAT(yfactor) ; force to exclude wrongly added ZEROS
;PRINT, spectraldata
;HELP, spectraldata
IF (show NE 0) THEN PLOT, spectraldata_x, spectraldata_y, title=title, xtitle=xunits, ytitle=yunits

PRINT, spefile + ':' + title + ', ' + date_exp
PRINT, ' nx ', N_ELEMENTS(spectraldata_x), ' xmin ', MIN(spectraldata_x), ' xmax ', MAX(spectraldata_x)
PRINT, ' ny ', N_ELEMENTS(spectraldata_y), ' ymin ', MIN(spectraldata_y), ' ymax ', MAX(spectraldata_y)

xunits = 'Wavenumber(' + STRLOWCASE(xunits) + ')'
yunits = 'Intensity (counts/channel)'
s = yunits & yunits = STRUPCASE(STRMID(s,0,1))+STRLOWCASE(STRMID(s,1,STRLEN(s)-1)) + ' (counts/channel)'

; check for whether the info items exist
IF (N_ELEMENTS(resolution) EQ 0) THEN resolution='0.5' ; default resolution is 0.5 [1/cm]
info = [spefile, date_exp, xunits, yunits, resolution] ; info is list of strings
;info = [title, date_exp, xunits, yunits, resolution] ; info is list of strings

; check for increasing x values ... routines are succesful only that way
spectraldata_x = REVERSE(spectraldata_x)
spectraldata_y = REVERSE(spectraldata_y)
IF (spectraldata_x(0) GT spectraldata_x(1)) THEN BEGIN
    spectraldata_x = REVERSE(spectraldata_x)
    spectraldata_y = REVERSE(spectraldata_y)
ENDIF
END
;-----
;-----
PRO read_jcamp_dx, dxfiles, spectraldata_x, spectraldata_y, info, show=show

IF (N_ELEMENTS(show) EQ 0) THEN show = 0

spefile_extension = '.dx.jdx'

IF (N_ELEMENTS(dxfiles) EQ 0) THEN BEGIN
    ;PRINT, 'NO jcamp DX file(s) given ... manual selection is requested ...'

```

```

    spefiles = DIALOG_PICKFILE(FILTER=['*.dx', '*.jdx'], $
    /FIX_FILTER, TITLE=spefile_extension+' file selection to be read')
ENDIF ELSE BEGIN
    spefiles = FINDFILE(dxfiles)
ENDELSE

;help, spefiles
;PRINT, spefiles(0)

IF(NOT(FILE_TEST(spefiles(0)))) THEN BEGIN ; no spectrum selection
    PRINT, 'NO jcamp DX/JDX selected ... read_jcamp_dx STOPPED'
    RETURN
ENDIF

nspefiles = N_ELEMENTS(spefiles)

IF(nspefiles NE 1) THEN BEGIN
    spefiles = spefiles(0)
    PRINT, 'Warning : more than file selected ... only first file is going to be read.'
ENDIF

spefile = spefiles

OPENR, unit, spefile, /GET_LUN
s=0
WHILE(NOT EOF(unit)) DO BEGIN
    ; read 1 spectrum
    read_jcamp_dx_spectrumbody, unit, headerline, t_firstx, t_lastx, t_spectraldata
    s = s + 1
    print, '    spectrum #', s
    WAIT, 0.5
    ; calculate spectrum
    calc_jcamp_dx_spectrum, spefile, headerline, t_firstx, t_lastx, t_spectraldata, s_spectraldata_x, s_spectraldata_y
    s_info, show=show
    ; check whether info(1) is empty string ... if so take the number s
    tempstring = STRCOMPRESS(s_info(1), /REMOVE_ALL)
    IF(STRLEN(tempstring) EQ 0) THEN s_info(1) = STRCOMPRESS(STRING(s), /REMOVE_ALL)
    IF(s EQ 1) THEN BEGIN
        spectraldata_x = s_spectraldata_x
        spectraldata_y = s_spectraldata_y
        info = s_info
    ENDIF ELSE BEGIN
        ; assume same dimensions for all individual RAMAN spectra
        spectraldata_x = [[spectraldata_x], [s_spectraldata_x]]
        spectraldata_y = [[spectraldata_y], [s_spectraldata_y]]
        info = [[info], [s_info]]
    ENDELSE
    ENDWHILE ; NOT EOF(unit)
CLOSE, unit
FREE_LUN, unit

END

;=====
; read dxfiles containing that could contain more than 1 spectrum
PRO read_jcamp_dx_files, dxfiles, spectraldata_x, spectraldata_y, info, show=show

IF(N_ELEMENTS(show) EQ 0) THEN show = 0

spefile_extension = '.dx.jdx'

IF(N_ELEMENTS(dxfiles) EQ 0) THEN BEGIN
    ;PRINT, 'NO jcamp DX file(s) given ... manual selection is requested ...'
    spefiles = DIALOG_PICKFILE(FILTER=['*.dx', '*.jdx'], $
    /FIX_FILTER, TITLE=spefile_extension+' file selection to be read')
ENDIF ELSE BEGIN
    nspefiles = N_ELEMENTS(dxfiles)
    IF(nspefiles EQ 1) THEN BEGIN
        ; filemask is given
        spefiles = FINDFILE(dxfiles)
    ENDIF ELSE BEGIN
        ; dxfiles is array of dx-filenames
        spefiles = dxfiles
    ENDELSE
ENDELSE

help, spefiles
PRINT, spefiles(0)

IF(NOT(FILE_TEST(spefiles(0)))) THEN BEGIN ; no spectrum selection
    PRINT, 'NO jcamp DX/JDX selected ... read_jcamp_dx STOPPED'
    RETURN
ENDIF

nspefiles = N_ELEMENTS(spefiles)
PRINT, '[read_jcamp_dx_files]', nspefiles, ' files to be read'

FOR s=0, nspefiles-1 DO BEGIN
    spefile = spefiles(s)
    OPENR, unit, spefile, /GET_LUN
    ; read 1 spectrum
    read_jcamp_dx_spectrumbody, unit, headerline, t_firstx, t_lastx, t_spectraldata

```

```

print, ' spectrum #', s
;WAIT,0.5
; calculate spectrum
calc_jcamp_dx_spectrum, spefile, headerline, t_firstx, t_lastx, t_spectraldata, s_spectraldata_x, s_spectraldata_y
, s_info, show=show
; check whether info(1) is empty string ... if so take the number s
tempstring = STRCOMPRESS(s_info(1),/REMOVE_ALL)
IF(STRLLEN(tempstring) EQ 0) THEN s_info(1) = STRCOMPRESS(STRING(s),/REMOVE_ALL)
nx = N_ELEMENTS(s_spectraldata_x)
IF(s EQ 0) THEN BEGIN
    spectraldata_x = s_spectraldata_x
    spectraldata_y = s_spectraldata_y
    info = s_info
    t_beg = s_spectraldata_x(0) ; table lowest wavenumber
    t_end = s_spectraldata_x(nx-1) ; table highest wavenumber
ENDIF ELSE BEGIN
    ; assume same dimensions for all individual RAMAN spectra
    ; check dimensions before joining adding data

    s_beg = s_spectraldata_x(0) ; spectrum lowest wavenumber
    s_end = s_spectraldata_x(nx-1) ; spectrum highest wavenumber

    IF(s_beg EQ t_beg AND s_end EQ t_end) THEN BEGIN
        ; do nothing ... table and spectrum to be added same length in wavenumber domain
        PRINT, 'Do NOTHING ...'
    ENDIF ELSE BEGIN
        ; different length table and spectrum to be added ... chunk
        PRINT, 'Do SOMETHING ...'
        new_beg = MAX([t_beg, s_beg])
        new_end = MIN([t_end, s_end])

        t_beg_i = WHERE(spectraldata_x(*,0) EQ new_beg)
        t_end_i = WHERE(spectraldata_x(*,0) EQ new_end)
        s_beg_i = WHERE(s_spectraldata_x EQ new_beg)
        s_end_i = WHERE(s_spectraldata_x EQ new_end)

        ; make spectraldata_x and s_spectraldata_x same length in wavenumber domain
        spectraldata_x = spectraldata_x(t_beg_i:t_end_i, *)
        s_spectraldata_x = s_spectraldata_x(s_beg_i:s_end_i)
        spectraldata_y = spectraldata_y(t_beg_i:t_end_i, *)
        s_spectraldata_y = s_spectraldata_y(s_beg_i:s_end_i)

        ; store new beg and end for table
        t_beg = new_beg
        t_end = new_end
    ENDELSE ; IF(s_beg NE t_beg OR s_end NE t_end)

    spectraldata_x = [[spectraldata_x], [s_spectraldata_x]]
    spectraldata_y = [[spectraldata_y], [s_spectraldata_y]]
    info = [[info], [s_info]]
ENDELSE
CLOSE, unit
FREE_LUN, unit
ENDFOR
END
;=====
;=====

```

A.2 calc_jcamp_dx_parameters.pro

The file `calc_jcamp_dx_parameters.pro` contains a set of IDL routines that are used to extract the information (position and intensity of peaks) from Raman spectra. The **calc_jcamp_dx_parameters** calculates the position (wave number) of peaks and the corresponding intensity, based on calculation of the first and second derivative of the spectrum. If the background is not given as input the calculation is done on the full spectrum. The **snip** routine estimates the background using the SNIP algorithm of Clayton, Ryan and co-workers. If `calc_jcamp_dx_parameters` is executed with the background as argument then the calculations are done on the background subtracted Raman spectrum; see routine `calc_jcamp_dx_parameters_using_background` for details. Also, if available by argument the background is used to decide whether a peak can be omitted on statistical considerations as explained in this work.

```
SYNTAX  calc_jcamp_dx_parameters, filemask, $
        input_x = input_x, input_y = input_y, $
        input_b = input_b, input_info = input_info, $
        d1_threshold = d1_threshold, d2_threshold = d2_threshold, $
        res_x, res_y, res_dx, res_yback

INPUT VALUES
filemask      filemask if no other input is given
input_x       vector or array (wave number, spectrum)
input_y       vector or array (intensity, spectrum)
input_b       vector or array (intensity, spectrum)
input_info    vector or array (info item, spectrum)
d1_threshold  threshold value equal to fraction of maximum change 1st derivative
d2_threshold  threshold value equal to fraction of maximum change 2nd derivative

RETURN VALUES
res_x         vector or array (wave number, spectrum number)
res_y         vector or array (intensity, spectrum number)
res_dx        vector or array (uncertainty wave number, spectrum number)
res_yback     vector or array (intensity, spectrum number)

SUBROUTINES
pderiv        programmed derivative with DOUBLE precision
ideriv        calculation of derivative by interpolation with polynomial

BACKGROUND ESTIMATION PROCEDURE
    snip       background estimation procedure SNIP of Clayton, Ryan and co
    isnip      iterative background estimation procedure SNIP
    example: yback = snip(input_x, input_y, 5, wvl_range=[50, 1800], /show)

EXAMPLES
• calc_jcamp_dx_parameters, 'test1.dx', wvl_range=[150,1400], $
  d1_threshold=0.02, d2_threshold=0.05, res_x, res_y, res_dx, $
  /labeled, psfile='test1.ps'
• read_jcamp_dx, 'test2.dx', i_x, i_y, info
  i_yback = snip(i_x, i_y, 5, wvl_range=[100, 1600], /show)
  calc_jcamp_dx_parameters_using_background, nonexistent_var, $
    input_x=i_x, input_y=i_y, input_b=i_yback, input_info=info, $
    wvl_range=[250,1800], d1_threshold=0.02, d2_threshold=0.01, $
    res_x, res_y, res_dx, res_yback, /labeled, psfile='test2.ps'
```

Listing of calc_jcamp_dx_parameters.pro

```

; calc_jcamp_dx_parameters.pro
; calculate parameters from graphs stored in the jcamp files
;
;
; how to call:
;
; output:
;   res_x(i)   wavenumber of maximum i
;   res_y(i)   intensity of maximum i
;   res_dx(i)  width of peak at maximum i
;
; e.g.:
; IDL> calc_jcamp_dx_parameters, 'gramsliber008blauw.DX', wvl_range=[200, 700], d1_threshold=0.02, d2_threshold=0.04
;-----
; pderiv      programmed derivative
FUNCTION pderiv, x, y

x = DOUBLE(x)
y = DOUBLE(y)
nx = N_ELEMENTS(x)
res_dx = DBLARR(nx)      ; holding the differential values

FOR i=0, nx-2 DO BEGIN
  res_dx(i) = ( y(i+1) - y(i) ) / ( x(i+1) - x(i) )
ENDFOR

res_dx(nx-1) = res_dx(nx-2)
RETURN, res_dx
END
;-----
; ideriv      calculation of derivative by interpolation with polynomial
FUNCTION ideriv, x, y

width = 21                ; odd !!!!

x = DOUBLE(x)
y = DOUBLE(y)
nx = N_ELEMENTS(x)
res_dx = DBLARR(nx)      ; holding the differential values

i_beg = (width / 2L)
i_end = nx - ((width / 2L) + 1)

FOR i=i_beg, i_end DO BEGIN
  x_range_i = (INDGEN(width)-i_beg) + i
  temp_x = x(x_range_i)
  temp_y = y(x_range_i)

  temp_coeff = POLY_FIT(temp_x, temp_y, 2)

  temp_b = temp_coeff(1)
  temp_c = temp_coeff(2)
  temp_deriv = temp_b + (2 * temp_c * temp_x)

  res_dx(i) = temp_deriv(i_beg)

  ; debug plotting
  ;plot, temp_x, temp_y, psym=4
  ;yfit = poly(temp_x, temp_coeff)
  ;oplot, temp_x, yfit
ENDFOR

FOR i=0, i_beg DO BEGIN      ; fill very first dx with first calculated value
  res_dx(i) = res_dx(i_beg)
ENDFOR
FOR i=i_end, i_end+i_beg DO BEGIN ; fill last dx with last calculated value
  res_dx(i) = res_dx(i_end)
ENDFOR

RETURN, res_dx
END
;-----
; background estimation procedure SNIP of Clayton, Ryan and coworkers
;
; input      i_x, i_y, i_n,                ; x & y values, and number of requested iterations i_n
;           ; x values are necessary in case a wavelength-range is given (wvl_range)
; output     o_b                            ; background estimation values
FUNCTION snip, i_x, i_y, i_n, wvl_range=wvl_range, show=show, ps=ps, waittime=waittime

IF(N_ELEMENTS(show) EQ 0) THEN show = 0      ; do not show by default
IF(N_ELEMENTS(ps) EQ 0) THEN BEGIN          ; parameters used by procedure calc_jcamp_dx_parameters
  ps=0
  sel_charsize = 2
  sel_charthick = 1
  sel_thick = 1
  sel_symsize = 1
ENDIF ELSE BEGIN
  ps=1
  sel_charsize = 1
  sel_charthick = 2
  sel_thick = 3
  sel_symsize = 0.7
ENDELSE
IF(N_ELEMENTS(waittime) EQ 0) THEN waittime=0

IF(show) THEN BEGIN
  pmulti_old = !P.MULTI
  !P.MULTI = [0, 1, 3]
  plotyrange = [MIN(i_y)*0.95, MAX(i_y)*1.05]
  PLOT, i_x, i_y, linestyle=1, XSTYLE=1, XRANGE=REVERSE(wvl_range), $
      YSTYLE=1, YRANGE=plotyrange, TITLE='Data Y'

  WAIT, waittime
ENDIF

nx = N_ELEMENTS(i_x)

```

```

IF(N_ELEMENTS(wvl_range) EQ 0) THEN BEGIN
  nbeg = 0
  nend = nx - 1
ENDIF ELSE BEGIN
  ; calculate range of i_y values corresponding to the wavelength range
  diff_x = i_x - wvl_range(0)
  temp_i = WHERE(diff_x GE 0)
  IF(temp_i(0) EQ -1) THEN BEGIN
    nbeg = 0
  ENDIF ELSE BEGIN
    nbeg = temp_i(0)
  ENDELSE
  diff_x = i_x - wvl_range(1)
  temp_i = WHERE(diff_x GE 0)
  IF(temp_i(0) EQ -1) THEN BEGIN
    nend = nx-1
  ENDIF ELSE BEGIN
    nend = temp_i(0)
  ENDELSE
ENDIF
; nbeg and nend holds ROI
PRINT, 'snip nbeg nend', nbeg, nend
IF(show) THEN BEGIN ; display selected region when asked
  OPLOT, i_x(nbeg:nend), i_y(nbeg:nend)
  WAIT, waittime
ENDIF

; calculate where to start: it all depends on the chosen width
; square root transformation
yback = i_y
yback(nbeg:nend) = SQRT(yback(nbeg:nend)>0)

width = 50 ; window FWHM ? fixed number for Raman ????????
; width=200 ... 5 expansion = 40 * 0.5/ch ... width of 20 1/cm
; width=50 width of 4 1/cm

NREDUC = 8
sqrt2 = SQRT(2)
red_fac = 1
iw = (red_fac * 2 * width) + 0.5
; calculate the borders to be stripped
FOR j=1, i_n DO BEGIN
  ; calculate width iw, reduce for last NREDUC iterations
  IF(j GT (i_n-NREDUC)) THEN red_fac = red_fac / SQRT2

  ; stripping
  IF(iw LE 0) THEN break

  FOR i=nbeg, nend DO BEGIN
    iw = (red_fac * 2 * width) + 0.5
    i1 = MAX([i-iw, nbeg])
    i2 = MIN([i+iw, nend])
    ;yback(i) = MIN([yback(i)+3*SQRT([yback(i)], 0.5*(yback(i1)+yback(i2))])
    yback(i) = MIN([yback(i), 0.5*(yback(i1)+yback(i2))])
  ENDFOR
ENDFOR

; inverse square root transformation
FOR i=nbeg, nend DO yback(i) = yback(i)^2

IF(show) THEN BEGIN
  PLOT, i_x, yback, YSTYLE=1, YRANGE=plotyrange, $
  ;PLOT, i_x, yback, YSTYLE=1, YRANGE=[MIN(yback(nbeg:nend))*0.95, MAX(yback(nbeg:nend))*1.05], $
  XSTYLE=1, XRANGE=REVERSE(wvl_range), linestyle=5, TITLE='Yback'
  OPLOT, i_x(nbeg:nend), yback(nbeg:nend)
  WAIT, waittime
ENDIF

IF(show) THEN BEGIN
  PLOT, i_x, i_y, YSTYLE=1, YRANGE=plotyrange, XSTYLE=1, XRANGE=REVERSE(wvl_range), linestyle=1
  OPLOT, i_x(nbeg:nend), yback(nbeg:nend), linestyle=5
  OPLOT, i_x(nbeg:nend), yback(nbeg:nend)+2*SQRT(yback(nbeg:nend)), linestyle=2 ; line of uncertainty n*sigma ... n addi
tional parameter ???
  WAIT, waittime
  !P.MULTI = pmulti_old
ENDIF

RETURN, yback
END

;-----
; iterative background estimation procedure SNIP of Clayton, Ryan and coworkers
; input i_x, i_y, ; x & y values,
; i_n ; array of number of requested iterations i_n
; ; x values are necessary in case a wavelength-range is given (wvl_range)
; output o_b ; background estimation values
FUNCTION isnip, i_x, i_y, i_n, wvl_range=wvl_range, show=show, ps=ps

i_times = N_ELEMENTS(i_n)

t_x = i_x
t_y = i_y

nx = N_ELEMENTS(i_x)
yback = DBLARR(nx) * 0.0
t_yback = yback

FOR i=0, i_times-1 DO BEGIN
  t_y = (i_y - yback) > 0
  t_yback = snip(t_x, t_y, i_n(i), wvl_range-wvl_range, show=show)
  yback = yback + t_yback
ENDFOR

RETURN, yback
END

;-----
; calculate reduced x, y and dx

```

```

;
; input  i_x, i_y, i_dx          i_dx is used to judge whether new peak starts (i.e. i_dx is instrumental parameter)
; output o_x, o_y, o_dx          o_x(i) indicate peak i position with intensity value o_y(i) with width o_dx(i)
PRO calc_reduced_x_y_dx, i_x, i_y, i_dx, $
    o_x, o_y, o_dx

nx = N_ELEMENTS(i_x)

; initialize accounting variables
temp_x = i_x(0)
temp_y = i_y(0)
flag_output = 0 ; no results in o_x yet
FOR i=0, nx-2 DO BEGIN
    nx_0 = i_x(i)
    nx_1 = i_x(i+1)
    dx = nx_1 - nx_0 ; always positive
    IF(dx GT i_dx OR i EQ nx-2) THEN BEGIN
        ; new peak
        ; calculate old peak

        temp_nx = N_ELEMENTS(temp_x)
        IF(temp_nx EQ 1) THEN BEGIN
            ; single point peak value
            IF(flag_output) THEN BEGIN
                ; add to results
                o_x = [o_x, temp_x(0)]
                o_y = [o_y, temp_y(0)]
                o_dx = [o_dx, i_dx] ; result cannot be better than instrumental precision
            ENDIF ELSE BEGIN
                ; first results
                o_x = temp_x(0)
                o_y = temp_y(0)
                o_dx = i_dx ; result cannot be better than instrumental precision
                flag_output = 1
            ENDELSE
        ENDIF ELSE BEGIN
            ; more than one value to consider
            temp_x_moment = MOMENT(temp_x)
            temp_y_moment = MOMENT(temp_y)
            IF(flag_output) THEN BEGIN
                ; add to results
                o_x = [o_x, temp_x_moment(0)] ; average
                o_y = [o_y, temp_y_moment(0)] ; average
                o_dx = [o_dx, temp_x(temp_nx-1)-temp_x(0)] ; o_dx is defined by the borders detected in this procedure
            ENDIF ELSE BEGIN
                ; first results
                o_x = temp_x_moment(0) ; average
                o_y = temp_y_moment(0) ; average
                o_dx = temp_x(temp_nx-1)-temp_x(0) ; o_dx is defined by the borders detected in this procedure
                flag_output = 1
            ENDELSE
        ENDIF ELSE BEGIN
            ; initialize accounting variables with new peak values
            temp_x = nx_1
            temp_y = i_y(i+1)
        ENDIF ELSE BEGIN
            ; still same peak
            temp_x = [temp_x, nx_1]
            temp_y = [temp_y, i_y(i+1)]
        ENDELSE
    ENDIF
ENDFOR

END

;-----
;-----
;-----
;-----
; If input_b is given THEN input_y is assumed to be a net peak intensity
PRO calc_jcamp_dx_parameters, filemask, $
    input_x = input_x, $ ; spectral data
    input_y = input_y, $ ; spectral data
    input_b = input_b, $ ; spectral data ... input_yback is ambiguous word
    input_info = input_info, $
    psfile = psfile, $
    labeled = labeled, $ ; add values at peaks
    wvl_range = wvl_range, $
    d1_threshold = d1_threshold, $
    d2_threshold = d2_threshold, $
    nowait = nowait, $
    res_x, res_y, res_dx, res_yback ; peak info

;wvl_range = [500, 1600]
;wvl_range = [1300, 1600]
;wvl_range = [500, 1000]
;wvl_range = [1000, 1200]
;wvl_range = [1010, 1020]

print, 'calc_jcamp_dx_parameters begin '
help, filemask
help, input_x
help, input_y
help, input_b
help, input_info

IF(N_ELEMENTS(nowait) EQ 0) THEN BEGIN
    waittime = 2
ENDIF ELSE BEGIN
    waittime = 0
ENDELSE

; postscript output or not
IF(N_ELEMENTS(psfile) EQ 0) THEN BEGIN
    ps=0

```

```

        subtitlestring='' ; no psfile
    ENDIF ELSE BEGIN
        ps=1
        subtitlestring=psfile ; add psfile on plots
        psb, psfile
    ENDELSE

    IF(N_ELEMENTS(labeled) EQ 0) THEN labeled = 0

    ; check thresholds
    IF(N_ELEMENTS(d1_threshold) EQ 0) THEN d1_threshold = 0.02
    IF(N_ELEMENTS(d2_threshold) EQ 0) THEN d2_threshold = 0.02

    ; background given or not
    IF(N_ELEMENTS(input_b) GT 0) THEN BEGIN
        yback = input_b
    ENDIF

    ; check what type of input is dealt with: filemask or (input_x, input_y)
    ; note that more than one Raman spectrum can be processed
    ; filemask has priority: if both are given then (input_x, input_y) is ignored

    ; files selection
    IF(N_ELEMENTS(filemask) EQ 0) THEN BEGIN
        ; check whether there is input of type (input_x, input_y)
        IF(N_ELEMENTS(input_x) EQ 0 OR N_ELEMENTS(input_y) EQ 0) THEN BEGIN
            ; absolute no intention of giving input via arguments ... ask for files
            PRINT, 'no filemask given... manual selection is requested...'
            dxfiles = DIALOG_PICKFILE(FILTER=['*.dx', '*.DX', '*.jdx', '*.JDX'], /FIX_FILTER, /MULTIPLE_FILES, $
                TITLE='DX/JDX files to be evaluated')
            filemode = 1
            nspectra = N_ELEMENTS(dxfiles)
        ENDIF ELSE BEGIN
            ; no filemask, input of type (input_x, input_y)
            filemode = 0
            ; find out how many spectra are given as input
            ndim_input_x = size(input_x, /n_dimensions)
            ndim_input_y = size(input_y, /n_dimensions)
            dim_input_x = size(input_x, /dimensions)
            dim_input_y = size(input_y, /dimensions)
            IF(ndim_input_x GT 2 OR ndim_input_y GT 2) THEN BEGIN
                PRINT, '[calc_jcamp_dx_parameters] ERROR input_x and/or input_y are vectors or matrices ... calculation canceled'
            ENDIF
            IF(ndim_input_x EQ 1) THEN BEGIN
                ; only one spectrum
                nspectra = 1
                IF(N_ELEMENTS(input_info) EQ 0) THEN BEGIN
                    dxfiles = 'input y=xj(i)j='+STRCOMPRESS(STRING(INDGEN(nspectra)+1),/REMOVE_ALL) ; check for filename in info !!!!
                ENDIF ELSE BEGIN
                    dxfiles = input_info(0)
                ENDELSE
            ENDIF ELSE BEGIN
                ; more than one spectrum: check for dimensions of input_x and input_y are matching
                IF(dim_input_x(0) NE dim_input_y(0) OR dim_input_x(1) NE dim_input_y(1)) THEN BEGIN
                    ; mismatch
                    PRINT, '[calc_jcamp_dx_parameters] ERROR mismatch of input_x and input_y ... calculation canceled'
                    RETURN
                ENDIF ELSE BEGIN
                    ; legal input of type (input_x, input_y)
                    nspectra = dim_input_x(1)
                    IF(N_ELEMENTS(input_info) EQ 0) THEN BEGIN
                        dxfiles = 'input y=xj(i)j='+STRCOMPRESS(STRING(INDGEN(nspectra)+1),/REMOVE_ALL) ; check for filename in info !!!!
                    ENDIF ELSE BEGIN
                        dxfiles = input_info(0)
                    ENDELSE
                ENDELSE
            ENDIF ELSE BEGIN
                dxfiles = FINDFILE(filemask)
                nspectra = N_ELEMENTS(dxfiles)
                filemode = 1
            ENDELSE
        ENDIF ELSE BEGIN
            nspectra = 0
        FOR i=0, nspectra-1 DO BEGIN
            pmulti_old = !P.MULTI
            !P.MULTI = [0, 1, 6]
            IF(filemode EQ 1) THEN BEGIN
                read_jcamp_dx, dxfiles(i), x, y, info
                titleinfo = dxfiles(i)
            ENDIF ELSE BEGIN
                x = input_x(*,i)
                y = input_y(*,i)
                IF(N_ELEMENTS(input_info) EQ 0) THEN BEGIN
                    info = ['input y=xj(i)j='+STRCOMPRESS(STRING(i+1),/REMOVE_ALL), 'none', 'none', 'none', 'none'] ; check for filename in info !!!!
                    titleinfo = info(0)
                ENDIF ELSE BEGIN
                    info = input_info(*,i) ; check this !!!!
                    temp_s = STRSPLIT(info(0), '/', /EXTRACT)
                    n_temp_s = N_ELEMENTS(temp_s)
                    titleinfo = temp_s(n_temp_s-1)+'#+'+STRCOMPRESS(STRING(i+1),/REMOVE_ALL)
                ENDELSE
            ENDIF ELSE
                x_resolution = x(1) - x(0) ; ??????????????????????
                x_resolution = 0.5
            ;-----
            ; selection of ROI
            wvl_beg = MIN(x)
            wvl_end = MAX(x)
            IF(N_ELEMENTS(wvl_range) EQ 0) THEN BEGIN
                PRINT, 'No selection of ROI ... full spectrum'
            ENDIF
        END FOR
    ENDIF

```

```

        wvl_range = [wvl_beg, wvl_end]
    ENDEF ELSE BEGIN
        wvl_beg = wvl_range(0)
        wvl_end = wvl_range(1)
    ENDELSE

; calculation of x_beg and x_end
x_beg = 0
x_end = N_ELEMENTS(x)-1

x = x(x_beg: x_end)
y = y(x_beg: x_end)
IF(N_ELEMENTS(input_b) GT 0) THEN yback = yback(x_beg: x_end)

; only look on selected ROI
x_sel_i = WHERE(x GE wvl_beg AND x LE wvl_end)
x = x(x_sel_i)
y = y(x_sel_i)
IF(N_ELEMENTS(input_b) GT 0) THEN yback = yback(x_sel_i)

nx = N_ELEMENTS(x)
xscale = 10 ; using xscale of 5 there is the risc to loose peaks !!!

x_orig = x
y_orig = y
IF(N_ELEMENTS(input_b) GT 0) THEN yback_orig = yback

x = CONGRID( DOUBLE(x), xscale * nx, 0, 0, /INTERP)
y = CONGRID( DOUBLE(y), xscale * nx, 0, 0, /INTERP)
IF(N_ELEMENTS(input_b) GT 0) THEN BEGIN
    ; background is given ... expand it also
    yback = CONGRID( DOUBLE(yback), xscale * nx, 0, 0, /INTERP)
    ;help, x, y, yback
    ;window, 3
    ;PLOT, x, y, ystyle=1, yrange=[0, MAX(yback)], $
    ; XSTYLE=1, REVERSE(wvl_range)
    ;OPLOT, x, yback
    ;OPLOT, x_orig, y_orig, linestyle=1
    ;OPLOT, x_orig, yback_orig, linestyle=1
    ;WAIT, waittime
ENDEF ELSE BEGIN
    ; no background given
ENDELSE
; x, y and yback are expanded data sets from here

IF(ps EQ 0) THEN BEGIN
    WINDOW, 0, RETAIN=2, xsize=800, ysize=900
    sel_charsize = 2
    sel_charthick = 1
    sel_thick = 1
    sel_symsize = 1
    ENDEF ELSE BEGIN
        ; postscript graph parameters
        sel_charsize = 1
        sel_charthick = 2
        sel_thick = 3
        sel_symsize = 0.7
    ENDELSE
; raw
PLOT, x_orig, y_orig, TITLE=titleinfo+ 'Raw y', SUBTITLE=subtitlestring, $
    charsize=sel_charsize, charthick=sel_charthick, thick=sel_thick, $
    xstyle = 1, xrange = REVERSE(wvl_range), $ ; xstyle=3
    YSTYLE=1, YRANGE = [MIN(y), MAX(y)]
;PLOT, x, y, TITLE=dxfiles(i)+ 'Raw y', xstyle = 1, charsize=2, xrange = wvl_range, $ ; xstyle=3
    YSTYLE=1, YRANGE = [MIN(y), MAX(y)]
;PLOTS, [MIN(x), MAX(x)], [0,0]

; smooth
ysmooth = SMOOTH(y, 2, /EDGE_TRUNCATE) ; parameter ???
;ysmooth = SMOOTH(y, 10, /EDGE_TRUNCATE) ; parameter ???
PLOT, x, ysmooth, title='Smoothed y', $
    charsize=sel_charsize, charthick=sel_charthick, thick=sel_thick, $
    linestyle=1, xstyle = 1, xrange = REVERSE(wvl_range), $
    YSTYLE=1, YRANGE = [MIN(ysmooth), MAX(ysmooth)]
;PLOTS, [MIN(x), MAX(x)], [0,0]

dl_orig = ideriv(x, y)
;dl_orig = pderiv(x, y) ; not enough precision !!!
;dl_orig = DERIV(y) ; not enough precision !!!
;dl_orig = DERIV(x, y) ; not enough precision !!!
PLOT, x, dl_orig, title='DERIV of raw y', psym=3, $
    charsize=sel_charsize, charthick=sel_charthick, thick=sel_thick, $
    xstyle = 1, xrange = REVERSE(wvl_range)
PLOTS, [MIN(x), MAX(x)], [0,0], /DATA

dl = ideriv(x, ysmooth)
;dl = DERIV(ysmooth) ; not enough precision !!!
;dl = DERIV(x, ysmooth) ; not enough precision !!!
PLOT, x, dl, title='DERIV of smoothed y', psym=3, $
    charsize=sel_charsize, charthick=sel_charthick, thick=sel_thick, $
    xstyle = 1, xrange = REVERSE(wvl_range)
;PLOTS, [MIN(x), MAX(x)], [0,0]
dl = smooth(dl, 10 * xscale, /EDGE_TRUNCATE)
dl = smooth(dl, 5 * xscale, /EDGE_TRUNCATE)
dl = smooth(dl, 3 * xscale, /EDGE_TRUNCATE)
PLOT, x, dl, title='Smooth DERIV of smoothed y', psym=3, $
    charsize=sel_charsize, charthick=sel_charthick, thick=sel_thick, $
    xstyle = 1, xrange = REVERSE(wvl_range)
PLOTS, [MIN(x), MAX(x)], [0,0]

;d2 = DERIV(x, dl_orig)
; no plot d2

d2 = ideriv(x, dl)
;d2 = DERIV(x, dl) ; faster but lower precision ???!!!

```

```

d2 = smooth(d2, 3 * xscale, /EDGE_TRUNCATE)
; d2 = smooth(d2, 5 * xscale, /EDGE_TRUNCATE)
; d2 = smooth(d2, 10 * xscale, /EDGE_TRUNCATE)
PLOT, x, d2, title='DERIV^2 of smoothed y', psym=3, $
charsize=sel_charsize, charthick=sel_charthick, thick=sel_thick, $
xstyle = 1, xrange = REVERSE(wvl_range)
PLOTS, [MIN(x), MAX(x)], [0,0]

;dlzeros_i = WHERE((ABS(d1_orig) LT 0.05 * MAX(d1_orig))) ; ????????? how close to ZERO
dlzeros_i = WHERE((ABS(d1) LT d1_threshold * MAX(d1))) ; ????????? how close to ZERO
dlzeros_x = x(dlzeros_i)
dlzeros_y = d1_orig(dlzeros_i)
zeros_y = y(dlzeros_i)
d2zeros_y = d2(dlzeros_i) ; d2 values where d1 is near zero

OPLLOT, dlzeros_x, d2zeros_y, PSYM=1

mind2 = MIN(d2)

temp_i = WHERE(d2zeros_y LT d2_threshold * mind2) ; !!!!!!!!!!!!! how small compared to GRAND MAX
;temp_i = WHERE(d2zeros_y GT 0.02 * maxd2) ; !!!!!!!!!!!!! how small compared to GRAND MAX
IF(temp_i(0) NE -1) THEN BEGIN
  dlzeros_posy_x = dlzeros_x(temp_i) ; x values for which: (i) 1st DERIV is near ZERO and (ii) 2nd DERIV positive
  zeros_y = zeros_y(temp_i) ; y values
  ENDEF ELSE BEGIN
    ; no x values for which (i) 1st DERIV is near ZERO and (ii) 2nd DERIV positiv
    dlzeros_posy_x = FLTARR(1)
    zeros_y = FLTARR(1)
    dlzeros_posy_x(0) = -9999
    zeros_y(0) = -9999
  ENDELSE
;PRINT, dlzeros_posy_x
;PRINT, min(dlzeros_posy_x), max(dlzeros_posy_x)
;PRINT, min(zeros_y), max(zeros_y)
;-----
; plot original raw data with symbol at maxima of y
!P.MULTI = pmulti_old
IF(ps EQ 0) THEN BEGIN
  WINDOW, 1, RETAIN=2, xsize=1200, ysize=900
  ENDEF ELSE BEGIN
    ; next plot is best in landscape
    DEVICE, /LANDSCAPE
  ENDELSE
PLOT, x, y, TITLE=titleinfo+ 'Raw y', SUBTITLE=subtitlestring, XTITLE=info(2), YTITLE=info(3), $
charsize=sel_charsize, charthick=sel_charthick, thick=sel_thick, $
xstyle = 1, xrange = REVERSE(wvl_range), $ ; xstyle=3
YSTYLE=1, YRANGE = [MIN(y)*0.95, MAX(y)*1.2]
n_dlzeros_posy_x = N_ELEMENTS(dlzeros_posy_x)

IF(labeled) THEN BEGIN
  USERSYM, [0,0], [-.5,0.5] ; vertical symbol
  labelyoffset = ((MAX(y)*1.2) - (MIN(y)*0.95)) / 30
  OPLLOT, dlzeros_posy_x, zeros_y + labelyoffset, PSYM=8, $ ; psym 1:+ 7:x 8:|
  thick=sel_thick
  ;FOR j=0, n_dlzeros_posy_x-1 DO BEGIN
  ; OPLLOT, dlzeros_posy_x, zeros_y, PSYM=7
  ; ENDFOR
  ENDEF ;IF(labeled)

WAIT, waittime ; waiting time between two plots
!P.MULTI = pmulti_old

;PRINT, dlzeros_posy_x
;PRINT, '-----'
;PRINT, zeros_y

;DELVAR, res_x, res_y, res_dx, res_yback

calc_reduced_x_y_dx, dlzeros_posy_x, zeros_y, x_resolution, res_x, res_y, res_dx

;print, 'calc_jcamp_dx_parameters end'
;help, res_x
;help, res_y
;help, res_dx
;print, res_x
;print, res_y
;help, input_b

; IF yback is given THEN remove peaks that can NOT be statistically distinguished from the background
; get background intensities corresponding to res_x
IF(N_ELEMENTS(input_b) EQ 0) THEN BEGIN
  ; background not given: no change of results
  ENDEF ELSE BEGIN
    ; check whether the peaks found are statistically different from the background
    temp_res_x = res_x
    temp_res_y = res_y
    temp_res_dx = res_dx
    ; res_b doesn't exist yet
    nresults = 0
    nres_x = N_ELEMENTS(temp_res_x)
    res_x = -9999. ; indicating no result
    FOR p=0, nres_x-1 DO BEGIN ; use p
      ; yback and x are expanded spectral data
      diffx_p = WHERE(ABS(x-temp_res_x(p)) LE 0.1)
      ;help, p, diffx_p
      IF(diffx_p(0) NE -1) THEN BEGIN
        ; background value of peak i is found
        temp_yb = MAX(yback(diffx_p)) ; take most pessimistic result (highest background)

        ;IF(p EQ 0) THEN BEGIN
        ; help, x, yback
        ; PRINT, 'temp_res_x(0)', temp_res_x(0)
        ; PRINT, 'MAX(yback(diffx_p))', temp_yb
        ; ENDEF

```

```

s_factor = 2. ; size factor of de sigma later in the comparison
; s_factor = 3. ; size factor of de sigma later in the comparison
; take into account increase of background because of statistics
temp_yb_max = temp_yb + (s_factor * SQRT(2. * temp_res_y(p) + temp_yb)) ; backmax = B+s_factor*SQRT(2P+B) do NOT change factor 2 !
; take also most pessimistic peak value (i.e. taking into account uncertainty)
temp_res_yp_min = temp_res_y(p) - (s_factor * SQRT(temp_res_y(p) + 2. * temp_yb)) ; peakmin = P-s_factor*SQRT(P+2B) do NOT change factor 2 !
; IF(temp_res_yp_min GT 3. * SQRT(temp_yb_max)) THEN BEGIN ; conservative 99%
; IF(temp_res_yp_min GT 2. * SQRT(temp_yb_max)) THEN BEGIN ; conservative 95%
; IF(temp_res_y(p) GT 3. * SQRT(temp_yb_max)) THEN BEGIN ;
; IF(temp_res_y(p) GT 2. * SQRT(temp_yb_max)) THEN BEGIN ;
; IF(temp_res_y(p) GT 3. * SQRT(temp_yb)) THEN BEGIN ; most optimistic
; peak is higher than background ... store results
IF(nresults EQ 0) THEN BEGIN
; first peak in list to store
res_x = temp_res_x(p)
res_y = temp_res_y(p)
res_dx = temp_res_dx(p)
res_yback = temp_yb
nresults = 1
ENDIF ELSE BEGIN
; add to list
res_x = [res_x, temp_res_x(p)]
res_y = [res_y, temp_res_y(p)]
res_dx = [res_dx, temp_res_dx(p)]
res_yback = [res_yback, temp_yb]
nresults = nresults + 1
ENDIF ELSE BEGIN
; peak should be considered as background
PRINT, ' rejected : x ', temp_res_x(p), ' y ', temp_res_y(p), ' yback ', temp_yb, ' backmax ', temp_yb_max, ' peakmin ', temp_res_yp_min
ENDELSE ; IF(res_y(p) GT 3. * SQRT(temp_yb))
ENDIF ELSE BEGIN
; problems with "LE 0.1" ... hopefully deadcode
ENDELSE ; IF(diffx_p(0) NE -1)
ENDFOR ; FOR i=0, nres_x-1
ENDELSE ; IF(N_ELEMENTS(input_b) EQ 0) THEN BEGIN

IF(labeled) THEN BEGIN
; output values on top of peaks found
; calculate offset of labels
labelyoffset = ((MAX(y)*1.2) - (MIN(y)*0.95)) / 20
IF(N_ELEMENTS(res_x) GT 0) THEN BEGIN
values_strings = STRCOMPRESS(STRING(res_x, FORMAT=' (F6.1) '),/REMOVE_ALL)
XYOUTS, res_x, res_y + labelyoffset, values_strings, ALIGNMENT=0.5, $
charsize=sel_charsize*0.4, charthick=sel_charthick
ENDIF
ENDIF ; IF(labeled)

help, info
ninfo = N_ELEMENTS(info)
FOR k=0, ninfo-1 DO BEGIN
i_string = STRCOMPRESS(STRING(k),/REMOVE_ALL)
PRINT, ' info (' + i_string + ') : ' + info(k) + ' '
ENDFOR

; build list of results: list_x list_y list_dx list_yback
; -----
; no data for i_yback ?
ndim_res_x = SIZE(res_x,/N_DIMENSIONS)

PRINT, ' '
PRINT, ' ***** '
PRINT, ' ndim_res_x is ', ndim_res_x
IF(N_ELEMENTS(res_x) GT 0) THEN PRINT, ' res_x ', res_x
PRINT, ' '
; WAIT, waittime

CASE ndim_res_x OF
0: BEGIN ; 1 or no peak
; check whether there 1 peak or no peak
IF(N_ELEMENTS(res_x) EQ 0) THEN BEGIN
; !!!!!!! what happens when there is no peak e.g. -9999
; !!!!!!! value non-existing peak still under consideration
res_x = -9999
res_y = -9999
res_dx = -9999
res_yback = -9999

dist_x = res_x
dist_y = res_y
dist_dx = res_dx
dist_yback = res_yback
npeaks = 1
ENDIF
IF(i EQ 0) THEN BEGIN
; first results
list_x = FLTARR(1) & list_x(0) = res_x(0)
list_y = FLTARR(1) & list_y(0) = res_y(0)
list_dx = FLTARR(1) & list_dx(0) = res_dx(0)
list_yback = FLTARR(1) & list_yback(0) = res_yback(0)
; nsamples is 1
PRINT, ' i=0 pos 1'
; WAIT, waittime
npeaks = 1
ENDIF ELSE BEGIN
; there are already results ... npeaks stays max number of peaks
temp_add_x = FLTARR(npeaks) & temp_add_x(0) = res_x(0)
temp_add_y = FLTARR(npeaks) & temp_add_y(0) = res_y(0)
temp_add_dx = FLTARR(npeaks) & temp_add_dx(0) = res_dx(0)
temp_add_yback = FLTARR(npeaks) & temp_add_yback(0) = res_yback(0)

list_x = [[list_x], [temp_add_x]]

```

```

list_y = [[list_y], [temp_add_y]]
list_dx = [[list_dx], [temp_add_dx]]
list_yback = [[list_yback], [temp_add_yback]]
; nsamples is i+1
ENDELSE
END
1: BEGIN ; more than 1 peak
n_res_x = N_ELEMENTS(res_x)
IF(i EQ 0) THEN BEGIN
; first results
list_x = res_x
list_y = res_y
list_dx = res_dx
list_yback = res_yback
; nsamples is 1
PRINT, '
; WAIT, waittime
npeaks = n_res_x
ENDIF ELSE BEGIN
; there are already results ... add to these results
; check whether an expansion of the list_* datamatrix is necessary
IF(n_res_x LE npeaks) THEN BEGIN
; npeaks stays max number of peaks: add results
temp_add_x = FLTARR(npeaks) & temp_add_x(0:n_res_x-1) = res_x
temp_add_y = FLTARR(npeaks) & temp_add_y(0:n_res_x-1) = res_y
temp_add_dx = FLTARR(npeaks) & temp_add_dx(0:n_res_x-1) = res_dx
temp_add_yback = FLTARR(npeaks) & temp_add_yback(0:n_res_x-1) = res_yback

list_x = [[list_x], [temp_add_x]]
list_y = [[list_y], [temp_add_y]]
list_dx = [[list_dx], [temp_add_dx]]
list_yback = [[list_yback], [temp_add_yback]]
; nsamples is i+1
ENDIF ELSE BEGIN
; n_res_x becomes max number of peaks: expand matrices storing the results and add
; nsamples is i+1
; expand the results matrices and store old results
temp_add_x = FLTARR(n_res_x, i+1) & temp_add_x(0:npeaks-1, 0:i-1) = list_x
temp_add_y = FLTARR(n_res_x, i+1) & temp_add_y(0:npeaks-1, 0:i-1) = list_y
temp_add_dx = FLTARR(n_res_x, i+1) & temp_add_dx(0:npeaks-1, 0:i-1) = list_dx
temp_add_yback = FLTARR(n_res_x, i+1) & temp_add_yback(0:npeaks-1, 0:i-1) = list_yback
; add new results
temp_add_x(*, i) = res_x & list_x = temp_add_x
temp_add_y(*, i) = res_y & list_y = temp_add_y
temp_add_dx(*, i) = res_dx & list_dx = temp_add_dx
temp_add_yback(*, i) = res_yback & list_yback = temp_add_yback
npeaks = n_res_x
ENDELSE ; IF(n_res_x LE npeaks)
ENDELSE ; IF(i EQ 0)
END
ELSE:
ENDCASE
; start from scratch next time
dummy = TEMPORARY(res_x)
dummy = TEMPORARY(res_y)
dummy = TEMPORARY(res_dx)
dummy = TEMPORARY(res_yback)
;-----
ENDFOR ; FOR i=0, nspectra-1 DO

res_x = list_x
res_y = list_y
res_dx = list_dx
res_yback = list_yback

IF(ps) THEN pse

END
;=====
; y is raw spectral data (P+B) ... net peak intensity will be calculated
PRO calc_jcamp_dx_parameters_using_background, filemask, $
    input_x = input_x, $ ; spectral data
    input_y = input_y, $ ; spectral data (actually P+B)
    input_b = input_b, $ ; spectral data ... input_yback is ambiguous word
    input_info = input_info, $
    psfile = psfile, $
    labeled = labeled, $ ; add values at peaks
    wvl_range = wvl_range, $
    d1_threshold = d1_threshold, $
    d2_threshold = d2_threshold, $
    nowait = nowait, $
    res_x, res_y, res_dx, res_yback ; peak info

i_ydiff = (input_y - input_b) > 0
plot, input_x, input_y
oplot, input_x, input_b, linestyle=1
oplot, input_x, i_ydiff
oplot, input_x, SQRT(input_b) * 2

; res_dx is not defined

; when calc_jcamp_dx_parameters is called with background, netto y is assumed
calc_jcamp_dx_parameters, nonexistent_var, input_x=input_x, input_y=i_ydiff, input_b=input_b, input_info=input_info, $
    wvl_range=wvl_range, d1_threshold=d1_threshold, d2_threshold=d2_threshold, nowait=nowait, $
    res_x, res_y, res_dx, res_yback, labeled=labeled, psfile=psfile
;help, res_x, res_y, res_dx, res_yback
;print, res_x
;print, res_y
;print, res_dx
;print, res_yback

END

```

Appendix B: Publications and activities

B.1 List of (contributions to) publications

1. de Veij, M., Deneckere, A., Vandenabeele, P., de Kaste, D., Moens, L. (2008) Detection of counterfeit Viagra® with Raman spectroscopy. *Journal of Pharmaceutical and Biomedical Analysis* 46: 303–309.
2. Calvo del Castillo, H., Deprez, N., Dupuis, T., Mathis, F., Deneckere, A., Vandenabeele, P., Calderón, T., Strivay, D. (2009) Towards the differentiation of non-treated and treated corundum minerals by ion-beam-induced luminescence and other complementary techniques. *Analytical and Bioanalytical Chemistry* 394: 1043–1058.
3. Deneckere, A., Schudel, W., Van Bos, M., Wouters, L., Bergmans, A., Vandenabeele, P., Moens, L. (2010) In situ investigations of mediaeval wall paintings in the Antwerp Cathedral. *Spectrochimica Acta Part A - molecular and biomolecular spectroscopy* 75: 511–519.
4. Deneckere, A., Hocquet, F-Ph., Born, A., Klein, P., Rakkaa, S., Lycke, S., De Langhe, K., Martens, M.P.J., Strivay, D., Vandenabeele, P., Moens, L. (2010) Direct analysis of the central panel of the so-called ‘Wyts triptych’ after Jan Van Eyck. *Journal of Raman Spectroscopy* 41: 1210–1219.
5. Deneckere, A., De Reu, M., Martens, M.P.J., De Coene, K., Vekemans, B., Vinzce L., De Maeyer, Ph., Vandenabeele, P., Moens, L. (2011) The use of a Multi-method approach to identify pigments in the 12th century manuscript Liber Floridus. *Spectrochimica Acta Part A - molecular and biomolecular spectroscopy*, 80: 125–132.

6. Deneckere, A., Vekemans, B., Van de Voorde, L., de Paepe, P., Vincze, L., Moens, L., Vandenabeele, P. (2011) Scanning porcelain cards with Raman spectroscopy and X-ray fluorescence spectroscopy. *Special issue of Applied Physics A - Optical Technologies in Art and Archaeology*, submitted.
7. Deneckere, A., Leeftang, M., Bloem, M., Chavannes-Mazel, C.A., Vekemans, B., Vincze, L., Vandenabeele, P., Moens, L. (2011) The use of mobile Raman spectroscopy to compare three full-page miniatures from the Breviary of Arnold of Egmond. *Spectrochimica Acta Part A - molecular and biomolecular spectroscopy*, Accepted.
8. Deneckere, A., de Vries, L., Vekemans, B., Van de Voorde, L., Ariese, F., Vincze, L., Moens, L., Vandenabeele, P. (2011) Identification of inorganic pigments used in porcelain cards based on fusing Raman and XRF data. *Applied Spectroscopy*, Accepted.

B.2 List of (contributions to) oral presentations

1. Workshop NACHO, Brussels, Belgium, 8 – 9 October 2009
 Oral presentation by Annelien Deneckere
 Deneckere, A., Hocquet, F.-P., Born, A., Klein, P., Rakkaa, S., Lycke, S., De Langhe, K., Martens, M. P. J., Strivay, D., Vandenabeele, P., Moens, L.:
Direct analysis of a so-called 'Wyts Triptych' after Jan Van Eyck.
2. Non-destructive Analysis of Cultural Heritage Objects PhD Day, Luik, Belgium
 2 July 2009
 Oral presentation by Annelien Deneckere
 Deneckere, A.:
In situ investigation of mediaeval wall paintings in the Antwerp cathedral.

3. 5th International Congress on the application of Raman Spectroscopy in Art and Archaeology, Bilbao (Spain), 14 – 18 September 2009

Oral presentation by Annelien Deneckere

Deneckere, A., Hocquet, F.-P., Born, A., Klein, P., Rakkaa, S., Lycke, S., De Langhe, K., Martens, M. P. J., Strivay, D., Vandenabeele, P., Moens, L.:

An in situ investigation of a so-called 'Wyts triptych' after Jan Van Eyck.

Best oral presentation

4. Workshop NACHO, IRPA/KIK, Brussels (Belgium), 8-9 October 2009

Oral presentation by Annelien Deneckere

Deneckere, A., Hocquet, F.-P., Born, A., Klein, P., Rakkaa, S., Lycke, S., De Langhe, K., Martens, M. P. J., Strivay, D., Vandenabeele, P., Moens, L.:

Direct analysis of the central panel of the 'Wyts triptych'.

5. 10th Flemish youth conference of Chemistry, Blankenberge (Belgium), 1-2 March 2010

Oral presentation by Annelien Deneckere

Deneckere, A., De Reu, M., Vekemans, B., Vincze, L., Vandenabeele, P., Moens, L.:

The analysis of the mediaeval manuscript 'Liber Floridus' with Raman and X-ray Fluorescence spectroscopy.

6. 9th International Conference on Raman Spectroscopy Applied to the Earth Sciences - Sensus Latus, Sydney (Australia), 28 June - 2 July 2010

Oral presentation by Annelien Deneckere

Deneckere, A., De Reu, M., De Coene, K., Vekemans, B., Vincze, L., Moens, L., Vandenabeele, P.:

Raman spectroscopy, supplemented with two other techniques, as tool to gather information about the mediaeval manuscript 'Liber Floridus'

7. 60th Annual conference on applications of X-ray Analysis, 1–5 August 2011
 Oral presentation by Bart Vekemans
 Deneckere, A., Vekemans, B., de Vries, L., Van de Voorde, L., De Paepe, P., Vincze, L., Moens, L., Vandenabeele, P.:
Investigation of porcelain cards using combined spectroscopic techniques.

8. 6th international congress on the application of Raman spectroscopy in art and archaeology, 5–8 September 2011
 Oral presentation by Annelien Deneckere
 Deneckere, A., Vekemans, B., de Vries, L., Vincze, L., Vandenabeele, P., Moens, L.:
A combination of Raman and X-ray fluorescence spectroscopy to investigate porcelain cards.

B.3 List of (contributions to) poster presentations

1. Technart 2009, Non-destructive and microanalytical techniques in Art and Cultural Heritage, Athens, 27 – 30 april 2009
 Poster presentation by Helena Calvo del Castillo
 Calvo del Castillo, H., Chêne, G., Dupuis, T., Mathis, F., Deneckere, A., Moens, L., Vandenabeele, P., Calderón, T., Strivay, D.:
Ongoing study of treated and non-treated corundum samples
 Best Poster Award

2. 8th International Conference on Raman Spectroscopy Applied to Earth Science – Sensus Latu, GeoRaman '08, Ghent, Belgium, 2–6 June 2008
 Poster Presentation by Annelien Deneckere
 Deneckere, A., Deprez, N., Calvo del Castillo, H., Strivay, D., Vandenabeele,

P., Moens, L., Calderón, T.:

Towards a differentiation of non-treated and treated corundum minerals by means of Raman microscopy: first results.

3. PhD symposium Faculty of sciences, Ghent, 28 april 2009

Poster presentation by Annelien Deneckere

Deneckere, A., Schudel, W., Van Bos, M., Wouters, L., Vandenabeele, P., Moens, L.:

In situ investigations of mediaeval wall paintings in the Antwerp Cathedral.

4. 5th International Congress on the application of Raman Spectroscopy in Art and Archaeology, Bilbao (Spain), 14 – 18 September 2009

Poster Presentation by Annelien Deneckere

Deneckere, A., De Reu, M., Vekemans, B., Lycke, S., Vincze, L., Vandenabeele, P., Moens, L.:

Raman analysis of the mediaeval manuscript 'Liber Floridus' at the library of Ghent University.

5. Archeometrie aan de UGent: een stand van zaken, Ghent (Belgium), 22 January 2010

Poster presentation by Annelien Deneckere

Deneckere, A., Hocquet, F.-P., Born, A., Klein, P., Rakkaa, S., Lycke, S., De Langhe, K., Martens, M. P. J., Strivay, D., Vandenabeele, P., Moens, L.:
Direct analysis of the so-called 'Wyts triptych' after Jan van Eyck.

6. International School Hubert Curien Structural and Molecular Archaeology: 3rd course non-invasive analysis of painting materials, Erice (Sicily), 14–21 June 2010

Poster Presentation by Annelien Deneckere

Deneckere, A., Vekemans, B., Van de Voorde, L., Vincze, L., De Paepe, P.,
Vandenabeele, P., Moens, L.:

Mapping of porcelain cards with Raman spectroscopy and X-ray fluorescence spectroscopy.

7. 9th International Conference on Raman Spectroscopy Applied to the Earth
Sciences - Sensu Latu, Sydney (Australia), 28 June - 2 July 2010

Poster presentation by Annelien Deneckere

Deneckere, A., Leeftang, M., Bloem, M., Chavannes-Mazel, C.A.,
Vandenabeele, P., Moens, L.:

*The use of Raman spectroscopy to compare three folios from the Breviary of
Arnold of Egmond.*

8. 9th International Conference on Raman Spectroscopy Applied to the Earth
Sciences - Sensu Latu, Sydney (Australia), 28 June - 2 July 2010

Poster presentation by Annelien Deneckere

Deneckere, A., Vekemans, B., Van de Voorde, L., Vincze, L., De Paepe, P.,
Vandenabeele, P., Moens, L.:

Mapping of porcelain cards with Raman spectroscopy and X-ray fluorescence spectroscopy.

9. XVIIIth congress of the GMPCA Archéométrie 2011, 11 - 15 April 2011

Poster presentation by Annelien Deneckere

Deneckere, A., Vekemans, B., Van de Voorde, L., De Paepe, P., Vincze, L.,
Vandenabeele, P., Moens, L.:

A multi-method approach for the characterising of porcelain cards.